Indirect control of flexible demand for power system applications.

Sossan, Fabrizio

Publication date:
2014

Document Version
Publisher's PDF, also known as Version of record

Fabrizio Sossan

Indirect control of flexible demand for power system applications

Ph.D. thesis, December 2013

www.elektro.dtu.dk
Department of Electrical Engineering
Center for Electric Power and Energy
Technical University of Denmark
Frederiksborgvej 399
Building 776
DK-4000 Roskilde Denmark
Tel: (+45) 45 25 38 00
Fax: (+45) 45 93 16 34
Email: info@elektro.dtu.dk

ISBN XX-XXXX-XX-X

Preface

This thesis was prepared at the Department of Electrical Engineering at the Technical University of Denmark in partial fulfillment of the requirements for acquiring the PhD degree in engineering. The PhD was funded by Flexpower project (project number n. 2010-1-10486).

The PhD project started on 1 December 2010 and it was completed on 9 December 2013.

The thesis deals with indirect control of electrical flexible consumption for supporting the operation of the electric power system and mitigating the effects of an increased penetration of renewable generation in the grid.

The thesis is composed by 7 chapters, 4 appendices and 6 attached papers. Four among the attached papers have been published in international peer-reviewed conferences. The other two papers have been submitted for journal publications and they are currently under review.

Fabrizio Sossan
9 December 2013

Summary

This thesis addresses the topic of control of flexible demand to provide support to the operation of the electric power system. We focus on the indirect control approach, a framework that enables demand response by means of a consumption incentive signal.

Initially, the concept of flexibility is defined and a classification of flexible electric loads is presented. In order to evaluate the potential of flexible demand, the storage capacity associated with the operation of a number domestic electric loads is quantified by means of simulations.

Subsequently, the topic of indirect control of flexible demand is addressed. We investigate the subject considering both how to achieve a shift in the consumption of the single DSRs, and how to generate the indirect control signal for a population of DSRs in order to support the operation of the grid. In the former case, we develop algorithms that achieve a shift in the consumption according to an indirect control signal. We present from simple control algorithms with a few requirements up to model predictive control strategies. The performance of the indirect control algorithms are compared by means of hardware-in-the-loop simulations using Power Flexhouse, a facility of DTU Elektro for testing demand side management strategies, as experimental site. In the latter case, we develop four applications where flexible demand is required to support power system operations. The applications are: integration of the operation of flexible demand and conventional generating units by means of unit commitment, mitigation of congestions in radial distribution networks, photo-voltaic self consumption and consumption peak shaving by means of a distributed optimization strategy.

Finally, motivated by the perspective of the interplay between flexible demand and storage in the operation of the future power system, we develop a model predictive control strategy for a smart building with the objective of supplying

space heating and providing regulating power to the grid according to a dynamic electricity price. We named this application *energy replacement* to indicate that the predictive control is able to switch among several energy sources to supply space heating according to the electricity cost.

In the process of developing this work, we propose novel validated mathematical models for a domestic refrigeration unit and a fuel cell. Models are realized applying a state-of-the-art grey-box methodology, using measurements from the following experimental devices: the freezer of Power Flexhouse and the 15 kW PEM fuel cell of the EPFL Distributed Electrical Systems Laboratory (EPFL-DESL).

Resumé (in danish)

Denne afhandling behandler indirekte kontrolleret fleksibelt elforbrug til effektregulering.

Først formuleres et forslag til en klassifikation af bygningers energifleksibilitet, og fleksibiliteten kvantificeres for en specifik klasse af forbrug.

Emnet indirekte kontrolleret fleksibelt forbrug er undersø gt dels i forhold til hvordan de enkelte enheder styres og dels i forhold til det aggregerede forbrug fra et stort antal enheder (demand side resources – DSR).

I første tilfælde er kontrolalgoritmer for prisstyret fleksibelt forbrug klassificeret i forhold til om de anvender prisforudsigelser eller ej. Forskellige kontrolalgoritmer er udviklet for begge klasser, og deres evner er sammenlignet i forhold til hhv brugerservice og energiændring.

I andet tilfælde er det aggregerede dynamiske respons fra mange enheder af en given klasse af indirekte kontrollerede DSR analyseret, og det fremgår, at der er dynamiske effekter, der ikke kan ses bort fra, hvis fleksibelt forbrug skal levere elsystemsydelser. En metode baseret på leveringsaftaler er udviklet med det formål at integrere fleksibelt forbrug i elsystemet, hvor de dynamiske egenskaber netop tages i regning.

Afhandlingen præsenterer to eksempler på brug af fleksibelt forbrug til andre formål end at levere effektregulering. Det første handler om tilskyndelse til lokalt forbrug af vedvarende energiproduktion, realiseret ved hjælp af model-prædiktion-kontrol (MPC). Det andet handler om brug af fleksibelt forbrug til at afhjælpe overbelastning i distributionsnettet ved hjælp af adaptiv lukket-sløjfe styring på netstation-niveau.

Et eksempel på optimerings-baseret styring af en samling frysere er udviklet med

det formål at tilskynde eget-forbrug af PV produktion og samtidig begrænse spidsbelastninger af nettet. En sådan anvendelse, løst gennem dobbelt dekompositionsalgoritme, er et eksempel på et optimeringsproblem hvor vilkår for både forbruger og elsystem tages i betragtning i optimeringsprocessen. Dette er en udvidelse og forbedring i forhold til traditionel økonomisk model-prædiktion-kontrol af DSR, hvor omkostningsfunktionen af det underliggende optimeringsproblem kun medtager forbrugervilkår.

Endelig er en substitutionsstrategi for en kraft-varme-enhed (CHP) præsenteret. Substitution er her defineret som forbrugerens mulighed for at vælge mellem to varmekilder til rumvarmen, hvilket viser sig at øge fleksibiliteten af forbruget. I dette tilfælde er anvendt en kombination af brændselscelle, elektrolysator, reaktanstanke og elektriske varmepaneler til levering af varme til en bygning.

Denne afhandling og tilhørende artikler indeholder desuden formuleringer af matematiske modeller for elektriske husholdningsvandvarmer, brændselscelle (med tilhørende hjælpekomponenter) og fryser. Modellerne er udviklet ved hjælp af grey-box metode med målinger på fysiske enheder. For vandvarmeren og fryseren er der målt påenheder i DTU PowerFlexHouse. For brændselscellen er der anvendt en 15 kW PEMFC i EPFL's Distributed Electrical System Laboratory (EPFL-DESL).

List of publications

Papers Included in the Thesis

Papers presented in international peer-reviewed conferences

[B] F. Sossan and H. Bindner. A comparison of algorithms for controlling DSRs in a control by price context using hardware-in-the-loop simulation. In *IEEE Power and Energy Society General Meeting*, pages 1–8, 2012.

[C] F. Sossan, A. M. Kosek, S. Martinenas, M. Marinelli, and H. W. Bindner. Scheduling of domestic water heater power demand for maximizing PV self-consumption using model predictive control. In *IEEE International Conference on Innovative Smart Grid Technologies (ISGT)*, 2013.

[D] F. Sossan and M. Marinelli. An auto tuning substation peak shaving controller for congestion management using flexible demand. In *IEEE International Universities Power Engineering Conference (UPEC)*, 2013.

[E] F. Sossan, X. Han, and H. Bindner. Dynamic behaviour of a population of controlled-by-price demand side resources. In *IEEE Power Engineering Society General Meeting*, 2014. Accepted for publication.

Journal Papers

[A] F. Sossan, V. Lakshmanan, G. Costanzo, M. Marinelli, P. Douglas, and H. Bindner. Grey-box modelling of a household refrigeration unit for energy consumption prediction and optimization using time series data. 2013. Currently unpublished.

[F] F. Sossan, H. Bindner, H. Madsen, L. Reyes, D. Torregrossa, and M. Paolone. A MPC replacement strategy for electric space heating including cogeneration of a fuel cell-electrolyzer system. *International Journal of Electrical Power & Energy Systems*, 2013.

Other Publications not Included

The following publications have been also prepared during the course of the Ph.D. study. They are omitted in this thesis because they are covered by other papers or are not directly related to the primary objective of the Ph.D. project.

- F. Sossan and H. Bindner. Evaluation of the performance of indirect control of many DSRs using hardware-in-the-loop simulations. In *IEEE Conference on Decision and Control (CDC)*, 2012.
- F. Sossan, M. Marinelli, G. Costanzo, and H. Bindner. Indirect control of DSRs for regulating power provision and solving local congestions. In *IEEE International Youth Conference on Energy (IYCE)*, 2013.

Papers as a contributing author

- M. Marinelli, F. Sossan, G. Costanzo, and H. Bindner. Testing of a predictive control strategy for balancing renewable sources in a microgrid. *IEEE Transactions on Sustainable Energy*, 2014.
- G. T. Costanzo, O. Gehrke, J. Parvizi, D. E. Morales Bondy, and H. Madsen. A coordination scheme for distributed model predictive control: Integration of flexible ders. In *IEEE International Conference on Innovative Smart Grid Technologies (ISGT)*, 2013.
- P. Douglass, R. Garcia-Valle, F. Sossan, J. Ostergaard, and P. Nyeng. Design and evaluation of autonomous hybrid frequency-voltage sensitive load controller. In *IEEE International Conference on Innovative Smart Grid Technologies (ISGT)*, 2013.
- V. Lakshmanan, M. Marinelli, A. M. Kosek, F. Sossan, and P. B. Nørgård. Domestic refrigerators temperature prediction strategy for the evaluation of the expected power consumption. In *IEEE International Conference on Innovative Smart Grid Technologies (ISGT)*, 2013.
- G. T. Costanzo, F. Sossan, M. Marinelli, P. Bacher, and H. Madsen. Grey-box modeling for system identification of household refrigerators: A step toward smart appliances. In *IEEE International Youth Conference on Energy (IYCE)*, 2013.

- M. Marinelli, F. Sossan, F. R. Isleifsson, G. T. Costanzo, and H. Bindner. Day-ahead scheduling of a photovoltaic plant by the energy management of a storage system. In *IEEE International Universities Power Engineering Conference (UPEC)*, 2013.

Project report

- F. Sossan, Indirect control algorithms for flexible demand, WP4 Flexpower project report, November 2013.

Acknowledgments

I would like to thank my supervisor Senior Scientist Henrik Bindner, my co-supervisors Senior Engineer Per Nørgård, Scientist Oliver Gehrke.

Thanks to Prof. Dr. Mario Paolone who hosted me for my external research stay at EPFL, Lausanne.

I would also like to thank the members of the examination committee Prof. Dr. Göran Andersson, Prof. Dr. Miguel F. Anjos and Prof. Dr. Pierre Pinson for their helpful reviews which served to improve the quality of this document and to convey the contributions of this thesis in a clearer form.

List of Abbreviations

AC	Alternating current
AGC	Automatic generation control
CHP	Combined heat and power
CLP	Cold load pickup
COP	Coefficient of performance
CTSM	Continuos time stochastic modelling
DC	Direct current
DD	Dual decomposition
DER	Distributed energy resource
DFIG	Double fed induction generator
DG	Distributed generation
DR	Demand response
DRE	Demand response event
DSO	Distribution system operator
DSR	Demand side resource
EV	Electric vehicle
EWH	Electric water heater
FC	Fuel cell

FIR	Finite impulse response
FSL	Frequency sensitive loads
FSM	Finite State Machine
HIL	Hardware in the loop
LS	Least squares
LV	Low voltage
MILP	Mixed integer linear programming
MIP	Mixed integer programming
MLE	Maximum likelihood estimation
MPC	Model predictive control
MV	Medium voltage
NWP	Numerical weather prediction
OCV	Open circuit voltage
ODE	Ordinary differential equation
PDF	Probability density function
PEM	Proton exchange membrane
PMSG	Permanent magnet synchronous generator
PV	Photo voltaic
SCUC	Secure Constrained Unit commitment
SDE	Stochastic differential equation
SOC	State of charge
SQ	State queue
TCL	Thermostatically controlled load
TSO	Transmission system operator
UC	Unit commitment

Contents

Chapter 1

Introduction

The increasing cost of traditional methods of electricity generation and the move towards a reduction in the impact of human activities on planet Earth are driving the need to integrate more renewable energy into the power grid. The Fukushima accident, as with the Chernobyl disaster in 1986, raised the question of the real sustainability of producing energy from nuclear fission. In response to these events, several countries worldwide are considering to shut down nuclear power plants in the long run in favor of other technologies, possibly increasing the proportion of renewable energy. As an example in Europe, the installed wind power capacity is expected to grow from the current 105 GW (2012) up to 140-180 GW by 2015 [124, 125]. The photovoltaic (PV) production capacity is also expected to increase, and at the end of 2012, in Europe, it was 69 GW [63].

The framework on which the power system is based is that electricity generation has to match consumption, and this is accomplished by keeping the system frequency at a constant value by regulating production. Increasing the proportion of energy generation from renewable sources decreases the amount of controllable generation in the power system. This same factor limits the penetration that renewables can achieve. There are two possible ways of restoring the lack of control capability:

1. storing the excess renewable production and using it when conditions are not sufficient to renewable power generation;
2. controlling the consumption.

Regarding case 1, the most well-known and established energy storage technology is hydroelectricity combined with pumped storage. However, availability of

hydropower is mainly limited to populated mountain regions, and installation in remote areas is not convenient due to high transmission cost. Five main energy storage technologies exist: electrochemical (battery), chemical (hydrogen-based, both direct used and as a source for synthesizing fuels), large scale thermal storage, mechanical (compressed air, flywheels) and electrical (super capacitors, magnetic energy storage). However nowadays, none of these technologies are able to offer a solution compatible with large-scale integration that merges economic feasibility, reliability, matureness and energy density [30, 93].

Regarding case 2, the consumption of electricity depends on consumers habits and, because the power system is designed to satisfy the consumers demand, consumption is not controlled. However, there exists a part of the demand for electricity that is characterized by an intrinsic flexibility, which allows the time at which power consumption occurs to be deferred. Flexible demand could be hence utilized to temporarily support the power system. Although this is not a new solution [43, 104], it has come to prominence in recent years because the advent of the smart grid opens up the possibility (in terms of required infrastructure) for realizing it on a large scale and in an automated way.

In order to contextualize the contribution of this thesis, an overview of both the power system and the issues related to an increase in the proportion of renewable energy generation is given in Section 1.1. In Section 1.2, the concept of smart grid is introduced and flexible energy demand is discussed. Section 1.3 provides an overview of the thesis, and states the thesis aim and main contributions.

1.1 The electric power system

The electric power system is a network of electrical components that generate and transmit electric power. Electric power is produced by thermal power plants, gas fired plants, hydropower stations and distributed renewable generation units (e.g. wind turbines and PV plants). In conventional generation plants, electricity production is achieved by mechanically coupling a prime mover with a synchronous generator, whose rotating frequency is regulated to 50 Hz (in Europe) by a droop controller. Electricity is generated and supplied in alternating current (AC) form. Electricity is transmitted at high voltage to reduce the energy loss in transmission lines. Conventional generation constitutes the backbone of production because it sustains the synchronism of the electric grid. Distributed renewable energy generation is usually connected to the electric grid by means of induction generators or power electronic interfaces. Induction generators are, for example, used in non-controlled rotational speed wind turbines [18]. Power electronic interfaces are used for PV, where an inverter is used for transforming the DC power supplied by the solar cells into AC, and for wind turbines equipped with permanent magnet synchronous generator (PMSGs) and double fed induction generators (DFIGs), where a back-to-back converter is used to control the rotational speed of the rotor and to transform electric power in

AC.

Power system ancillary services

Reliable operation of the electric power system is guaranteed by so-called ancillary services. The term *ancillary services* refers to a broad class of activities that deal with several technical aspects of power system. According the classification in [3, 40], ancillary services are:

- Scheduling and dispatch. Scheduling refers to the assignment of generation resources before the operation, while dispatch refers to the services for actuating the production plans and managing the power plants.
- Regulation and frequency response. This service is responsible for keeping the electric grid synchronized. This is achieved by adjusting the active power generation by regulating the frequency, and in conventional power plants is implemented by automatic control loops (droop regulators and AGCs). This automatic regulation is also referred to as primary and secondary frequency regulation, with the former faster than the latter [37].
- Reactive power supply and voltage control. In transmission lines, the voltage along the feeders depends primarily on the reactive power in the lines [2], which can be used for keeping the voltage inside acceptable margins. Voltage regulation along the feeders can be achieved with different kinds of devices, such as transformer taps and capacitors banks.
- Energy imbalance service refers to the financial settlement required for compensating for differences between the scheduled and actual delivery of energy during the period of operation.
- Operating reserves and spinning reserves. This service is for ensuring that enough spinning reserve is available for supplying the system frequency regulation service. Spinning reserve is composed of interruptible loads and generators already synchronized with the system frequency.
- Supplemental reserve service. Supplemental reserve refers to the amount of power that can be activated on short notice in order to restore the correct amount of spinning reserve in the system. It will be referred to as *regulating power*.

Effects of increased penetration of renewable generation

Increasing the penetration of variable generation imposes significant challenges to the electric grid due primarily to the need to reallocate the ancillary services.

The issues that are related to an increase in the penetration of variable renewable generation in the system are [34, 33]:

- Thermal stability. Variability of the production provokes variations in the power flow through transmission lines (for example in the case of a big wind farm) thus increasing mechanical stress and the risk of breaking components.
- Voltage stability. Feeders and distribution networks are designed for one-way power flow. Increasing the penetration of distributed generation (DG) causes voltage gradients in the network.
- Spinning reserve. In high penetration scenarios, an increased amount of spinning reserve is required in order to support during sudden generation deficits common with, for example, wind generation.
- Ramping duty. An increased penetration of renewables decreases the inertia of the system, as less rotating mass is present. Hence it should be possible for the units that are supplying frequency regulation to change their production set-points quickly (fast reserve). Virtual inertia response from wind turbines might be a partial solution to this problem [87, 45].
- Supplemental reserve. A minimum amount of controllable generation should always be available in the power system. This requires an increased amount of supplemental regulating power for use during unexpected variations in generation by renewable sources.
- Grid reinforcement: the capability of absorbing excess renewable production requires the power system to manage variable power flow with higher peaks. This requires the development of the current transmission and distribution infrastructures.

1.2 The smart grid concept

Traditionally, the power grid was a vertically integrated system characterized by single direction power flow, i.e. all electric power was produced from a few big power plants and transported to consumers through high voltage transmission and medium and low voltage distribution lines.

The increased penetration of *plug-and-forget* distributed renewable generation changed the traditional setup, and generation is nowadays also present both at medium and low voltage distribution levels. However, ancillary services are still provided by conventional power systems.

The smart grid concept is a broad topic that refers to a modernization process which the power system should undergo in the future. The first stage in the

evolution of the present power system towards a smart grid is to facilitate communication between the different components of the power system, both on the production side (power plants and DR) and the consumption side (e.g. flexible demand and electric vehicles), as shown in Fig. 1.1. This is necessary in order to enable the implementation of services that can drive the transition to a more sustainable power system, a more efficient use of energy and a greater reliability through monitoring and responding in real time [9].

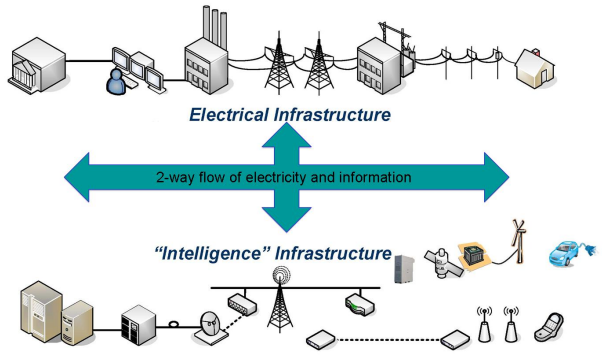

Figure 1.1: Electric and communication infrastructures of a smart grid [39].

Flexible demand

A smart grid could make it possible for ancillary services to be supported through flexible demand. Flexible demand is defined as that part of consumption which can be shifted in time without compromising the quality of the primary services it is supplying to the consumers. Electric loads which exhibit this capability are referred to as Demand Side Resources, DSRs. The change in power consumption that is achieved by consumers is referred to as Demand response (DR) [24]. In this thesis, flexible demand associated with electricity consumption in buildings is considered. According to [126], electricity consumption in buildings accounts for 40% of global demand.
The idea on which the concept of controlling flexible demand relies is that the contribution in terms of electric power from a single DSR is negligible while the aggregated and coordinated contribution from a large population of flexible DSRs might have significant size and, hence, a significant impact on the operation of the electric grid. A coordinated response from a group of DSRs is referred to as aggregate consumption.

Control strategies for flexible demand

An overview of the control strategies for flexible demand is given in [69], with control schemes classified in three main types (direct control, transactional con-

trol and indirect control) according to a bivariate criteria, as shown in Fig. 1.2.

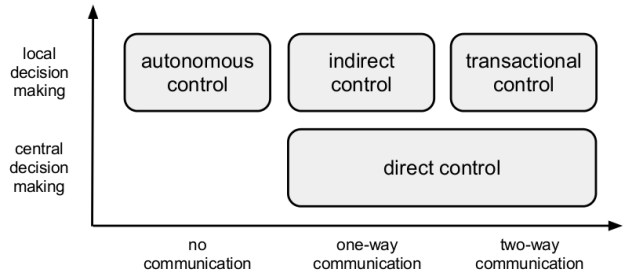

Figure 1.2: Classification of control algorithms for flexible demand [69].

Other works, such as [62, 54], propose a classification according to communication requirements only. In this case two main approaches are recognized: direct and indirect control. In the case of direct control, bidirectional communication with the DSR is required, and the electricity that the DSR should consume is determined by a central entity or by means of an energy handshaking process between an aggregator and the DSR itself (respectively direct and transactional control, as defined in [69]). Examples of direct control implementation are given in [14], where each DSR negotiates the electricity consumption with a central aggregator with demand weighted according to a price/energy curve, and in [27], where an admission control strategy for optimizing the schedule of a portfolio of domestic loads is developed, with admission dependent for example on the maximum value of power consumption.

Indirect control relies on one-way communication only. An individual control signal is used to induce a shift in the power consumption of a DSRs population. The dynamic electricity price is often proposed as a possible control signal because it gives the consumer a clear economic incentive for shifting the consumption. This assumes the existence of a (real-time) market for electric energy where DSRs can also bid. In this thesis no market considerations are given and the control signal responsible for indirect control is sometimes referred to as the *indirect control signal*.

Indirect control allows the simplification of the complex task of controlling a big population of DSRs, as a single control signal is adopted for all of them. Furthermore, this can be achieved by simple ICT infrastructure [92] as the only hardware necessary are those responsible for implementing the capability of sending and receiving a price signal. On the other hand, the response given by indirect control is not known *a priori* because the response of the units to the indirect control signal is on a spontaneous basis, according to local preferences, and cannot be communicated back to the aggregator. In the case of direct control, the aggregator knows what the consumption of flexible demand

is. Nevertheless, the direct control approach is more complex because it requires the definition of a multi-level aggregation infrastructure [68].

Overview on demand response programs

An overview of the global state of DR programs is provided in [61]. [119] summarizes the opportunity of DR experience in Europe, where the main demand side programs are nowadays focusing on monitoring user behaviour by installing smart meters. Current demand side programs are concerned with load shedding for large consumers (typically industrial loads). DR programs at consumer level (manually operated) are operated by, for example, the Italian and French distributed system operators (DSOs) [36, 129]. In the US, DR programs have been setup in several states [53, 130, 21], with the main objective of peak shaving the electric power consumption. For example, the Californian energy retailer SCE offers a wide range of DR programs, suitable for both small (on/off indirect control) and large consumers (using real time pricing).
D. J. Hammerstrom et al. describe in [52] the implementation and results of a demonstration test where, a wide class of DSRs are automatically controlled by price in order to supply peak shaving services to the grid.

1.3 Thesis overview

Thesis objective and contributions

As developed above, increasing the penetration of renewables will pose severe challenges to the power system. On the other hand, the advent of smart grid will enable monitoring of and interaction with the demand. The objective of the thesis is to investigate the potential of flexible demand in supporting the operation of the grid and mitigating the effects of an increased penetration of renewables. We focus on the indirect control approach, a simple framework that is extensively advocated in literature for enabling demand response since it relies on only a few ICT requirements.

We develop the topic of indirect control of flexible demand considering two aspects. The first addresses the concern of how to achieve a shift in the consumption of a single DSR provided an indirect control signal.The second concerns how to generate the indirect control signal for a population of DSRs according to the service that flexible demand is meant to provide to the grid. In the latter case, we conceive the following four applications:

- scheduling of the operation of flexible demand using unit commitment (UC). Motivated by the need of investigating the interaction between conventional generation, renewable generation and flexible demand, we outline a method based on the UC formulation that allows to determine the

indirect control signal for a population of DSRs together with the operation schedule of conventional generating units;

- mitigation of congestions in radial distribution networks by means of indirect control of flexible demand. Although not directly connected with renewable generation, this application has been considered because congestion management is a key priority for assuring a reliable delivery of electricity;
- PV self consumption. We propose a control strategy that shifts the consumption of an electric water heater (EWH) in order to self consume the electricity generated by a local PV plant, thus reducing transmission losses and improving voltage stability;
- transactional control of a cluster of freezers with the objective of peak shaving the consumption. We relax the hypothesis of one-way communication, and we show how the problem of limiting the aggregated power consumption of a cluster of DSRs can be formulated as a distributed optimization problem.

Finally, in the perspective of the interplay between flexible demand, storage and conventional generation in the operation of the future grid, we develop a control strategy for a smart building with the objective of supplying space heating by means of combining the operation of flexible demand, storage and combined heat and power generation, while providing regulating power to the grid according to a dynamic electricity cost.

In the process of developing this work, the following mathematical models have been developed using a state of the art grey-box modelling methodology (Appendix A):

- a domestic refrigeration unit, using measurements from a freezer available in Power Flexhouse, the experimental facility of DTU Elektro for testing demand side strategies;
- a proton exchange membrane fuel cell (PEMFC), using measurements from the 15 kW PEMFC of the DESL facility at EPFL, Lausanne.

Thesis outline

The thesis is organized in 6 self-contained chapters, 4 appendices and 6 attached papers. Some of the chapters rely on the contributions of the attached papers. When it is important for the sake of comprehension and in order to facilitate the reader, the main contributions of the papers are summarized in the chapters.

In Chapter 2, the concept of flexibility is defined, and a classification of DSRs is presented. Moreover, the amount of flexibility associated to the operation of a number of domestic DSRs is quantified by means of Monte Carlo simulations.

In Chapter 3, indirect control algorithms for DSRs are discussed . A *control algorithm* is the algorithm that, provided an indirect control signal, achieves a shift in the consumption of the associated DSR. Several control algorithms are developed, from simple ones with a few requirements up to state-of-the-art MPC strategies. The performance of the proposed algorithms are tested in a hardware-in-the-loop (HIL) simulations framework using Power Flexhouse as the experimental site.

In Chapter 4, the focus is moved on studying the aggregated power consumption of flexible demand. It is shown by simulations that controlling a population of thermostatically controlled loads (TCLs) by means of a consumption incentive signal introduces dynamics in the aggregated power consumption that have to be taken into account if flexible demand is to provide power system services.

In Chapter 5, the applications of flexible demand that have been developed in the thesis are discussed.

In Chapter 6, a model predictive control strategy for scheduling the operation of storage, flexible demand and combined heat and power generation is developed. The objective of the predictive control is to provide space heating to a smart building and regulating power to the grid according to a dynamic electricity price. We named this application *energy replacement* to indicate the capability of the control to switch among several sources for supplying space heating according to the cost of the electricity.

Finally, in Chapter 7, conclusions are stated together with a summary of the results, thesis contributions and future work.

Chapter 2

Identification of electric flexible demand

This chapter explores the concepts of flexible demand and demand side resources. Two primary reasons to explain flexible consumption are discussed, and a classification of demand side resources is presented. Finally, we determine the storage capacity associated with the operation of a number of thermostatically controlled loads by means of Monte Carlo simulations.

2.1 Introduction

Flexible demand is that part of the electric power consumption which can be shifted in time without compromising the quality of the primary services it is supplying to the consumers. Electric loads that exhibit this ability are referred to as Demand Side Resources, DSRs. In the existing literature, the utilization of flexible demand is advocated for allowing to increase the proportion of electricity generated from variable renewable sources [74, 100] by means of supporting the operation of the power system [52, 127]. Before proceeding to develop control algorithms for DSRs, it is necessary to explore the concept of flexibility, identify those electric loads capable of flexible operation and quantify their amount of flexibility.

In [99], Petersen et al. identify a classification for DSRs according to three categories depending on the power requirements of the electric loads. Such a classification is similar to the one proposed in this chapter, and it will be discussed more into details in the next section. A qualitative assessment of the level of demand responsiveness among domestic appliances is performed in [51], while a method for quantifying the amount of flexibility of a population of space heating units using observations of the baseline consumption of a city is proposed in [131]. In [83], Mathieu et al. identify the economic revenue that

several types of thermostatically controlled loads (TCLs) can achieve by bidding their flexibility in electricity markets: their level of flexibility is determined by means of bottom-up simulations, and it is described in terms of power and energy capacities, which are defined as the power consumption of the population of TCLs and the energy that the TCLs can store in the thermostatic range, respectively.

In this chapter, we define the concept of flexibility, and we propose a classification of DSRs. Finally, the amount of flexibility associated with the operation of a number of TCLs is evaluated by means of Monte Carlo simulations. The characterization of the storage capacity of TCLs is carried out separately for the cases of providing up-regulating or down-regulating power to the grid, because this leads to different results.

2.2 Classification of flexible demand

We identify two prime reasons to explain the flexibility that exists at demand side level:

1. the availability of the consumer to reduce the power consumption in response to a varying electricity price. For instance in [118, 38], this type of flexibility is described by a price elasticity factor, which is defined as the percentage change in demand resulting from a percentage change of the electricity price. This kind of flexibility will be referred to as **Type I**.
2. the implicit flexibility associated with the operation of some electric loads that allows to change the consumption pattern without affecting the services that are provided to the consumers. For instance, the phase of the thermostat operation of a TCL can be shifted without violating the temperature thermostatic thresholds. This kind of flexibility will be referred to as **Type II**.

Type I flexibility depends on consumer demand habits, and quantifying its amount is complex because it requires to evaluate how consumer behaviour will be affected by changing from the current consumption paradigm to a price driven one. Type II is a technical kind of flexibility because is only related to the operation of the DSR. Hence, in the latter case, the amount of flexibility can be estimated without involving any assumption on the electricity demand habits of the consumers. The topic of quantifying the amount of Type II flexibility will be discussed in Section 2.4.

Load shifting and load shedding In the existing literature, two operating modalities of flexible demand are usually discerned (e.g. [69, 42]): load shifting and load shedding. The former indicates that the power consumption of an

electric load is moved from one period to another, while the latter indicates a reduction in the consumption.

Load shifting can be achieved by means of using either Type I flexibility, Type II flexibility or a combination of the two. For example, the first case is when a consumer decides to defer or anticipate the operation of a dishwasher. An example of the second case has been given in 2. The third case is when, for example, the temperature set-point of a TCL is changed and eventually returned to the original reference: the transient deviation of the thermostatic set-point might temporarily compromise the temperature comfort of the consumer (Type I flexibility), and the associated thermal mass prevents large variations of the temperature (Type II flexibility).

Load shedding operation is only due to Type I flexibility: in fact, decreasing the consumption of an electric load implies that the consumer renounces, steadily, to a part of the service that the electric load is providing.

In this thesis, we will focus on load shifting only. We will not consider load shedding because we think that assuming that a portion of the demand is curtailable at the power system convenience without investigating the consumer behavior (which is not in the scope of this thesis) is not a realistic assumption.

2.3 Classification of DSRs

Three types of flexible electric loads are identified in the domestic and commercial sectors: continuous operation TCLs, bulk loads and electric loads with batteries, and they will be discussed in the next three sections. Petersen et al. propose a similar taxonomy in [99], and they classify DSRs into the following three categories:

- *bucket* with a leakage, a metaphor to indicate a DSR with a shiftable comfort level and that has an energy requirement in order to maintain it;
- *battery*, a DSR with a comfort level that depends on the energy that is consumed and withdrawn;
- *bakery*, a process with a fixed consumption pattern and a flexible operating starting point.

As regards the industry sector, two types of flexible processes are identified [35]: tasks which have deferrable serving time, and continuous processes with variable production throughput.

In the following of this thesis, only household and commercial DSRs are considered.

Continuous operation TCLs

Thermostatic control is used in applications which require, the temperature to be regulated. The operation principle of a thermostat is based on a temperature hysteresis cycle, and, considering for example heating applications, it is described by the following relationship:

$$P_{e,i} = \begin{cases} P_{e,\text{nominal}}, & \text{if } T_i < T_{\text{set-point}} - h \\ 0, & \text{if } T_i > T_{\text{set-point}} + h \\ P_{e,i-1}, & \text{otherwise} \end{cases}, \tag{2.1}$$

where $P_{e,i}$ is the electric power consumption of the TCL at time i, $P_{e,\text{nominal}}$ is the nominal power consumption of the TCL, T_i is the temperature to regulate, h is the amplitude of the hysteresis cycle and $T_{\text{set-point}}$ is the temperature set-point.

The flexibility of a TCL is due to the associated thermal mass, which allows to change the power consumption without this provoking a steep change of the temperature. Continuous operation TCLs are, for example, devices for electric space heating (radiators, heat pumps), electric water heaters (EWHs), electric air conditioning units and cold appliances. A simple mathematical model that describes the comfort level of a TCL is derived in Example 2.1.

Example 2.1 *Given a generic TCL, let ΔT [°C] be the temperature offset that should be maintained with respect to environment (i.e. the difference between the thermostatic set point and the temperature of the environment). Assuming that the TCL temperature evolves according to a dominant time constant, the dynamic quantity $\Delta T(t)$ can be approximated by the first order linear model*

$$\dot{\Delta T}(t) = -a\Delta T(t) + bP_e(t), \tag{2.2}$$

where $P_e(t) > 0$ [W] is the controllable electric power, $a > 0$ is a parameter that depends on thermal inertia and heat losses, and b is a scale factor, and it is negative for cooling applications and positive for heating ones. Let $\Delta T_{\max}$ and $\Delta T_{\min}$ be the thermostatic upper and lower thresholds with respect to the temperature environment. It is assumed that $|\Delta T_{\max}| > |\Delta T_{\min}| > 0$ and $\operatorname{sgn}(\Delta T_{\max}) = \operatorname{sgn}(\Delta T_{\min})$. We describe the comfort level of the TCL by means of the SOC index (state of charge), which in this case is defined as:

$$SoC(t) = \frac{\Delta T(t) - \Delta T_{\min}}{\Delta T_{\max} - \Delta T_{\min}}. \tag{2.3}$$

The SOC is maintained in the interval $[0, 1]$ by the thermostat control action. The model in Eq. (2.3) shows that, although a certain amount of flexibility is available, electricity is required in order to maintain a minimum SOC.

Bulk loads

Bulk loads are those electric loads which are manually activated by the users, e.g. appliances. In [27], Costanzo et al. proposes a modelling approach based on the finite state machine (FSM) representation. In FSM representation, each phase of the operation of the device is described by a state with an associated consumption pattern. The transitions between states are described by a transition matrix, and the length of the stays in each state is defined in terms of the duration of the operation. The structure of a FSM describing the operation of a generic white appliance is shown in Fig. 2.1.

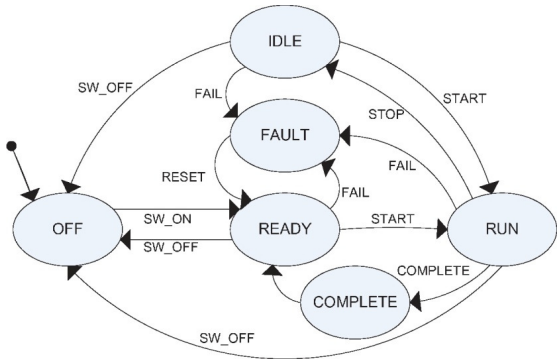

Figure 2.1: FSM representation of a domestic appliance [27]. The nodes and the edges of the graph represent the states and the transition events of the appliance, respectively.

Battery-based electric loads

Grid-connected devices equipped with electrochemical storage, and that must satisfy an energy requirement rather than a power requirement, are flexible since they can achieve the energy target by means of different power absorption trajectories. Electric vehicles (EVs) are the most significant representative of such a category of DSRs. If EVs charging stations are equipped with bidirectional converters, the power flow can be reversed and the energy in the batteries can be used to support power system operation [22]. The results from an analysis performed in [82] show that the average charging time of the EVs is 4 hours, and the average plug-in time is 12 hours: this suggests that two third of the plug-in time could be used for EVs flexible operation. However, in the case of deployment of EVs, the time frame available for flexible operation could be drastically reduced by smart charging strategies, which may require to fractionate the charging process in order to relieve congestions in the distribution grid [97]. A simple model of a battery based electric load is developed in Example 2.2

Example 2.2 *The evolution in time of the state of charge* $SoC(t) \in [0,1]$ *of a battery with capacity* C_b *[J] is*

$$\dot{SoC}(t) = \frac{1}{C_b} P_e(t) \tag{2.4}$$

where $P_e(t)$ *[W] is the electric power, positive if used for charging the battery and vice versa. By comparing Eq. (2.2), Eq. (2.3) with Eq. (2.4), it can be seen that the model of the TCL can be seen as a generalization of the battery model.*

2.4 Quantification of the amount of flexibility

In this section, the amount of flexibility associated with four domestic TCLs is quantified by means of a statistical analysis performed with Monte Carlo simulations. The TCLs are as follows: electric space heating, an EWH and two refrigeration units, namely a freezer and a fridge. The flexibility of the TCLs is evaluated using mathematical models, which are introduced in Section 2.4.1. The flexibility that is considered is of Type II and is evaluated according to the method described in Section 2.4.2.

2.4.1 Models of the thermostatically controlled loads

The TCLs considered in this section are those available in Power Flexhouse, the experimental facility of DTU Elektro for testing demand side control strategies. A description of Power Flexhouse is provided in Appendix D. The flexibility of the TCLs is evaluated using their respective mathematical thermal models. The thermal models, with the exception of the EWH, are obtained by means of applying the grey-box modelling methodology and are formulated using stochastic differential equations (SDEs). Grey-box modelling allows to identify a model incorporating its physical knowledge with information obtained from measurements: a short treatise regarding the grey-box methodology is given in Appendix A, while a practical application of the grey-box method is described in Paper **[A]**. The main characteristics of the experimental Power Flexhouse TCLs are summarized in Table 2.1.

Table 2.1: Characteristics of the TCLs of Power Flexhouse. The nominal power consumption values of the fridge and freezer are from measurements.

TCL	Size	Nominal power [kW][1]
Space heating	120 m^2	10
Water heater	30 L	1.2
Freezer	70 L	0.06
Fridge	40 L	0.08

Power Flexhouse space heating

Power Flexhouse is a 8 rooms, 125 m^2 free standing building situated at DTU Risø Campus. Space heating is supplied by 10 1 kW electric radiators. In [96], Bacher et al. present a collection of linear dynamic thermal models for Power Flexhouse. Each model describes the evolution of Power Flexhouse indoor air temperature $T(t)$ as a function of time, building characteristics and three exogenous inputs: power consumption $P_e(t)$ [W] of the radiators, solar insolation $\phi_s(t)$ [$\mathrm{W\,m^{-2}}$] and outside air temperature $T_{\mathrm{out}}(t)$ [°C]. The applied heat dynamics models all use the approximation that the interior of the building is one room. In this analysis, we use the first order model, whose deterministic skeleton is given as

$$\dot{T}(t) = -\frac{1}{R_e C_l} T(t) + P_e(t) + \frac{A}{C_l}\phi_s(t) + \frac{1}{R_e C_l} T_{\mathrm{out}}(t), \tag{2.5}$$

where C_l, R_e, A are the lumped thermal capacity of the building, the thermal resistance of the envelope of the building and the global surface of the windows, respectively. The values and the units of the parameters of Eq. (2.5) are given in Table 2.2.

In order to provide a better description of the indoor temperature dynamics, it is usually recommended to use a second order thermal model since it allows to account for the different thermal capacities of the building envelope and air content [76]. In this case, the choice of the first order model is motivated by the fact that the amount of flexibility is evaluated using the steady state thermostatic consumption pattern, which is not influenced by higher order dynamics.

Table 2.2: Parameters of the thermal model of Power Flexhouse space heating.

Name	Unit	Value
C_l	$\mathrm{J\,°C^{-1}}$	1.23×10^7
R_e	$\mathrm{°C\,W^{-1}}$	4.87×10^{-3}
A	$\mathrm{m^2}$	10.7

Power Flexhouse electric water heater

In Paper **[C]**, we develop a first order dynamic model that describes the evolution of the temperature of the water of a domestic thermostatically controlled EWH. The model only accounts for the global thermal energy content of the water, and does not describe the thermal stratification of the water inside the tank (cfr. [121, 66]). The model is described by the following first order differential

equation:

$$\dot{T}(t) = \left(-\frac{1}{R_e C_w} - \frac{q(t)}{C_w/C_p} \right) T(t) + \\ + \frac{1}{C_w} P_e(t) + \frac{1}{R_e C_w} T_{\text{room}} + \frac{q(t)}{C_w/C_p} T_{\text{inlet}}(t), \tag{2.6}$$

where $T(t)$ is the water temperature, $q(t)$ [$\mathrm{L\,s^{-1}}$] is the water consumption, P_e is the power consumption of the heating element, T_{room} is the temperature of the room where the EWH is located, T_{inlet} is the temperature of the inlet water and C_w and R_e are the parameters of the model. The parameter C_w denotes the thermal capacity associated with the EWH and is approximated by the thermal capacity of the water contained in the tank. The thermal capacity of the tank structure is neglected because the mass and the specific heat of the insolation layer and tank complex ($\approx 5\,\mathrm{kg}$ and $1400\,\mathrm{J\,kg^{-1}\,K^{-1}}$, respectively, assuming polyurethane foam as insolation material [4]) are significantly smaller than those of the water ($30\,\mathrm{kg}$ and $4190\,\mathrm{J\,kg^{-1}\,K^{-1}}$, respectively). The thermal resistance R_e was found minimizing the sum of the squared output errors of the model with the least squares method (LS, see Appendix B) and using measurements performed with the Power Flexhouse EWH. The value of R_e and C_w are given in Table 2.3. A similar model was described in [88].

Table 2.3: Parameters of the thermal model of Power Flexhouse EWH.

Name	Unit	Value
C_w	$\mathrm{J\,°C^{-1}}$	1.257×10^5
R_e	$\mathrm{°C\,W^{-1}}$	1.2

Power Flexhouse Freezer

In Paper **[A]**, we present a number of dynamic models to describe the temperature evolution $T(t)$ of the Power Flexhouse freezer as a function of the room ambient temperature $T_{\text{room}}(t)$ and the power consumption $P_e(t)$ of the compressor of the freezer. The first order model is given as

$$\dot{T}(t) = -\frac{1}{R_e\, C_l} T(t) + \frac{1}{R_e\, C_l} T_{\text{room}}(t) + \frac{\text{COP}}{C_l} P_e(t), \tag{2.7}$$

where the parameters C_l, R_e, COP are the lumped thermal capacity of the freezer, the thermal resistance of the freezer envelope and the coefficient of performance of the refrigeration cycle, respectively. Their values and units are given in Table 2.4.

Table 2.4: Parameters of the thermal model of Power Flexhouse freezer.

Name	Unit	Value
C_l	$\mathrm{J\,°C^{-1}}$	3.0×10^4
R_e	$\mathrm{°C\,W^{-1}}$	0.6
COP	-	3.01×10^{-1}

Power Flexhouse fridge

In [26], Costanzo et al. present a collection of linear models for describing the temperature evolution $T(t)$ of the Power Flexhouse fridge as a function the room ambient temperature $T_{\mathrm{room}}(t)$ and the power consumption $P_e(t)$ of the compressor of the fridge.

$$\dot{T}(t) = -\frac{1}{R_e C_l} T(t) + \frac{1}{R_e C_l} T_{\mathrm{room}}(t) + \frac{\mathrm{COP}}{C_l} P_e(t), \tag{2.8}$$

where the parameters have the same meaning as those of the previous model and their values are given in Table 2.5.

Table 2.5: Parameters of the thermal model of Power Flexhouse fridge.

Name	Unit	Value
C_l	$\mathrm{J\,°C^{-1}}$	0.95×10^4
R_e	$\mathrm{°C\,W^{-1}}$	1.47
COP	-	0.3

2.4.2 Determination of Type II flexibility

Given a generic TCL, the determination of Type II flexibility consists in analysing the amount of energy that can be shifted with respect to a baseline consumption without violating the thermostatic temperature limits. The baseline consumption is defined as the consumption profile of the TCL during normal operation, i.e. , without any demand response event (DRE). A DRE can be of two types: a decrease or an increase of the consumption of flexible demand, according to if the grid requires up-regulating or down-regulating power, respectively. In the following analysis, these two cases will be analysed separately.

The nomenclature used in this section is graphically introduced in Fig. 2.2, which sketches the temperature evolution during one *on-off* cycle of a generic TCL for heating applications. The blue line shows the evolution of the temperature, which is constrained by the thermostatic control action in the interval denoted

by T_{up} and T_{low}, which are the upper and lower thresholds of the thermostat, respectively. The thermostatic cycle in Fig. 2.2 is composed by a warming phase $dT/dt > 0$ with duration $d \cdot \tau$, and a cooling phase $dT/dt < 0$ with duration $(1-d)\tau$. The coefficients d and τ are the duty cycle and the period, respectively, of the sketched thermostatic cycle. The TCL power consumption, not indicated in Fig. 2.2, equals P during the warming phase, and 0 otherwise.

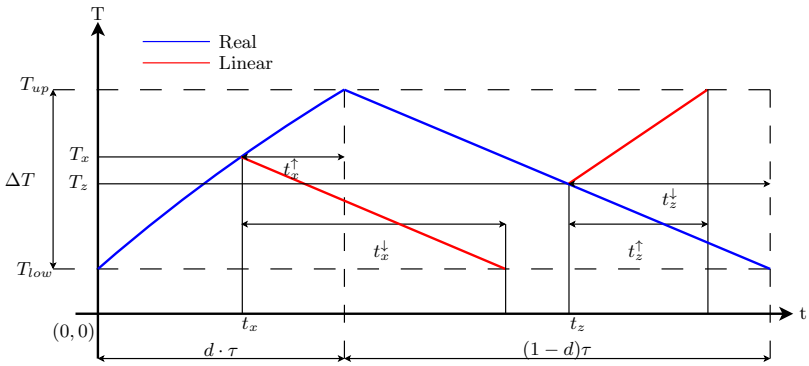

Figure 2.2: The temperature of a generic TCL during an *on-off* cycle of the thermostat. The blue line represents the temperature evolution, and the two red lines are linear approximations of the temperature profile during the cooling and warming phases.

Support to up-regulation In the case when the power system needs up-regulating power, the production should increase, or alternatively, the consumption should be lowered. By picking a uniformly distributed random time instant t_x on the interval $[0, T)$, the probability of the TCL being in *on* state is given by d. Hence, the expected amount of power $E[P_{up}]$ that can be curtailed by switching off the TCL is given as

$$E[P_{up}] = P \cdot d. \tag{2.9}$$

Provided the TCL thermostat being on, i.e. $t_x \in [0, d \cdot T)$, the amount of electricity consumption E that can be deferred by turning the consumption off at t_x, without violating the temperature lower value, is given by the nominal power consumption P times the quantity $t_x^{\downarrow}$, which, in Fig. 2.2, is defined as the duration of the left-hand red line, and it is the time that temperature takes to go from T_x to T_{low} when the TCL is turned off. However, in absence of the DRE, the TCL was going to switch off naturally at time $d \cdot T$, whose distance from t_x is denoted by $t_x^{\uparrow}$. Hence, the deviation in the consumption from a hypothetical baseline demand profile without the DRE is given as

$$E_{up} \mid t_x \in [0, d \cdot T) = P \cdot \min(t_x^{\downarrow}, t_x^{\uparrow}), \tag{2.10}$$

where the function $\min(\cdot)$ denotes the minimum value among the two arguments. The durations $t_x^{\downarrow}, t_x^{\uparrow}$ can be found analytically by approximating the first order temperature profile in Fig. 2.2 with a linear function of the time. The rates of the linearly approximated heating and cooling process are given by:

$$m^{\uparrow} = \frac{\Delta T}{d \cdot T} \tag{2.11}$$

$$m^{\downarrow} = -\frac{\Delta T}{(1-d)T}. \tag{2.12}$$

Let T_x be the temperature value at the instant of time t_x, then the terms $t_x^{\downarrow}$ and $t_x^{\uparrow}$ are given by the following expressions:

$$t_x^{\downarrow} = \frac{T_x - T_{down}}{\Delta T} d \cdot T \tag{2.13}$$

$$t_x^{\uparrow} = \frac{T_{up} - T_x}{\Delta T} (1-d)T. \tag{2.14}$$

Support to down-regulation It is now considered the case that the electric grid requires down-regulating power, i.e. the production should decrease, or alternatively the consumption should increase. By picking a uniformly distributed random time instant t_z on the interval $[0, T)$, the expected amount of power that can be consumed by switching on the TCL is

$$E[P_{down}] = P(1-d). \tag{2.15}$$

Provided the thermostat in *off* state, i.e. $t_z \in [d \cdot T, T)$, the amount of electricity E that can be consumed by turning the consumption on at t_z, without violating the thermostat upper threshold, is given by the nominal power consumption P times the duration $t_z^{\uparrow}$, which is the time that the temperature takes to reach the upper threshold of the thermostat when the TCL is on. Similarly to the previous case, it is of interest evaluating the difference in the consumption from the baseline demand, which is given as

$$E_{down} \mid t_z \in [d \cdot T, T) = P \cdot \min(t_z^{\uparrow}, t_z^{\downarrow}), \tag{2.16}$$

where the quantities $t_z^{\uparrow}$ and $t_z^{\downarrow}$ can be evaluated with the same expression previously introduced for $t_x^{\uparrow}$ and $t_x^{\downarrow}$ (Eq. (2.14) and Eq. (2.13), respectively). It is worth noting by comparing Eq. (2.10) and Eq. (2.16), that $\left|E_{up} \mid t_x\right| = |E_{down} \mid t_z|$. This means that the amount of energy that the TCL can release for supporting power system up-regulation or down-regulation power is the same (provided the respective event to happen). This was to expect since the amount energy that the TCLs can temporarily provide is the one stored in the thermostatic temperature range. However, the probability of the events *thermostat being on* and *thermostat being off* can be different, so as the marginal expectations of the amounts of energy that the TCL can provide.

Populations of the TCLs For each type of TCL, a population of TCLs is generated by means of replicating the nominal models and changing their parameters according to statistical distributions. The nominal models are those presented in Section 2.4. The population of space heating units is generated with the method described in Paper **[E]**. In the case of the other three types of TCLs, the populations are obtained by changing the respective thermal capacities. The thermal capacity is assumed to vary linearly with the volume, which is randomly generated from Gaussian distributions. The exogenous inputs of the model are assumed constant both in time and across the TCLs populations. User behaviour is not taken into account in this analysis. Table 2.6, Table 2.7, Table 2.8 and Table 2.9 report the characteristics of the populations of buildings, EWHs, fridges and freezers, respectively.

Simulation method The amounts of up-regulating power and down-regulating power that is possible to extract from each TCL of the populations is calculated using the simulation algorithm described in Listing 1, which uses the concepts and equations developed above.

Algorithm 1 Monte Carlo simulation algorithm for determining the flexibility of the TCLs.

Generate random populations of TCLs
Determine temperature and consumption profiles of TCLs under normal operation
Generate random vector $\boldsymbol{t_x}$ of uniform distributed random variables
for each value at index i **in** $\boldsymbol{t_x}$ **do**
    for each TCL j of the populations **do**
        $t^{\downarrow}$ = calculate Eq. (2.13)
        $t^{\uparrow}$ = calculate Eq. (2.14)
        $t = \min(t^{\downarrow}, t^{\uparrow})$
        if TCL j is *on* state **then**
            $E_{up}[i,j] = t \cdot P$ ▷ TCL energy contribution to up-regulation
            $E_{down}[i,j] = 0$
            $P_{up}[i,j] = P$ ▷ TCL power contribution to up-regulation
            $P_{down}[i,j] = 0$
        else
            $E_{up}[i,j] = 0$
            $E_{down}[i,j] = t \cdot P$ ▷ TCL energy contribution to down-regulation
            $P_{up}[i,j] = 0$
            $P_{down}[i,j] = P$ ▷ TCL energy contribution to down-regulation
        end if
    end for
end for
▷ Determine the expected energy and power contributions
$\mathbf{E_{up}}$ = average E_{up} along the first dimension
$\mathbf{E_{down}}$ = average E_{down} along the first dimension
$\mathbf{P_{up}}$ = average P_{up} along the first dimension
$\mathbf{P_{down}}$ = average P_{down} along the first dimension

Table 2.6: Characteristics of the population of space heating units.

Parameters	Unit	Value
Thermostat set-point	°C	$\sim \mathcal{N}(21, .5^2)$
Thermostat hysteresis	°C	$\sim \mathcal{N}(\pm 1.5, .1^2)$
Ambient temperature	°C	10
Solar irradiance	$\mathrm{W\,m^{-2}}$	0
Thermal capacity	$\mathrm{J\,°C^{-1}}$	from Paper **[E]**

Table 2.7: Characteristics of the population of EWHs.

Parameters	Unit	Value
Thermostat set-point	°C	$\sim \mathcal{N}(70, .4^2)$
Thermostat hysteresis	°C	$\sim \mathcal{N}(\pm 2.0, .2^2)$
Ambient temperature	°C	20
Cold water temperature	°C	8
Thermal capacity	$\mathrm{J\,°C^{-1}}$	$\sim \frac{C_w}{30} \cdot \mathcal{N}(50, 5^2)$
Water consumption profile	$\mathrm{L\,s^{-1}}$	from [64] (scaled for 4 people)

Table 2.8: Characteristics of the population of fridges.

Parameters	Unit	Value
Thermostat set-point	°C	$\sim \mathcal{N}(4, .2^2)$
Thermostat hysteresis	°C	$\sim \mathcal{N}(\pm 1.5, .1^2)$
Ambient temperature	°C	20
Thermal capacity	$\mathrm{J\,°C^{-1}}$	$\sim \frac{C_l}{30} \cdot \mathcal{N}(60, 10^2)$

Table 2.9: Characteristics of the population of freezers.

Parameters	Unit	Value
Thermostat set-point	°C	$\sim \mathcal{N}(-17, .5^2)$
Thermostat hysteresis	°C	$\sim \mathcal{N}(\pm 1.5, .1^2)$
Ambient temperature	°C	20
Thermal capacity	$\mathrm{J\,°C^{-1}}$	$\sim \frac{C_l}{70} \cdot \mathcal{N}(70, 10^2)$

2.4.3 Simulation results

Fig. 2.3 and Fig. 2.4 show the expected power and energy contributions that the TCLs can deliver for up-regulation and down-regulation, respectively. In the plots, the amount of support provided by flexible demand is compared with the one provided by three different batteries: the SYSLAB 15 kW/120 kWh vanadium battery, a 40 kW/22 kWh lithium battery pack of a Peugeot Ion and a 12 V/60 Ah lead-acid battery for a car. In order to be congruent with the expected values representation used for TCLs, the batteries are considered half charged.

2.4.4 Discussion

Results in Fig. 2.3 and Fig. 2.4 show that the TCLs that can provide the largest expected amount of energy and power are electric space heating units. This was to expect since the larger thermal capacities of buildings with respect to the other types of TCLs. The order of magnitude of the storage capacities of space heating units is comparable with the one of an EV battery. It is worth to note that the duty cycles and the periods of the thermostatic consumption patterns of electric space heating units are strongly affected by environmental conditions (e.g. outside temperature and insolation), hence the inherent flexibility is expected to undergo relevant changes during the time of the day and the period of the year.

Regarding EWHs, it is interesting to observe that the expected amount of support they can provide is very different in the two analysed cases. This is due to the fact that their thermostatic cycles are very asymmetric ($d << 0.5$), and the probability of finding a unit in *on* state is low. This is reflected into a reduced capacity of providing up-regulating power. In the case of providing down-regulating power, EWHs are more effective.

Finally, the results show that the flexibility inherent the thermostatic operations of freezers and fridges is very limited: their storage capacities are one order of magnitude less than a lead-acid battery for a car.

Two differences between batteries and TCLs are to mention. The first difference is that if batteries are grid-connected (such as EVs during the charging phase), their power converter may allow to charge and discharge the batteries at any rate. This does not happen with TCLs since they only have two states of consumption. The second difference is that TCLs are subject to an energy requirement, i.e. once they have used their flexibility they must consume electricity in order to keep the comfort of the consumer. On the contrary, the charging process of batteries may be postponed.

Moreover, it must be mentioned that modifying the steady state consumption of a population of TCLs leads to synchronizing their states: this introduces

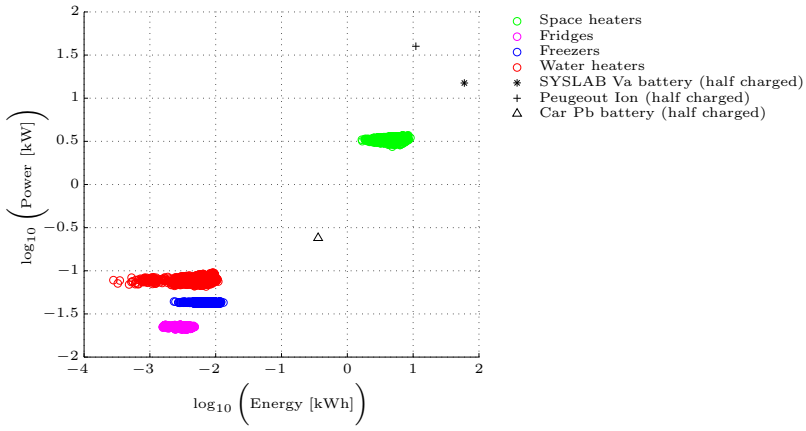

Figure 2.3: The flexibility inherent in the consumption of several TCLs in the case of supplying up-regulating power to the grid. As a comparison, the energy and power contributions of several batteries are indicated.

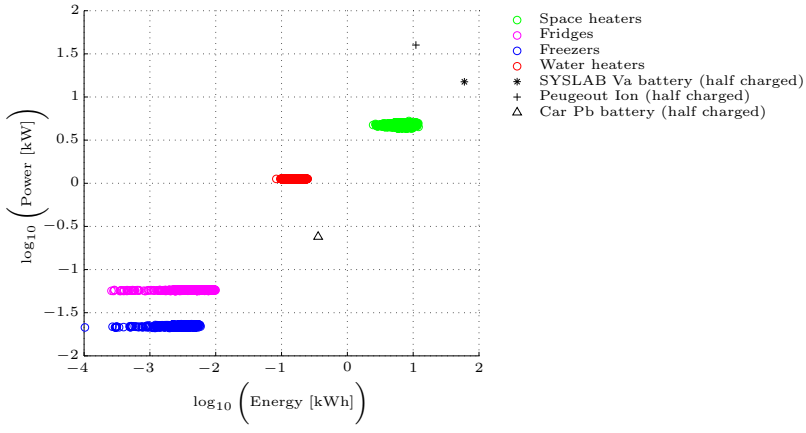

Figure 2.4: The flexibility inherent in the consumption of several TCLs in the case of supplying down-regulating power to the grid. As a comparison, the energy and power contributions of several batteries are indicated.

relevant dynamics into the aggregated power consumption, as it will be shown in Chapter 4.

2.5 Conclusions

In this chapter, we investigated the concept of flexibility and presented a classification of DSRs. Moreover, the storage capacity associated with the operation of four types of TCLs was evaluated by means of Monte Carlo simulations. Among the types of TCLs that were analysed, electric space heating was the one with the largest intrinsic flexibility, followed by EWH, freezers and fridges: this explains why, in the following of this thesis, flexible demand will mainly consist of electric space heating units. The flexibility of fridges and freezers was very limited, and it was estimated around one order of magnitude less than a lead-acid battery for a car: hence their use should be considered for applications which require a limited contribution of energy, such as transient support to primary frequency regulation.

Chapter 3

Control algorithms for indirect control of flexible demand

In this chapter, control algorithms for indirect control of flexible demand are developed. The term "control algorithm" refers to the algorithm that achieves changes of the power consumption of a DSR according to a broadcasted consumption incentive signal. Algorithms are divided into two classes, according to if they use forecast in their decision-making process or not. Finally, the performance and requirements of the algorithms are compared.

3.1 Introduction

A way that is extensively advocated in existing literature for enabling demand response is to use dynamic electricity prices. The electricity price is sent at regular time intervals to the DSRs subscribed to DR programs and is meant to act as an economic incentive for the consumers to shift their consumption, according to the intuitive mechanism that the demand should increase when the price is low and vice versa. This approach is sometimes referred to as *control by price* and, in a broader context, is indicated as *indirect control* for pointing out its opposition to *direct control*, which requires two-way communication instead.

In the thesis, *price signal* is a shortened term used to indicate the *dynamic electricity price*, while *indirect control signal* is used in a more general context to refer to a consumption incentive signal.

In this chapter, we focus on the control algorithms for indirect control of flexible demand. A control algorithm is implemented in connection with a DSR and can control its power consumption (or activation state) and access its operation conditions, for example, by means of measurements. The main objective of a control algorithm is to control the power consumption of the associated DSR

according to the indirect control signal, while taking into account the comfort level of the consumer, and the flexibility and the operational constraints of the DSR. The indirect control signal is received at discrete time intervals through a one-way communication channel, which can be used for fetching other information, such as numerical weather predictions (NWPs). In this chapter, the way that the indirect control signal should be generated is not of concern.

In [59, 50, 49], DSRs are controlled by load shedding mechanisms based on the electricity price. According to [20], demand side strategies should have imperceptible effect on the end-use performance (*nondisruptive control*), thus suggesting that control algorithms should achieve load shifting rather than load shedding. A control algorithm for TCLs that produces transient deviations of the thermostat set-point according to a price signal is proposed in [52, 92, 28], and it will be discussed in the next section. A methodology that is often proposed in the existing literature to indirectly control a DSR is economic predictive control (MPC). The economic MPC framework consists in an optimization problem that minimizes the operating cost of the DSR, while obeying the constraints of the consumer and DSR. Economic MPC strategies for building space heating have been described in [47, 132, 133, 134, 135, 136], where the price signal is the historical Nord Pool regulating power price, whereas in [95] the price signal is the marginal production cost of conventional generating units. Economic MPC applied to commercial refrigeration units are described in [55] and in [57]. The latter describes the formulation of a chance constraints MPC, which is characterized by enhanced robustness properties against uncertainties. Indirect control strategies that do not use price signals are developed in [128, 31, 32], where flexible loads respond to variations of the system frequency (frequency sensitive loads, FSLs). Although, this approach is envisaged to support primary frequency regulation.

In this chapter, control algorithms are classified into two classes depending on if the decision-making process that they implement utilizes forecast of the indirect control signal or not. In the latter case, algorithms are said *myopic*[1]. In the former case, control algorithms can be developed using the economic MPC formulation. The mathematical formulation of a number of myopic and MPC algorithms is described in Section 3.2 and Section 3.3, respectively. The performance and requirements of myopic and MPC algorithms are compared in Section 3.4. Finally, the conclusions of this chapter are provided in Section 3.5.

3.2 Myopic control algorithms

The decision-making process of myopic control algorithms is based on the elaboration of the current and past values of the indirect control signal. The myopic algorithms presented in this section are developed for heating loads, and they

[1]This term was originally used for indicating policies for inventory models.

are meant to operate on the top of a thermostatic control loop.

3.2.1 Controller A

In [52], D. Hammerstrom et al. propose a control-by-price algorithm for TCLs that consists in adjusting the thermostatic set-point according to the electricity price. The thermostatic set point T_{ref} at the discrete instant of time i is given as

$$T_{\text{ref},i} = T^o + \Delta T_i, \tag{3.1}$$

where T^o is the consumer optimal set-point, and ΔT_i is the temperature offset. The latter is calculated as

$$\Delta T_i = -k\ \hat{p}_i, \tag{3.2}$$

where k is an arbitrary coefficient that adjusts the sensitivity of the algorithm. The term $\hat{p}_i$ is called *relative price signal*, and is defined as

$$\hat{p}_i = \frac{p_i - \overline{p}_i}{\sigma_i},\ \sigma_i \neq 0, \tag{3.3}$$

where p_i is the current price signal, $\bar{p}_i$ and σ_i are the average and the standard deviation, respectively, of the price signal history computed on a rolling window. The standard deviation at the denominator of Eq. (3.3) serves as a normalizing factor, and it reduces the risk of the consumer of being exposed to high volatility of the price p. At steady state ($dp/dt = 0$), the relative price $\hat{p}_i$ in Eq. (3.3) tends to zero since the price p_i tends to match its average $\bar{p}_i$: therefore the user comfort is not affected, in the sense that $T_{\text{ref, steady state}} = T^o$. During transients, the temperature offset ΔT_i is unbounded. This could be of concern for the comfort of the consumer.

3.2.2 Controller B

Controller B is based on the simple principle that, when the temperature is in thermostatic range, the TCL power consumption is turned on if the current electricity price is smaller than the average cost of electricity, and vice versa. The following relation holds:

$$P_{e,i} = \begin{cases} P_{e,\text{nominal}}, & \text{if } (T_i \leq T_{\min} \ \text{ or } \ p_i \leq \overline{p}_i) \\ 0, & \text{if } (T_i > T_{\max} \ \text{ or } \ p_i > \overline{p}_i) \end{cases}. \tag{3.4}$$

The temperature of the TCL is always bounded in the range defined by $T_{\min}$ and $T_{\max}$.

3.2.3 Controller C

Controller C changes the thermostatic set-point of a TCL according to

$$T_{\text{ref},i} = T^o + \Delta T_i, \tag{3.5}$$

where the offset ΔT_i is obtained high-pass filtering the indirect control signal by means of the following discrete time transfer function

$$H(z) = \frac{\Delta T(z)}{p(z)} = b\frac{1 - z^{-1}}{1 - az^{-1}}, \tag{3.6}$$

where z^{-1} is the delay operator, and a and b are the parameters of the filter. At steady state, the contribution of controller C is null and the thermostat set-point matches the optimal consumer set-point T^o. The controller does not implement any mechanism for bounding the temperature deviation ΔT during transients. This control algorithm has been used in Paper **[E]**.

3.3 Economic model predictive control

MPC techniques have been originally developed in relation to tracking problems while controlling constrained industrial processes [1]. The economic MPC in application to the control of the power consumption of a DSR consists in determining the power consumption trajectory at the lowest cost over a time horizon into the future, while respecting DSR and consumer constraints. The MPC strategy relies on an optimization problem, and it is implemented using the receding horizon policy, which consists in solving, at each discrete time interval, the optimization over the whole time horizon, but only actuating the first step of the optimal decision sequence. Although normally present in the feedback loop in real life applications, in this thesis we do no not consider the design of state estimators.

In this section, two formulations of the economic MPC problem are described. The first one in Section 3.3.1 shows how the optimization can be solved using the steepest gradient descent method , while the second in Section 3.3.2 is a generic representation of the optimization problem which is suitable for convex optimization libraries, such as CVXOPT or those in Matlab or R.

3.3.1 Model predictive control using the steepest gradient descent method

We show how the MPC problem can be solved using the steepest gradient descent method. Such a methodology utilizes the *Euler-Lagrange* equations, which are derived from the calculus of variations theory and are the necessary conditions for optimality [115]. This MPC formulation was implemented in Java and was used for the experimental application with Power Flexhouse described in Paper **[B]**.

Euler-Lagrange equations It is given a dynamic system described by

$$\dot{\boldsymbol{T}} = \boldsymbol{f}\big(\boldsymbol{T}(t), P_e(t), t\big), \tag{3.7}$$

and a Bolza cost function to minimize:

$$\min_{P_e(t)} \quad \phi\big(\boldsymbol{T}(t_f), t_f\big) + \int_{t_0}^{t_f} \mathcal{L}\big(\boldsymbol{T}(t), P_e(t), t, p(t)\big), \tag{3.8}$$

where $\boldsymbol{T}$ is a temperature state vector of a building, $\boldsymbol{f}$ is a dynamic thermal model, $P_e(t)$ is the power consumption of the electric space heating and $p(t)$ is the dynamic electricity price. The *Hamiltonian* function $\mathcal{H}$ is defined as

$$\mathcal{H}\big(\boldsymbol{T}(t), P_e(t), \boldsymbol{\lambda}(t), t, p(t)\big) = \mathcal{L}\big(\boldsymbol{T}(t), P_e(t), t, p(t)\big) + \boldsymbol{\lambda}^T(t)\boldsymbol{f}\big(\boldsymbol{T}(t), P_e(t), t\big), \tag{3.9}$$

where $\boldsymbol{\lambda}(t)$ are Lagrangian multipliers. The *Euler-Lagrange* equations are

$$\dot{\boldsymbol{\lambda}}^T(t) = \frac{-\partial\mathcal{H}\big(\boldsymbol{T}(t), P_e(t), \boldsymbol{\lambda}(t), t, p(t)\big)}{\partial \boldsymbol{T}} \tag{3.10}$$

$$\boldsymbol{\lambda}^T(t_f) = \frac{\partial\phi\big(\boldsymbol{x}(t), t\big)}{\partial \boldsymbol{T}}\bigg|_{t=t_f} \tag{3.11}$$

$$\frac{\partial\mathcal{H}\big(\boldsymbol{T}(t), P_e(t), \boldsymbol{\lambda}(t), t, p(t)\big)}{\partial u} = 0 \tag{3.12}$$

and are the three necessary conditions for optimality according to calculus-of-variations [115]. These equations are not global criteria, in the sense that they do not preclude the existence of more than one power consumption optimizing paths for the problem in Eq. (3.8). The condition for global optimality is given by the *convexity* condition:

$$\frac{\partial^2\mathcal{H}\big(\boldsymbol{T}(t), P_e(t), \boldsymbol{\lambda}(t), t, p(t)\big)}{\partial u^2} > 0, \tag{3.13}$$

which will be verified later for the case of the MPC applied to control the space heating of Power Flexhouse.

Gradient steepest descent algorithm The gradient steepest descent algorithm allows to determine the power consumption trajectory $P_e(t)$ that satisfies the Euler-Lagrange equations (3.10)-(3.12). The algorithm starts from a nominal power consumption profile (e.g. the thermostatic consumption profile). At each iteration of the algorithm, the state trajectory $\boldsymbol{x}(t)$ is computed with Eq. (3.7) and the vector $\boldsymbol{\lambda}(t)$ is obtained integrating back from the terminal condition (3.11) using Eq. (3.10). Once these two quantities are known, the path of the Hamiltonian function $\mathcal{H}$ can be determined with Eq. (3.9). If the partial derivative of the Hamiltonian function in Eq. (3.12) is zero along the state and

power consumption trajectories, the three conditions of optimality are satisfied. This latter condition acts as a stop criteria for the algorithm. If the stop criteria is not met, the control history is perturbed according to

$$P_{e,k+1}(t) = P_{e,k}(t) - \alpha \frac{\partial \mathcal{H}_k(t)}{\partial u}, \tag{3.14}$$

where k indicates the iteration step of the algorithm and α determines the amplitude of the variation.

Power Flexhouse model predictive control In Paper **[B]**, the gradient descent MPC was applied to control the power consumption of the heaters of Power Flexhouse according to a dynamic electricity price $p(t)$. The dynamic system $f(\cdot)$ in (3.7) is given by the first order Power Flexhouse thermal model [96]:

$$\dot{T}(t) = f(\cdot) = \frac{1}{R_e C_l} T(t) + P_e(t) + \frac{A}{C_l}\phi_s(t) + \frac{1}{R_e C_l} T_{\text{out}}(t), \tag{3.15}$$

where the parameters R_e and C_l were previously defined in Table 2.2, and T^{out} and $\phi_s(t)$ denote NWPs of the ambient temperature and insolation, respectively. The cost function to optimize in Eq. (3.8) is composed by the following two terms:

$$\theta = \big(T(t_f) - T_{\text{ref}}\big)^2 \tag{3.16}$$

$$\mathcal{L} = \big(T(t) - T_{\text{ref}}\big)^2 + \log P_e(t) + -\log\big(10 - P_e(t)\big) + p(t)P_e(t). \tag{3.17}$$

Eq. (3.17) is composed by a quadratic temperature term, which penalizes deviations from the temperature set-point, and two logarithmic barrier functions, which implement the constraints on the minimum and maximum power consumption of the heaters, i.e. 0 kW and 10 kW, respectively. The barrier functions tend to infinite when the power consumption approaches the minimum and maximum allowed values, hence favouring, in the optimization process, less extreme values of the power consumption, while having lower impact for intermediate values. The last term in Eq. (3.17) is the cost of consuming power, that is the power consumption times the electricity price. All the functions on the right hand side of Eq. (3.17) are convex, and since nonnegative weighted sums preserve convexity [16], also the function $\mathcal{L}$ is convex.

Replacing Eq. (3.9) in Eq. (3.13) yields to

$$\frac{\partial^2 \mathcal{L}(\cdot)}{\partial u^2} + \frac{\partial^2 \boldsymbol{f}(\cdot)}{\partial P_e^2} > 0. \tag{3.18}$$

The Power Flexhouse model (3.15) is linear in the power consumption P_e, hence the second addend on the left-hand side of Eq. (3.18) is null. This means that the convexity criteria in Eq. (3.18) only depends on the function $\mathcal{L}$, which is convex. Since the convexity criteria is satisfied, the Power Flexhouse MPC achieves the global optimum.

3.3.2 Formulation of model predictive control problems using model state space representation

In this section, we show how the MPC problem can be formulated using the state space representation of a dynamic model. We formulate and illustrate the properties of MPC with a linear cost function, linear cost function and soft constraints, and quadratic cost function.

Linear cost function MPC with hard constraints

The cost function of the optimization problem is

$$J = \sum_{i=0}^{n-1} p_i P_{e,i}, \tag{3.19}$$

where p and P_e are the electricity cost (or a generic consumption incentive signal) and the power consumption of electric space heating, respectively, at the discrete time step i. Using the matrix product, Eq. (3.19) can be expressed as

$$J = \boldsymbol{p}^T \boldsymbol{P_e}, \tag{3.20}$$

where $\boldsymbol{p}, \boldsymbol{P_e} \in \mathbb{R}^n$ and are obtained stacking the respective values for $i = 0, \ldots, N-1$. The MPC problem is given by

$$\boldsymbol{P_e^o} = \arg\min_{\boldsymbol{P_e}} J \tag{3.21}$$

$$\text{s.t.} \quad T_{\min,i} \leq T_i \leq T_{\max,i}, \quad i = 0, \ldots, n-1 \tag{3.22}$$

$$P_{\min,i} \leq P_{e,i} \leq P_{\max,i}, \quad i = 0, \ldots, n-1. \tag{3.23}$$

The constraints in (3.22) and (3.23) define the limits of the building temperature and electric power consumption of the space heating, respectively.

Let $A \in \mathbb{R}^{n \times n}$ and $B_P, B_T, B_S, C^T \in \mathbb{R}^n$ be the matrices that describe the following state space thermal model of a building:

$$\boldsymbol{x}_{i+1} = A\boldsymbol{x_i} + B_P P_{e,i} + B_T T_{\text{out},i} + B_S S_i \tag{3.24}$$

$$T_i = C\boldsymbol{x}_i, \tag{3.25}$$

where $\boldsymbol{x} \in \mathbb{R}^n$ is the state vector, T_{out} is the outside air temperature, S is the insolation value and T is the indoor air temperature. Developing Eq. (3.24) and Eq. (3.25) for $i = 1$ and $i = 2$, respectively, yields

$$\boldsymbol{x}_1 = A\boldsymbol{x}_0 + B_P P_{e,0} + B_T T_{\text{out},0} + B_S S_0 \tag{3.26}$$

$$T_2 = C\big(A\boldsymbol{x}_1 + B_P P_{e,1} + B_T T_{\text{out},1} + B_S S_1\big). \tag{3.27}$$

Replacing Eq. (3.26) into Eq. (3.27) gives

$$\begin{aligned} T_2 =& CA\big[A\boldsymbol{x}_0 + B_P P_{e,0} + B_T T_{\text{out},0} + B_S S_0\big] + \\ &+ CB_P P_{e,1} + CB_T T_{\text{out},1} + CB_S S_1. \end{aligned} \tag{3.28}$$

Iterating this procedure, juxtaposing the input quantities in column vectors and using matrix product notation yields to

$$\begin{aligned} \begin{bmatrix} T_1 \\ T_2 \\ \vdots \\ T_{n+1} \end{bmatrix} = \begin{bmatrix} CA \\ CA^2 \\ \vdots \\ CA^{n+1} \end{bmatrix} T_0 + \begin{bmatrix} CB_P & 0 & \cdots & 0 \\ CAB_P & CB_P & \cdots & 0 \\ \vdots & \vdots & \ddots & \vdots \\ CA^n B_P & CA^{n-1}B_P & \cdots & CB_P \end{bmatrix} \begin{bmatrix} P_{e,0} \\ P_{e,1} \\ \vdots \\ P_{e,n} \end{bmatrix} + \\ + \begin{bmatrix} CB_T & 0 & \cdots & 0 \\ CAB_T & CB_T & \cdots & 0 \\ \vdots & \vdots & \ddots & \vdots \\ CA^n B_T & CA^{n-1}B_T & \cdots & CB_T \end{bmatrix} \begin{bmatrix} T_{\text{out},0} \\ T_{\text{out},1} \\ \vdots \\ T_{\text{out},n} \end{bmatrix} + \\ + \begin{bmatrix} CB_S & 0 & \cdots & 0 \\ CAB_S & CB_S & \cdots & 0 \\ \vdots & \vdots & \ddots & \vdots \\ CA^n B_S & CA^{n-1}B_S & \cdots & CB_S \end{bmatrix} \begin{bmatrix} S_0 \\ S_1 \\ \vdots \\ S_n \end{bmatrix}. \end{aligned} \tag{3.29}$$

Introducing the matrices $\Phi \in \mathbb{R}^n, \Theta, \Gamma, \Delta \in \mathbb{R}^{n\times n}$, Eq. (3.29) can be written as

$$\boldsymbol{T} = \Phi T_0 + \Theta \boldsymbol{P_e} + \Gamma \boldsymbol{T}_{\text{out}} + \Delta \boldsymbol{S}, \tag{3.30}$$

which is the finite impulse response (FIR) of the building thermal model plus the bias due to the initial condition. This form can be used to express the two inequality constraints in (3.22), which become

$$\Phi T_0 + \Theta \boldsymbol{P_e} + \Gamma \boldsymbol{T}_{\text{out}} + \Delta \boldsymbol{S} \leq \boldsymbol{T_{\max}} \tag{3.31}$$

$$\Phi T_0 + \Theta \boldsymbol{P_e} + \Gamma \boldsymbol{T}_{\text{out}} + \Delta \boldsymbol{S} \geq \boldsymbol{T_{\min}}. \tag{3.32}$$

Inequalities (3.31) and (3.32) can be rearranged as

$$\Theta \boldsymbol{P_e} \leq \boldsymbol{T_{\max}} - \Phi T_0 - \Gamma \boldsymbol{T}_{\text{out}} - \Delta \boldsymbol{S} \tag{3.33}$$

$$-\Theta \boldsymbol{P_e} \leq -\boldsymbol{T_{\min}} + \Phi T_0 + \Gamma \boldsymbol{T}_{\text{out}} + \Delta \boldsymbol{S}, \tag{3.34}$$

where the right-hand sides are composed by a sum of known terms and the left-hand sides are linear in the decision vector.

Using matrix product, constraints in (3.23) can be written as

$$I_{n\times n} \boldsymbol{P_e} \leq \boldsymbol{P_{\max}} \tag{3.35}$$

$$-I_{n\times n} \boldsymbol{P_e} \leq -\boldsymbol{P_{\min}}. \tag{3.36}$$

The constraints (3.33)-(3.36) are in the form

$$A_c \boldsymbol{P_e} \leq \boldsymbol{b_c}, \tag{3.37}$$

where A_c is

$$A_c = \begin{bmatrix} \Theta \\ -\Theta \\ I_{n\times n} \\ -I_{n\times n} \end{bmatrix}, \tag{3.38}$$

and $\boldsymbol{b_c}$ is

$$\boldsymbol{b_c} = \begin{bmatrix} \boldsymbol{T_{max}} - \Phi T_0 - \Gamma \boldsymbol{T}_{\text{out}} - \Delta \boldsymbol{S} \\ -\boldsymbol{T_{min}} + \Phi T_0 + \Gamma \boldsymbol{T}_{\text{out}} + \Delta \boldsymbol{S} \\ \boldsymbol{P_{max}} \\ -\boldsymbol{P_{min}} \end{bmatrix}. \tag{3.39}$$

Summarizing, the initial MPC problem (3.21)-(3.23) has been rewritten as

$$\boldsymbol{P_e^o} = \arg\min_{\boldsymbol{P_e}} \boldsymbol{p}^T \boldsymbol{P_e} \tag{3.40}$$

$$\text{s.t.} \quad A_c \boldsymbol{P_e} \leq \boldsymbol{b_c}. \tag{3.41}$$

The optimization in (3.40)-(3.41) is convex (see Appendix B). This MPC is said linear MPC because the cost function is linear in the decision variable $\boldsymbol{P_e}$, and it can be solved, for example, using the function *linprog* in Matlab.

Model predictive control with temperature soft constraints

Temperature constraints in (3.33) and (3.34) are formulated as hard constraints, i.e. the temperature is allowed only in the range determined by the upper and lower constraints. Soft constraints can be implemented by adding an offset $\boldsymbol{s} \in \mathbb{R}^n$ to the temperature inequality constraints, as shown in the following:

$$\Phi T_0 + \Theta \boldsymbol{P_e} + \Gamma \boldsymbol{T}_{\text{out}} + \Delta \boldsymbol{S} \leq \boldsymbol{T_{max}} + \boldsymbol{s} \tag{3.42}$$

$$\Phi T_0 + \Theta \boldsymbol{P_e} + \Gamma \boldsymbol{T}_{\text{out}} + \Delta \boldsymbol{S} \geq \boldsymbol{T_{min}} - \boldsymbol{s}, \tag{3.43}$$

where the vector $\boldsymbol{s}$ is a slack variable and it is added in the cost function through a vector of coefficients $\boldsymbol{\sigma}$. The new formulation of the optimization problem is given in 3.44 and 3.45.

$$\begin{bmatrix} \boldsymbol{P_e^o} \\ \boldsymbol{s^o} \end{bmatrix} = \arg\min_{[\boldsymbol{P_e}, \boldsymbol{s}]} \begin{bmatrix} \boldsymbol{p} \\ \boldsymbol{\sigma} \end{bmatrix}^T \begin{bmatrix} \boldsymbol{P_e} \\ \boldsymbol{s} \end{bmatrix} \tag{3.44}$$

$$\text{s.t.} \quad \begin{bmatrix} \Theta & -I_{n\times n} \\ -\Theta & -I_{n\times n} \\ I_{n\times n} & 0 \\ -I_{n\times n} & 0 \end{bmatrix} \begin{bmatrix} \boldsymbol{P_e} \\ \boldsymbol{s} \end{bmatrix} \leq \mathbf{b}_c \tag{3.45}$$

There exist two main reasons to implement temperature soft constraints rather than hard constraints in a MPC:

- if the temperature initial condition of the thermal model does not belong to the range defined by the hard constraints, the MPC with hard constraints is impossible to solve. On the contrary, the MPC with soft constraints can be solved even if the temperature initial condition is not in the allowed range. This aspect is relevant during the receding horizon policy in real life applications: in this case, during the update phase of the thermal model, the temperature initial condition may drift out of the range specified by the temperature hard constraints because, for example, of system noise or inaccuracy of the model.
- the MPC with hard constraints does not allow the DSR to react to a stepwise variation of the consumption incentive signal. This situation is sketched in Fig. 3.1, which compares the behaviour of the MPC with hard constraints (plots in the upper panel) and soft constraints (plots in the lower panel) when a stepwise decrease of the dynamic electricity price occurs at time $t = 10$ h (plots in the third column). The MPC with hard constraints let the temperature of the building lay at the lowest allowed temperature limit: when the price signal drops, the MPC strategy does not alter the power consumption, since the best it can do is to minimize the power consumption while respecting the hard constraints. In the case of the MPC with soft constraints, the slack variables $\boldsymbol{s}$ in (3.44) allows the trade between the amount of temperature deviation from the lower set-point and the electricity cost: in this case, as visible in the lower panel plots of Fig. 3.1, the space heating power consumption is decreased at time $t \approx 10$ h and increased again when the lower electricity price occurs.

Quadratic MPC

In the linear MPC, the building indoor temperature is allowed in the range defined by $\boldsymbol{T_{\min}}$ and $\boldsymbol{T_{\max}}$. In the MPC formulation of this section, we introduce a penalty term in the cost function in order to penalize the deviation from a temperature set-point, which is defined using the vector $\boldsymbol{T}_{\text{ref}} \in \mathbb{R}^n$. We impose that the temperature of the building $\boldsymbol{T}$ has to match the temperature set-point plus the offset $\boldsymbol{T}_{\text{offset}}$:

$$\boldsymbol{T} = \boldsymbol{T}_{\text{ref}} + \boldsymbol{T}_{\text{offset}}. \tag{3.46}$$

Using the description introduced in Eq. (3.30), the equation above becomes

$$\Phi T_0 + \Theta \boldsymbol{P_e} + \Gamma \boldsymbol{T}_{\text{out}} + \Delta \boldsymbol{S} = \boldsymbol{T}_{\text{ref}} + \boldsymbol{T}_{\text{offset}}, \tag{3.47}$$

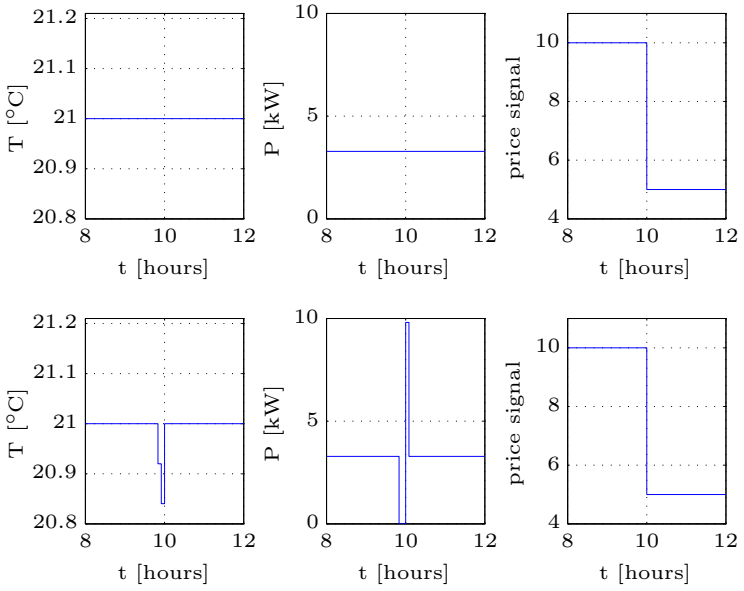

Figure 3.1: Comparison between the responses of the MPC with temperature hard constraints (plots in the upper panel) and soft constraints (plots in the lower panel) to a stepwise decrease of the dynamic electricity price signal (plots in the third column). The former MPC does not react to the price signal variation, while the latter achieves to consume a larger amount of power when the electricity cost is lower and vice versa.

which can be rearranged and written using the matrix product notation as shown in the following:

$$\Theta \boldsymbol{P_e} - \boldsymbol{T}_{\text{offset}} = \boldsymbol{T}_{\text{ref}} - \Phi T_0 - \Gamma \boldsymbol{T}_{\text{out}} - \Delta \boldsymbol{S} \tag{3.48}$$

$$\begin{bmatrix} \Theta \\ -\mathbb{I}_{n\times n} \end{bmatrix}^T \begin{bmatrix} \boldsymbol{P_e} \\ \boldsymbol{T}_{\text{offset}} \end{bmatrix} = \boldsymbol{T}_{\text{ref}} - \Phi T_0 - \Gamma \boldsymbol{T}_{\text{out}} - \Delta \boldsymbol{S}. \tag{3.49}$$

The vector $\begin{bmatrix} \boldsymbol{P_e} & \boldsymbol{T}_{\text{offset}} \end{bmatrix}^T$ in Eq. (3.49) is the new decision vector of the optimization problem. The cost function of the optimization problem is given as

$$J = \begin{bmatrix} \boldsymbol{P_e} \\ \boldsymbol{T}_{\text{offset}} \end{bmatrix}^T \begin{bmatrix} 0 & 0 \\ 0 & \mathbb{I}_{n\times n} \end{bmatrix} \begin{bmatrix} \boldsymbol{P_e} \\ \boldsymbol{T}_{\text{offset}} \end{bmatrix} + \begin{bmatrix} \boldsymbol{p} \\ 0 \end{bmatrix}^T \begin{bmatrix} \boldsymbol{P_e} \\ \boldsymbol{T}_{\text{offset}} \end{bmatrix} \tag{3.50}$$

Eq. (3.50) and Eq. (3.49) compose a convex optimization with quadratic cost function in the form:

$$\begin{aligned} \boldsymbol{x^o} = \arg\min_{\boldsymbol{x}} \; & \boldsymbol{x}^T Q \boldsymbol{x} + \boldsymbol{c}^T \boldsymbol{x} \\ \text{s.t.} \quad & A\mathbf{x} = \mathbf{b}, \end{aligned}$$

which can be solved, for example, using the function *quadprog* in Matlab. The quadratic MPC achieves to trade between the temperature comfort (in terms of deviation from the temperature set-point $\boldsymbol{T}_{\text{ref}}$) and the electricity cost.

Hard constraints to limit the temperature offset can be implemented by adding to the previous optimization the following constraint:

$$\begin{bmatrix} 0 & \mathbb{I}_{n\times n} \end{bmatrix} \begin{bmatrix} \boldsymbol{P_e} \\ \boldsymbol{T}_{\text{offset}} \end{bmatrix} \leq \boldsymbol{T}_{\text{offset,max}}.$$

Length of the optimization horizon

The MPC formulation requires to choose the length of the optimization horizon t_f or N. A qualitative method that is adopted to assign it consists in choosing it large enough in order that the next set of forecast does not alter the decision at the current time step. This criteria can be visualized if thinking about the receding horizon formulation: it has been said that at each time step the optimization problem is solved for the whole optimization horizon, but only the first decision out of the optimized profile is actuated. If the horizon is too short, a new step of the receding horizon policy may alter the optimal trajectory defined at the step before, hence invalidating its actual utility. If the horizon length is long enough, this does not happen because the decision at the current time step has a reduced effect on the system dynamics in the far future.

3.4 A comparison between the classes of controllers

Two classes of price responsive controllers for DSRs have been presented in this chapter. The former class was named *myopic*, in the sense that predictions were not used in the decision-making process. The latter class of algorithms uses forecast of the price signal and a prediction model of the DSR. In this section, the performance and the requirements of the two classes of algorithms are discussed.

3.4.1 A systematic comparison of the performance of indirect control algorithms

A comparison of the performance of a number of control algorithms was presented in Paper **[B]**. In this section, we present a summary of the most relevant results of the paper. Four group of buildings were simulated by means of

thermal models, and their space heating units were controlled by controller A (Section 3.2.1), controller B (Section 3.2.2), steepest gradient descent MPC (Section 3.3.1) and a traditional thermostatic controller, respectively. The buildings were subject to the same weather conditions, and for MPC controllers, NWPs from DTU Wind Energy department were used. In the simulations, the price signal was artificial and built in order to highlight and spot the differences between the behaviors of the control algorithms. The forecast of the price signal were assumed known without error. Simulations were performed using a hardware-in-the-loop (HIL) simulation strategy that is described in the next section.

The comparison between the performance of the controllers was carried out by means of defining metrics regarding the consumer comfort and electricity cost. In the former case, the results of the comparison are shown in Fig. 3.2, while in the latter case, they are shown in Fig. 3.3.

The plot in the upper panel of Fig. 3.2 shows, for each group of buildings, the average temperature deviation from the average temperature set-point (23 °C). The averages are calculated across each group of buildings. The plots in the middle and lower panels show the evolutions of two indicators, which are defined as follows:

- indicator 1 is the normalized cumulative absolute value of the temperature deviation from the set-point, with the states of under temperature ($T < T_{\text{set-point}}$) weighted 20% more than the sates that are overheated ($T > T_{\text{set-point}}$);
- indicator 2 is the normalized cumulative value of the temperature deviation when the temperature is outside the thermostatic range ($23 \pm 3°C$).

For convenience of visualization, both indicator are normalized with respect to their respective final values.

The thermostatic and the MPC controllers are the algorithms with the better performance in the case of the indicator 1 and indicator 2, respectively. In the case of the thermostatically controlled group of buildings, the value of the indicator 2 is different than zero even if, by formulation, thermostatic control should assure the building temperature not to leave the thermostatic range. The reason for such a behaviour is that measured weather conditions were used to perform the simulations, and the period under consideration was characterized by relative high values of insolation: this caused the overheating of the buildings during the day time. This did not happen for the group of buildings controlled by the MPC algorithms: in this case, the MPC strategy could benefit of the weather forecast to decide in advance on opportune counteractions to avoid the overheating (i.e. disconnect the heating before the sunrise).

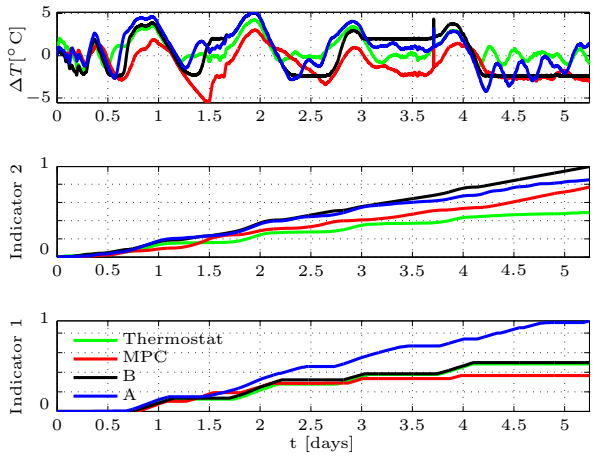

Figure 3.2: The plot in the upper panel shows the average temperature deviation from the thermostat set-point of the four populations of buildings. The plots in the middle and lower panels show two performance indicators, which are described in the body of the thesis.

In Fig. 3.3, we compare the performance of the controllers in terms of electricity costs. The plot in the upper panel shows the evolution in time of the average electricity bill. Since, in the simulations, an artificial price signal was used, the monetary values on the y-axis are not measured using an existing currency, and they should be regarded to as a generic cost indicator. The plot in the lower panel of Fig. 3.3 shows the cost savings that the control algorithms achieve compared to the thermostatic control, which is considered as the base case. The MPC is the controller that achieves the best performance in terms of cost reduction.

Real-time hardware-in-the-loop simulations

Results in Paper **[B]** were obtained using a HIL simulation strategy that consisted in carrying out the simulations of a population of buildings in parallel to an experiment with Power Flexhouse. The operation principle of the HIL simulation strategy is sketched and described in Fig. 3.4.

It is worth to note that using the prediction error of Power Flexhouse thermal model to perturb the conditions of all the simulated thermal models is not fully rigorous because the prediction error may change from building to building. However, the main objective of the HIL strategy is to introduce into the simu-

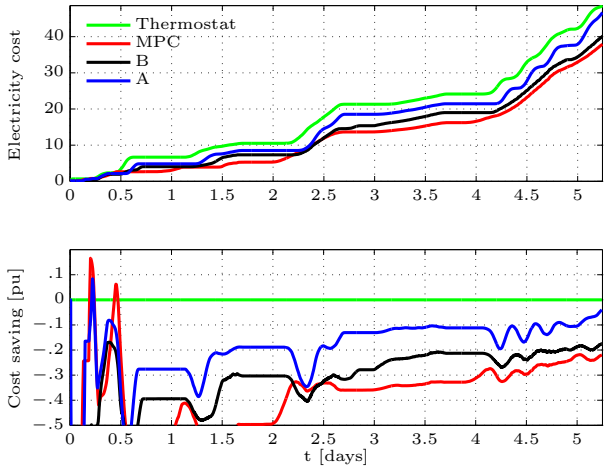

Figure 3.3: The plot in the upper panel shows the evolution of the electricity cost. The plot in the lower panel shows the cost savings the control algorithms achieve compared to the thermostatic control, which is considered as the base case.

lations stochastic disturbances coherent with real operating conditions, such as the cooling effect of the wind, which is not described in the thermal models. The HIL simulation strategy is valuable when evaluating the performance of MPC controllers (e.g. robustness against uncertainties) because the predictions of the thermal models are not exact anymore. Moreover, the HIL simulation framework allows to evaluate the performance of indirect control algorithms both in a real-life environment (e.g. by means of measuring the temperature comfort in Power Flexhouse) and in terms of (simulated) aggregated response of a large population of DSRs.

3.4.2 A remark about the optimality of economic MPC controllers

MPC control strategies are formulated upon an optimization problem and, in respect to the cost function they implement, are said to be optimal. In the formulation proposed in Section 3.3, and more in general in [48, 29, 133, 55], the optimization problem is formulated accounting for the interest of the consumer (i.e. minimization of the electricity cost, while respecting comfort conditions). It is worth noting that the economic MPC framework does not offer any guarantees that the operation of the DSR is optimal in respect to the service that flexible demand is meant to supply to grid: the optimality of the operation of flexible demand in respect to the power system rather comes from a correct formulation

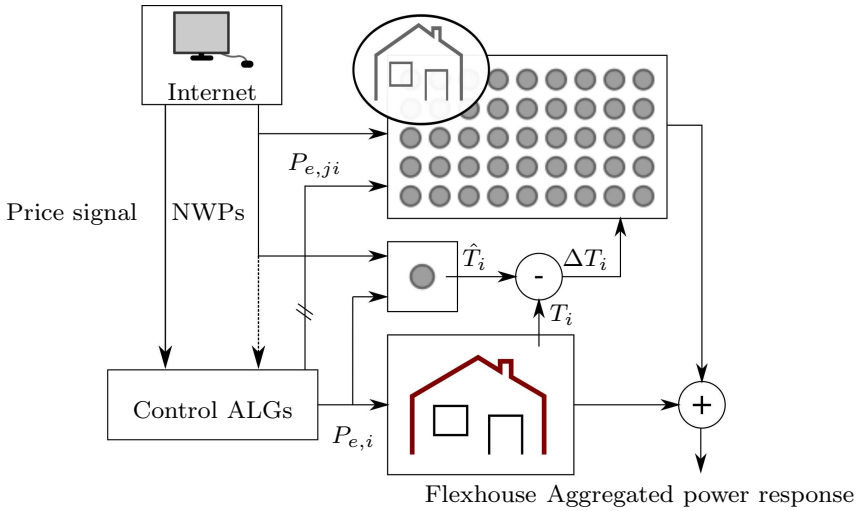

Figure 3.4: Diagram of the HIL real-time simulation framework. The price signal and the NWPs required by the control algorithms are fetch from the Internet. The control algorithms (one for each building) determine the power consumption profile $P_{e,ji}$ of the respective simulated buildings, which are indicated by the circles in the top-right corner. One among the control algorithms determines the power consumption of Power Flexhouse$P_{e,i}$. This signal is applied both to Power Flexhouse and to Power Flexhouse thermal model. This allows to determine the one-step ahead prediction error ΔT_i of Power Flexhouse thermal model. The prediction error ΔT_i is used as an offset for perturbing the initial conditions of the simulated buildings. This is done with the aim of introducing into the simulations of the buildings a stochastic components that is derived from the real experiment with Power Flexhouse.

of the price signal and price signal forecast. Reflecting into the price signal the need of the power system (for example, regulating power) requires the capability of predicting the dynamic behaviour of flexible demand.

On the other hand, myopic algorithms are not optimal from the consumer perspective because there are no explicit guarantees on the comfort conditions and cost saving that they achieve. The decision-making process of myopic algorithms leads to an intuitive behaviour of DR since the consumption is induced to decrease when the price increases and vice versa (cfr. Fig. 3.1). With myopic algorithms the consumption could be, for example, forced to an immediate disconnection (compatibly with the indirect control time scale) in the case of an unforeseen emergency event (e.g. sudden loss of generation).

3.4.3 Implementation of indirect control algorithms

Myopic and MPC algorithms achieve different results in terms of amount of regulating power they can provide by means of controlling flexible demand (see for example Fig. 4 in Paper **[B]**). Hence, the use of one or another control algorithm should be specifically addressed when determining the indirect control signal. This also suggests that algorithms belonging to different classes might not coexist since they require different indirect control signals.

Requirements of myopic and MPC algorithms

Fig. 3.5 and Fig. 3.6 show the input-output diagrams of myopic and MPC algorithms, respectively. The main difference between the two classes of algorithms is that MPC requires a prediction model of the DSR, forecast of the price signal and forecast of the quantities to compute the evolution of the state of the DSR model (e.g. NWPs).

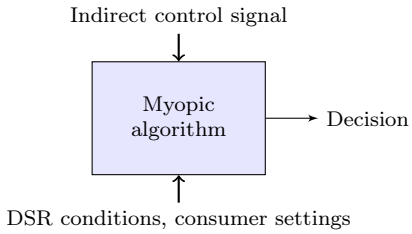

Figure 3.5: Input output diagram of myopic algorithms.

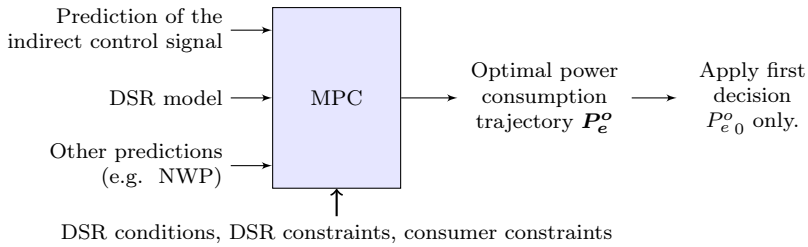

Figure 3.6: Input output diagram of MPC algorithms.

The optimized power consumption sequence $\boldsymbol{P_e^o}$ in Fig. 3.6 is a vector of real values. If the DSRs to control are of *on-off* type, such as TCLs, an additional layer to convert from the power reference $P_{e,0}^{o} \in \mathbb{R}$ to binary pulses should be implemented. This can be done, for example, by means of PWM (Pulse Width Modulation), which is a binary signal whose energy content over a specified period is the same as the power reference. PWM do not alter the overall

performance of MPC because:

- disregarding the power consumption binary state is of concern as it may lead to violate the process constraints during the PWM period. However, the time interval of the receding horizon policy can be chosen short enough so to assure that the variations in the interval of the constrained variables are smaller than arbitrary coefficients, which could be implemented as a back-off terms in the respective constraints;
- said T_s the period of the receding horizon policy, from the definition of PWM follows that the amount of electricity that the PWM signal delivers during T_s equals the one of the continuous value of the MPC. Provided that the price signal is constant during T_s, the electricity cost does not change in the two cases. Thus, the PWM consumption signal achieves the same minimum electricity cost as the MPC with continuous decision variables.

It is worth to note that the PWM approach allows to deal with TCLs without the requirement of formulating the optimization problem as a binary integer programming, hence preserving the convex structure of the optimization.

When, for safety reasons, it is not possible to directly control the state or the power consumption of the DSR, control algorithms may still achieve controllability by changing the quantity that triggers the power consumption. For example, in [117], the power consumption of a heat pump is controlled by means of varying the temperature of the water of the hydronic system by actuating the valves of the radiators. It is worth to note that in such a case, a MPC policy is recommendable because there is a delay (introduced by the thermal inertia of the water) between controlling the water flow and changing the consumption profile.

Computational power From the point of view of the computational power, MPC-based algorithms require to solve a convex optimization problem, which is of polynomial time complexity [16]. Myopic algorithms are less demanding than MPC strategies, and they require to calculate a few algebraic relationships only. Nevertheless, considering that potential DSRs need a hardware upgrade in order to achieve the ability of communicating, and that computational power is nowadays cheap, the hardware requirements are not considered as a distinguishing factor in favor of myopic algorithms.

3.5 Conclusions

In this chapter, a number of control algorithms for indirect control of flexible demand have been presented. Control algorithms have been classified into two macro groups, depending on if their decision-making processes use forecast of

the price signal (MPC algorithms) or not (myopic algorithms). Myopic control algorithms have an intuitive response behaviour, because whenever the price rises, the DSRs are induced to consume less power and vice versa. In the case of MPC algorithms, the behaviour is complex because the power consumption depends on the prediction of the electricity price and system dynamics of the DSR. The implementation of one control algorithm or another should be taken into account while formulating the indirect control signal. Receding horizon economic MPC algorithms allow to manage in an optimal way the flexibility of the DSRs because the consumption is scheduled in advance. The economic MPC strategy is optimal from a consumer point of view since it achieves the minimization of the operating cost while obeying comfort constraints. On the other hand, MPC strategies have more requirement than myopic algorithms, which are based on a simple decision-making process.

Chapter 4

Aggregated response of flexible demand

In this chapter, we show that indirectly controlling a population of TCLs induces a synchronization of the states of the units, causing the aggregated power consumption to oscillate. These dynamics must be be taken into account if flexible demand is meant to supply power system services.

4.1 Introduction

The paradigm on which the concept of controlling flexible demand relies is that, although the power consumption of a single DSR is negligible, the aggregated and coordinated change of consumption of a large population of DSRs may have relevant size, and hence it can be controlled to support the operation of the grid. This states the motivation to investigate the dynamics of the aggregated power consumption of groups of DSRs. In Paper **[E]**, we show by means of simulations that shifting or shedding the consumption of a population of thermostatically controlled space heating units induces a synchronization in the states of the TCLs and provokes oscillations of the aggregated power consumption.

The problem of the synchronization in the consumption was originally investigated in [85, 86] in connection to service restoration after power system outages during cold periods. In [79], Malhamé and Chong developed a model based on the coupled Fokker-Planck equations to describe the dynamics of the aggregated power consumption of an indirectly controlled population of water heaters. The synchronization effect due to controlling EWHs and air conditioning units has been described in [73] and [98], respectively.

In this chapter, the main contributions from Paper **[E]** are summarized. Section 4.2 describes the setup utilized to simulate the aggregated power consumption of a population of TCLs. TCLs are electric space heating units, and they

are controlled with an algorithm that achieves load shifting. In Section 4.3, we analyse the transient response of the aggregated power consumption of the population of TCLs when a stepwise variation of the indirect control signal is applied. In Section 4.4, the analysis described above is repeated, but considering load shedding instead of load shifting. In Section 4.5, the results are discussed, and in Section 4.6, the conclusions are stated.

4.2 Simulation setup

A population of 10^5 buildings equipped with electric space heating is simulated using a bottom-up approach, i.e. by aggregating the simulated power consumption of the individual buildings. Each building is modelled using a first order linear thermal model, the same discussed in Chapter 2. In order to account for differences across the population, the floor areas of the buildings have been variated according to the gamma distribution shown in Fig. 4.1, whose parameters are reported in Paper **[E]** and have been determined applying MLE on data from the BBR database (the Danish national register of buildings[1]).

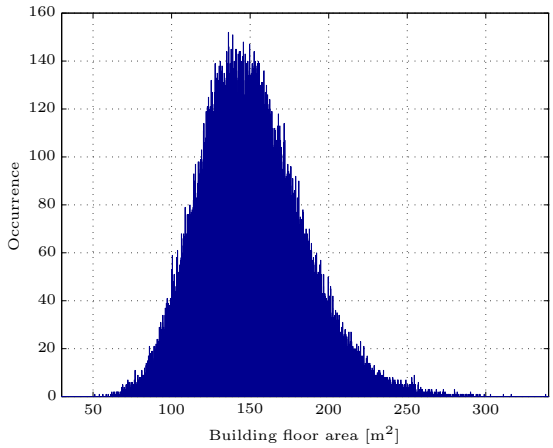

Figure 4.1: Histogram of 10^5 realizations of the gamma distribution representative of the floor area of the class of buildings similar to Power Flexhouse.

The space heating of each building is controlled by a thermostat. On the top of the thermostat, *controller C* (see Section 3.2.3) is implemented in order to achieve load shifting according to a consumption incentive signal. The diagram of the indirect control configuration of each building is shown in Fig. 4.2, where p is the indirect control signal and $H_j(z)$ is the high-pass filter of the controller.

[1] Bygnings- og Boligregistret, http://www.bbr.dk/.

The parameters of the controllers, the hysteresis values of the thermostats and the comfort set-points T_j^{in} are distributed according to the Gaussian PDFs that are characterized in Paper **[E]**. Weather conditions are constant in time and across the population.

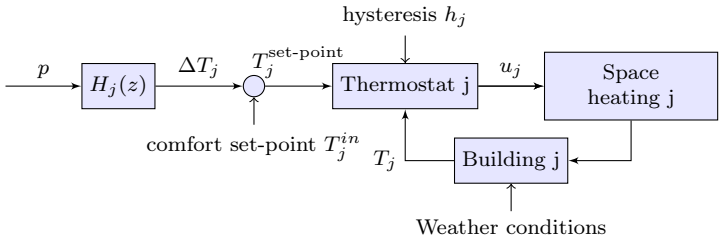

Figure 4.2: Control layout of the electric space heating of the building j.

4.3 Step response of the aggregated power consumption

In the indirect control framework, shifting the operation of flexible demand is achieved by means of changing the indirect control signal, e.g. by modifying the electricity cost at discrete time intervals. In Paper **[E]**, the step response of the aggregated power consumption of the aforementioned population of buildings is studied with the objective of determining its dynamic properties. The plots in the three panels of Fig. 4.3 show, respectively, the aggregated power consumption of the population of space heating units, the indirect control signal p and the average temperature offset applied to the thermostatic set-point of the buildings. Four points of interest have been identified along the aggregated power consumption profile, and they are indicated by the coloured marks.

Red mark (steady state) The aggregated power consumption does not show any major variations. This is a steady state situation and, statistically, for each thermostat turning on, there is one turning off and vice versa. The histogram in Fig. 4.4 shows that the distribution of the distances between the temperatures of the buildings and the respective set-points is uniform across the population. The buildings moving rightward in the histogram are those whose space heating is in the *on* state, and those which eventually pass the right threshold are switched off by the thermostat, and vice versa.

Green mark The price signal variation is perceived by the indirect control algorithms, which therefore decrease the temperature set-points of the respective buildings. In Fig. 4.5, all the units that are in the *on* state and that have the temperature larger that the new respective thermostatic set-points are switched off. This provokes a drop in the power consumption. Moreover, for a certain period of time, no units will be able to trigger the consumption *on* because they

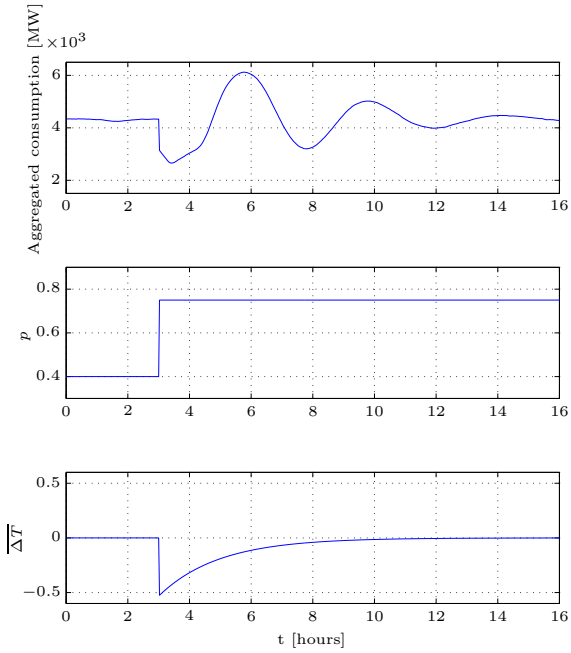

Figure 4.3: The plot in the upper panel shows the aggregated power consumption of the population of space heating units. The plots in the middle and lower panels show the indirect control signal p and the average of the temperature offsets $\Delta T_j,\ j = 1, \ldots, 10^5$ applied by the indirect control algorithms, respectively.

need to reach a new lower thermostatic threshold; the unbalance between the number of units triggering the consumption *on* and *off* causes the aggregated power consumption to decrease further, as shown in the top panel of Fig. 4.3 between the green and orange marks.

Orange mark The aggregated power consumption reaches the lowest value. By comparing the histograms in Fig. 4.5 and Fig. 4.6, it is possible to notice that there is a *wave* moving leftwards, indicating that a large number of buildings are cooling down. It is worth to note that while time passes, the indirect control algorithms of the buildings gradually remove the temperature offsets, as shown in the plot in the lower panel of Fig. 4.3: this contributes to redistribute the temperature of the buildings in the middle of the thermostatic thresholds (Fig. 4.6).

Magenta mark The aggregated power consumption assumes the same value as during steady state. However, this situation does not result in an equilibrium

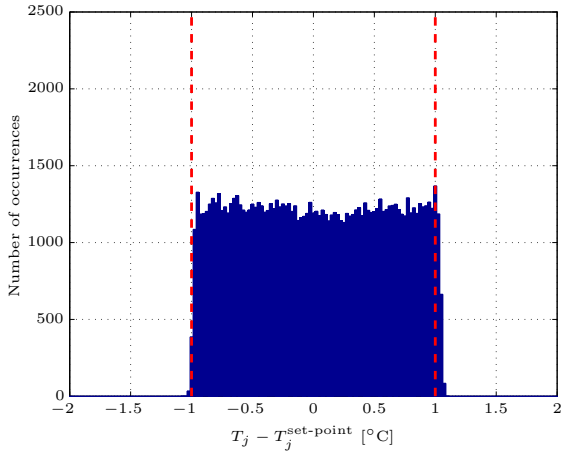

Figure 4.4: Histogram of the distances between the temperatures of the buildings and the respective thermostatic set-points at steady state (red mark). The two vertical lines shows the average thermostat hysteresis value across the population of buildings.

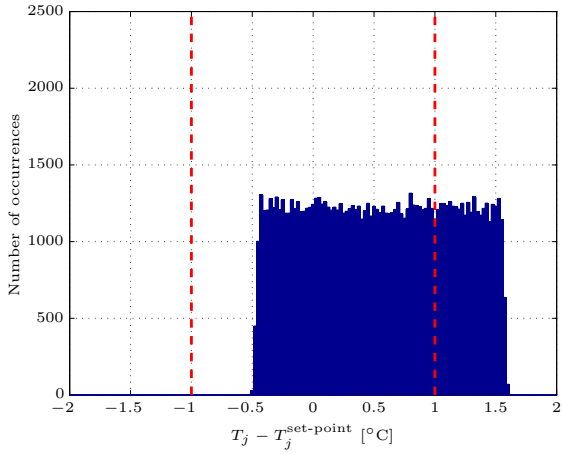

Figure 4.5: Histogram of the temperature distance from the respective set-point at the green mark in the plot in the upper panel of Fig. 4.3.

point because the flow of units trespassing the right thermostatic threshold does not equal the flow in the opposite direction. The progressive activations of space

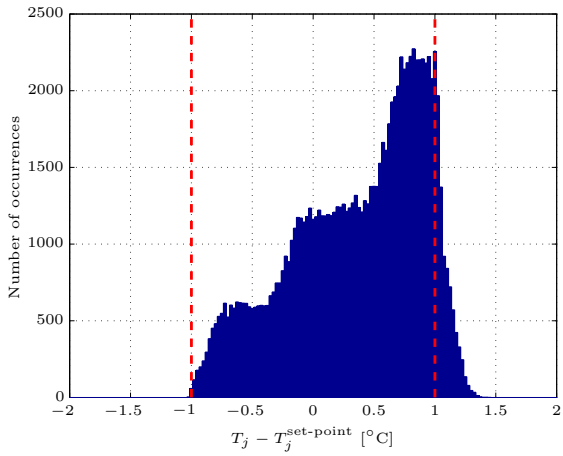

Figure 4.6: Histogram of the temperature distance from the respective set-point at the orange mark in the plot in the upper panel of Fig. 4.3.

heating units will cause the aggregated power consumption to increase, leading to the kickback effect of flexible demand.

Black mark The black mark indicates the peak of the kickback effect of the aggregated power consumption. After the black mark, the aggregated power consumption undergoes to a period with damped oscillations and, finally, reaches a new steady state at time $t \approx 15$ h. The new steady state power consumption is equal to the initial one because the DC gain of the filter $H_j(z)$ is null (i.e. the final thermostatic set-point matches the initial one) and the weather conditions are constant in time.

4.4 Step response of load shedding

One might wonder if the kickback effect can be reduced by implementing a load shedding policy instead of a load shifting one. This is shown in Fig. 4.7. In this case, the temperature offsets applied by the indirect control algorithms are step variations. Such a setup achieves load shedding because decreasing the temperature set-points of the buildings determines a reduction of the consumption. Also in this case, the kickback effect is well visible.

4.5 Discussion

The idea on which the indirect control framework relies is that the consumption can be controlled by means of a consumption incentive signal. It this chapter,

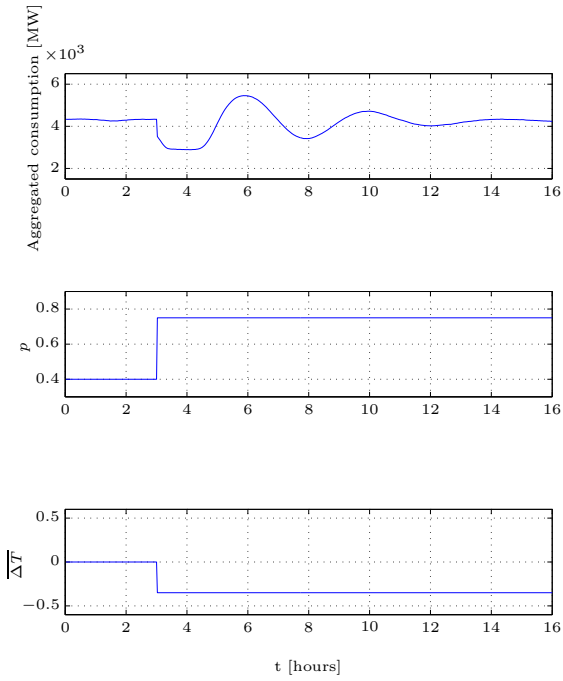

Figure 4.7: The plot in the upper panel shows the aggregated power consumption of the population of space heating units. The plots in the middle and lower panels show the indirect control signal p and the average of the temperature offsets $\Delta T_j,\ j = 0, \ldots, N-1$ applied by the indirect control algorithms, respectively. In this case, the temperature offsets are step signals and not anymore high-pass filtered versions of the indirect control signal.

the response of the aggregated power consumption of a population of TCLs to a stepwise variation of the indirect control signal was studied. It was shown that the reaction of flexible demand, although initially congruent with the variation of the indirect control signal, exhibits a kickback effect. In the case of load shifting, the kickback effect is to ascribe to two causes. The first cause is implicit in the concept of load shifting: if the flexible demand is subject to an energy requirement, the electricity consumption over a certain period must be constant, hence decreasing the power consumption requires a future increase, and vice versa. The second cause is given by the fact that indirect control provokes a synchronization in the states of the TCLs: this leads to amplify the kickback effect because when the synchronized units are all on, the power consumption is much larger than at the steady state condition. In the case of load shedding, only

the latter cause subsists. In Paper **[E]**, it has been also shown that increasing the diversity among the TCLs reduces the kickback effect and contributes to damp the oscillations of the aggregated power consumption.

4.6 Conclusions

In this chapter, the aggregated power consumption of a population of TCLs equipped with an indirect control algorithm was analysed. It has been shown by simulations that a stepwise variation of the indirect control signal causes a consumption kickback and induces transient oscillations in the aggregated power consumption. Clearly, these dynamics are not desirable for the grid and they have to be taken into account if TCLs are meant to deliver power system services.

Chapter 5

Flexible demand in power system applications

In this chapter, four applications of flexible demand are presented. We investigate how to integrate the operation of flexible demand and conventional generation by means of unit commitment, how flexible demand can be used to mitigate congestions in radial distribution networks and how to achieve PV self consumption by means of shifting the consumption of an EWH. In the last application, we relax the requirement of one-way communication, and we show how to limit the aggregated power consumption of a cluster of DSRs by means of a distributed optimization algorithm.

5.1 Introduction

In the future electric grid, a large share of electricity will be produced from renewable energy sources. In such a scenario, flexible demand is expected to contribute to support the grid since conventional generation may not have enough capacity and flexibility to assure secure and reliable operations of the power system.

This chapter presents four applications where flexible demand is used to support power system services through indirect control. We call them *applications*, because in contrast to Chapter 3, we now determine how to generate the indirect control signal according to the service that flexible demand is meant to deliver to the power system.

The first application in Section 5.2 addresses the problem of how to integrate flexible demand into the power system operation. We do this by means of formulating an unit commitment (UC) problem that accounts for the system dynamics of flexible demand. With this setup, we achieve the objective of scheduling the

production of conventional generation together with the activation of DR.

In Section 5.3, flexible demand is used for mitigating congestions in radial LV distribution networks. Although this application does not directly concern with issues related to an increased penetration of renewable generation, it is considered because congestion management is a key priority to assure a reliable delivery of electricity. Moreover, the proposed method can be used for accommodating the charging demand of EVs, whose diffusion is considered a major breakthrough, not only for transportation, but also for the electricity sector since EVs are expected to increase the flexibility at demand side level [65].

In Section 5.4, we address the topic of PV self consumption, which is a policy recently introduced in some European countries that aims at promoting direct utilization of PV electricity as it reduces transmission losses and voltage gradients in the grid. We propose to utilize a domestic EWH to absorb PV generation. The control strategy is formulated using MPC and utilizing an EWH prediction model and forecast of the PV production.

Finally, in Section 5.5, we consider a cluster of domestic refrigeration units and we show how they can be controlled in order to self consume PV electricity, while limiting the aggregated power consumption according to a threshold defined by the power system. In this case, we relax the one-way communication requirement of indirect control and we formulate the control problem using distributed MPC.

5.2 Scheduling flexible demand operation using unit commitment

In existing literature, the performance of control algorithms for DSRs are often evaluated using historical prices from the regulating power market as in [137, 47, 56, 135, 46, 94, 92], and as also done in the attached Paper **[B]** and Paper **[F]**. Such an approach results in an open loop control scheme, because the historical electricity prices do not consider demand response. In order to account for the closed loop interactions between the electricity markets and DR, real-time pricing schemes for small consumers have to be developed. In the Flexpower project [5], it is proposed to modify the setup of the current intraday electricity market allowing DSRs to bid their flexibility in an aggregated way. In [138], Zugno et al. develop a real-time pricing schemes by means of a bilevel optimization which maximizes the profit of an electricity retailer and a consumer, this latter using economic MPC for controlling electric space heating.

In this section, we propose to integrate flexible demand in the operation of the power system using a novel formulation of the UC. UC is an optimization problem used to determine the operation schedule of conventional generating units at a specific time interval with varying loads under different constraints and scenarios [10, 103, 105]. The conventional UC problem is modified by including

a dynamic model that describes the aggregated consumption of a population of DSRs as a function of the indirect control signal. The proposed UC achieves to schedule the activation of DR together with the operation of conventional generating units; solving the UC problem allows to determine the production schedules of the power plants and the indirect control signal for flexible demand. The topic of including DR into a UC problem was presented, for example, in [11], where flexible demand was described as a static function of the price signal. The novelty of the proposed approach consists in using a dynamic model of flexible demand, which allows to account for the dynamics of the aggregated power consumption of a population of TCLs described in the previous chapter.

In the following of this section, the formulation of the proposed UC is presented. As an application of the UC, we show how flexible demand can be used to absorb excess wind generation in a scenario with high wind penetration.

5.2.1 Setup of the unit commitment problem

The UC problem is modelled considering a subset of the power system composed by conventional power generation, wind generation and conventional demand. Besides this traditional setup, the UC problem also includes flexible demand, which is described by a linear dynamic model that expresses the aggregated power consumption of a population of TCLs as a function of the indirect control signal. The model of flexible demand is estimated using measurements of the global power consumption. The setup of the UC problem is sketched in Fig. 5.1. In a real-life application, the proposed method could be applied, for example, in a receding horizon manner, as done with MPC algorithms. At this stage, we do not consider implementation aspects.

5.2.2 Formulation of the unit commitment problem

The unit commitment problem consists of minimizing the following cost function

$$J = J_{\text{gen}} + J_{\text{startup}} + J_{\text{curt}}, \tag{5.1}$$

where on the right-hand side there are the production cost of conventional generation, the startup cost of power plants and the cost associated to performing wind generation curtailment. The production cost is given as

$$J_{\text{gen}} = \sum_{i=0}^{N-1} \sum_{j=1}^{n} \Phi_j P_{ij} T_s + \Psi_j s_{ij} \tag{5.2}$$

$$s_{ij} = \begin{cases} 0, & \text{if } P_{ij} = 0 \\ 1, & \text{if } P_{ij} > 0, \end{cases} \tag{5.3}$$

where Φ_j and Ψ_j are the unitary production cost and fixed cost of the power plant j, respectively. The conventional generation portfolio is composed by n

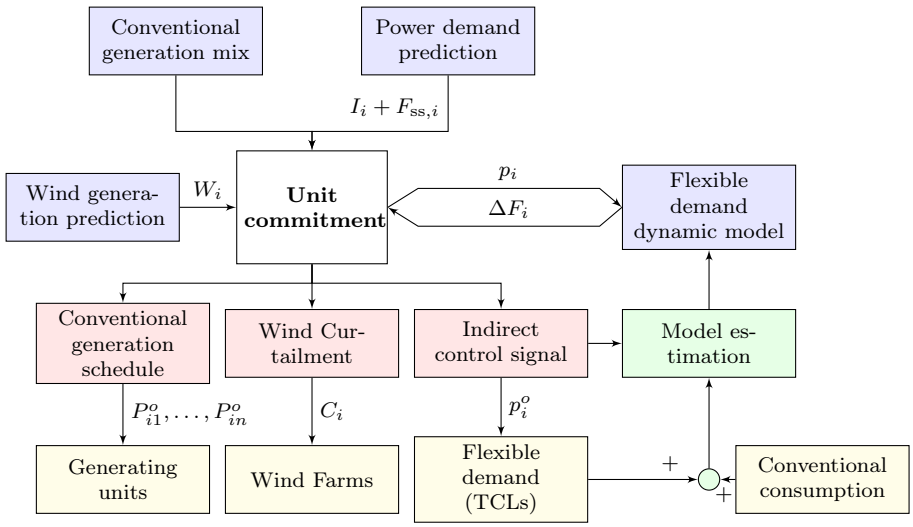

Figure 5.1: Concept of the UC with flexible demand. The blue and the red blocks denote the inputs and the outputs, respectively, of the optimization problem. The yellow blocks indicate the power system operation phase, while the green block highlights the estimation procedure of the model of flexible demand, which is carried out using observations of the aggregated power consumption and of the indirect control signal. In comparison with conventional UC setups, this formulation allows to determine the indirect control signal $p^o(t)$ while taking into account the aggregated dynamic behaviour of flexible demand.

power plants, and the length of the optimization horizon is N. T_s is the duration, in seconds, of the discrete time interval. The binary variable s_{ij} in Eq. (5.3) defines the state (offline or online) of the power plant j during the time interval i. The power plants startup cost is given as

$$J_{\mathrm{startup}} = \sum_{i=0}^{N-1} \sum_{j=1}^{n} \Upsilon_j \left[(s_{ij} - s_{i-1j}) s_{ij} \right], \tag{5.4}$$

where Υ_j is the cost of starting the operation of the generating unit j, and the term in the square bracket is 1 when the power plant is required to start operating, 0 otherwise. The cost of performing wind curtailment is given as

$$J_{\mathrm{curt}} = \sum_{i=0}^{N-1} \alpha C_i T_s, \tag{5.5}$$

where α is a cost coefficient. The reason to implement in the UC the cost of performing wind curtailment is explained in the following. Wind generation is

cost-free and is usually prioritized ahead of conventional generating units; this does not occur when an expensive generating unit delivers power instead of a cheaper one, which does not meet the constraint on the minimum production level: in such a case, a reduction in the global operating cost may be achieved by performing wind curtailment, in order to allow the activation of the cheaper generating unit. Implementing wind curtailment cost, as in Eq. (5.5), prevents such a situation.

The lower generation limits of conventional generating units are given as

$$P_{ij} \geq P_{\min,j}, \text{ if } s_{ij} = 1,\ i = 0, \ldots, N-1,\ j = 1, \ldots, n \tag{5.6}$$
$$P_{ij} = 0, \text{ if } s_{ij} = 0,\ i = 0, \ldots, N-1,\ j = 1, \ldots, n, \tag{5.7}$$

and the upper generation limits are:

$$P_{ij} \leq P_{\max,j},\ i = 0, \ldots, N-1,\ j = 1, \ldots, n. \tag{5.8}$$

The ramp-up constraints of conventional generating units are:

$$P_{i+1j} - P_{ij} \leq R_j,\ i = 0, \ldots, N-1,\ j = 1, \ldots, n. \tag{5.9}$$

The condition that, during power system operation, the consumption should match the demand is implemented as

$$W_i - C_i + \sum_{j=1}^{n} P_{ij} = D_i, \quad i = 0, \ldots, N-1, \tag{5.10}$$

where W_i is the wind production, C_i is the curtailment to the wind production and D_i is the demand, which is given as

$$D_i = I_i + F_i(p_i), \quad i = 0, \ldots, N-1, \tag{5.11}$$

where I_i and F_i are the inflexible demand (or conventional demand) and flexible demand, respectively. The latter is a function of the indirect control signal p_i, and it is described by the dynamic model discussed in the next section.

Constraints not implemented Constraints usually found in UC problems but that were not implemented in the proposed formulation are the minimum uptime and downtime and spinning reserve requirements. The latter is of relevant concern for scenarios with high wind penetration because it can be be used as a security margin against uncertainty of wind generation forecast.

Solving the unit commitment The UC is formulated as the following optimization problem

$$\begin{aligned} \boldsymbol{\theta}^o = \arg\min_{\boldsymbol{\theta}}\ & J \\ \text{s.t.}\ & (5.7) - (5.11), \end{aligned} \tag{5.12}$$

where $\boldsymbol{\theta} = \{\boldsymbol{P_1}, \cdots, \boldsymbol{P_n}, \boldsymbol{p}, \boldsymbol{C}\}$. The optimization in Eq. (5.12) is a MILP (mixed integer linear programming) and allows to determine the generation schedule of the power plants $\boldsymbol{P_1^o}, \cdots, \boldsymbol{P_n^o}$, the amount of wind generation $\boldsymbol{C^o}$ to curtail and the trajectory of the indirect control signal $\boldsymbol{p^o}$. The UC problem is formulated in GAMS and solved using Couenne library.

5.2.3 Inputs of the unit commitment

Conventional generation

The mix of conventional generation is composed considering the currently available statistics on the Danish power system [6], and it is summarized in Table 5.1. Electricity generation costs for coal and gas power plants are from [60] (EU average). Power plants characteristics are summarized in Table 5.2.

Table 5.1: Production costs and generation capacities of conventional generating units.

Kind of plant	Number of plants	Production Cost Φ [\$/MW]	Total capacity [MW]
Coal-fired	1	59	500
Gas CT	2	72	2×100
Hydro	1	150	150

Table 5.2: Characteristics of conventional generation units [120].

Kind of plant	Power output rate of change R_j [% of rated power·min^{-1}]	Minimum power output $P_{\min,j}$[% of rated power]
Coal-fired	2	40
Gas CT	5	50
Hydro	100	0

Although hydro power generation is not present in Denmark, it was included in the generation mix as a flexible generation resource that represents the value of having a strongly interconnected electric grid (by means, for example, of HVDC, high voltage direct current). This is the case of Denmark, whose grid is connected to those of Germany, Sweden and Norway. Such interconnections allow to share regulating power and excess wind generation. The cost of hydro power was chosen deliberately larger than conventional generation because it represents the power that must be imported from or exported to another portion of the power system.

Wind generation

Wind generation profiles are generated from time series of the global Danish wind production (data are from Danish TSO Energinet.dk), and are shown in Fig. 5.2. Thirty daily wind generation profiles were randomly chosen from the available measurements, and have been uniformly scaled in order that their average covers the 50% of the global electricity demand, as the 2020 Danish wind electricity production objective. In such a high wind penetration scenario, the wind exceeds the demand during some periods, hence decreasing the actual proportion of the demand satisfied by wind generation. The objective of the UC simulations presented at the end of this section is to determine if flexible demand can absorb the excess wind generation by means of shifting the consumption.

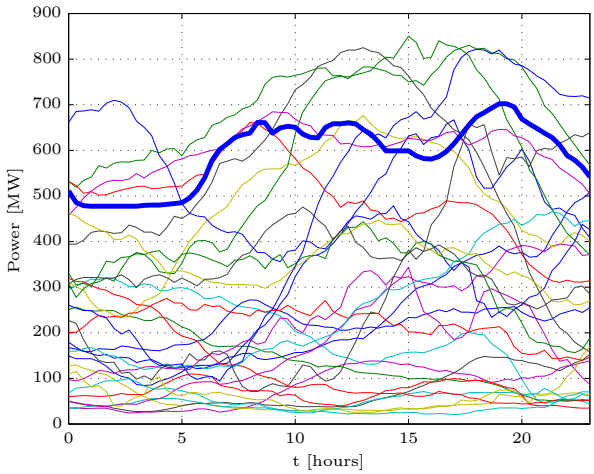

Figure 5.2: Daily wind generation profiles and electricity demand profile (thick blue line). The average of the wind generation profiles covers 50% of the electricity requirement of conventional demand. However, during some periods, the wind production exceeds the consumption: this requires to curtail wind production, hence decreasing the actual proportion of demand supplied by wind. Can the consumption of flexible demand be shifted in order to absorb the excess of wind production?

Each wind generation profile of Fig. 5.2 determines a day scenario that is simulated with the UC model. Real wind generation profiles are preferred to artificial ones (e.g. [91]) because they naturally contain a smoothing effect due to diversity of wind turbines and spatial distribution of the wind resource.

Inflexible demand

Inflexible demand (or conventional demand) is the part of the electricity consumption that does not respond to variations of the indirect control signal. The conventional demand profile is generated aggregating the daily domestic and commercial consumption patterns specified in [19]. Domestic, commercial and aggregated demand profiles are shown in Fig. 5.3. The domestic inflexible consumption is scaled considering 10^5 buildings with a nominal power consumption of 3.1 kW each.

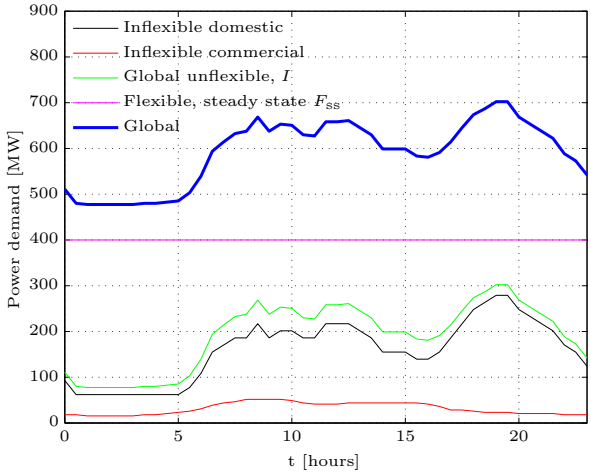

Figure 5.3: Electric power demand profiles.

Flexible demand

We consider the indirect control setup presented in Chapter 4, i.e. a population of 10^5 space heating units that are indirectly controlled by the myopic controller C according to an indirect control signal $\boldsymbol{p}$. The aggregated consumption of flexible demand, introduced initially in Eq. (5.11), is decomposed as

$$F_i(p_i) = F_{\mathrm{ss},i} + \Delta F_i(p_i), \tag{5.13}$$

where the first term on the right-hand side denotes the demand when the indirect control signal does not change since long time (steady state component), and the second term is the transient variation of the aggregated power consumption due to a DRE, and it is a function of the indirect control signal p_i. The steady state component $F_{\mathrm{ss},i}$ is the heat required by the population of buildings, and is shown in Fig. 5.3 with the magenta line: its profile is constant in time because weather

conditions are assumed constant during the day. The transient component of flexible demand is described by means of a black-box model, which is discussed in the next paragraph.

Flexible demand dynamic model The transient variation of the aggregated power consumption of flexible demand is described by the following output error model [75]:

$$\Delta F_i = \frac{\theta_0 + \theta_1 z^{-1}}{1 - \phi_1 z^{-1} - \cdots - \phi_p z^{-p}} + \epsilon_i, \tag{5.14}$$

where $\boldsymbol{\theta} = (\theta_1, \theta_2)$ and $\boldsymbol{\phi} = (\phi_1, \ldots, \phi_p)$ are parameters to be estimated, and ϵ_i is an i.i.d. (independent and identically distributed) Gaussian noise term. The model is based on the empirical property that the variations of the power consumption observed during different DREs are characterized by a similar profile when normalized with respect to the variations of the indirect control signal. This property was observed by simulations of the DSRs population of Chapter 4 and is valid under the assumption that DREs are triggered when flexible demand is at the steady state (in the sense defined in Section 4.3). The degree of the denominator of the model in Eq. (5.14) is chosen using an empirical method that consists in increasing the value of p until the output error of the fitted model does not exhibit relevant variations. The numerator of the model is of the first order, and its parameters are opposite, i.e. $\theta_0 = -\theta_1$: this because the model describes a transient response with a null steady state value. The parameters $\boldsymbol{\theta}$ and $\boldsymbol{\phi}$ are determined applying LS using observations of the detrended global power consumption. Detrending is achieved by removing the average consumption and allows to isolate the transient behaviour of flexible demand from the global consumption, hence avoiding the use of two-way communication with the TCLs; the approximation done in this case is that conventional consumption does not vary during the DR transient.

Assumptions behind the proposed model of flexible demand For the sake of clarity and for paving the way for the future development of the model, the assumptions that were introduced while developing the model of flexible demand are summarized. The assumptions are:

- constant weather conditions were assumed during the day. Considering diurnal weather variations requires to formulate a model for describing the aggregated heat demand of the buildings as a function of outside air temperature and insolation, as done for example in [90, 12]. An alternative approaches consist in utilizing a dynamic thermal model of a building, as for example the one used in Chapter 2, and using a bottom up approach to compute the aggregated power consumption;
- the linear model in Eq. (5.14) was derived using the following empirical property: the transient variations of the aggregate power consumption

of flexible demand during different DREs consist of damped oscillations normalized with respect to the variations of the indirect control signal. This property, thus the model, is valid only when DREs occur at the steady state. This requirement is implemented in the UC by means of adding a constraint which permits to utilize flexible demand only once every twelve hours, that, from Chapter 4, is the time that flexible demand, once activated, takes to reach a new steady state.

5.2.4 Results

Thirty UC scenarios are simulated. Each simulation scenario is 24 hours long and is characterized by a different profile of the wind generation. Two cases are considered in each scenario: in the first case (denoted as case I), flexible demand is not activated, and in the second case (denoted as case II) flexible demand is controlled by the indirect control signal $\boldsymbol{p}^o$, which is generated by the UC framework.

Two simulation scenarios are selected among the thirty for a detailed analysis, and they are shown from Fig. 5.4 to Fig. 5.7. Each figure is composed by two stacked plots. In the upper panel plot, the blue profile shows the amount of demand not supplied by wind generation and the red profile indicates the curtailment of wind generation. The lower panel plot shows the production plans of conventional generating units and, in the case where flexible demand is activated, the variation of the aggregated power consumption of flexible demand (cyan profile).

Table 5.3 and Table 5.4 summarize the simulation results of the two scenarios, and they indicate the amount of wind curtailment that was performed, the proportion of electricity production from wind that was achieved, the daily cost to produce electricity and the amount of hydroelectricity that was used (which represents the source of fast and expensive regulating power).

5.2.5 Discussion

Scenario 1 The plot in the lower panel of Fig. 5.4 shows that, until $t = 13$ h, the demand is supplied by coal generation, which is the cheapest energy resource available in the generation mix. In the next period, wind generation increases and, at $t = 13$ h, the demand not covered by wind production falls below the minimum power production level of coal generation, requiring the activation of gas generation. At $t = 15$ h, the wind production exceeds the demand and hence is curtailed. Fig. 5.5 shows the same scenario, but with the support of flexible demand. At $t \approx 16$ h, flexible demand is activated and increases the power consumption, allowing to decrease the wind generation curtailment. At $t = 19$ h, the kickback effect of flexible demand occurs: this causes a decrease of the amount of consumption. Numerical results in Table 5.3 show that, for

the day in analysis, the activation of flexible demand allows to avoid 40 MWh of wind curtailment.

Table 5.3: Summary of the simulation results of scenario 1.

	unit	Case I	Case II
Wind Curtailment	[MWh]	108	68
Wind Share	[%]	60.3	61.0
Total Generation Cost	[pu]	1	0.97
Hydro energy	[MWh]	5.0	27.8

Scenario 2 The plot in the top panel of Fig. 5.6 shows that there is a considerable amount of excess wind generation during the central part of the day. In the case II, the plot in the lower panel of Fig. 5.7 shows that flexible demand is induced to increase the consumption of nearly 200 MW. The DR kickback effect occurs at time $t \approx 14$ h, and it causes to increase the amount of wind curtailment in respect to case I. The oscillations of flexible demand during the evening hours absorb almost the whole amount of excess wind generation. The results summarized in Table 5.4 show that the contribution of DR allows to decrease by 190 MWh the amount of curtailment to wind generation.

Table 5.4: Summary of the simulation results of scenario 2.

	unit	Case I	Case II
Wind Curtailment	[MWh]	1079	899
Wind Share	[%]	84.6	90.0
Total Generation Cost	[pu]	1	0.95
Hydro energy	[MWh]	100	50

5.2.6 Conclusions

In this section, we proposed the formulation of a UC problem that included a model to describe the dynamics of the power consumption of flexible demand. Flexible demand was represented by a population of space heating units, which were indirectly controlled by means of a consumption incentive signal. The proposed UC framework allowed to schedule the activation of DR together with the operation of conventional generating units: solving the UC problem allowed to determine the consumption incentive signal for flexible demand and the generation schedule of the power plants.

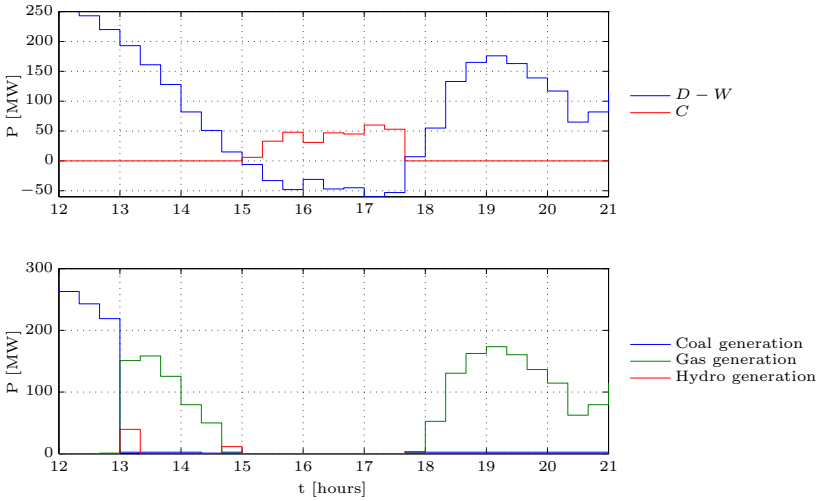

Figure 5.4: Scenario 1, Case I. The plot in the upper panel shows the demand not supplied by wind generation (blue profile) and the curtailment to wind generation (red profile). The plot in the lower panel shows the schedules of conventional generating units.

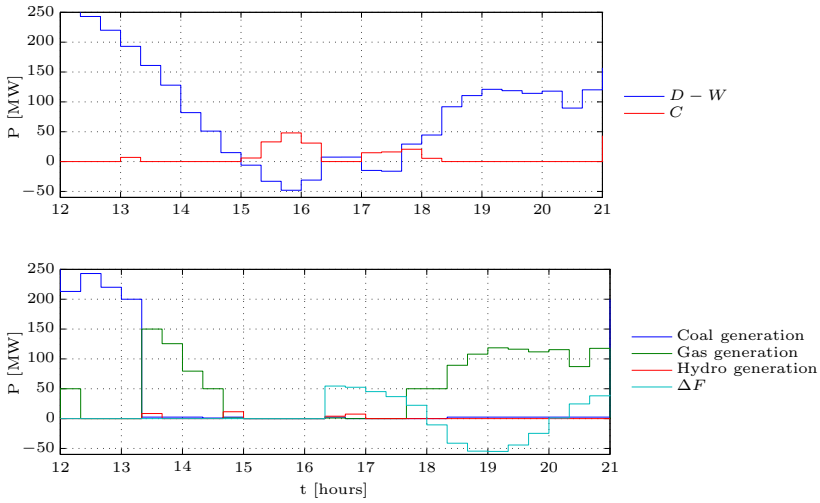

Figure 5.5: Scenario 1, Case II. The transient response of flexible demand, denoted by the cyan line in the lower panel plot, allows to absorb part of the excess wind generation.

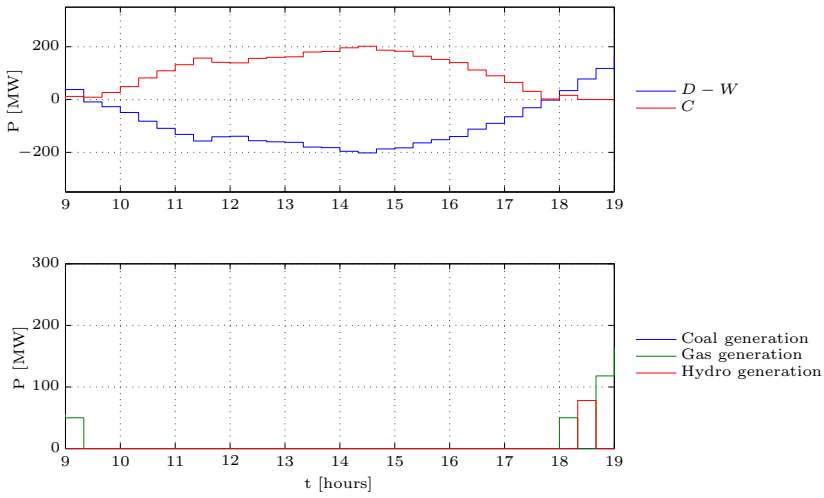

Figure 5.6: Scenario 2, Case I. The plot in the upper panel shows the demand not supplied by wind generation (blue profile) and the curtailment to wind generation (red profile). The plot in the lower panel shows the schedules of conventional generating units.

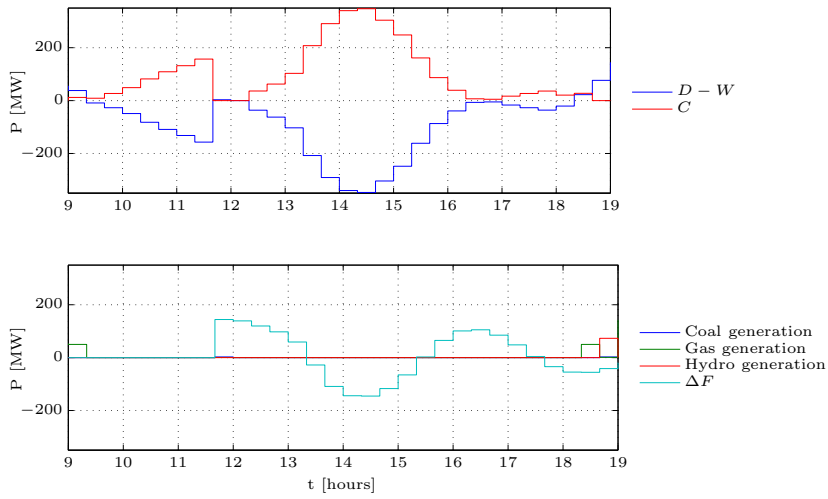

Figure 5.7: Scenario 2, Case II. Flexible demand absorbs the excess wind generation during late morning and evening hours.

5.3 Grid congestion management

In this section, we investigate the topic of using flexible demand for relieving congestions in LV radial distribution networks, which is a key priority for achieving a reliable delivery of the electricity. Congestion management has been extensively investigated especially in connection with transmission lines connecting several portions of the power system [70]. In this context, control-by-price strategies were proposed to reschedule the production and remove congestions from overloaded segments of the network (e.g. [44]). However, these methods only apply to meshed networks. Congestion management in radial distribution networks has been treated in connection with EVs smart charging algorithms in scenarios with high penetration of EVs [58, 116]. In [53], Herter et al. investigate the potential of manually activated demand response with application to peak shaving services, and they estimate that, in average, consumers can reduce the consumption by 5% when required to do so.

In Paper **[D]**, we propose to mitigate congestions in radial distribution networks by means of shifting the consumption of a population of electric space heating units. A feedback controller, implemented at substation level, detects congestions by measuring the power flow through the transformer. When a congestion occurs, the controller discourages the consumption by broadcasting an indirect control signal to the flexible loads of the substation. On demand side level, an indirect control algorithm perceives the variations of the price signal and shifts the consumption of the associated DSR. The work proposed in the paper is loosely based on the study in [28], where a heat pump is controlled in order to decrease congestions in a feeder. The control strategy in [28] was realized with a closed loop controller with statically assigned gains and was simulated in a small grid with one congested node. We extend this configuration, by implementing an auto tuning procedure in order to automatically determine the gains of the regulator according to the sensitivity of flexible demand with respect the consumption incentive signal. We show the proof-of-concept of the proposed congestion management strategy by simulations and using a reference network with seven LV substations and different penetration of flexible demand.

5.3.1 Grid layout

The CIGRE' MV European reference network is used as a case study [19]. The feeders of the reference network are three-phase and either of meshed or radial structure. Each feeder includes a number of laterals at which MV/LV transformers can be connected. The nominal voltage is 20 kV and the system frequency is 50 Hz. The study has been performed in an urban feeder whose main characteristics are:

- 11 MV buses and 11 LV buses;

- 4590 kVA of transformer MV/LV capacity;
- 2.82 km overhead lines and 12.2 km cable lines;
- radial configuration.

The LV network in the substations is not modelled into details. Each substation of the network is composed by 3 controllable loads that represent the aggregated consumption of flexible demand, residential demand and commercial demand. The power consumption of the aggregated flexible demand corresponds to the global power consumption of a subset of a population of DSRs. The size of each subset depends on the nominal power of the transformer of the substation to which flexible demand is connect. The residential and commercial aggregated demands are simulated using the daily consumption patterns described in [19]. In order to show the proof-of-concept of the proposed controller being able to clear congestions, the consumption patterns are scaled by a factor of 1.3.

5.3.2 Flexible demand

Flexible demand is represented by a population of 346 buildings equipped with electric radiators for space heating. The population is generated with the same approach as discussed in Chapter 4, although the buildings are simulated with a second order linear model for a better representation of the thermal transients. The space heating units of the buildings are controlled by the myopic controller A (Section 3.2.1).

5.3.3 Congestion controller

The discrete time control loop implemented in each substation of the network is shown in Fig. 5.8.

Fig. 5.9 shows the structure of the substation controller. The core of the controller is a discrete time PI regulator with gains proportional to the term s_m, which is determined by the auto tuning procedure discussed in the next section.

Determination of the regulator gain s_m

The coefficient s_i is defined as the value of the variation of the indirect control signal $\Delta p_i = p_i - p_{i-1}$ that induces a unitary change of the aggregated power consumption $\Delta P_i = P_i - P_{i-1}$, and it is given as

$$s_i = \frac{\Delta p_i}{\Delta P_{e_i}}, \ \Delta P_{e_i} \neq 0. \tag{5.15}$$

Assuming to know s_i at each instant of time i, the deviation of the indirect control signal that should be applied for changing the aggregated power con-

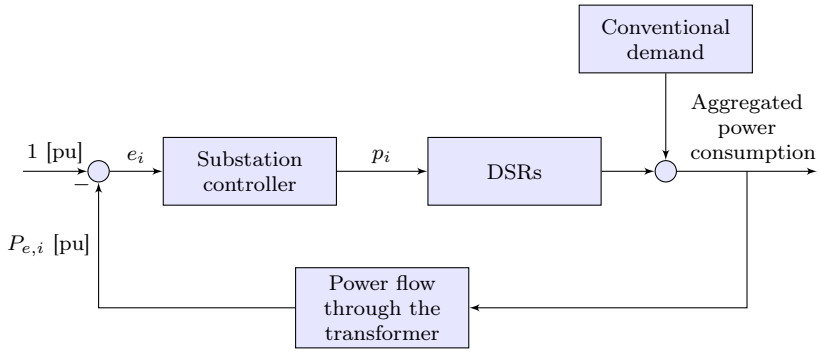

Figure 5.8: The feedback control loop that is implemented in the substations. When the power flow through the substation transformer $P_{e,i}$ exceeds the transformer nominal capacity, the substation controller disincentives consumption of flexible demand by means of the indirect control signal p_i.

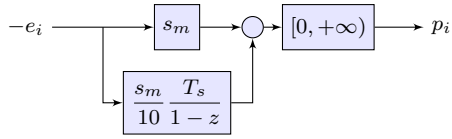

Figure 5.9: The substation controller is a discrete PI regulator with gains proportional to the adaptive coefficient s_m. The objective of the controller is to decrease the power consumption of flexible demand when congestions occur by means of the consumption incentive signal p_i. The saturation block on the output side prevents the controller to incentivize the power consumption when congestions do not occur. The integral regulator is equipped with an anti-windup configuration, which is not shown in the diagram.

sumption of a generic amount x would be simply given as

$$\Delta p_i = x s_i. \tag{5.16}$$

Provided to know the amount of overload x at a given substation, Eq. (5.16) allows to determine the variation to apply to the indirect control signal in order to reduce the consumption of flexible demand and clear the congestion. The term s_i is a time varying quantity and a function of DSRs conditions; moreover, its value is not known at time $t = i$. The method that is adopted in Paper **[D]** consists in replacing the unknown value s_i with the value s_m, which is computed as

$$s_m = \min\{s_{i-1}, s_{i-2}, \dots\}. \tag{5.17}$$

The coefficient s_m is used as the gain of the PI regulator of the substation controller. Determining s_m in Eq. (5.17) requires to evaluate the expression in

Eq. (5.15), and, hence, to access measurements of the aggregated power consumption of the population of DSRs. It is of interest to determine the deviation of the power consumption to variation of the indirect control signal: since conventional demand does not react to the indirect control signal, the measurements of the global power consumption (i.e. the power flow through the transformer) can be used instead of the measurements of the aggregated power consumption of flexible demand; hence, two-way communication with DSRs is not a requirement of the proposed indirect control framework. The adaptive regulator discussed in this section is implemented in all the substations of the network. The controllers do not require any manual intervention for adjusting the gains. An initial training phase is required to determine the value of the coefficient s_m through Eq. (5.17). During operation, s_m is updated on-line, and it is scaled by a forgetting factor in order to allow s_m to be updated with recent values of s_i.

5.3.4 Results and discussion

The auto tuning congestion controller is implemented in each substation of the CIGRE' reference network. Simulations are performed in a co-simulation environment composed by Matlab Simulink and a Python simulation engine. The former is used to simulate the electric network, while the latter performs the simulations of the thermal dynamics of buildings.

Two scenarios A and B are analyzed: scenario A is when congestion controllers are disabled, and scenario B is when they are enabled. The profiles of the power flows through the substations transformers are shown in Fig. 5.11 and Fig. 5.11 for scenario A and B, respectively. Fig. 5.11 shows that, when congestion controllers are not activated, the consumption exceeds of up to 0.3 pu the nominal capacities of the transformers, which, in the plot, are denoted by the black line at 1 pu. The congestions that occur at time $t \approx 20$ h are due to the evening consumption peak of conventional demand.

Fig. 5.11 shows that, when congestions controllers are activated, the congestions are reduced in all the substations. A closer inspection of the profiles in Fig. 5.11 during the time frame when the congestions occur shows that:

- a number of profiles oscillate around 1 pu. This case occurs when s_m underestimates indirect control ability of achieving a shift in the consumption. Flexible demand is very sensitive to the variations of the indirect control signal. The control action is mainly of proportional type and induces the aggregated power consumption to oscillate.
- a number of profiles slowly decreases to 1 pu. The value of the coefficient s_m overestimates the sensitivity of flexible demand to variations of the indirect control signal. In this case, the control action is mainly due to the integral part of the regulator, which slowly disincentives the consumption by increasing the magnitude of the indirect control signal.

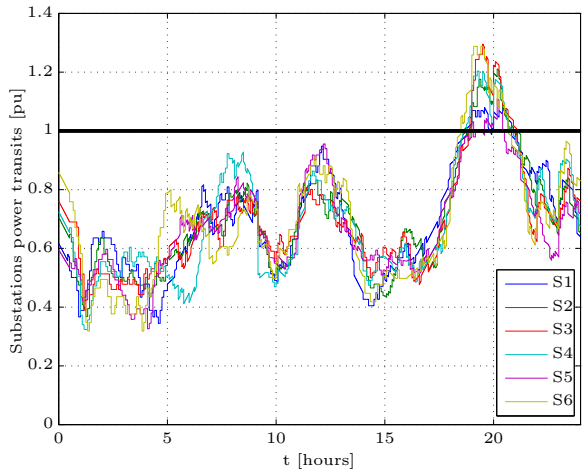

Figure 5.10: The power flows through the transformers of the substations of the network in scenario A, when congestion controllers do not operate. Congestions occur during the evening hours.

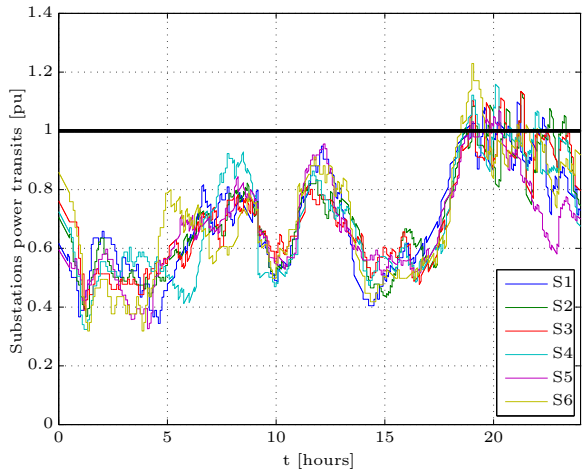

Figure 5.11: The power flows through the transformers of the substations of the network in scenario B, when congestion controllers are active.

- the peak values of all the consumption profiles are reduced and there is a wake of high consumption during night hours. This is due to the kickback

effect of flexible demand described in Chapter 4. However, in this application, the kickback effect does not compromise the overall performance of the congestion controllers because it occurs at late night, when the peak of conventional consumption is over.

Table 5.5 summarizes in numerical form a number of relevant information regarding the power flows through the transformers of the substations of the network. In all the substations, congestion controllers are able to trim the consumption peaks and to achieve consumption mean values close to the unit.

Table 5.5: Substations power transits during congestion.

Power transit	Scenario	S1	S2	S3	S4	S5	S6
peak value	A	1.08	1.21	1.30	1.20	1.11	1.29
	B	1.08	1.09	1.11	1.16	1.07	1.23
mean	A	1.05	1.09	1.15	1.11	1.02	1.16
	B	0.98	0.98	0.98	1.00	1.01	1.02

5.3.5 Conclusions

In this section, it was shown how flexible demand can be controlled by means of a consumption incentive signal in order to mitigate congestions in LV distribution networks. The indirect control signal was generated by a consumption feedback regulator, which was implemented at substation level and detected congestion by measuring the power flow through the transformer. The proposed solution did not require two-way communication with the DSRs. The gains of the regulator were assigned with an auto tuning procedure that identified the elasticity of the demand. It was shown by simulations that the controllers achieved a reduction of the congestion levels during the evening peak consumption period. In the simulations, the kickback effect of flexible demand discussed in Chapter 4 occurred at late night and did not affect the performance of the congestion controllers. We conclude that the dynamics of the considered flexible demand are compatible with the requirements of peak shaving the evening peak of power demand.

An improvement that we envisage to this setup consists in replacing the simple space heating control algorithm with an economic MPC (as those proposed in Chapter 3): this would allow to enhance the performance of flexible demand since the consumption of DSRs is planned in advance. In this case, the forecast of the indirect control signal may be generated using prediction of the consumption of conventional demand. The proposed congestion management could be considered to support the integration of EVs, whose diffusion is of concern for

DSO since it requires reinforcement at distribution level for accommodating the charging demand.

5.4 PV self consumption

With regard to grid connection policies for PV plants, two mainstream approaches are recognized in Europe: net-metering and self-consumption [8]. The former consists in the opportunity for the consumer to inject into the grid the excess PV production and to withdraw it for consumption in a different time frame. In this case, the grid is seen as a long term storage solution, and the consumer pays the difference between the total consumption and total production during a billing time frame (usually one year long). The latter aims at promoting the instantaneous consumption of the generated electricity, and it is referred to as PV self consumption. PV self consumption policies have been introduced in Germany and Italy since 2011 and 2013, respectively. Considering that the PV installed capacity is expected to increase in the coming years [7], PV self consumption is a topic that requires to be investigated since it promotes the transition to a more efficient power system (fewer transmission losses) and reduces voltage gradients in the distribution network, caused by an increased penetration of DG. In the existing literature, control algorithms for achieving PV self consumption using electrochemical storage have been described, for example, in [17, 23]. However, before planning specialized storage devices, it is worth to investigate the potential of flexible demand of achieving PV self consumption since DSRs are normally present at demand side level.

Paper **[C]** presents an active demand side control strategy for shifting the power consumption of a domestic EHW with the objective of absorbing the electricity generated by a PV plant, hence achieving PV self consumption. The methods and main results from the paper are summarized in the following of this section.

5.4.1 Self consumption strategy

We investigate the ability of a domestic EWH to achieve PV self consumption. The self consumption strategy is realized by means of the following MPC

$$\boldsymbol{P^o} = \arg\min_{\boldsymbol{P}} \sum_{i=0}^{N-1} \left| \frac{\max(\boldsymbol{P_s}) - P_{s,i}}{\max(\boldsymbol{P_s})} \right| P_i, \ \max(\boldsymbol{P_s}) \neq 0 \tag{5.18}$$

$$\text{s.t.} \quad T_{i+1} = f(T_i, T_{\text{room},i}, q_i, T_{\text{inlet},i}, P_i), \quad i = 0, \dots, N-1 \tag{5.19}$$

$$T_{\min} \leq T_i \leq T_{\max}, \quad i = 0, \dots, N-1 \tag{5.20}$$

$$P_{\min} \leq P_i \leq P_{\max}, \quad i = 0, \dots, N-1, \tag{5.21}$$

where $\boldsymbol{P^o}$ is the optimized power consumption trajectory of the EWH for $i = 0, \dots, N-1$, $\boldsymbol{P_s}$ is a vector composed by stacking the production forecast of the PV plant for the time horizon $i = 0, \dots, N-1$, P is the consumption of the

EWH, T is the average temperature of the hot water in the tank, $f(\cdot)$ is the dynamic model of the EWH, T_{room} is the temperature of the room where the EWH is located, q and T_{inlet} are the flow [L/s] and temperature of the water flowing out and in, respectively. The inequality constraints in (5.20)-(5.21) determine the allowed ranges of the water temperature and the power consumption, respectively. The cost function in Eq. (5.18) is the sum over the optimization horizon of the power consumption multiplied by a known coefficient, which is a function of the PV production forecast. Such a coefficient can be regarded as a consumption incentive signal, which is small when P_{s_i} approaches the maximum forecasted PV production value (incentivizing the consumption) and vice versa.

The problem in (5.19)-(5.21) is a linear optimization problem and is solved using the methodology presented in Section 3.3.2. The continuous consumption trajectory calculated by the MPC is converted to *on-off* pulses as described in Section 3.4.3.

5.4.2 Models and forecast

In Paper **[C]**, a linear dynamic model of an EWH is formulated. The model was realized applying a mixed white/grey-box methodology and using the approximation that the water in the tank is a mass at uniform temperature. We assumed that the thermal capacity of the EHW is only given by the water content. The thermal resistance of the EWH model was estimated applying LS and using measurements from the experimental 30 L 1.2 kW EWH of Power Flexhouse.

The PV production forecast are realized using a white-box PV model from the literature [67]. The PV model is developed for one of the PV array of SYSLAB, a 5.95 kWp poly-cristalline ground mounted plant. The PV model determines the component of the insolation incident to the panel, which is subsequently converted in the amount of produced power according to an empirical efficiency factor that depends on the technology of the panels and the temperature of the cells. The PV model requires as an input the NWPs of the insolation on the horizontal plane. Grey-box PV models, such as those in [123, 78], could be consider in order to generalize the control strategy to other PV layouts.

The hot water consumption profiles are from [64], and they have been scaled considering the demand of four people.

5.4.3 Results and discussion

In order to evaluate the capability of the MPC to actuate self consumption, the optimized power consumption trajectory calculated by the MPC is compared with the consumption profile of a conventional thermostat. The proposed simulations refer to one step of the receding horizon policy, and they are realized using real PV production data from SYSLAB. In the simulation, deterministic

conditions are assumed for the model of the EWH, while the forecast of the insolation are from DTU Wind Energy department, hence subject to forecast errors. The other relevant information regarding the simulation scenarios are summarized in Table 5.6.

Table 5.6: Summary of the simulation scenarios of PV self consumption.

Component	Attribute	Value
PV plant	Nominal power	2 kWp
Water Heater Model	Nominal power	1.26 kW
	Tank capacity	30 l
	R (model parameter)	$2\ K \cdot W^{-1}$
Thermostatic controller	Temperature set-point	$55 \pm 5°C$
MPC controller	Optimization length	12 hours

Fig. 5.12 shows the PV production profile (yellow area) and the consumption profiles of thermostatic and MPC controllers. From Fig. 5.12, it is possible to notice that the MPC is able to shift the consumption in the central part of the day, when PV production is available.

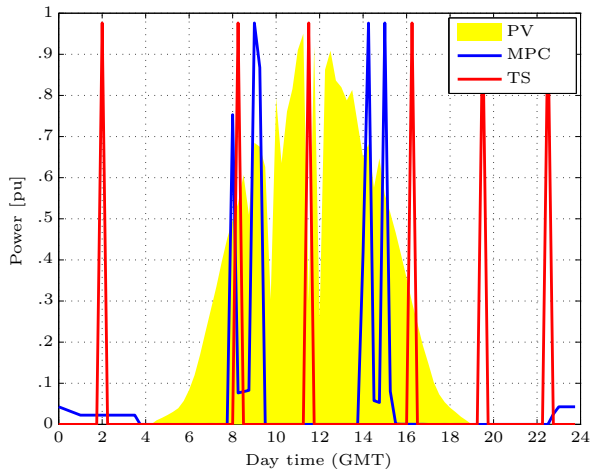

Figure 5.12: Power consumption profiles of the thermostatic control action and the MPC controller (red profile and blue profile, respectively). The yellow surface denotes the PV production.

Table 5.7 summarizes in numerical form the composition of the power require-

ments of the two controllers, and it shows that the MPC achieves to increase by 200% the amount of PV self consumption with respect to conventional thermostatic control. The last column of Table 5.7 shows the economic revenues of the controllers, which is computed using the Italian tariffs of electricity consumption, PV feed-in and PV self consumption[1]. According to an estimation done in Paper **[C]**, such a solution could save 18 € per year.

Table 5.7: Summary of the operations of the controllers during a 24 hours simulation.

Controller	Energy sold [kWh]	Energy bought [kWh]	Self consumed [kWh]	Revenue [€]
Thermostat	11.86	1.28	0.57	2.15
MPC	10.75	0.21	1.67	2.31

5.4.4 Conclusions

Increasing the penetration of PV generation in the distribution network increases transmission losses and voltage gradients along the feeders. In order to mitigate these problems, PV self consumption policies have been introduced in some European countries. In this section, the ability of a domestic EWH to absorb PV generation and achieve PV self consumption was shown by simulations. The EWH control strategy was formulated by means of a MPC strategy and considering forecast of the PV production. The MPC controller increased by 200% the amount of PV self consumption with respect to conventional thermostatic control. Since flexible consumption is present at demand side level, the proposed setup should be considered instead of or for supporting specialized PV self consumption configurations, such as those based on electrochemical storage.

5.5 Transactional control of a cluster of freezers

Paper **[A]** describes the modelling process of a domestic refrigeration unit, namely a freezer. Several models are proposed and, using the methodology defined by the grey-box framework, are analysed and tested against each other in order to determine which one gives the best representation of the relationship between electricity consumption and freezer temperature. Models are formulated using SDEs, and they are estimated using MLE and measurements from the Power Flexhouse freezer. Both linear and nonlinear models are considered. Nonlinear models are based on a reversed Carnot cycle representation of the

[1]Erratum: Paper **[C]** reports wrong values in the last column of Table II: the values are inverted for the two controllers and column header should be *(economic) revenue* rather than *energy bill*; this error does not affect any of the conclusions stated in the paper. The correct version of the table is Table 5.7 of this thesis.

refrigeration cycle [84]. The single phase induction motor that drives the compressor of the freezer is not described in the model, and its efficiency is assumed lumped in the estimated value of the freezer COP. Literature review, extended descriptions and validation results of the modelling process are discussed in the attached paper.

As an application of the model, we propose here a transactional control strategy for a cluster of freezers. The objective of the proposed transactional control is to achieve PV self consumption and peak shaving the aggregated power consumption of the cluster. This latter requirement is implemented by means of constraining the power flow at the virtual point of common coupling (PCC) of the freezers according to a threshold defined by the power system. The control strategy is realized using the MPC framework and it is solved using dual decomposition (DD) algorithm.

In Section 5.5.1, we present the model of the freezer that we use in this application. In Section 5.5.2, the formulation of the transactional control strategy is presented. Section 5.5.3 is for results and discussion. Conclusions are stated in Section 5.5.4.

5.5.1 Freezer model

According to Paper **[A]**, the model that better describes the thermal dynamics of the freezer is a nonlinear third order model. In the model, the nonlinearity is introduced by modelling the refrigeration cycle COP as a function of the reversed Carnot cycle:

$$\mathrm{COP}(T) = \eta \frac{T + 273}{T_{\mathrm{room}} - T}, \tag{5.22}$$

which is nonlinear in the freezer temperature T, and where η is an efficiency factor that describes how much the real COP differs from the theoretical one. In the linear models of the freezer, the COP is essentially described by a zero order Taylor expansion of Eq. (5.22), calculated at the freezer temperature set-point. For this application, we chose the second order linear model which, according to the statistics developed in the paper, performs a 20 minutes ahead prediction with a mean and standard deviation error of 0.223 °C and 0.914 °C, respectively, against −0.044 °C and 0.825 °C of the best model. In spite of the worse performance (that could be accounted for by means of using robust MPC, e.g. [57]), the linear model has been chosen because it is of easier implementation in the MPC. The deterministic continuous state space representation of the

model is given as

$$\begin{bmatrix} \dot{T} \\ \dot{V}_e \end{bmatrix} = \begin{bmatrix} -\frac{1}{C_a R_w} - \frac{1}{C_a R_e} & \frac{1}{C_a R_e} \\ \frac{1}{C_e R_e} & -\frac{1}{C_e R_e} \end{bmatrix} \begin{bmatrix} T \\ V_e \end{bmatrix} + \begin{bmatrix} \frac{1}{C_a R_w} & 0 \\ 0 & -\frac{\mathrm{COP}}{C_e} \end{bmatrix} \begin{bmatrix} T_{\mathrm{room}} \\ P_e \end{bmatrix}, \tag{5.23}$$

where C_a, C_e, R_w, R_e are the estimated parameters presented in the paper, T and V_e are the temperatures of the freezer and freezer envelope, respectively, T_{room} is the temperature of the room where the freezer is located and P_e is the electric power consumption of the freezer.

5.5.2 Problem formulation

It is given the problem of determining the electric power consumption trajectories of n freezers in order to promote PV self consumption and limiting the power flow at the PCC. Initially, the optimization problem is formulated in a centralized way. Later, it is shown how the PCC constraint can be moved in the cost function by means of introducing a Lagrangian function, and how the centralized optimization problem can be decomposed and solved using the methodology of dual decomposition (DD) algorithm.

Centralized optimization The part of the optimization concerned with PV self consumption is formulated in the same way as done in Section 5.4, i.e. by means of introducing a consumption incentive signal that is a function of the forecast $\boldsymbol{P_s}$ of the PV production. For each freezer j of the cluster, the PV self consumption objective function is defined as

$$J_j = \sum_{i=0}^{N-1} \frac{1}{P_{s,i}} P_{e,ij}, \quad P_{si} \neq 0, \tag{5.24}$$

where $P_{e,ij}$ is the electric power consumption of the freezer j at the discrete instant of time i, and N is the length of the optimization horizon. The centralized optimization is formulated merging the cost functions J_j and the constraints of each MPC problem for $j = 1, \ldots, n$. Constraining the power flow at the virtual PCC is achieved imposing that the sum of the power consumption trajectories of the freezers should be lower than $\boldsymbol{P_{\mathbf{max}}}$, as indicated in Eq. (5.28). The

centralized linear MPC is as follows:

$$\boldsymbol{\mathcal{P}}^o = \arg\min_{\boldsymbol{\mathcal{P}}} \sum_{j=1}^{n} J_j \tag{5.25}$$

$$\text{s.t. Freezer model, } \; i = 0, \ldots, N-1, \; j = 1, \ldots, n \tag{5.26}$$

$$\text{Freezer constraints, } \; i = 0, \ldots, N-1, \; j = 1, \ldots, n \tag{5.27}$$

$$\sum_{j=1}^{n} P_{e,ij} < P_{\max i}, \;\; i = 0, \ldots, N-1, \tag{5.28}$$

where

$$\boldsymbol{\mathcal{P}} = \left[\boldsymbol{P^o_{e\,1}}, \ldots, \boldsymbol{P^o_{e\,n}} \right] \tag{5.29}$$

is the decision vector obtained by stacking the power consumption profiles of all the freezers. The freezer model and freezer constraints in (5.26)-(5.27) will be introduced later for convenience.

Lagrangian function The inequality constraint in (5.28) can be expressed as

$$\sum_{j=1}^{n} \left(P_{e,ij} - \frac{1}{n} P_{\max i} \right) < 0, \;\; i = 0, \ldots, N-1. \tag{5.30}$$

We define a new cost function (said Lagrangian, $\mathcal{L}$) as

$$\mathcal{L} = \sum_{j=1}^{n} J_j + \boldsymbol{\lambda}^T \left(\boldsymbol{P_{e}}_j - \frac{1}{n} \boldsymbol{P_{\max}} \right), . \tag{5.31}$$

The equation above is obtained by moving the constraint (5.30) in the cost function (5.25) by means of a vector of weight coefficients $\boldsymbol{\lambda} \in \mathbb{R}^N$. The new optimization problem is defined as

$$\boldsymbol{\mathcal{P}}^o = \arg\min_{\boldsymbol{\mathcal{P}}} \mathcal{L} \tag{5.32}$$

$$\text{s.t. } \; (5.26), (5.27). \tag{5.33}$$

Dual decomposition The Lagrangian cost function (5.31) can be written as

$$\mathcal{L} = \sum_{j=1}^{n} \mathcal{L}_j, \tag{5.34}$$

where

$$\mathcal{L}_j(J_j, \boldsymbol{\lambda}, \boldsymbol{P_{e}}_j) = J_j + \boldsymbol{\lambda}^T \left(\boldsymbol{P_{e}}_j - \frac{1}{n} \boldsymbol{P_{\max}} \right). \tag{5.35}$$

Eq. (5.35) is the Lagrangian function of the refrigeration unit j of the cluster. The DD algorithm [15] allows to split the optimization in (5.32)-(5.33) into n subproblems that can be solved in parallel. The algorithm consists in iterating

$$\begin{aligned} \boldsymbol{P_e}_j^{k+1} = \arg\min_{\boldsymbol{P_e}_j^k} \ & \mathcal{L}_j^k(J_j, \boldsymbol{\lambda}^k, \boldsymbol{P_e}_j^k) \\ \text{s.t.} \ & (5.26), (5.27) \end{aligned}, \quad j = 1, \dots, n \tag{5.36}$$

$$\boldsymbol{\lambda}^{k+1} = \boldsymbol{\lambda}^k + \alpha \left(\sum_{j=1}^{n} \boldsymbol{P_e}_j^{k+1} - \boldsymbol{P_{max}} \right), \ \alpha > 0 \tag{5.37}$$

until a stop criteria is met. In Eq. (5.37), the coefficient α determines the speed of convergence of the algorithm, and the index k is the iteration step of the algorithm.

Summarizing, the initial centralized optimization problem (5.25)-(5.28) has been decomposed in n subproblems, and the PCC constraint (5.28) has been moved into the cost function of the subproblems by means of a vector of Lagrangian multipliers $\boldsymbol{\lambda}$. The DD algorithm consists in solving, at each iteration, n optimizations in parallel plus carrying out the updates of the weights of the Lagrangian multipliers. This procedure is repeated until a stop criteria is verified, that is given by meeting the PCC constraint. The pseudo code of the DD algorithm is shown in Listing 2.

Algorithm 2 Dual decomposition algorithm.

```
Initialize λ^0, α
k = 0
while Σ_{j=1}^{n} P_ej^k ≤ P_max do
    for j = 1, ..., n do
        P_ej^{k+1} = solve (5.36)
    end for
    λ^{k+1} = from (5.37)
    k = k + 1
end while
```

The interesting part of such a method is that the mathematical decomposition matches the physical distribution of the units, i.e. (5.36) is a MPC problem that can be solved in the same fashion as the economic MPC strategies of Chapter 3. On the other hand, the $\boldsymbol{\lambda}$ update in Eq. (5.37) requires the presence of an aggregator, i.e. a service that collects information from all the freezers of the cluster, as shown in Fig. 5.13. The DD algorithm requires bidirectional communication, because each freezer has to communicate its intermediate power consumption intention $\boldsymbol{P_e}_j^k$ to the aggregator.

The role of the Lagrangian multipliers $\boldsymbol{\lambda}$ is to carry the information on the state of congestion at the PCC into the single MPC problems: when the PCC is

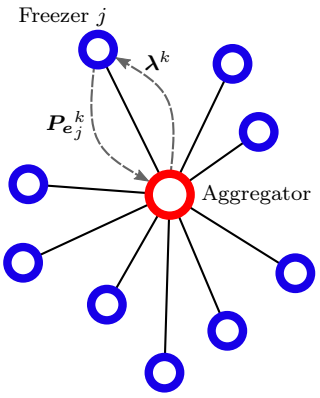

Figure 5.13: Layout of the transactional control strategy. The freezers and the aggregator of the cluster are denoted by the blue circles and red circle, respectively. At each step k of the DD algorithm, the information exchanged between the freezers and the cluster are the intermediate power consumption trajectories $\boldsymbol{P_e}_j^k,\ j = 1, \dots n$ and the consumption incentive signal $\boldsymbol{\lambda}^k$. For convenience of visualization, only the communication between the freezer j and the aggregator is shown.

congested, the values of the weight coefficients $\boldsymbol{\lambda}$ increase and discourage the consumption of the freezers. Although the problem is solved as the economic MPC at demand side level, the DD algorithm pursues to maximize the benefit for the community rather than achieving those of the single consumers.

5.5.3 Results and discussion

A cluster of 25 freezers is considered. Each freezer is modelled using the second order linear model discussed above, where the thermal capacity has been randomly variated across the population for accounting for differences among units. User behaviour is not considered at this stage. We use the simplification that the consumption of the freezers is continuous instead of being *on-off* type. This allows to maintain a convex structure of the MPC problems and it does not require MILP algorithms. The constraints of the local MPC problem, which were not indicated explicitly in (5.36), are

$$T_{i+1j} = f(T_{ij}, C_{aj}, P_{e,ij}, T_{\text{room}}),\ \ i = 0, \dots, N-2,\ \ j = 1, \dots, n \tag{5.38}$$

$$0 \leq P_{e,ij} \leq P_{e,\max},\ \ i = 0, \dots, N-2,\ \ j = 1, \dots, n \tag{5.39}$$

$$T_{\min} \leq T_{ij} \leq T_{\max},\ \ i = 0, \dots, N-2,\ \ j = 1, \dots, n, \tag{5.40}$$

where $f(\cdot)$ in Eq. (5.38) is the discretized freezer thermal model introduced above, and the other symbols are defined, together with the simulation conditions, in Table 5.8.

Table 5.8: Conditions for the simulation of the transactional control strategy.

Parameters	Description	Value
$T_{\max}$	Maximum freezer temperature	$-15\,^{\circ}\mathrm{C}$
$T_{\min}$	Minimum freezer temperature	$-23\,^{\circ}\mathrm{C}$
T_{room}	Room temperature	$22\,^{\circ}\mathrm{C}$
$P_{e,\max}$	Maximum freezer power consumption	$60\,\mathrm{W}$
$C_{a,j}$	Thermal mass	$\in \mathcal{N}\left(C_a, C_a^2/100\right)$
N	MPC optimization horizon length	$15\,\mathrm{h}$

The PV production forecast used to calculate the consumption incentive signal in Eq. (5.24), are shown in Fig. 5.14.

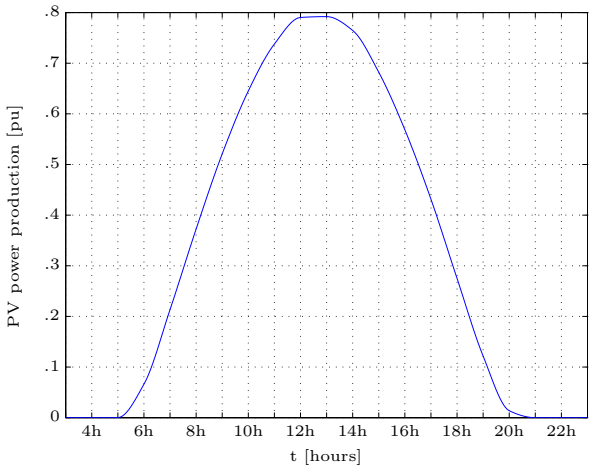

Figure 5.14: PV solar production during the day considered for simulations. This production profile is used for determining the consumption incentive signal for incentivizing PV self consumption.

In order to appraise the performance of the transactional control strategy, we compare the aggregated consumption profile of the same cluster of freezers when controlled by the DD algorithm, an economic MPC and a traditional thermostatic control. The simulation of the freezers controlled by the economic MPC is performed using the same simulation framework as the DD algorithm in Listing 2, with the difference that we do not perform any iteration, i.e. for each $j = 1, \ldots n$ the MPC cost function is given by $\mathcal{L}_j^0$ and the optimized power

consumption trajectory of the freezer is $\boldsymbol{P}_{e_j}^{1}$.

The aggregated power consumptions of the three clusters of freezers are shown in Fig. 5.15. The magenta profile is the aggregated power consumption of the group of thermostatically controlled freezers. In this case, the freezers consume power according to the their needs. Since thermostatic control does not implement any demand response ability, it does not react either to the self consumption signal or the PCC constraint. It is worth to note that, except for evening hours, the PCC constraint is steadily larger than the thermostatic consumption. If this is not the case, the freezers MPC strategies may fail because not enough transmission capacity is available.

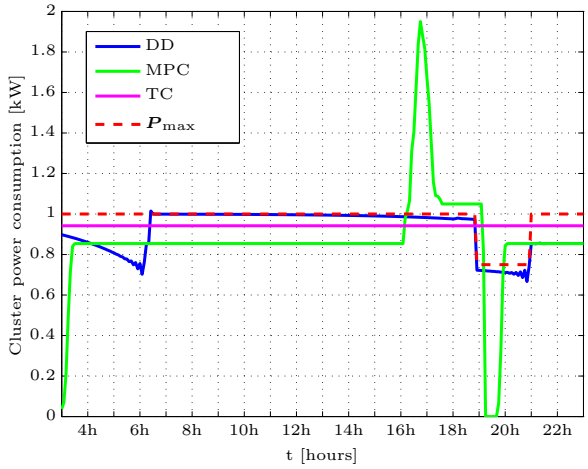

Figure 5.15: Aggregated power consumption of the cluster of freezers under three different control strategies: DD (dual decomposition), economic MPC and conventional thermostatic control. The red profile shows the maximum allowed power flow at the PCC.

The aggregated power consumption of the freezers controlled by MPC does not react to the self consumption signal for the whole central part of the day. The freezers are kept at the minimum consumption level and they do not have enough flexibility to absorb the relative slow varying PV generation. At $t \approx 16$ h, the freezers manage to absorb part of the afternoon production; this allows the freezers to reduce the consumption in the evening hours, when the constraint on the power flow at the PCC becomes stricter.

When the cluster is controlled by the DD algorithm, the aggregated power consumption is kept at the value of the PCC constraint during the whole central part of the day. In this case, freezers are incentivized to consume because the

PV self consumption policy. Fig. 5.16 shows the temperature profile of each freezer of the cluster. It is visible that, during the day, the freezers tend to store thermal energy by means of decreasing their respective temperatures. Storing energy allows the freezers to decrease the power consumption when required by the PCC constraint at $t = 19$ h.

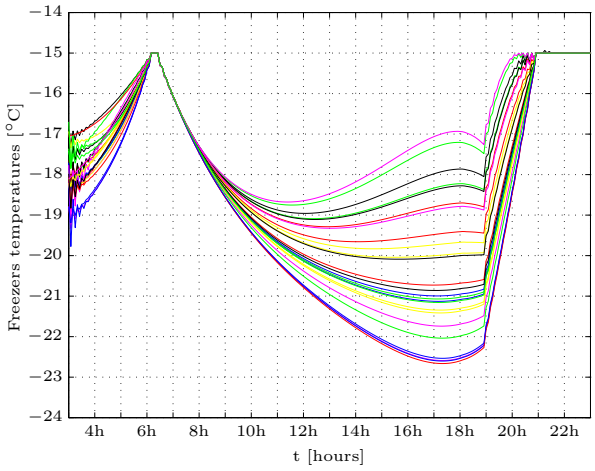

Figure 5.16: Temperature profiles of the freezers of the cluster when controlled by the DD algorithm. It is visible that the freezers store thermal energy in the central part of the day by means of decreasing the temperature of the associated thermal mass. This allows the freezers to reduce the consumption when required to do so at time $t = 19$ h.

5.5.4 Conclusions

A transactional control strategy was formulated with the objectives of peak shaving the aggregated power consumption of a cluster of freezer and achieving PV self consumption. Initially, the problem was formulated as a centralized optimization, which was obtained by means of aggregating the single MPC problems in a single optimization and adding a constraint to limit the power flow at the virtual PCC. It was shown how the centralized optimization can be decomposed by means of moving the PCC constraint in a new cost function using Lagrangian multipliers.

The mathematical decomposition of the centralized optimization matches with the layout of the cluster, in the sense that each subproblem of the DD algorithm is solved by one of the freezers of the cluster. The DD algorithm requires the existence of an aggregator, which is due to collect the power consumption

intention of each freezer and update the weights of the Lagrangian multipliers according to the state of congestion of the PCC.

Compared to the economic MPC strategies discussed in Chapter 3, the proposed transactional control pursues to maximize the benefit of the community rather than the single profits of the owners of the freezers. In fact, the transactional control formulation implements the additional constraint regarding the maximum allowed power flow at the PCC, which serves to redistribute among the freezers the duty of reducing the consumption.

This method can be regarded as an evolution of the indirect control approach because it allows to determine the consumption incentive signal for the DSRs. Although dual decomposition requires two-way communication, the information that the freezers has to exchange with the central aggregator is of reduced amount, and it consists of the intermediate power consumption trajectories of the MPC only; no other information (such as the type of DSR, DSR operational constraints, consumer comfort requirements, local conditions) are required.

Chapter 6

A energy replacement strategy for building space heating

This chapter presents a model predictive control strategy for a smart building equipped with conventional electric radiators, combined heat and power generation and storage. This application has been named energy replacement because the control is able to switch among several energy sources according to the dynamic cost of the electricity, which reflects the need for regulating power of the grid.

6.1 Introduction

The operation of the future power system will be characterized by the interplay between renewable generation, storage, flexible demand and conventional generation. Motivated by this perspective, in Paper **[F]** we develop a control strategy that combines the operation of flexible demand, storage and combined heat and power (CHP) generation to provide space heating to a building and regulating power to the grid according to the electricity cost.

The setup considered in Paper **[F]** is a smart building equipped with electric radiators for space heating and a CHP/storage system, composed by a fuel cell, an electrolyzer, two tanks and electric compressors to store the reactants. The diagram of the setup is sketched in Fig. 6.1. The control strategy is developed using the MPC framework, and its task is to schedule the operation of the components in order to minimize the operating cost, while obeying consumer and components constraints. We named this application *energy replacement* to indicate that the control can choose among multiple space heating sources according to the cost of the electricity. From the grid operation point of view, such a setup is expected to provide greater flexibility because energy can be

stored not only in the thermal energy of the building, but also by means of producing and storing the reactants.

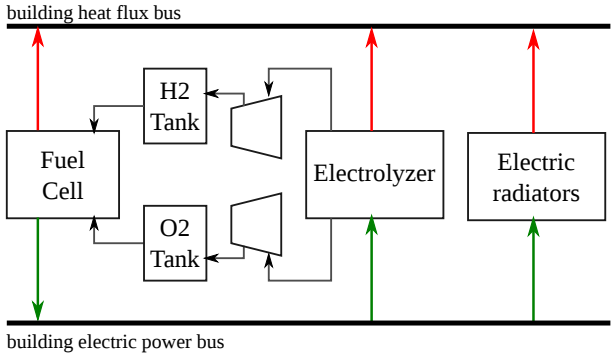

Figure 6.1: The components of the energy replacement strategy. Building space heating is provided by conventional electric radiators, a fuel cell and an electrolyzer. The reactants are pressurized by compressors and stored in tanks.

In this chapter, the main contributions of Paper **[F]** are summarized. Section 6.2 outlines the formulation of the MPC strategy, Section 6.3 summarizes the results and Section 6.4 states the conclusions. The attached paper also describes the formulation of a grey-box model of a proton exchange membrane fuel cell (PEMFC), which was realized using measurements from the 15 kW PEMFC of the Distributed Electrical Systems Laboratory at EPFL. In Appendix C, we describe the general properties of PEMFCs and the experimental setup that was adopted to collect the measurements required by the grey-box modelling process.

6.2 Energy replacement economic model predictive control

The energy replacement strategy is formulated using the MPC framework. The cost function of the underlying optimization problem is as follows

$$J = \sum_{i=0}^{N} \big[-P_{FC,i} + P_{EL,i} + P_{co,i} + P_i \big] p_i + s_i S_i + \lambda_i \big[n_i - n_{\max} \big], \qquad (6.1)$$

where $P_{FC,i}$ is the power generated by the FC, $P_{EL,i}, P_{co,i}, P_i$ are the power consumptions of the electrolyzer, compressors and electric radiators, respectively, p_i is the electricity cost, s_i is the FC state (*on* or *off*), S_i is the startup cost and the last term is a cost for penalizing those operation schedules that requires the FC to go through more than $n_{\max}$ on-off cycles (n_i is the number of FC on-off

cycles). The FC power is given as

$$P_{FC,i} = i_{FC,i} \cdot v_{FC,i}\big(T_{FC,i}, i_{FC,i}\big) \tag{6.2}$$

where $i_{FC,i}$ is the current supplied by the FC, $v_{FC,i}(\cdot)$ is the model of the stack voltage (or model of the polarization curve) and $T_{FC,i}$ is the temperature of the FC stack, which is described by the following discrete time dynamic model:

$$T_{FC,i+1} = f\big(T_{FC,i}, i_{FC,i}, T_{\text{room},i}, Q_{FC}\big), \tag{6.3}$$

where T_{room} is the temperature of the room where the FCs located and Q_{FC} is the heat extracted by the FC cooling system. In a similar fashion as the FC, the electrolyzer power $P_{EL,i}$ in Eq. (6.1) is given as

$$P_{EL,i} = i_{EL,i} \cdot v_{EL,i}\big(i_{EL,i}\big), \tag{6.4}$$

where $v_{EL,i}(\cdot)$ is determined using an electrolyzer model from the literature. Finally, the compressors power $P_{co,i}$ in Eq. (6.1) is described as a function of i_{EL}, i_{FC} and the reactants pressures according to a model we developed. All the mathematical models used in the replacement strategy are discussed into details in Paper **[F]**.

The constraints of the components of the energy replacement setup are:

$$0 \leq i_{FC,i} \leq i_{FC,\max} \tag{6.5}$$
$$0 \leq i_{EL,i} \leq i_{EL,\max} \tag{6.6}$$
$$p_{H_2,\min} \leq p_{H_2,i} \leq p_{H_2,\max} \tag{6.7}$$
$$T_{FC,i} \leq T_{FC,\max} \tag{6.8}$$
$$i_{FC,i+1} - i_{FC,i} \leq \Delta i_{FC,\max} \tag{6.9}$$
$$P_{\min} \leq P_i \leq P_{\max} \tag{6.10}$$
$$T_{\min} \leq T_i \leq T_{\max}, \tag{6.11}$$

which are for limiting the current of FC and electrolyzer, the pressure of hydrogen in the tank, the FC temperature, the FC current rate of change, the power of the electric radiators and the temperature of the building. The constraints for the oxygen pressure of the tank are not implemented because they are redundant in the optimization: in fact, the oxygen and hydrogen quantities are defined by the respective stoichiometric coefficient of the water reaction; hence, the pressure of the oxygen can be derived by knowing the hydrogen pressure and the sizes of the storage tanks.

The MPC problem is solved minimizing the cost expression in Eq. (6.1) subject to the operation constraints and the models of the components. The decision variables of the problem are the FC current, the electrolyzer current and FC

cooling system heat flux trajectories. The optimization problem is given as

$$\begin{aligned} \theta^o = \arg\min_{\theta} \; & J \\ \text{s.t.} \; & (6.5) - (6.11) \\ & \text{Building model} \\ & \text{FC model} \\ & \text{Electrolyzer model} \\ & \text{Compressor model} \\ & \text{Tank model} \end{aligned} \tag{6.12}$$

where $\theta = \{\boldsymbol{i}_{FC}, \boldsymbol{i}_{EL}, \boldsymbol{Q}_{FC}\}$. For convenience of visualization, the models of the component are not shown in (6.12). The reader is referred to Paper **[F]** for the mathematical formulation of the models. The optimization in (6.12) is a nonlinear MIP (mixed integer programming) and is formulated in GAMS and solved using CONOPT algorithm.

6.3 Results and discussion

The performance of the energy replacement strategy is compared with the performance of a conventional economic MPC, whose setup is composed by a building with electric radiators only. In order to evaluate the extent to which the two setups are able to track the variations of the indirect control signal, several scenarios are simulated in Paper **[F]**. The simulations scenarios are characterized by sinusoidal price signals with different periods. Among those proposed in the paper, we show one selected simulation scenario with the objective of illustrating the energy replacement principle. The price signal is shown Fig. 6.2, and the operation of the economic MPC and energy replacement MPC are shown in Fig. 6.3 and Fig. 6.4, respectively.

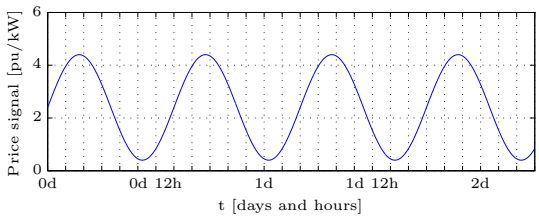

Figure 6.2: The artificial price signal used to compare the energy replacement MPC and economic MPC.

Both controllers show the tendency of consuming power when the electricity cost is low, as shown in the plots in the lower panels of Fig. 6.3 and Fig. 6.4. During

the period with large electricity prices, the energy replacement MPC activates the FC in order to export electricity to the grid and increase the profit.

The operation of the energy replacement MPC is illustrated in Fig. 6.5 and Fig. 6.6, which show the power consumption of the components and the heat flux contributions of radiators, FC and electrolyzer to building space heating, respectively.

Economic revenue Table 6.1 shows the total cost of electricity achieved by three different controllers: energy replacement MPC, economic MPC and thermostatic, the last two not implementing replacement and not equipped with the FC-electrolyzer system. Costs are referred to a five days period and are calculated using the regulating prices of the NordPool intra-day electricity market. The larger flexibility of the energy replacement setup allows to achieve a cost saving of 25% and 20% in respect to thermostatic control and economic MPC, respectively.

Table 6.1: Cost of the electricity requirements of the controllers during a 5 days simulation.

Configuration	Electricity cost [EUR]
Energy replacement MPC	7.27
Economic MPC	9.10
Thermostatic control	9.70

6.4 Conclusions

In Paper **[F]**, a energy replacement strategy for a smart building has been developed. Energy replacement is defined as the ability of the consumer to switch among several sources for supplying space heating according to a dynamic electricity price. Simulations showed that the proposed energy replacement MPC was able to schedule the operation of radiators, FC, electrolyzer and compressors in order to reduce the global operating cost while obeying to comfort and components constraints. From the point of view of the power system, the achievement of the paper was the development of a control framework that was able to integrate the operation of flexible demand and storage and provide an extended amount of flexibility to support the operation of the grid.

In the process of developing this application, a novel dynamic grey-box model of a PEMFC was developed and is presented in Paper **[F]**.

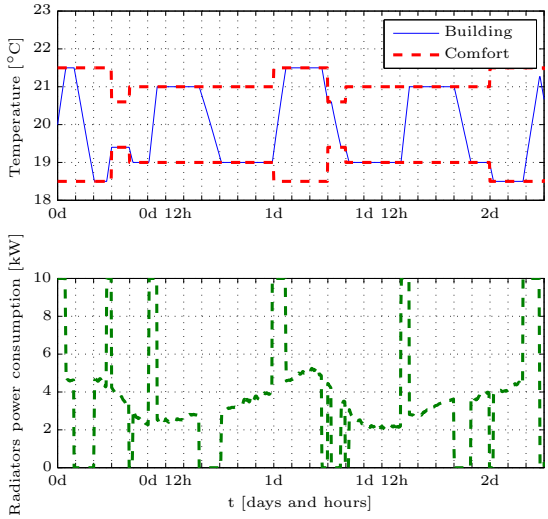

Figure 6.3: Economic MPC operation. The plot in the upper panel shows the temperature of the building (blue profile) and the consumer comfort range (red profile). The plot in the lower panel shows the space heating electric power consumption.

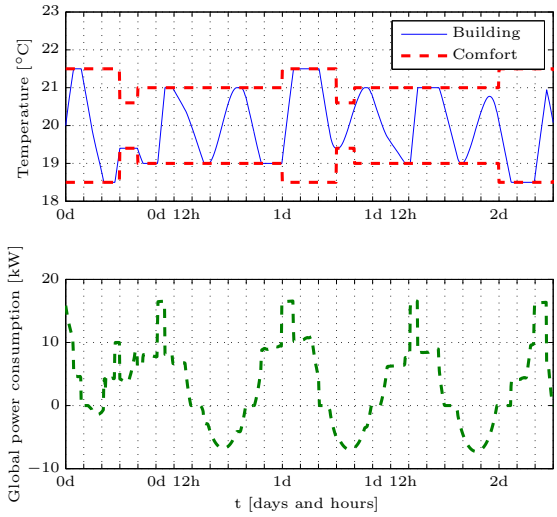

Figure 6.4: Energy replacement MPC operation. Negative values in the plot in the lower panel indicate that electric power is exported to the grid.

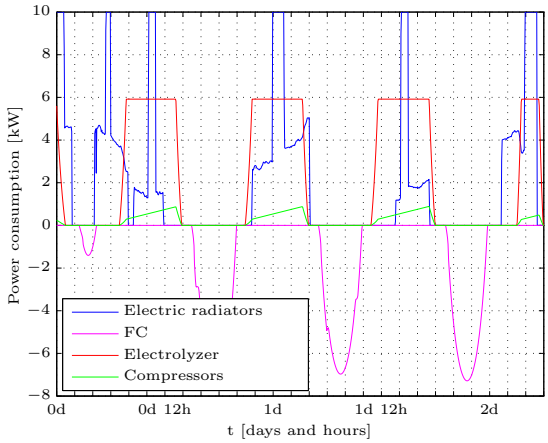

Figure 6.5: Power consumption profiles of the components of the energy replacement strategy.

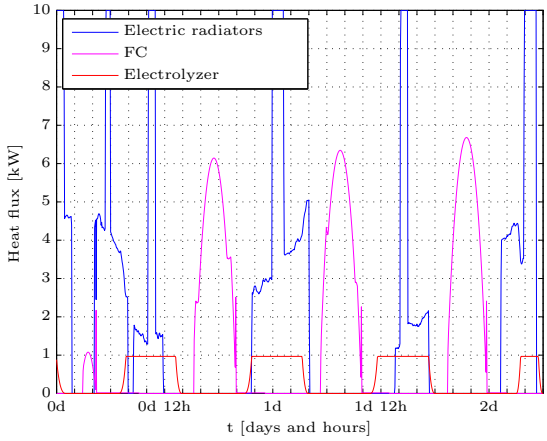

Figure 6.6: Contributions in terms of heat flux supplied to the space heating of the components of the energy replacement strategy.

Chapter 7

Conclusions

7.1 Thesis overview and main results

This thesis addressed the topic of control of flexible demand to provide support to the operation of the electric power system. We focused on the indirect control approach, a framework that enables demand response by means of a consumption incentive signal (e.g. dynamic electricity cost) and relies on one-way communication. A key aspect of the indirect control framework is achieving a shift in the consumption of the individual units as well as determining how the contribution of flexible demand (in particular the aggregated response) can be used to support the power system. A central part of the thesis work was to describe the nature of the dynamics of flexible demand and investigate how it can be utilized in the operation of the power system considering the dynamics of the flexibility and important operational issues, such as UC, self consumption of PV electricity, grid congestion and peak shaving.

In Chapter 2, the concept of flexibility was defined, and the flexibility associated with the operation of selected DSRs was quantified by means of Monte Carlo simulations and benchmarked with the storage capacity of a number of electrochemical batteries. Simulations showed that the DSRs with the largest storage capacity are electric space heating units, followed by EWHs and domestic refrigeration units.

In Chapter 3, the indirect control algorithms for achieving a shift in the consumption of single DSRs were investigated. Several algorithms were formulated, from simple with few requirements up to model predictive control (MPC). Their performance were evaluated by means of hardware-in-the-loop simulations using Power Flexhouse as experimental site. It was shown that MPC achieves the best

performance in terms of consumer comfort and reduction of the operation costs. On the other hand, the MPC framework is complex since it requires a model of the DSR and forecast of the indirect control signal.

The paradigm on which the concept of controlling flexible demand relies is that, although the power consumption of single DSRs is negligible, the aggregated and coordinated change of consumption of large populations of DSRs may have relevant size, and hence it can be used to support the operation of the grid. This stated the need for investigating the aggregated power consumption of a large population of DSRs. In Chapter 4, we showed that the indirect control of a population of TCLs introduces significant dynamic effects in the aggregated power consumption. This phenomena must be taken into account if flexible demand is meant to supply power system services.

In Chapter 6, four applications of flexible demand to support power system operations were presented. The first application consisted in integrating the operation of flexible demand, conventional generation and non dispatchable renewable generation by means of the UC formulation. UC is a well established method used for determining the operation schedule of conventional generating units at a specific time interval with varying loads under different constraints and scenarios. The novelty of the proposed approach consisted in accounting for the aggregated dynamic behaviour of a population of DSRs, which was modelled as a function of the indirect control signal. The proposed UC allowed to determine the consumption incentive signal for flexible demand.

In the second application, we looked at how flexible demand can be used to mitigate congestion in radial distribution networks, which is a key priority for assuring a reliable delivery of the electricity. A population of electric space heating units was controlled according to the state of congestion of the grid by means of a consumption incentive signal, which was generated by an auto tuning feedback controller placed at substation level. It was shown that the proposed framework is able to mitigate congestion in all the simulated substations of the network.

The third application concerned the use of flexible demand for implementing PV self consumption, which is a policy that has been introduced in a number of European countries with the objective of mitigating the impact of a large penetration of PV generation in the distribution network. A PV self consumption strategy for an EWH was developed by means of MPC and considering forecast of the PV production. We showed by simulations that the proposed strategy was able to shift the consumption of the EWH during periods with PV production, allowing to increase by 300% the amount of PV self consumption compared to traditional thermostatic control.

In the fourth application, we developed a transactional control strategy with the objective of limiting the aggregated power consumption of a cluster of DSRs.

The transactional control method was developed using the dual decomposition algorithm, and consisted in each DSR of the cluster to solve an economic MPC problem and communicate the resulting optimized power consumption profile to an aggregator, which was in charge of computing the consumption incentive signal. Although the single DSRs solved the same type of MPC as those discussed in Chapter 3, the proposed transactional control strategy pursued to maximize the benefit of the community rather than achieving minimum operation costs of the single consumers. In contrast to previous applications, transactional control of DSRs required two-way communication. As far as the communication infrastructure is concerned, we think that communication requirements do not represent a relevant distinguishing factor in favor of indirect control schemes with one-way communication. It is reasonable to assume that communication with DSRs will be implemented over the Internet, which is a mature technology that counts on a well established infrastructure and that intrinsically allows for two-way communication. Although, control schemes based on two-way communication must face the increased complexity of managing the feedback signals and information of a large number of DSRs. In this regard, the proposed transactional control method was effective because it required to communicate the consumption incentive signal and the power consumption trajectories only. The other information of the DSRs, such as characteristics and consumer constraints, were elaborated locally, allowing to simplify the task of the aggregator (since it had to elaborate power consumption data only) and reduce the amount of data to communicate.

In Chapter 6, in an effort to integrate the operation of flexible demand and storage with the objective of increasing the amount flexibility of the demand, we presented an *energy replacement* MPC strategy for space heating. The objective of the energy replacement method was to schedule the operation of flexible demand, storage and combined heat and power generation while respecting the temperature comfort of the consumer and supply regulating power to the grid according to a dynamic electricity price. The energy replacement method was applied to a setup composed by a smart building, conventional electric radiators, a fuel cell, an electrolyzer and tanks to store the reactants. Simulation results showed that the energy replacement method achieved lower operation costs than setups controlled by economic MPC and thermostat.

In the process of developing these results, we also proposed novel validated mathematical models of a domestic freezer and a PEM fuel cell. The dynamic models were obtained applying a grey-box methodology and using measurement from experimental units: a domestic freezer available in Power Flexhouse (DTU Elektro) and the 15 kW PEMFC of DESL microgrid facility (EPFL), respectively. The models are intended for simulation purposes or use with MPC strategies.

7.2 Main contributions

The central theme of the thesis was to incorporate the indirect control concept in frameworks that allowed to generate the consumption incentive signal for DSRs according to the service that flexible demand was meant to deliver to the grid, and while considering the dynamics of flexibility. In the applications proposed in the thesis, the intrinsic open loop nature of the indirect control approach (which, in general, is not an appealing method for controlling a system) was resolved by means of implementing:

- feedback controllers, as done for mitigating congestions in distribution networks;
- MPC strategies, as done for the UC and the transactional control method.

The results in Chapter 5 showed that the methods developed in the thesis were able to provide support to different services of the grid by means of utilizing the flexibility of DSRs. The main limitation of flexible demand consisted of the limited amount of storage capacity of DSRs, which did not allow to shift the consumption for long periods of time. The effects of the restricted flexibility, in confluence with the consumption kickback of TCLs, were evident in the simulations of the UC, where the use of flexible demand allowed to reduce the wind generation curtailment by marginal amounts only. In those applications where the need for electricity reduction was for shorter periods, the use of flexible demand allowed to achieve better performance. The problem of the limited amount of flexibility was tackled by developing the energy replacement strategy, which achieved to integrate the operation of flexible demand, storage and CHP generation.

7.3 Future work and perspectives

There are several directions to investigate for extending the contributions of this thesis.

The UC framework was proposed with the objective of integrating the operation of flexible demand and conventional generating units. An immediate continuation of this work consists of improving the adaptive prediction model that describes the aggregated power consumption of flexible demand. The main limitation of the proposed model was that it could capture the dynamics of flexible demand only when variations of the indirect control signal occurred at steady state. We believe that improving the model of flexible demand will eventually allow the UC to generate safe pulse variations of the indirect control signal in order to mitigate the kickback effect of flexible demand, which represents a significant concern when dealing with large populations of DSRs.

Although the proposed UC structure was scalable with respect to flexible demand (because variations of the population of DSRs could be captured by the adaptive flexible demand model), the topic of mixing different types of DSRs in the flexible demand portfolio needs to be further investigated. In fact, different types of DSRs (i.e. space heating and EHWs) have different levels of flexibility and this may require different dynamic models to describe the aggregated consumption.

An aspect that needs to be addressed in the proposed UC is how to tackle the uncertainties related with the demand and the intermittent renewable generation. This could be done, for example, by means of stochastic or robust optimization formulations [10]. It is worth to remind that the formulation of the proposed UC did not account for several operational aspects of a real power grid: in order to account for more advanced aspects of the grid operation (such as limits on transmission lines and reactive power requirements), the implementation of a secured constrained unit commitment (SCUC) may be considered [122].

As a perspective of the proposed transactional control strategy, we could imagine a hierarchical structure of heterogeneous clusters of DERs, individually controlled using transactional control, and with the overall objective of achieving controllability according to explicit power set-points from the grid. This structure may be considered as the control framework of a *virtual power plant*.

The proposed UC and transactional control strategies represent two well distinct indirect control approaches for integrating flexible demand in the power system. The former approach was congruent with the traditional framework of indirect control, i.e. it relied on one-way communication only, while the latter opened up the possibility of using two-way communication. As a future work, we envisage a comparative analysis between the two proposed strategies, including also existing control schemes from the literature (e.g. [13, 68]). The analysis should consider aspects such as efficiency and effectiveness of supplying power system services using flexible demand, stability properties, scalability, reliability, requirements, costs and robustness against uncertainties.

Considering that the estimated storage capacities of EVs and electric space heating units are of the same order of magnitude (as we showed in Chapter 2), we suggest investigating the use of the proposed congestion management framework with application to accommodate the charging demand of EVs (as an alternative or as a support to smart charging algorithms). Introducing EVs in the demand mix opens the perspective of researching on coordinated control strategies for domestic flexible demand and EVs. For example, the operation of domestic DSRs can be shifted in order to support the EVs charging demand, and EVs can be used to support power system operation by means of V2G (vehicle-to-grid) systems, which will allow to deliver and withdraw precise amounts of power thanks to power electronic interfaces. In this context, coordinated control strategies can count on the extended amount of flexibility provided by EVs batteries, which

have a charging demand that is perfectly predictable (provided that the residual and the desired final SOCs are known) because, in contrast to domestic flexible demand, is not subject to consumer behavior and environmental conditions.

Appendix A

Grey-box stochastic modelling

A.1 Grey-box modelling

Grey-box methodology is a modelling technique that allows to model a dynamic system by incorporating the physical knowledge of the process with evidence obtained from experimental data. The adopted grey-box procedure is composed by six steps, which are described in the following.

Experiments design Given a process or a device to model, suitable physical quantities should be selected for measurements. The process should be excited in all the frequency operation range so to explore all the dynamics of the system. A convenient signal to use for probing the system is the PRBS (Pseudo Binary Random Signal), that is a signal that assumes two states (on and off) and whose duty cycle is randomly chosen from a uniform distribution. Ideally, two datasets should be available, one for parameters estimation and a second one for validation of the model.

Data acquisition and measurements post-processing The physical quantities of interest should be measured using appropriate sensors, discretized with convenient sampling time, sampled at opportune resolution and stored. Data post-processing might be required to remove from the measurements information not inherent to the physical process to model.

Model formulation This phase consists in identifying a set of suitable physical relationships that describes the nature and the working principles of the process to model.

Parameters estimation The aim of this phase is to find the most suitable set of values for the parameters of the model. Two approaches are usually possible. The first one is based on minimizing the sum of the squared output errors over the observation horizon (OEM, Output Error Method). The second one is based on maximizing the likelihood function of the observation (MLE, Maximum Likelihood Estimation) [75], i.e. determining the set of parameters that maximizes the probability of observing the events described by the measurements.

Model validation This phase consists in verifying that the model with the freshly identified parameters is actually able to describe the physical phenomena it was intended for. For example, by evaluating any correlations in the model 1-step ahead prediction errors (or residuals) it is possible to infer if the model can capture all system dynamics or not.

Model expansion If the validation process is not satisfactory, an expansion of the model should be considered, for example by adding a new state, new parameters or an alternative representation of the physical process. Each time a new model is defined, the parameters identification and validation procedures should be repeated again (as discussed in the previous two paragraphs). Once the new model and the values of its parameters are available, statistical tests (e.g. likelihood ratio test [77, 89]) should be performed in order to verify if the model extension that has been introduced is meaningful. This allows to avoid overfitting due to an excess of parameters.

A.2 Continuous time stochastic modelling (CTSM)

CTSM is a R library that performs continuous time stochastic modelling. In CTSM, models are formulated using state space representation, and the unknown parameters are estimated from measurements using maximum likelihood estimation (MLE).

Maximum Likelihood Estimation

Given a model with parameters $\boldsymbol{\theta}$, the problem is to find a set of parameters that maximizes the likelihood function of a set of measurements $\Upsilon(k)$, defined as follows:

$$\Upsilon(k) = [\boldsymbol{y}_k, \boldsymbol{y}_{k-1}, \cdots, \boldsymbol{y}_1] \tag{A.1}$$

The likelihood function L is defined as the joint probability of the measurements given the parameters, as given in Eq. (A.2).

$$L\big(\boldsymbol{\theta}; \Upsilon(k)\big) = p\big(\Upsilon(k)|\boldsymbol{\theta}\big) \tag{A.2}$$

$$= \left(\prod_{j=1}^{k} p\big(\boldsymbol{y}_j|\Upsilon(j-1), \boldsymbol{\theta}\big) \right) p(\boldsymbol{y}_0|\boldsymbol{\theta}) \tag{A.3}$$

For passing from Eq. (A.2) to Eq. (A.3), the rule $P(A \cap B) = P(A|B)P(B)$ has been applied k times to form a product of conditional probability densities. The following notation is introduced:

$$\hat{\boldsymbol{y}}(k|k-1) = E[\boldsymbol{y}(k)|\boldsymbol{y}(k-1), \boldsymbol{\theta}] \tag{A.4}$$

$$R(k|k-1) = V[\boldsymbol{y}(k)|\boldsymbol{y}(k-1), \boldsymbol{\theta}] \tag{A.5}$$

The values of Eq. (A.4) and Eq. (A.5) are obtained by applying a Kalman filter [115], conventional if the model to estimate is linear and time invariant, or extended if the model is time variant or nonlinear.
The one step prediction error of the model is defined as:

$$\boldsymbol{\epsilon}(k) = \boldsymbol{y}(k) - \hat{\boldsymbol{y}}(k|k-1). \tag{A.6}$$

By assuming that the conditional probability are Gaussian distributed, the likelihood function Eq. (A.3) can be written as follows

$$L\big(\boldsymbol{\theta}; \boldsymbol{y}(k)\big) = \left(\prod_{j=1}^{k} \frac{\exp\big(-\frac{1}{2}\boldsymbol{\epsilon}(j)^T R(j|j-1)^{-1}\boldsymbol{\epsilon}(j)\big)}{\sqrt{\det(R(j|j-1))}\sqrt{2\pi}^{k}} \right) p(\boldsymbol{y}_0|\boldsymbol{\theta}). \tag{A.7}$$

Defining $l = -\ln(L)$, l can be written as:

$$\begin{aligned} l\big(\boldsymbol{\theta}; \boldsymbol{y}(k)|\boldsymbol{y}_0\big) = \frac{1}{2}\sum_{j=1}^{k} \ln\big(\det(R(j|j-1))\big) + \boldsymbol{\epsilon}(j)^T R(j|j-1)^{-1}\boldsymbol{\epsilon}(j) \\ + \frac{1}{2}\ln 2\pi \sum_{j=1}^{k} N \end{aligned} \tag{A.8}$$

Maximizing the log likelihood function is equivalent to minimize the expression in Eq. (A.8). The parameters of the model are found using the following optimization

$$\hat{\boldsymbol{\theta}} = \arg\min_{\boldsymbol{\theta}} l\big(\boldsymbol{\theta}; \boldsymbol{y}(k)|y_0\big). \tag{A.9}$$

Appendix B

Notes on optimization

B.1 General formulation

The conventional notation for a mathematical optimization problem is shown in Eq. (B.1), where $\boldsymbol{x} \in \mathbb{R}^n$ is the optimization variable and $f_i, i = 0, \ldots, m$ and $h_i - 1, \ldots, p$ are functions $\mathbb{R}^n \to \mathbb{R}$ [16].

$$\begin{aligned} \min \quad & f_0(\boldsymbol{x}) \\ \text{s.t.} \quad & f_i(\boldsymbol{x}) \leq 0, \ i = 1, \ldots, m \\ & h_i(\boldsymbol{x}) = 0, \ i = 1, \ldots, p \end{aligned} \tag{B.1}$$

The variable $\boldsymbol{x}$ is called *optimization variable*. Functions $f_i, i = 1, \ldots, m$ and $h_i, i = 1, \ldots, p$ describe inequality and equality constraints, respectively.
Solving the optimization problem in Eq. (B.1) consists in finding a $\boldsymbol{x}$ that minimizes the function $f(\boldsymbol{x})$ and that satisfies the m equalities $f_i(x) = 0$ and the p inequalities $h_i(x) \leq 0$. If such a $\boldsymbol{x}$ exists, it is called solution of the problem.
An optimization problem that does not have constraints is called unconstrained.

B.2 Convex optimization

The optimization problem (B.1) is convex when it meets three additional requirements: the objective functions f_0 is convex, the inequality constraint functions $f_i, i = 1, \ldots, m$ are convex and the equality constraint functions $h_i, i = 1, \ldots, p$ are affine, i.e. in the form $\boldsymbol{a}^T\boldsymbol{x} = \boldsymbol{b}$. A function f is said convex if its domain [1],

[1] A convex set is defined as the set of points such that the line connecting each couple of points of the set lies entirely in the set.

dom$f$, is convex and

$$f\big(\theta x + (1-\theta)y\big) \leq \theta f(x) + (1-\theta)f(y), \tag{B.2}$$

for all $x, y \in \mathbf{dom}f,\ 0 \leq \theta \leq 1$ [16]. Examples of convex functions are linear functions in $\mathbb{R}$, affine functions on $\mathbb{R}$, positive quadratic functions on $\mathbb{R}$ and the negative logarithmic function on $\mathbb{R}^+$.

The most appealing property of convex optimization problems is that the solution of the problem, if exists, is globally optimal. Moreover, solution methods for convex optimization problems are quite well established [16].

Least squares Least squares (LS) is a type of unconstrained convex problem whose solution can be found in a closed form. An example of the application of LS is polynomial regression. Consider the problem of determining the coefficients of a polynomial of degree n given $\boldsymbol{x},\ \boldsymbol{y} \in \mathbb{R}^p,\ p > n$ which are a vector of input values and observations, respectively. The value of the polynomial in x_0 is given as

$$\hat{y}_0 = a_0 + a_1 x_0 + \ldots + a_n x_0^n. \tag{B.3}$$

Writing Eq. (B.3) for $0, \ldots, p-1$ and using the matrix product leads to

$$\hat{\boldsymbol{y}} = H\boldsymbol{p}, \tag{B.4}$$

where the input matrix

$$H = \begin{bmatrix} 1 & x_0 & \ldots & x_0^n \\ 1 & x_1 & \ldots & x_1^n \\ \vdots & \vdots & \ddots & \vdots \\ 1 & x_{p-1} & \ldots & x_{p-1}^n \end{bmatrix} \tag{B.5}$$

and the vector of coefficients $\boldsymbol{p} = [a_0, \ldots, a_n]$ have been introduced. The matrix H cannot be inverted because $p > n$, and a reasonable approach to determine p is to minimize the norm of the residuals squared, where the residuals are defined as the difference between the observations the polynomial output.

$$||r||^2 = (\boldsymbol{y} - H\boldsymbol{p})^2 = \boldsymbol{p}^T H^T H\boldsymbol{p} - 2\boldsymbol{y}^T H\boldsymbol{p} + \boldsymbol{y}^T\boldsymbol{y} \tag{B.6}$$

whose minimum can be found by setting its gradient respect to $\boldsymbol{p}$ to zero:

$$2H^T H\boldsymbol{p} - 2\boldsymbol{y}^T H = 0 \tag{B.7}$$

$$\boldsymbol{p} = (H^T H)^{-1} H^T \boldsymbol{y} \tag{B.8}$$

Appendix C

Proton exchange membrane fuel cells

C.1 Proton exchange membrane fuel cells generalities

A fuel cell is an electrochemical device that allows the electrons that are exchanged during a chemical reaction to flow in a external electric circuit, hence generating electric power. The chemical elements which are used in the conversion process are a fuel and an oxidizing agent, usually oxygen and hydrogen. In some applications, hydrogen is supplied by means of fuel reforming technologies, for example using methane [106]. The main FC technologies are e.g. PEM (Proton Exchange Membrane), solid oxyde and alkaline fuel cells [72]. We consider a PEMFC directly supply by hydrogen and oxygen. PEMFCs are mainly developed for automotive applications and are characterized by high power density, high durability and resistance to corrosion and capability to work at low temperature (20 °C-80 °C). The components of a PEMFC system are:

- fuel cell stack composed by individual cells placed in series in order to increase the voltage available at the stack terminals;
- inlet manifold systems (pipelines and valves) to allow the reagents (oxygen and hydrogen) to reach the stack;
- humidifiers adding water to the reactants to assure proper hydration of the membrane;
- drainage system to collect the water that is produced in the reaction;
- compressor to recirculate the oxygen in excess in the inlet circuit. This is because PEMFCs work in excess of oxygen assuring higher reactant pressure and higher conversion efficiency;
- thermostatically controlled cooling system to extract the heat in excess;

- local control system to implement control loops and allow communication;
- tank for the hydrogen supply;
- tank for the oxygen supply (or air compressor, in the case of automotive applications).

C.1.1 The PEMFC reaction

The working principle of PEMFCs is shown in Fig. C.1. The anode and the cathode are separated by a membrane and they are electrically connected by a load.

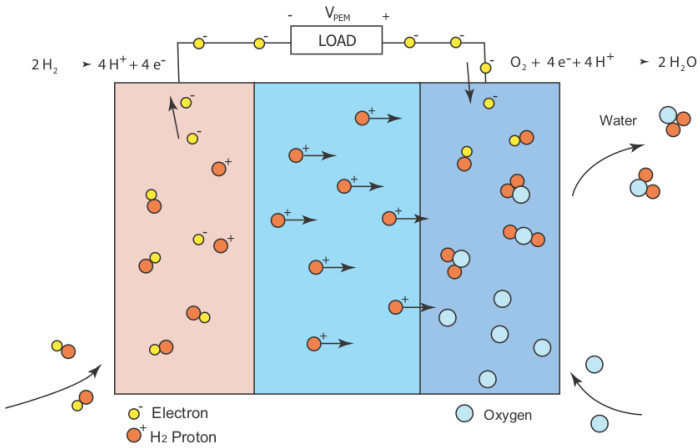

Figure C.1: Fuel cell reaction [102].

Hydrogen is supplied at the anode, where the action of the catalyst provokes the molecule to split into positive charged ions and free electrons, according to the reaction

$$H_2 \rightarrow 2H^+ + 2e^-. \tag{C.1}$$

The electrolyte membrane that separates the cathode from the anode allows the positive hydrogen ions to flow through while blocking the electrons, which are forced through the electric load. At the cathode side, both hydrogen ions and electrons combine with the oxygen forming water according to the reaction

$$2H^+ + 2e^- + \frac{1}{2}0_2 \rightarrow H_2O. \tag{C.2}$$

Hydrogen flow The amount of hydrogen consumed during the reaction is calculated starting from the value of the electric current provided by the FC.

This because the current depends on the number of electrons and the only path for the electrons is the electric load. According to the international system of units, the current i [A] is defined as the amount of electric charge [C] per second. Hence the number of electrons in one second is given by

$$\frac{\text{number of electrons}}{t} = 6.24 \times 10^{18} i. \tag{C.3}$$

Each molecule of hydrogen has two electrons. The number of molecules needed for creating the electrons flow in Eq. (C.3) is

$$\frac{\text{number of } H_2 \text{ molecules}}{t} = \frac{6.24 \times 10^{18}}{2} i, \tag{C.4}$$

which is converted to number of moles dividing by the number of Avogadro N:

$$\frac{mol_{H_2}}{t} = i \frac{6.24 \times 10^{18}}{2N}. \tag{C.5}$$

The known quantity $N/6.24 \times 10^{18}$ in Eq. (C.5) is the Faraday constant F. Substituting F into Eq. (C.5) yields to

$$\frac{mol_{H_2}}{t} = \frac{1}{2F} i, \tag{C.6}$$

which is the molar rate of hydrogen. The molar rate is converted to mass rate [$\mathrm{g\,s^{-1}}$] multiplying by the molar mass of the hydrogen molecule (2 g), hence

$$\dot{m}_{H_2} = \frac{1}{F} i. \tag{C.7}$$

A FC is composed by n stacked cells for increasing the terminal voltage. The total hydrogen consumption is

$$\dot{m}_{H_2} = n \frac{1}{F} i \tag{C.8}$$

Oxygen flow From Eq. (C.2), each mole of oxygen combines with two moles of hydrogen. Using Eq. (C.6), it is possible to calculate the oxygen molar rate as

$$\frac{mol_{O_2}}{t} = \frac{1}{4F} i. \tag{C.9}$$

Similarly to what done before, the oxygen mass rate is obtained dividing by the molecular molar weight of oxygen (32 g). Multiplying by n gives the total oxygen consumption

$$\dot{m}_{H_2} = n \frac{8}{F} i. \tag{C.10}$$

C.1.2 Fuel cell stack voltage

In a FC, not all the energy released by the chemical reaction is transformed into electricity, and a part of it is lost in the form of heat. The losses occur in form of drops of the voltage available at the FC stack terminal. The equivalent circuit representing the FC stack terminal voltage is shown in Fig. C.2, where E is the modified Nernst potential, v_{act}, v_{conc}, R_{ohm} are denoting voltage activation loss, concentration loss and ohmic loss, respectively.

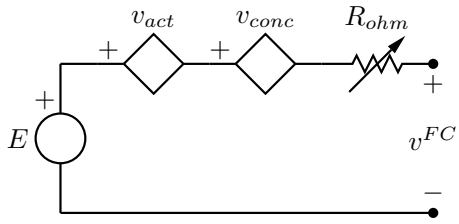

Figure C.2: Fuel cell stack voltage.

Ideal FC voltage The modified Nernst potential is ([101])

$$E = 1.23 - 0.85 \times 10^{-3}(T - 298.15) + 4.31 \times 10^{-5} T[\ln p_{H_2} + \frac{1}{2} \ln p_{O_2}] \quad \text{(C.11)}$$

and depends on the temperature at which the reaction occurs T [K] and on the partial pressure p_{H2} and p_{O_2} [bar] of the reactants. Increasing T, p_{H_2} or p_{O_2} leads to higher value of the Nernst potential.

Activation loss This kind of loss is due to the overpotential that is the difference between the expected voltage from thermodynamic laws and the collected voltage at the terminal of the fuel cell. Overpotential is caused by the fact that a small amount of energy is spent to push the reaction to occur.

Ohmic loss Ohmic loss is due to the resistivity of the membrane which separates the anode from the cathode. Ohmic loss depends on the thickness and resistivity of the membrane. The resistivity of the membrane varies as a function of operating conditions (FC stack temperature and membrane humidity).

Concentration loss During the FC reaction, reactants are consumed and they need to be replaced. High reaction rates provoke the reactants partial pressure to decrease. Concentration loss depends on stack temperature.

C.2 Experimental setup for the FC modelling

In Paper **[F]**, the grey-box model of the 15 kW PEMFC of the EPFL DESL facility is presented. In this section, the experimental setup that has been used for collecting the measurements from the FC is described. The target of the experiments is to collect measurements for determining the parameters of the FC polarization curve model at different stack temperature. The experiment requirements are to measure the temperature, the voltage and to absorb from the FC a determined amount of electric current. The experimental setup is shown in Fig. C.3. The FC is connected to a programmable DC electronic loads. The electronic load is interfaced through RS-232 with a PC, which provides the electric current set-points. On the same PC, a CAN bus interface implements communication with the FC accessing stack temperature information, fuel cell state, diagnostic messages and maximum current value.

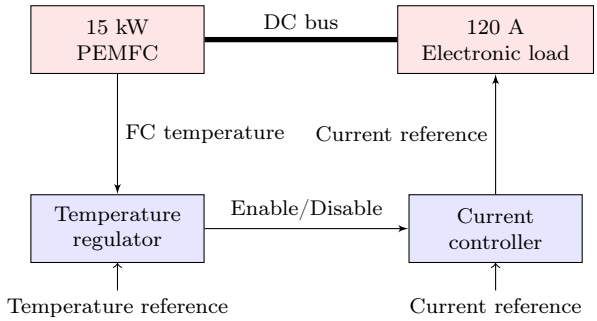

Figure C.3: Diagram of the experimental setup. The red and blue blocks denote the hardware and software layers, respectively.

The electric current set-points that are applied to the electronic loads are calculated by a LABVIEW script, which also indirectly controls the temperature of the stack acting on the current set-point: this is achieved by forcing the set-point of the electric current to zero when the FC needs to cool down.

Appendix D

SYSLAB and Power Flexhouse

D.1 SYSLAB

SYSLAB is a small scale experimental low voltage power grid of DTU Elektro located at DTU Risø campus [41]. The power system components of SYSLAB are:

- a 48 kW/60 kVA diesel generator;
- a 15 kW/120 kWh Vanadium battery;
- a 80 kW dumpload;
- 3 PV arrays with 2×10 kWp and 7 kWp of nominal power, respectively, and different configurations (i.e. different types of cells and installation);
- 2 wind turbines, an 11 kW unit an induction generator and a 10 kW unit with an PMSG generator;

SYSLAB can operate both in grid-connected mode and islanded mode (i.e. disconnected from the main grid). The electrical infrastructures of SYSLAB is characterized by a flexible structure that allows to configure different network layouts by means of automated switchboards, as shown in Fig. D.1.

The SCADA system of SYSLAB is based on an Ethernet network of Linux machines, which are called SYSLAB nodes. Each SYSLAB node is connected to the device that is control (e.g. switches) or to access (e.g. power measurements units) by means of lower level interfaces (such as RS-232 and CAN bus). The high level interface of the SCADA system is coded in Java. In SYSLAB, measurements are performed synchronously and with a sample rate of 1 Hz, while

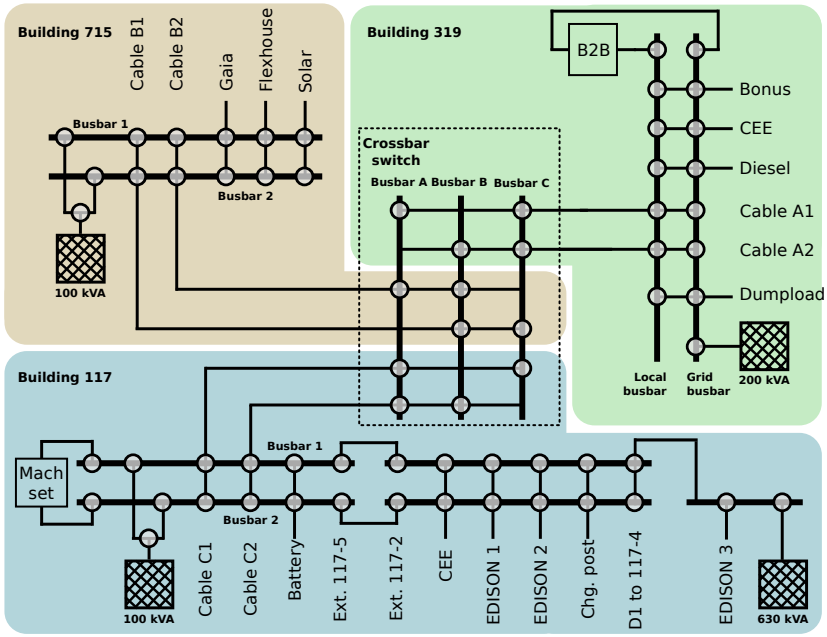

Figure D.1: The components and the electric network infrastructure of SYSLAB. The components are physically distributed over DTU Risø campus. A number of remotely controllable switches, denoted by the circles at the intersections between the power lines, allow to reproduce different network configurations.

actuation is by event (asynchronous). Control algorithms for SYSLAB can be developed directly in Java or by means of Matlab and Python APIs.

D.2 Power Flexhouse

Power Flexhouse is the facility of DTU Elektro for testing demand side management strategy. Power Flexhouse, located at DTU Risø campus, is a free standing building on one level composed by 8 rooms and with a total floor area of 125 m^2. The building is connected to SYSLAB laboratory, with which it shares the same high-level hardware configurations and software structures. Power Flexhouse is equipped with the following devices:

- 10 1 kW electric radiators to provide space heating;
- 5 air conditioning units;
- 2 fridges;

- 1 freezer;
- 1 1.2 kW 30 L EWH;
- doors and window actuators for simulating user presence;
- controllable lights.

Each load is controlled by an actuator. The state of the actuators is accessible and controllable from remote through the Java software platform. Power Flexhouse is instrumented with a number of sensors which allow to measure the user comfort and the environmental conditions. The sensors are:

- temperatures sensors for the rooms, refrigeration units and EWH;
- lights sensors;
- insolation, outside temperature and wind speed and direction sensors;
- flow meter for the hot water consumption.

In Power Flexhouse, both measurements and actuations are asynchronous, i.e. measurements are updated when the variations of the variables to measure are larger than configurable thresholds, and actuators are commanded when the respective remote actuation events are fired. The visualization interface of Power Flexhouse is shown in Fig. D.2.

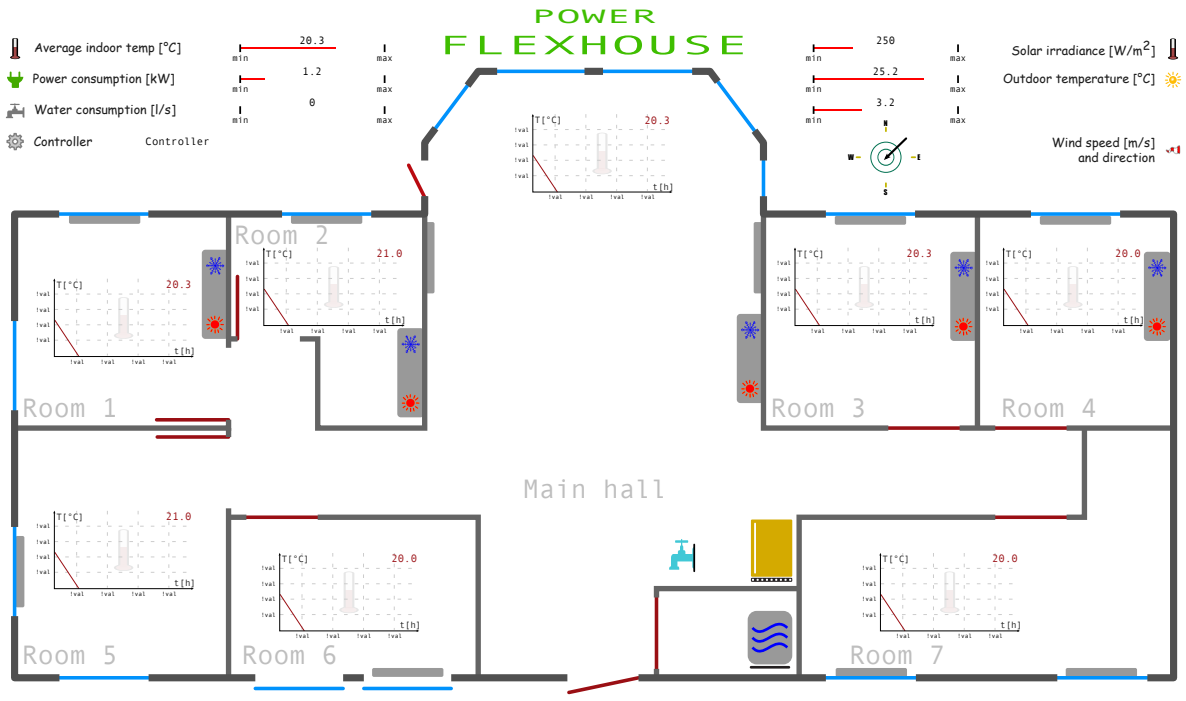

Figure D.2: The visualization interface of Power Flexhouse, which is the laboratory for testing demand side management strategies of DTU Elektro. The house is composed by a number of DSRs and is instrumented with sensors and actuators for measuring consumer comfort and environmental conditions and actuating the decision of control strategies and simulating user behaviour.

Bibliography

[1] Model predictive control: Theory and practice—a survey. *Automatica*, 25:335–348, 1989.

[2] *Power System Stability And Control*. EPRI power system engineering series. McGraw-Hill Education (India) Pvt Limited, 1994.

[3] Promoting wholesale competition through open access non-discriminatory transmission services by public utilities; recovery of stranded costs by public utilities and transmitting utilities. *Order*, 888:24, 1996.

[4] Thermal insulation materials made of rigid polyurethane foam. Technical report, Federation of European Rigid Polyurethane Foam, 2006.

[5] Flexpower project, 2010. http://goo.gl/D8XkIh.

[6] Energy statistics 2011. Technical report, Danish Energy Agency, 2011.

[7] Global market outlook for photovoltaic until 2016. Technical report, EPIA, European Photovoltaic Industry Association, May 2012.

[8] Self consumption of pv electricity. Technical report, EPIA, European Photovoltaic Industry Association, July 2013.

[9] Smart grid consumer benefits, 2013.

[10] M. F. Anjos. Recent progress in modeling unit commitment problems. In *Modeling and Optimization: Theory and Applications*, pages 1–29. Springer, 2013.

[11] H. Arasteh, M. P. Moghaddam, M. Sheikh-El-Eslami, and A. Abdollahi. Integrating commercial demand response resources with unit commitment. *International Journal of Electrical Power & Energy Systems*, 51:153–161, 2013.

[12] P. Bacher, H. Madsen, H. Nielsen, and B. Perers. Short-term heat load forecasting for single family houses. *Energy and Buildings*, 65:101–112, 2013.

[13] A. Bernstein, L. Reyes-Chamorro, J.-Y. L. Boudec, and M. Paolone. A composable method for real-time control of active distribution networks with explicit power setpoints. *arXiv preprint arXiv:1403.2407*, 2014.

[14] F. Bliek, A. van den Noort, B. Roossien, R. Kamphuis, J. de Wit, J. van der Velde, and M. Eijgelaar. Powermatching city, a living lab smart grid demonstration. In *IEEE International Conference on Innovative Smart Grid Technologies (ISGT)*, 2010.

[15] S. Boyd, N. Parikh, E. Chu, B. Peleato, and J. Eckstein. Distributed optimization and statistical learning via the alternating direction method of multipliers. *Foundations and Trends in Machine Learning*, 3, 2011.

[16] S. Boyd and L. Vandenberghe. *Convex Optimization*. Cambridge University Press, 2004.

[17] M. Braun, M. Budenbender, Z. Perrin, D. Feng, and Magnor. Photovoltaic self-consumption in Germany. In *24th European Photovoltaic Solar Energy Conference*, September 2009.

[18] T. Burton, N. Jenkins, D. Sharpe, and E. Bossanyi. *Wind Energy Handbook*. Wiley.

[19] C. T. F. C6.04.02. Benchmark systems for network integration of renewable and distributed energy resources. Technical report, Cigre' International Council on large electric systems, July 2009.

[20] D. Callaway and I. Hiskens. Achieving controllability of electric loads. *Proceedings of the IEEE*, 99, 2011.

[21] P. Cappers, C. Goldman, and D. Kathan. Demand response in u.s. electricity markets: Empirical evidence. *Energy*, 35:1526–1535, 2010.

[22] M. Caramanis and J. M. Foster. Management of electric vehicle charging to mitigate renewable generation intermittency and distribution network congestion. In *IEEE Conference on Decision and Control (CDC)*, pages 4717–4722, 2009.

[23] E. Castillo-Cagigal, A. Caamaño-Martín, D. Gutiérrez, F. Masa-Bote, J. Monasterio, E. Porro, J. Matallanas, and Jiménez-Leube. Self-consumption of pv electricity with active demand side management: The gedelos-pv system. In *25th European Photovoltaic Solar Energy Conference*, September 2010.

[24] F. E. R. Commission et al. Assessment of demand response and advanced metering. *Department of Energy, Washington, DC*, 2006.

[25] G. T. Costanzo, O. Gehrke, J. Parvizi, D. E. Morales Bondy, and H. Madsen. A coordination scheme for distributed model predictive control: Integration of flexible ders. In *IEEE International Conference on Innovative Smart Grid Technologies (ISGT)*, 2013.

[26] G. T. Costanzo, F. Sossan, M. Marinelli, P. Bacher, and H. Madsen. Grey-box modeling for system identification of household refrigerators: A step toward smart appliances. In *IEEE International Youth Conference on Energy (IYCE)*, 2013.

[27] G. T. Costanzo, G. Zhu, M. F. Anjos, and G. Savard. A system architecture for autonomous demand side load management in smart buildings. *IEEE Transactions on Smart Grid*, 3:2157–2165, 2012.

[28] Z. Csetvei, J. Ostergaard, and P. Nyeng. Controlling price-responsive heat pumps for overload elimination in distribution systems. In *IEEE International Conference on Innovative Smart Grid Technologies (ISGT)*, 2012.

[29] M. Damm, M. Lukic, S. Mahlknecht, J. Haase, C. Grimm, and V. Malbasa. Shifting of thermal and schedulable loads based on abstract cost profiles. In *IEEE International Conference on Innovative Smart Grid Technologies (ISGT)*, 2012.

[30] K. Divya and J. Østergaard. Battery energy storage technology for power systems — an overview. *Electric Power Systems Research*, 79:511–520, 2009.

[31] P. Douglass, R. Garcia-Valle, P. Nyeng, J. Ostergaard, and M. Togeby. Smart demand for frequency regulation: Experimental results. *IEEE Transactions on Smart Grid*, PP, 2013.

[32] P. Douglass, R. Garcia-Valle, F. Sossan, J. Ostergaard, and P. Nyeng. Design and evaluation of autonomous hybrid frequency-voltage sensitive load controller. In *IEEE International Conference on Innovative Smart Grid Technologies (ISGT)*, 2013.

[33] I. Dudurych, M. Holly, and M. Power. Secure operation of power system with high wind penetration. EirGrid.

[34] I. Dudurych, M. Holly, and M. Power. Integration of wind power generation in the Irish grid. In *IEEE Power Engineering Society General Meeting*. IEEE, 2006.

[35] S. Emec, M. Kuschke, M. Chemnitz, and K. Strunz. Potential for demand side management in automotive manufacturing. In *IEEE International Conference on Innovative Smart Grid Technologies (ISGT)*, 2013.

[36] Enel.it. Conto energia (in Italian), 2010. http://goo.gl/aoEO1a.

[37] Energinet. Technical regulation for thermal power station units of 1.5 MW and higher. Technical report, Energinet.dk, 2008.

[38] P. Faria and Z. Vale. Demand response in electrical energy supply: An optimal real time pricing approach. *Energy*, 36:5374–5384, 2011.

[39] N. I. for Standard and Technology. Smart grid, 2013.

[40] J. C. Galvis and A. P. Feltrin. Power system ancillary services. In *Handbook of Networks in Power Systems I*, pages 555–579. Springer, 2012.

[41] O. Gehrke. *Self-Organising Distributed Control of a Distributed Energy System with a High Penetration of Renewable Energy*. Ph.D. thesis, Risoe DTU, 2010.

[42] O. Gehrke and F. Isleifsson. An aggregation friendly information model for demand side resources. In *Local Computer Networks (LCN), 2010 IEEE 35th Conference on*, 2010.

[43] C. Gellings. The concept of demand-side management for electric utilities. *Proceedings of the IEEE*, 1985.

[44] H. Glavitsch and F. Alvarado. Management of multiple congested conditions in unbundled operation of a power system. In *International Conference on Power Industry Computer Applications*, pages 374–380, 1997.

[45] S. Grillo, M. Marinelli, F. Silvestro, F. Sossan, O. Anaya-Lara, and G. Burt. Transient support to frequency control from wind turbine with synchronous generator and full converter. In *IEEE Universities Power Engineering Conference International Conference*, 2010.

[46] R. Halvgaard, P. Bacher, B. Perers, E. Andersen, S. Furbo, J. B. Jørgensen, N. K. Poulsen, and H. Madsen. Model predictive control for a smart solar tank based on weather and consumption forecasts. *Energy Procedia*, 30:270–278, 2012.

[47] R. Halvgaard, N. Poulsen, H. Madsen, and J. Jørgensen. Economic model predictive control for building climate control in a smart grid. In *IEEE International Conference on Innovative Smart Grid Technologies (ISGT)*, 2012.

[48] R. Halvgaard, N. K. Poulsen, H. Madsen, and J. B. Jørgensen. Economic model predictive control for building climate control in a smart grid. In *IEEE International Conference on Innovative Smart Grid Technologies (ISGT)*, 2012.

[49] V. Hamidi and F. Li. Responsive demand to increase the value of wind power.

[50] V. Hamidi, F. Li, and F. Robinson. Responsive demand in networks with high penetration of wind power. In *Transmission and Distribution Conference and Exposition, 2008. IEEE/PES*, 2008.

[51] V. Hamidi, F. Li, and F. Robinson. Demand response in the uk's domestic sector. *Electric Power Systems Research*, 79(12), 2009.

[52] D. J. Hammerstrom, R. Ambrosio, T. A. Carlon, J. G. Desteese, R. Kajfasz, and R. G. Pratt. Pacific Northwest GridWise Testbed Demonstration Projects Part I . Olympic Peninsula Project. *Contract*, page 157, 2007.

[53] K. Herter and S. Wayland. Residential response to critical-peak pricing of electricity: California evidence. *Energy*, 35:1561–1567, 2010.

[54] K. Heussen, S. You, B. Biegel, L. Hansen, and K. Andersen. Indirect control for demand side management-a conceptual introduction. In *IEEE International Conference on Innovative Smart Grid Technologies (ISGT)*. IEEE, 2012.

[55] T. Hovgaard, L. Larsen, and J. Jørgensen. Flexible and cost efficient power consumption using economic MPC a supermarket refrigeration benchmark. In *IEEE Conference on Decision and Control (CDC)*, pages 848–854, 2011.

[56] T. G. Hovgaard, S. Boyd, L. F. Larsen, and J. B. Jørgensen. Nonconvex model predictive control for commercial refrigeration. *International Journal of Control*, 86:1349–1366, 2013.

[57] T. G. Hovgaard, L. F. Larsen, K. Edlund, and J. B. Jørgensen. Model predictive control technologies for efficient and flexible power consumption in refrigeration systems. *Energy*, 44:105–116, 2012.

[58] J. Hu, S. You, M. Lind, and J. Østergaard. Coordinated charging of electric vehicles for congestion prevention in the distribution grid. *IEEE Transactions on Smart Grid*, 2012.

[59] S.-J. Huang and C.-C. Huang. An adaptive load shedding method with time-based design for isolated power systems. *International Journal of Electrical Power & Energy Systems*, 22:51–58, 2000.

[60] IEA and NEA. Projected costs of generating electricity. Technical report, International Energy Agency, Nuclear Energy Agency, 2010.

[61] IFC. Demand response resources: the US and international experience. *Energy*, 35, 2010.

[62] M. Ifland, N. Exner, and D. Westermann. Appliance of direct and indirect demand side management. In *IEEE Energytech conference*, 2011.

[63] A. Jäger-Waldau. PV status report 2012, 2012.

[64] S. Kalogirou and Y. Tripanagnostopoulos. Hybrid pv/t solar systems for domestic hot water and electricity production. *Energy Conversion and Management*, 2006.

[65] W. Kempton and J. Tomić. Vehicle-to-grid power implementation: From stabilizing the grid to supporting large-scale renewable energy. *Journal of Power Sources*, 144(1):280–294, 2005.

[66] S. Koch. *Demand Response Methods for Ancillary Services and Renewable Energy Integration in Electric Power Systems*. Ph.D. thesis, ETH, 2012.

[67] C. Koch-Ciobotaru, L. Mihet-Popa, F. R. Isleifsson, and H. Bindner. Simulation model developed for a small-scale pv-system in a distribution network. In *International Symposium on Applied Computational Intelligence and Informatics*, pages 257–261, 2012.

[68] J. K. Kok, C. J. Warmer, and I. G. Kamphuis. Powermatcher: multiagent control in the electricity infrastructure. In *International conference on autonomous agents and multiagent systems*, pages 75–82, 2005.

[69] A. M. Kosek, G. T. Costanzo, H. W. Bindner, and O. Gehrke. An overview of demand side management control schemes for buildings in smart grids. In *IEEE International Conference on Smart Energy Grid Engineering*, 2013.

[70] T. Krause and G. Andersson. Evaluating congestion management schemes in liberalized electricity markets using an agent-based simulator. In *IEEE Power Engineering Society General Meeting*, 2006.

[71] V. Lakshmanan, M. Marinelli, A. M. Kosek, F. Sossan, and P. B. Nørgård. Domestic refrigerators temperature prediction strategy for the evaluation of the expected power consumption. In *IEEE International Conference on Innovative Smart Grid Technologies (ISGT)*, 2013.

[72] J. Larminie and A. Dicks. *Fuel Cell Systems Explained*. J. Wiley, 2003.

[73] S. Lee and C. Wilkins. A practical approach to appliance load control analysis: a water heater case study. *IEEE Transactions on Power Apparatus and Systems*, (4), 1983.

[74] H. Lund. Large-scale integration of wind power into different energy systems. *Energy*, 30:2402–2412, 2005.

[75] H. Madsen. *Time Series Analysis*. Chapman & Hall/CRC Texts in Statistical Science. Taylor & Francis, 2007.

[76] H. Madsen and J. Holst. Estimation of continuous-time models for the heat dynamics of a building. *Energy and Buildings*, 22:67–79, 1995.

[77] H. Madsen and P. Thyregod. *Introduction to General and Generalized Linear Models*. Chapman & Hall/CRC Texts in Statistical Science Series. Chapman & Hall/CRC, 2011.

[78] G. Makrides, B. Zinsser, M. Schubert, and G. E. Georghiou. Energy yield prediction errors and uncertainties of different photovoltaic models. *Progress in Photovoltaics: Research and Applications*, 2011.

[79] R. Malhamé and C.-Y. Chong. Electric load model synthesis by diffusion approximation of a high-order hybrid-state stochastic system. *IEEE Transactions on Automatic Control*, 30:854–860, 1985.

[80] M. Marinelli, F. Sossan, G. Costanzo, and H. Bindner. Testing of a predictive control strategy for balancing renewable sources in a microgrid. *IEEE Transactions on Sustainable Energy*, 2014.

[81] M. Marinelli, F. Sossan, F. R. Isleifsson, G. T. Costanzo, and H. Bindner. Day-ahead scheduling of a photovoltaic plant by the energy management of a storage system. In *IEEE International Universities Power Engineering Conference (UPEC)*, 2013.

[82] F. Marra, D. Sacchetti, A. Pedersen, P. Andersen, C. Traholt, and E. Larsen. Implementation of an electric vehicle test bed controlled by a virtual power plant for contributing to regulating power reserves. In *Power and Energy Society General Meeting, 2012 IEEE*. IEEE, 2012.

[83] J. Mathieu, M. Dyson, and D. Callaway. Using residential electric loads for fast demand response: The potential resource and revenues, the costs, and policy recommendations. *Proceedings of the ACEEE Summer Study on Buildings, Pacific Grove, CA*, 2012.

[84] Y. Mayhew and M. Hollingsworth. *Engineering Thermodynamics Work and Heat Transfer*. Number v. 2. Longman Scientific & Technical, 1996.

[85] J. McDonald and A. M. Bruning. Cold load pickup. *IEEE Transactions on Power Apparatus and Systems*, (4), 1979.

[86] D. Miller and T. Sleva. Cold load pickup issues. Technical report, Power System Relay Committee of The IEEE Power Engineering Society, May 2008.

[87] J. Morren, J. Pierik, and S. W. De Haan. Inertial response of variable speed wind turbines. *Electric power systems research*, 76:980–987, 2006.

[88] M. Nehrir, R. Jia, D. Pierre, and D. Hammerstrom. Power management of aggregate electric water heater loads by voltage control. In *IEEE Power Engineering Society General Meeting*, 2007.

[89] J. A. Nelder and R. W. Wedderburn. Generalized linear models. *Journal of the Royal Statistical Society. Series A (General)*, pages 370–384, 1972.

[90] H. A. Nielsen, H. Madsen, et al. *Predicting the heat consumption in district heating systems using meteorological forecasts*. Citeseer, 2000.

[91] P. Norgaard and H. Holttinen. A multi-turbine power curve approach. In *Nordic Wind Power Conference*, volume 1, 2004.

[92] P. Nyeng and J. Ostergaard. Information and communications systems for control-by-price of distributed energy resources and flexible demand. *IEEE Transactions on Smart Grid*, 2:334 –341, 2011.

[93] T. F. of Technical University of Denmark. Energy storage options for future sustainable energy systems. Technical report, DTU, November 2013.

[94] F. Oldewurtel, A. Parisio, C. Jones, M. Morari, D. Gyalistras, M. Gwerder, V. Stauch, B. Lehmann, and K. Wirth. Energy efficient building climate control using stochastic model predictive control and weather predictions. In *American Control Conference (ACC), 2010*, pages 5100–5105, 2010.

[95] F. Oldewurtel, A. Ulbig, A. Parisio, G. Andersson, and M. Morari. Reducing peak electricity demand in building climate control using real-time pricing and model predictive control. In *IEEE Conference on Decision and Control (CDC)*, 2010.

[96] H. M. P. Bacher, A. Thavlov. Models for energy performance analysis. Technical report, DTU-IMM, 2010.

[97] J. Peas Lopes, F. Soares, and P. Almeida. Identifying management procedures to deal with connection of electric vehicles in the grid. In *IEEE PowerTech*, 2009.

[98] C. Perfumo, E. Kofman, J. H. Braslavsky, and J. K. Ward. Load management: Model-based control of aggregate power for populations of thermostatically controlled loads. *Energy Conversion and Management*, 55:36–48, 2012.

[99] M. H. Petersen, K. Edlund, L. H. Hansen, J. D. Bendtsen, and J. Stoustrup. A taxonomy for flexibility modeling and a computationally efficient algorithm for dispatch in smart grids.

[100] P. Pinson, H. Madsen, H. Bindner, H. Hansen, K. Andersen, and H. L.H. Indirect control by prices – basic concepts, applications and requirements. Technical report, iPower, July 2012.

[101] J. Pukrushpan. *Modeling and Control of Fuel Cell Systems and Fuel Processors*. Ph.D. thesis, The University of Michigan, 2012.

[102] J. Pukrushpan, A. Stefanopoulou, and H. Peng. Modeling and control for pem fuel cell stack system. In *Proceedings of the American Control Conference*, volume 4, pages 3117–3122, 2002.

[103] B. Saravanan, S. Das, S. Sikri, and D. Kothari. A solution to the unit commitment problem: a review. *Frontiers in Energy*, 7:223–236, 2013.

[104] F. Schweppe, R. Tabors, J. Kirtley, H. Outhred, F. Pickel, and A. Cox. Homeostatic utility control. *IEEE Transactions on Power Apparatus and Systems*, 1980.

[105] S. Sen and D. Kothari. Optimal thermal generating unit commitment: a review. *International Journal of Electrical Power & Energy Systems*, 20:443–451, 1998.

[106] B. Sorensen. *Hydrogen and Fuel Cells: Emerging Technologies and Applications*. Sustainable World. Elsevier Science, 2005.

[107] F. Sossan and H. Bindner. A comparison of algorithms for controlling DSRs in a control by price context using hardware-in-the-loop simulation. In *IEEE Power and Energy Society General Meeting*, pages 1–8, 2012.

[108] F. Sossan and H. Bindner. Evaluation of the performance of indirect control of many DSRs using hardware-in-the-loop simulations. In *IEEE Conference on Decision and Control (CDC)*, 2012.

[109] F. Sossan, H. Bindner, H. Madsen, L. Reyes, D. Torregrossa, and M. Paolone. A MPC replacement strategy for electric space heating including cogeneration of a fuel cell-electrolyzer system. *International Journal of Electrical Power & Energy Systems*, 2013.

[110] F. Sossan, X. Han, and H. Bindner. Dynamic behaviour of a population of controlled-by-price demand side resources. In *IEEE Power Engineering Society General Meeting*, 2014. Accepted for publication.

[111] F. Sossan, A. M. Kosek, S. Martinenas, M. Marinelli, and H. W. Bindner. Scheduling of domestic water heater power demand for maximizing PV self-consumption using model predictive control. In *IEEE International Conference on Innovative Smart Grid Technologies (ISGT)*, 2013.

[112] F. Sossan, V. Lakshmanan, G. Costanzo, M. Marinelli, P. Douglas, and H. Bindner. Grey-box modelling of a household refrigeration unit for energy consumption prediction and optimization using time series data. 2013. Currently unpublished.

[113] F. Sossan and M. Marinelli. An auto tuning substation peak shaving controller for congestion management using flexible demand. In *IEEE International Universities Power Engineering Conference (UPEC)*, 2013.

[114] F. Sossan, M. Marinelli, G. Costanzo, and H. Bindner. Indirect control of DSRs for regulating power provision and solving local congestions. In *IEEE International Youth Conference on Energy (IYCE)*, 2013.

[115] R. Stengel. *Optimal Control and Estimation*. Dover Books on Advanced Mathematics. Dover Publications, 1994.

[116] O. Sundstrom and C. Binding. Flexible charging optimization for electric vehicles considering distribution grid constraints. *IEEE Transactions on Smart Grid*, 3:26–37, 2012.

[117] F. Tahersima, J. Stoustrup, H. Rasmussen, and S. A. Meybodi. Economic cop optimization of a heat pump with hierarchical model predictive control. In *IEEE Conference on Decision and Control (CDC)*, pages 7583–7588. IEEE, 2012.

[118] P. Thimmapuram, J. Kim, A. Botterud, and Y. Nam. Modeling and simulation of price elasticity of demand using an agent-based model. In *IEEE International Conference on Innovative Smart Grid Technologies (ISGT)*, 2010.

[119] J. Torriti, M. G. Hassan, and M. Leach. Demand response experience in europe: Policies, programmes and implementation. *Energy*, 35(4):1575–1583, 2010.

[120] C. Trueblood, S. Coley, T. Key, L. Rogers, A. Ellis, C. Hansen, and E. Philpot. Pv measures up for fleet duty : Data from a Tennessee plant are used to illustrate metrics that characterize plant performance. *IEEE Power and Energy Magazine*, 11:33–44, 2013.

[121] K. Vanthournout, R. D'hulst, D. Geysen, and G. Jacobs. A smart domestic hot water buffer. *IEEE Transactions on Smart Grid*, 3:2121–2127, 2012.

[122] J. Wang, M. Shahidehpour, and Z. Li. Security-constrained unit commitment with volatile wind power generation. *Power Systems, IEEE Transactions on*, 23(3):1319–1327, 2008.

[123] C. Whitaker, T. Townsend, J. Newmiller, D. King, W. Boyson, J. Kratochvil, D. Collier, and D. Osborn. Application and validation of a new pv performance characterization method. In *IEEE Photovoltaic Specialists Conference*, 1997.

[124] J. Wilkes and J. Moccia. Wind in power: 2012 european statistics. Technical report, EWEA, European Wind Energy Association, February 2013.

[125] W. Winter. European wind integration study (ewis). In *14. Kasseler Symposium Energie-Systemtechnik*, page 25, 2010.

[126] World Business Council for Sustainable Development (WBCSD). Transforming the market: Energy efficiency in the buildings, 2009.

[127] Z. Xu, J. Ostergaard, and M. Togeby. Demand as frequency controlled reserve. *IEEE Transactions on Power Systems*, 26(3), 2011.

[128] Z. Xu, J. Ostergaard, M. Togeby, and C. Marcus-Moller. Design and modelling of thermostatically controlled loads as frequency controlled reserve. In *IEEE Power Engineering Society General Meeting*, 2007.

[129] P. J. Yves Dherbécour. Demand response technology roadmap, 2009.

[130] J. W. Zarnikau. Demand participation in the restructured electric reliability council of texas market. *Energy*, 35:1536–1543, 2010.

[131] Q. Zhao, M. Li, and H. Zhang. Spinning reserve from responsive load via intelligent energy management network. In *IEEE International Conference on Networking, Sensing and Control*, pages 715–720, 2006.

[132] Y. Zong, D. Kullmann, A. Thavlov, O. Gehrke, and H. Bindner. Active load management in an intelligent building using model predictive control strategy. In *IEEE PowerTech*, 2011.

[133] Y. Zong, D. Kullmann, A. Thavlov, O. Gehrke, and H. Bindner. Model predictive control strategy for a load management research facility in the distributed power system with high wind penetration -towards a Danish power system with 50% wind penetration. In *Power and Energy Engineering Conference (APPEEC)*, 2011.

[134] Y. Zong, D. Kullmann, A. Thavlov, O. Gehrke, and H. Bindner. Application of model predictive control for active load management in a distributed power system with high wind penetration. *IEEE Transactions on Smart Grid*, 3, 2012.

[135] Y. Zong, D. Kullmann, A. Thavlov, O. Gehrke, and H. Bindner. Application of model predictive control for active load management in a distributed power system with high wind penetration. In *IEEE Power and Energy Society General Meeting*, 2012.

[136] Y. Zong, L. Mihet-Popa, D. Kullmann, A. Thavlov, O. Gehrke, and H. Bindner. Model predictive controller for active demand side management with pv self-consumption in an intelligent building. In *IEEE International Conference on Innovative Smart Grid Technologies (ISGT)*, 2012.

[137] Y. Zong, L. Mihet-Popa, D. Kullmann, A. Thavlov, O. Gehrke, and H. Bindner. Model predictive controller for active demand side management with pv self-consumption in an intelligent building. In *IEEE International Conference on Innovative Smart Grid Technologies (ISGT)*, 2012.

[138] M. Zugno, J. M. Morales, P. Pinson, and H. Madsen. A bilevel model for electricity retailers participation in a demand response market environment. *Energy Economics*, 2012.

Paper A

Grey-box modelling of a household refrigeration unit for energy consumption prediction and optimization using time series data

Grey-box Modelling of a Household Refrigeration Unit for Energy Consumption Prediction and Optimization Using Time Series Data

Fabrizio Sossan[a,*], Venkatachalam Lakshmanan[a], Giuseppe Tommaso Costanzo[a], Mattia Marinelli[a], Philip J. Douglass[a], Henrik Bindner[a]

[a] *DTU Elektro, Frederiksborgvej 399, 4000, Roskilde, Denmark*

Abstract

This paper describes the application of a grey-box modelling methodology to the system identification of a domestic refrigeration unit utilizing measurements from an instrumented commercially available freezer. The proposed models are formulated using stochastic differential equations (SDEs), estimated from the measurements applying maximum likelihood estimation (MLE), validated through the model residuals analysis and cross-validated to detect model overfitting. We show that including a nonlinear description of the coefficient of performance (COP) of the refrigeration cycle improves the ability of the models to explain the dynamics observed from the measurements. As an application, we show how the proposed models can be utilized to predict and optimize the electricity consumption of a freezer in a smart grid scenario utilizing model predictive control (MPC). The proposed methodology and models can be adopted and adapted to identify other kinds of refrigeration units and for real-time online estimation of the parameters.

Keywords: Power demand, Modelling, Refrigerators, Smart grids, Demand Response.

1. Introduction

According to [1], household refrigerators account for 7% of the total electricity consumption in the residential sector in US. Methodologies to estimate and validate mathematical models of refrigeration units are of importance to assess the energy efficiency and predict the energy consumption of freezers and fridges. Additionally nowadays, household and commercial refrigerators are seen with increased interest as they can provide demand response exploiting the consumption flexibility due to their thermal mass [2–4]. In this context,

*Corresponding author
Email address: fabrizio.sossan@elektro.dtu.dk (Fabrizio Sossan)

validated mathematical models are required to develop intelligent energy management strategies, such as model predictive control (MPC) [5, 6]. In this paper, we describe the application of a state-of-the-art grey-box modelling methodology to identify power consumption-to-temperature models of a domestic freezer suitable for prediction of the temperature and optimization of the consumption. The discussed modelling effort aims to the system identification of the physical processes associated with the operation of the freezer, i.e. heat transfer and refrigeration cycle coefficient of performance (COP). Modelling of the consumer behavior is not considered at this stage. In the existing literature, dynamic thermal models are mainly developed using first principles approaches (or white-box), as for example in [7–9]. Dynamic linear models for a fridge developed with a grey-box procedure similar to the one adopted here are discussed in [10]. We extend the work already present in the literature by implementing novel nonlinear thermal models of a domestic freezer based on stochastic differential equations (SDEs) and estimated using measurements obtained from an instrumented and commercially available freezer. It is shown that the proposed nonlinear description of the refrigeration cycle based on the reversed Carnot formula improves the performance of the models, allowing to explain the most of the time dynamics observable from the measurements. The model identification is carried out utilizing a grey-box methodology which, in contrast to first principles approaches, is an adaptive modelling strategy as based on measurements and can be applied to model other kinds of freezers as well as on-line estimation of the parameters. Finally, as an application of the proposed models, a convex MPC is developed to optimize the consumption of the freezer according to a dynamic electricity price.

The structure of the paper is as follows. Section 2 describes the experimental setup realized to collect the measurements to identify the models. Section 3 describes the steps of the adopted grey-box methodology and provides to the reader an insight on the mathematical formulation of MLE and the logic of the inference process used to cross-validate the models. In Section 4, the models are presented in a sequential fashion and in order of complexity. For each model, the model fitting through MLE, validation and cross-validation are carried out. A detailed descriptions of the validation and cross-validation procedures are respectively given when presenting the first two models: in the case of the other models only the results are presented, since the adopted procedures are the same. In Section 5, a comparison between the proposed grey-box models and the white-box estimated physical characteristics of the freezer is carried out with the main objective to understand if the parameters of the former are capable of capturing the physical characteristics of the freezer. Moreover, the quality of the predictions of the models are assessed statistically using validation data sets. In Section 6, the results of the modelling process are summarized and a general discussion regarding the identified models is given. In Section 7, the MPC application is formulated and the respective simulation results are presented. Finally, Section 8 is for conclusions.

2. Experimental setup

The objective of the experimental setup is to collect the measurements required to identify the proposed freezer thermal models. The instrumented unit is a Bosch GSN40A21, a commercially available domestic freezer with 333 L capacity and a single-phase compressor. The freezer belongs to Power Flexhouse, the experimental facility of DTU Elektro for testing demand side management strategies for smart grid applications. The requirements of the model identification process are measuring the freezer and room temperatures, the freezer total active power consumption and controlling the on-off state of the unit. Temperatures are measured using 10k NTC thermistors. Such a kind of thermistors can measure temperatures in the range -30 to 80°C with an accuracy of ± 0.2 °C at 25°C and are characterized by a fast measurements response. Each thermistor is connected to a 12bit ADC through a resistance-to-voltage transducer. The freezer power consumption is measured using a DEIF MIC-2, an instrument under the accuracy class 0.5. This device is able to measure voltages up to 400 V and current flows up to 5 A on a three phases bus, although only one is used for this application. The state of the freezer is controlled using a controllable power plug. All the sensors and instruments are interfaced with a conventional PC and are accessed by a JAVA software, which also serves to log the measurements and allows for the remote control of the state of the freezer. Measurements and actuations are synchronous with a sample time of 0.1 Hz.

3. The grey-box modelling methodology

The grey-box methodology is a framework that allows to identify and validate a mathematical model incorporating its physical knowledge together with measurements from a real device. The adopted modelling methodology consists of a number of steps, which are explained in the following.

3.1. Experiment design

In order to observe from measurements the dynamics inherent a system, the device to model should be excited in a wide range of frequency using an appropriate control signal. This was done by means of activating the compressor of the freezer according to a pseudo random binary signal (PRBS), a signal that can assume two states, on or off, with a fixed period and uniformly distributed random duty cycle. The action of the freezer thermostat, which normally controls the state of the compressor, was overridden by setting the thermostatic set-point at the lowest temperature: in this way, it was possible to control the state of the compressor by triggering the power consumption of the unit using a controllable plug. In order to avoid to damage the compressor of the freezer, the PRBS cycles with on-to-off transitions shorter than 30 seconds were disregarded: this had the effect of not being able to observe very short transients. Nevertheless, fast dynamics are of limited interest when dealing with predictions, simulation and optimization of the freezer power consumption, which is

mostly influenced by slower thermal transients, as those due to the freezer thermal mass. The power consumption and temperature measurements used for the model identification were collected for 50 hours and are shown in Fig. 1. In the plot in the upper panel of Fig. 1, the action of the PRBS signal triggering on and off the power consumption of the freezer for random time periods is well visible. We believe that this set of measurements is of sufficient length to identify the models because includes several cycles of the PRBS signal and is considerably longer than the dominant time constant of the system ($\approx$ 4 hours[1]). A second and a third 40 hours long sets of measurement, respectively with PRBS and conventional thermostatic control, were collected and used as validation data to assess the prediction performance of the models (Section 5.2). During the experiment, the freezer was empty and the door closed.

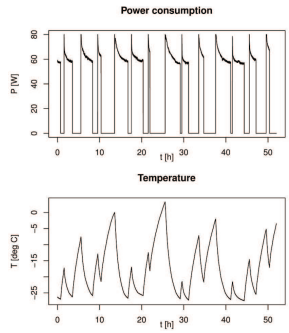

Figure 1: The measurements used to identify the thermal models of the freezer. The plot in the upper and lower panels respectively show the post-processed power consumption and temperature of the freezer.

3.2. Data acquisition and measurements post-processing

The physical quantities that are measured in the experiment are the temperatures of the freezer and room and the freezer total power consumption. Although the temperature measurements did not require any post-processing, the power consumption time series was filtered to remove those components not directly related to the mechanical work required by the refrigeration cycle since could interfere with the identification of the models parameters: initially, the approximately constant power consumption of the auxiliary components of the freezer (i.e. control logic and user display) was removed by subtracting it from the total power consumption; subsequently, the consumption spikes, due to the inrush currents of the induction motor that drives the compressor, were

[1] A rule-of-thumb to determine the dominant time constant is to take 1/5 of the time that the system states takes to reach the steady state condition.

removed by means of a statistical filter for detecting outliers. The consumption spikes were observed being of short duration (< 40 seconds) and they were removed from the total power consumption because the associated dynamics are considerably faster than the dominant thermal time constants. Moreover, this transitory phenomena is closely related to the nature of the induction motor and mainly represents the initial investment of energy required to accelerate the rotor and the associated mass rather than the energy spent in the thermodynamic transformation.

3.3. Model Formulation

In this phase, a set of suitable physical relationships that describes the nature and the working principles of the process that is to be modelled is identified. The thermal models of the freezer are formulated using SDEs and state-space representation. The models will be presented in Section 4.

3.4. Parameters estimation

The parameters of the model are found utilizing CTSM (continuous time stochastic modelling), a software library for R that implements maximum likelihood estimation (MLE) [11]. MLE consists in maximizing the likelihood function of the model, i.e. maximizing the probability that the model can explain the observations (or measurements). The mean and variance of the 1-step ahead prediction of the candidate model with parameters θ at the time step k are defined as

$$\hat{\boldsymbol{y}}_{k|k-1} = E[\boldsymbol{y}_{k|k-1}(\boldsymbol{\theta})] \tag{1}$$

$$R_{k|k-1} = \mathrm{Var}[\boldsymbol{y}_{k|k-1}(\boldsymbol{\theta})], \tag{2}$$

respectively, where $\boldsymbol{y}_{k|k-1}$ indicates the prediction of the model provided the information up to time $k-1$. The 1-step ahead prediction error of the model, or *model residual*, at the step k is defined as

$$\boldsymbol{\epsilon}_k = \boldsymbol{y}_k - \hat{\boldsymbol{y}}_{k|k-1}, \tag{3}$$

where $\boldsymbol{y}_k$ is the observation at the time interval k. Assuming that the predictions of the stochastic model are Gaussian distributed, the likelihood function is

$$L\big(\boldsymbol{\theta}, \boldsymbol{y}(k)\big) = \Bigg(\prod_{j=1}^{k} \frac{\exp\big(-\frac{1}{2}\boldsymbol{\epsilon}_j^T R_{j|j-1}^{-1} \boldsymbol{\epsilon}_j \big)}{\sqrt{\det(R_{j|j-1})}\sqrt{2\pi}^{k}} \Bigg) p(\boldsymbol{y}_0|\boldsymbol{\theta}), \tag{4}$$

which is the joint probability of the prediction errors obtained as the product of the single conditional probability density. The parameters of the model are found by minimizing the logarithm of Eq. (4).

3.5. Model validation through the residuals analysis

This phase consists in evaluating if the candidate model with the respective identified parameters is able to describe all the dynamics observable in the measurements or not. The model validation is performed by carrying out the model residuals analysis, which consists in evaluating any autocorrelation in time of the model residuals: if a model were exact, the model residuals should not show any autocorrelation, meaning that none of the time dynamics observed from the measurements were left unexplained by the model. The validation of the proposed models will be described in Section 4.

3.6. Model extension and cross validation

If the residuals analysis is not satisfactory, an extension of the model should be realized by means of, for example, increasing its order or adopting an alternative mathematical description of the physical processes. Once a new model is formulated, the parameters estimation and model validation procedures described in Sections 3.4 and 3.5 must be performed again. At this point, the new extended model has to be cross validated with the previous to check if the introduced extension is statistically meaningful. This is done by applying the method described in the following. Given two models, say 0 and 1, respectively with parameters $\boldsymbol{\theta} \in \Omega_0$ and $\boldsymbol{\theta} \in \Omega_1$, where $\Omega_0 \in \mathbb{R}^m$, $\Omega_1 \in \mathbb{R}^k$, $k > m$ and $\Omega_0 \subset \Omega_1$, the likelihood ratio λ is defined as

$$\lambda(\mathbf{y}) = \frac{L(\boldsymbol{\theta} \in \Omega_0 \mid \mathbf{y})}{L(\boldsymbol{\theta} \in \Omega_1 \mid \mathbf{y})}, \tag{5}$$

where L and $\mathbf{y}$ respectively denotes the likelihood function minimized in the MLE and the set of measurements used to fit the model. According to Wilk's theorem, the following statistic

$$D = -2 \log_{10}(\lambda(\mathbf{y})) \tag{6}$$

converges in law to a $\chi^2(k-m)$-distribution, i.e. a chi-squared distribution with $k - m$ degrees of freedom [12, 13]. The expression above can be reformulated as:

$$D = 2\big(\log_{10} L(\boldsymbol{\theta} \in \Omega_1 \mid \mathbf{y}) - \log_{10} L(\boldsymbol{\theta} \in \Omega_0 \mid \mathbf{y})\big). \tag{7}$$

The statistic D in Eq. (7) is used to test the null hypothesis $H_0 : \boldsymbol{\theta} \in \Omega_0$ against the alternative $H_1 : \boldsymbol{\theta} \in \Omega_1$. In other words, the Wilk's likelihood ratio test allows to infer which among Ω_0 and Ω_1 is the most suitable set for the vector of parameters $\boldsymbol{\theta}$. This is done by analyzing the p-value, and if it is smaller than an arbitrary small threshold (chosen as 2%), the null hypothesis is rejected and the model with $\boldsymbol{\theta} \in \Omega_1$ is considered a meaningful extension of model 0; otherwise, if the null hypothesis is not rejected, the extended model is not a valid extension of the model and is disregarded. The likelihood ratio test acts as a stopping criterion for the model extension process: in fact, extended models are with a larger number of parameters and usually perform better than the originals

because the increased number of freedom degrees of the optimization problem. On the contrary, the likelihood ratio test allows to determine statistically if the larger number of parameters is justified, and eventually prevents over-fitting to occur. A detailed example of the application of this method will be provided in Section 4 when cross validating the models.

4. Freezer thermal models

In this section, the models of the freezer that have been identified are presented. In general, refrigeration units, such as freezers and fridges, implement a thermodynamic cycle that achieves to transfer heat from a cold to a hot reservoir by a mean of supplying mechanical work to the system. The basic thermodynamic concepts that are used to formulate the models are introduced in the following while presenting the models. The models are formulated using the state-space description and are derived using the analogy between thermal and electric circuits, which consists in considering temperatures and heat fluxes as voltages and currents, respectively. The models are presented in increasing order of complexity. For each model, the estimation of the parameters is performed using MLE and the model validation is carried out applying the model residuals analysis, as previously described in Sections 3.4 and 3.5. The extension from one model to another is cross validated utilizing the method described in Section 3.6.

4.1. Model A (linear first order)

4.1.1. Model formulation

The equivalent electric circuit of Model A is shown in Fig. 2.

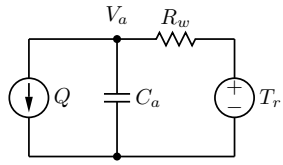

Figure 2: The equivalent electric circuit of Model A.

The current generator Q and the associated current respectively represent the freezer compressor and the heat flux that is extracted from the cold chamber of the freezer. In this and the following linear models, the heat flux Q is a function of the measured electric power consumption P according to the relationship

$$Q = P \cdot \mathrm{COP}, \tag{8}$$

where COP is the coefficient of performance of the refrigeration cycle, a dimensionless quantity defined as the amount of heat transferred from the cold to

the hot reservoir per unit of mechanical work supplied to the system. In the proposed models, the COP includes also the loss due to the electric motor: this explains why, in Eq. (8), the electric power P is utilized instead of the mechanical power. In Fig. 2, the capacitor C_a is a lumped description of the freezer cold thermal mass (air content, heat exchanger and freezer envelope) and V_a is the measured freezer temperature. The electric current flowing through the resistance R_w represents the lumped thermal resistance of the freezer to the external environment (room) which is at the measured temperature T_r. The first order linear model of the freezer is given by Kirchoff's voltage law (KVL) applied to the circuit of Fig. 2 and is as

$$\frac{dV_a}{dt} = -\frac{1}{R_w\ C_a}V_a + \frac{1}{R_w\ C_a}T_r - \frac{\mathrm{COP}}{C_a}P + e^{\theta}\frac{dw}{dt}, \tag{9}$$

where R_w, C_a, COP and θ are the parameters to be estimated and V_a and T_r are measurements. The last additive term of Eq. (9) denotes system noise and is composed by the Wiener process $w(t) \in \mathcal{N}(0,1)$ scaled by the factor e^{θ}. The observation equation of Model A is

$$T = V_a \tag{10}$$

and denotes that the freezer temperature T corresponds to the voltage V_a on the capacitor C_a.

4.1.2. Model identification and validation

Fig. 3 shows the logarithm of the absolute value of the normalized autocorrelation function of the model residuals. As mentioned in Section 3.5, checking for the presence of any autocorrelation in the model residuals allows to determine if the model was able to capture all the dynamics contained in the measurements or not. Comparing the autocorrelation functions of the model residuals and white noise permits an effective visual assessment of the performance of the model, since white noise is uncorrelated by definition. The 95% confidence interval of the white noise autocorrelation function is indicated in Fig. 3 and following plots with the blue dotted line, which should be hence intended as the threshold that indicates autocorrelation. The autocorrelation functions are plotted utilizing the semi-logarithmic scale in order to allows a clear visualization of small values.

As shown in Fig. 3, the Model A residuals are very much correlated as they are well above the blue line, which should be considered as a threshold. This means that the model is not able to capture the dynamics of the system and is hence suitable for being extended. The estimated values of the parameters of Model A are summarized in Table 1.

4.2. Model B (linear second order)

4.2.1. Model formulation

It was observed from the measurements that when the compressor of the freezer turns on, the freezer temperature does not decrease immediately. This

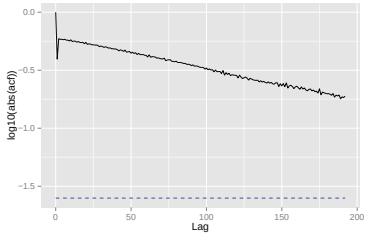

Figure 3: The autocorrelation functions of Model A residuals and white noise (in blue and black, respectively). In this case, Model A is not able to explain all the dynamics of the system.

Table 1: Model A identification summary.

Parameter	Unit	Value	σ
C_a	$[\mathrm{J\,K^{-1}}]$	2.99×10^{3}	5.00×10^{4}
R_w	$[\mathrm{K\,W^{-1}}]$	5.69×10^{-1}	7.50×10^{-1}
θ	–	-4.54	7.0×10^{-3}
COP	–	3.01×10^{-1}	6.07×10^{-3}
log-likelihood value		19833.1	-

is due to the fact that the heat exchanger needs to be cooled down before that heat is actually extracted from inside the freezer. The linear second order model shown in Fig. 4 is built in order to account for this fact. The additional components C_e and R_e respectively represent the thermal mass of the heat exchanger and the thermal contact resistance between the heat exchanger and the rest of the freezer cold mass.

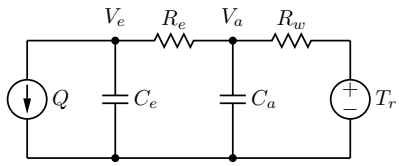

Figure 4: Model B electric equivalent circuit.

The state-space description of Model B is given as

$$\begin{bmatrix}\dot{V}_a\\ \dot{V}_e\end{bmatrix} = \begin{bmatrix}-\frac{1}{C_a R_w}-\frac{1}{C_a R_e} & \frac{1}{C_a R_e}\\ \frac{1}{C_e R_e} & -\frac{1}{C_e R_e}\end{bmatrix}\begin{bmatrix}V_a\\ V_e\end{bmatrix} +$$
$$+\begin{bmatrix}\frac{1}{C_a R_w} & 0\\ 0 & -\frac{\mathrm{COP}}{C_e}\end{bmatrix}\begin{bmatrix}T_r\\ P\end{bmatrix} + \begin{bmatrix}e^{\theta_0} & 0\\ 0 & e^{\theta_1}\end{bmatrix} d\mathbf{w} \tag{11}$$
$$T = \begin{bmatrix}1 & 0\end{bmatrix}\begin{bmatrix}V_a\\ V_e\end{bmatrix}. \tag{12}$$

4.2.2. Model identification and validation

Fig. 5 shows that the autocorrelation of Model B residuals is reduced in comparison to Model A, meaning that the additional state C_e absorbs part of the dynamics left unexplained by the previous model. Although, for time lags up to 100, the autocorrelation of the model residuals is consistently larger than the 95% confidence interval of white noise. This suggests that Model B could benefit of a further extension.

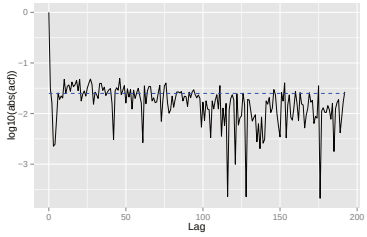

Figure 5: The comparison of the autocorrelation functions of the 1-step ahead prediction error of Model B (in black) and white noise (in blue) in semilogarithmic scale used to perform the validation as explained in 3.5.

The values of the estimated parameters of Model B are reported in Table 2. For the sake of completeness and although the model residuals analysis gave already an encouraging indication regarding the better performance of the current model with respect to the previous, we will proceed to apply the method described in Section 3.6 to evaluate if Model B is a valid extension of Model A. While extending from Model A to Model B, two parameters have been added to the model, hence according to Wilk's theorem (see Section 3.5), the statistic D in Eq. (7) converges in law to a $\chi^2(2)$-distribution. We use this result to establish the probability that Model B is not a better model of Model A, which is the null hypothesis to reject. The calculated value of Eq. (7) for the proposed model extension is

$$D = 10665, \tag{13}$$

and is determined using the the log-likelihood function values given in Table 1 and Table 2. Since the distribution of the stochastic variable D is known from

the Wilk's theorem and, from Eq. (5), a larger value of D implies a larger likelihood function of the less complex model, it is possible to assess the probability that Model B had worse performance than Model A as

$$p = \Pr(x > D) \tag{14}$$

which is known as the *p-value* and is determined as

$$\Pr(x > D) = 1 - \Phi(D), \tag{15}$$

where $\Phi(D)$ is the cumulative distributed function (CDF) of the $\chi^2(2)$-distribution and can be computed using, for example, the *chi2cdf* function in Matlab. In this case, the p-value is very close to zero, indeed smaller than the chosen 2% level of confidence interval. The null hypothesis, according to which Model B is not a statistically meaningful extension of Model A, is hence rejected.

Table 2: Model B identification summary.

Parameter	Unit	Value	σ
C_a	$[\mathrm{J\,K^{-1}}]$	9.74×10^3	2.12×10^3
C_e	$[\mathrm{J\,K^{-1}}]$	2.28×10^3	1.67×10^2
R_e	$[\mathrm{K\,W^{-1}}]$	9.74×10^{-2}	7.03×10^{-3}
R_w	$[\mathrm{K\,W^{-1}}]$	9.93×10^{-1}	1.80×10^{-1}
θ_0	–	-1.36×10^1	2.76
θ_1	–	-2.59	1.45×10^{-1}
COP	–	1.04	1.87×10^{-1}
log-likelihood value		25165.4	–

4.3. Model C (linear third order)

4.3.1. Model formulation

In this model, an additional state C_w is added in order to decouple between the thermal mass of the air inside the freezer and the freezer envelope. The resulting circuit is shown in Fig. 6, where R_a represents the thermal contact resistance between the air inside the freezer cold chamber and the freezer envelope.

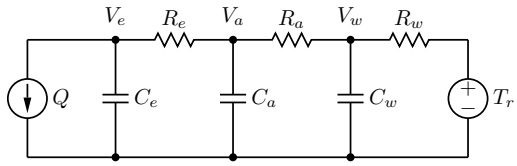

Figure 6: Model C electric equivalent circuit.

The state-space description of the model is given as

$$\begin{bmatrix} \dot{V}_e \\ \dot{V}_a \\ \dot{V}_w \end{bmatrix} = \begin{bmatrix} \frac{-1}{C_e R_e} & \frac{1}{C_e R_e} & 0 \\ \frac{1}{C_a R_e} & \frac{-1}{C_a R_a} + \frac{-1}{C_a R_e} & \frac{1}{C_a R_a} \\ 0 & \frac{1}{C_w R_a} & \frac{-1}{C_w R_w} + \frac{-1}{C_w R_a} \end{bmatrix} \begin{bmatrix} V_e \\ V_a \\ V_w \end{bmatrix} + \\ + \begin{bmatrix} 0 & -\frac{\mathrm{COP}}{C_e} \\ 0 & 0 \\ \frac{1}{C_w R_w} & 0 \end{bmatrix} \begin{bmatrix} T_r \\ P \end{bmatrix} + \begin{bmatrix} e^{\theta_0} & 0 & 0 \\ 0 & e^{\theta_1} & 0 \\ 0 & 0 & e^{\theta_2} \end{bmatrix} d\mathbf{w} \tag{16}$$

$$T = \begin{bmatrix} 1 & 0 & 0 \end{bmatrix} \begin{bmatrix} V_a \\ V_e \\ V_w \end{bmatrix}. \tag{17}$$

4.3.2. Model identification and validation

The autocorrelation of Model C residuals is shown in Fig. 7. An evident autocorrelation is still visible when compared to the 95% confidence interval of the autocorrelation function of white noise.

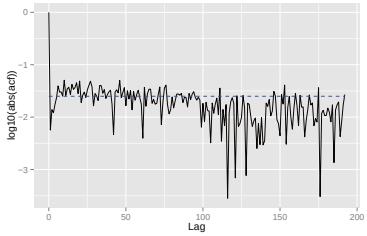

Figure 7: The comparison of the autocorrelation functions of the 1-step ahead prediction error of Model C (in black) and white noise (in blue) in semilogarithmic scale used to perform the validation as explained in 3.5.

As the autocorrelation functions of Model B and Model C residuals are very similar, we will proceed to cross validate the model to verify if the extension from the linear second order to the linear third order model is statistically relevant. The calculated value of the D statistic for the proposed model extension is

$$D = 6.8 \tag{18}$$

and is computed using Eq. (7) and the values given in Tables 2 and 3. Two parameters were added while passing from Model B to Model C, thus the D statistic converges in law to a $\chi^2(2)$-distribution. As the associated p-value is 0.0334 and the level of the confidence interval was chosen at 2%, the null hypothesis cannot be rejected: hence the extension from Model B to Model C is not considered statistically relevant. Since adding a state to the second order linear model did not contribute to improve the prediction performance, in the following models, a nonlinear description of the refrigeration cycle will be implemented to verify if it can describe the unexplained dynamics.

Table 3: Model C identification summary.

Parameter	Unit	Value	σ
C_a	$[\mathrm{J\,K^{-1}}]$	4.90×10^3	7.71×10^2
C_e	$[\mathrm{J\,K^{-1}}]$	2.26×10^3	1.89×10^3
C_w	$[\mathrm{J\,K^{-1}}]$	1.04×10^4	3.12×10^3
R_a	$[\mathrm{K\,W^{-1}}]$	3.92×10^{-1}	6.50×10^{-2}
R_e	$[\mathrm{K\,W^{-1}}]$	5.11×10^{-2}	1.24×10^{-2}
R_w	$[\mathrm{K\,W^{-1}}]$	9.99×10^{-1}	2.36×10^{-1}
θ_0	–	-3.31	1.7×10^{-2}
θ_1	–	-3.94	3.8×10^{-2}
θ_2	–	-9.97	2.6×10^{-1}
COP	–	7.68×10^{-1}	1.65×10^{-1}
log-likelihood value		25168.8	–

4.4. Model D (nonlinear second order)

4.4.1. Model formulation

As known, the COP of an ideal refrigeration cycle is expressed by the reversed Carnot cycle formula, which is given as:

$$\overline{\mathrm{COP}}(T_L, T_H) = \frac{T_L + 273}{T_H - T_L}, \tag{19}$$

where T_L and T_H are the temperatures in Celsius of the cold and hot reservoirs, respectively. In an equivalent way, the expression above can be written as

$$\overline{\mathrm{COP}}(T_L, T_H) = \frac{T_H + 273}{T_H - T_L} - 1 = \frac{T_H + 273}{\Delta T} - 1, \tag{20}$$

which highlights the nonlinear relationship between the COP and ΔT. In other words, the difference between the temperatures of the hot and cold reservoirs affects the ability of the thermodynamic cycle to transfer heat from the freezer cold chamber to the room. This phenomena was not taken into account in the linear models, where the COP was simply a constant scale factor of the power

consumption P. In the following nonlinear models, the COP is described as a linear function of the reversed Carnot cycle formula, i.e.

$$\mathrm{COP}(T_L, T_H) = \eta \cdot \overline{\mathrm{COP}}(T_L, T_H), \tag{21}$$

where the coefficient η can be regarded to as an efficiency factor that denotes how much the COP of the real refrigeration cycle differs from the ideal one. The structure of Model D is equivalent to the one of Model B, unless the expression of the heat extracted from the freezer Q, which is now expressed as

$$Q(V_e, T_r) = P_e \cdot \mathrm{COP}(V_e, T_r), \tag{22}$$

where the function $\mathrm{COP}(V_e, T_r)$ is given as in Eq. (21), and V_e and T_r are the temperature of the heat exchanger and room, respectively. The complete nonlinear state-space description of Model D is given as

$$\begin{aligned}\begin{bmatrix}\dot{V}_a \\ \dot{V}_e\end{bmatrix} &= \begin{bmatrix}-\frac{1}{C_a R_w} - \frac{1}{C_a R_e} & \frac{1}{C_a R_e} \\ \frac{1}{C_e R_e} & -\frac{1}{C_e R_e}\end{bmatrix}\begin{bmatrix}V_a \\ V_e\end{bmatrix} \\ &+ \begin{bmatrix}\frac{1}{C_a R_w} & 0 \\ 0 & -\frac{\eta}{C_e}\end{bmatrix}\begin{bmatrix}T_r \\ P\frac{V_e+273}{T_r - V_e}\end{bmatrix} + \begin{bmatrix}e^{\theta_0} & 0 \\ 0 & e^{\theta_1}\end{bmatrix} d\mathbf{w}.\end{aligned} \tag{23}$$

4.4.2. Model identification and validation

The autocorrelation of Model D residuals is shown in Fig. 8. In comparison to the previous linear models, the autocorrelation is reduced, indicating that Model D has an improved ability of capturing the dynamics contained in the set of measurements.

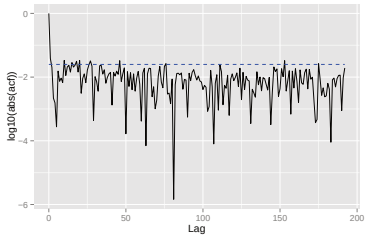

Figure 8: The comparison of the autocorrelation functions of the 1-step ahead prediction error of Model D (in black) and white noise (in blue) in semilogarithmic scale used to perform the validation as explained in 3.5.

The values of the estimated parameters of Model D are summarized in Table 4. It is worth to note that the value of the log-likelihood function of Model D is larger than for Model B and Model C, although the current model has respectively an equal and smaller number of parameters than the previous two. In this case, the Wilk's likelihood ratio test is not applied because Model D is not an extension of the previous models, but rather relies on a different modelling principle of the refrigeration cycle COP.

Table 4: Model D identification summary.

Parameter	Unit	Value	σ
C_a	$[\mathrm{J\,K^{-1}}]$	2.13×10^4	8.23×10^2
C_e	$[\mathrm{J\,K^{-1}}]$	2.35×10^3	2.34×10^3
R_e	$[\mathrm{K\,W^{-1}}]$	8.40×10^{-2}	2.16×10^{-2}
R_w	$[\mathrm{K\,W^{-1}}]$	5.65×10^{-1}	2.23×10^{-2}
η	–	3.85×10^{-1}	4.03×10^{-2}
θ_0	–	-1.12×10^1	2.53
θ_1	–	-2.00	6.5×10^{-2}
log-likelihood value		25179.8	–

4.5. Model E (nonlinear third order)

4.5.1. Model formulation

Model E has the same form as Model C unless that the heat flux Q is expressed using Eq. (22), in the same way as done for Model D.

4.5.2. Model identification and validation

The autocorrelation of the model residuals is shown in Fig. 9: very few values of the autocorrelation function of the model residuals exceed the 95% confidence interval of white noise, thus indicating that the current model is able to capture almost all the dynamics contained in the measurements.

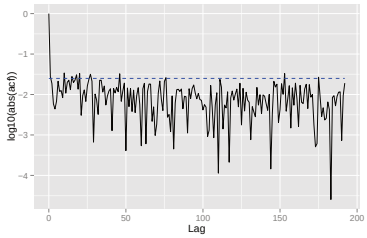

Figure 9: The comparison of the autocorrelation functions of the 1-step ahead prediction error of Model E (in black) and white noise (in blue) in semilogarithmic scale used to perform the validation as explained in 3.5.

The estimated values of the parameters of Model E are summarized in Table 5. As previously done, the extension from model D to E is evaluated applying the Wilk's likelihood ratio test. The value of the statistic D is

$$D = 15.6, \tag{24}$$

and the associated p-value is 4×10^{-4}. Since the p-value is very close to zero, the null hypothesis is rejected, and Model E is considered as a valid extension of Model D.

Table 5: Model E identification summary.

Parameter	Unit	Value	σ
C_a	$[\mathrm{J\,K^{-1}}]$	1.25×10^4	3.80×10^{-1}
C_e	$[\mathrm{J\,K^{-1}}]$	1.22×10^3	1.03×10^2
C_w	$[\mathrm{J\,K^{-1}}]$	8.30×10^3	1.59×10^2
R_a	$[\mathrm{K\,W^{-1}}]$	1.61×10^{-1}	8.66×10^{-5}
R_e	$[\mathrm{K\,W^{-1}}]$	1.47×10^{-1}	8.49×10^{-4}
R_w	$[\mathrm{K\,W^{-1}}]$	6.32×10^{-1}	3.53×10^{-3}
η	–	5.67×10^{-1}	2.97×10^{-1}
θ_0	–	-7.20	1.1×10^{-1}
θ_1	–	-3.66	3.4×10^{-2}
θ_2	–	-1.1×10^1	2.2×10^{-2}
log-likelihood value		25187.6	–

5. Models performance

5.1. Estimation of the physical values of the parameters

In this section, we perform a white-box estimation of the physical values of the parameters of the freezer in order to evaluate if the values and time constants estimated in the previous MLEs are of reasonable order of magnitude and if the circuit components of the proposed models captured those system dynamics they were meant for. The empirically estimated physical values of the parameters are shown in Tables 6 and 7. The thermal capacities are calculated as

$$C = V \cdot \rho \cdot c, \tag{25}$$

where V, ρ and c are respectively the volume, density and specific heat capacity. The volumes are estimated by measuring the components. If the components are not accessible for being measurement, their size is reasonably guessed. The thermal resistance of the isolation layer is estimated as

$$R = \frac{1}{\lambda} \cdot \frac{T}{S} \tag{26}$$

where λ is the thermal conductivity, T is the thickness and S is the lateral surface of the isolation layer. It is worth to note that this process is to intend as a further validation test of the proposed grey-box models and not a replacement of the grey-box modelling procedure. Grey-box is yet a more powerful modelling tool as allows to identify models using only time series data and regardless of difficult-to-get information, such as composition, materials physical constants, geometry and size of the freezer.

By comparing Tables 6-7 with 4-5, a discrepancy between the empirical and the estimated values of the thermal capacities of Model D and Model E can be

Table 6: The empirically estimated thermal capacities of the freezer main components [$\mathrm{J\,K^{-1}}$].

Component	Material	Thermal capacity
Chamber	Air	$\approx 5 \times 10^2$
Isolation envelope	Polyurethane foam [14]	$\approx 1 \times 10^4$
Heat exchanger	Iron	$\approx 1 \times 10^4$

Table 7: The empirically estimated thermal resistance of the freezer isolation [$\mathrm{K\,W^{-1}}$].

Component	Material	Thermal resistance
Isolation layer	Polyurethane foam [14]	≈ 0.54

noted. For example, in the case of Model E, the value of C_a is approximately 2 order of magnitude larger than the empirically calculated thermal capacity of the air, and vice-versa in the case of C_e and the thermal capacity of the heat exchanger. This indicates that the capacitors of the model did not absorbed those dynamics that they were originally meant for. It is hence not possible to state, for example, that C_a represents the thermal capacity of the air, but is rather a lumped description of the thermal masses of several parts of the freezer. In spite of this, the total value of the thermal capacities of Model D and Model E are of the same order of magnitude as the total empirical one, as well as the thermal resistance, thus denoting that the identified models parameters values are reasonable and overall close to the empirically estimated physical characteristics of the freezer. In the next section, we will show the ability of the proposed models to produce reliable temperature predictions.

5.2. Prediction errors of the models

Table 8 shows the absolute value of the mean and variance of the 20-minutes ahead prediction errors of the identified models. The statistics are realized utilizing a validation data set with a PRBS as the activation signal of the freezer compressor. The best temperature predictions are those provided by the nonlinear models since are unbiased and with the smallest standard deviation. As expected from the results of the validation process, Model A performs poorly and is implicitly excluded from the following discussion.

Although, the PRBS control signal usually induces the freezer temperature to vary in an extended range of values, as it was visible in Fig. 1: this is not the case of any practical applications since the food temperature is kept below a maximum level to preserve its quality. In order to verify if there is any substantial difference between linear and nonlinear models while predicting the freezer temperature in real operating conditions, we perform a second analysis considering, in this case, a validation data set measured during conventional thermostatic regime. The statistics of the prediction errors of this latter analysis are realized for both short and long-term forecast (5-minutes and 20-minutes) and are summarized in Table 9. As visible, the difference between linear and

Table 8: Twenty-minutes ahead prediction statistics with PRBS.

Model	$\lvert\bar{e}\rvert$ [°C]	σ_e [°C]
Model A	0.59	2.8
Model B	0.22	0.91
Model C	0.22	0.91
Model D	0.086	0.64
Model E	0.044	0.45

nonlinear models is reduced if compared to the previous case, especially when shortening the prediction horizon: in this case the predictions of Model C are even statistically better than those provided by nonlinear Model D.

Table 9: Five and twenty-minutes ahead prediction statistics for a thermostatic cycle.

	5-minutes ahead		20-minutes ahead	
Model	$\lvert\bar{e}\rvert$ [°C]	σ_e [°C]	$\lvert\bar{e}\rvert$ [°C]	σ_e [°C]
Model B	0.034	0.17	-0.15	0.73
Model C	0.012	0.10	-0.080	0.31
Model D	0.026	0.018	-0.084	0.55
Model E	0.003	0.001	-0.023	0.32

6. Discussion

A number of stochastic grey-box models to describe the thermal dynamics of a domestic freezer as a function of the power consumption were identified using time series data and maximum likelihood estimation. The measurement for fitting the models were obtained using an instrumented commercially available domestic freezer controlled by PRBS. The performance of each model was validated by means of the autocorrelation analysis of the model residuals, that allowed to determine if the models were able to capture all the dynamics observable from the measurements. The extension from one model to another was validated using the Wilk's likelihood ratio test. Two mainstream classes of thermal models were proposed: linear and nonlinear. The former class was characterized by a linear relationship between the power consumption and the refrigeration heat (i.e. constant COP). The latter included a nonlinear description of the refrigeration cycle based on the reverse Carnot cycle formula and allowed to describe the dependencies between the COP and the freezer temperature. It was shown that the first order linear model could not describe the freezer dynamics and that the increase of performance when passing from the second to the third order linear model was to ascribe mainly to overfitting rather

than a meaningful extension of the model. On the contrary, the identification process benefited of the inclusion of a nonlinear COP model based on the reversed Carnot cycle formula. Although, the statistics in Section 5.2 showed that when the models are used to predict the freezer temperature during real operating conditions (such as conventional thermostatic operation), the difference between linear and nonlinear models is reduced: this is explained by the fact that the temperature is limited in a smaller range than in the case of PRBS, and consequently the nonlinearities due to COP variations are less visible. The choice of the model to adopt is hence to be done evaluating the overall performance of the models as well as according to the requirements of the application. For example, in the next section, Model B is utilized to provide short-term predictions of the freezer temperature because it offers a good compromise between complexity and quality of the predictions when the temperature is constrained in a normal operation range. It is worth to note that the proposed grey-box models and the associated parameters are valid only for the instrumented freezer that was considered in this paper. However, both the described methods and models structures can be tested and applied to identify other kinds of freezers and for on-line real time estimation of the parameters also. As far as the consumer behavior is concerned, unmodelled phenomenas such as door openings and variable food content can alter significantly the consumption and temperature patterns of the freezer. These dynamics are difficult to capture with the grey-box framework because do not respond to any precise physical process as mainly depend on user habits. A perspective on how to capture the general operation pattern of a freezer including also consumer behavior is, for example, to test a two-layers model: the base layer implements a grey-box model, such as those proposed in this paper, to describe the freezer heat transfer and COP, and the upper layer is composed by a consumer behavior model derived, for example, utilizing pattern recognition techniques.

7. Models application: optimizing the power consumption of the freezer using model predictive control

Since the progressive extension of communication and metering infrastructures, controlling the electricity demand is becoming of increasing interest in the context of providing power system services, such as in the US to peak shave the demand [15–17] and Europe to allow the integration of more renewables into the power system [18, 19]. A method that is commonly envisaged in the existing literature to achieve demand response is to use a dynamic electricity price and expect that the consumers will adjust their flexible demand according to it [20, 21]. Flexible demand is that part of the consumption which can be shifted in time without compromising the quality of the primary service it is supplying to the consumer. The loads with this ability are referred to as demand side resources (DSRs) and are, for example, thermostatically controlled loads (TCLs), such as electric space heating and refrigeration units. Provided the forecast of the electricity price and a prediction model of a given TCL, the electricity consumption of the TCL can be controlled in order to minimize

the total electricity cost while maintaining the comfort of the consumer and respecting the operation limits of the device. This control strategy is known as economic model predictive control (MPC) and, in the case of the freezer, can be formulated as the following optimization:

$$[P_0^o, \cdots, P_{N-1}^o] = \underset{[P_0,\cdots,P_{N-1}]}{\arg\min} \sum_{i=0}^{N-1} p_i P_i \tag{27}$$

$$\text{s.t.} \quad T_{\min,i} \leq T_i \leq T_{\max,i}, \quad i = 0, \ldots, N-1 \tag{28}$$

$$P_{\min,i} \leq P_i \leq P_{\max,i}, \quad i = 0, \ldots, N-1 \tag{29}$$

$$T_{i+1} = f(T_i, P_i, T_r), \tag{30}$$

where p_i, P_i, T_i are respectively the price signal, the freezer power consumption and temperature at the time interval i. The constants $T_{\min,i}$, $T_{\max,i}$, $P_{\min,i}$ and $P_{\max,i}$ determine the bounds for the freezer temperature and power consumption. The function f is the model of the freezer, and T_r is the room temperature. The output of the optimization problem is the sequence $[P_0^o, \ldots, P_{N-1}^o]$, i.e. the trajectory of the freezer power consumption that minimizes Eq. (27) while satisfying the inequality constraints (28)-(30). The MPC strategy is usually actuated applying the receding horizon policy, which consists in, at each time step i, solving the optimization (27)-(30) and applying only the first set-point of the optimal decision sequence.

7.1. A tractable formulation of a convex economic MPC for the freezer

In this section, it is shown how the optimization problem in (27)-(30) can be formulated as a convex, which is appealing because it admits a global optimum (provided that a solution exists) and can be solved with well established and effective solution methods [22]. In order the optimization to be convex, the model function f in Eq. (30) must be linear. We choose to utilize Model B, as it is linear and because, in this application, the prediction horizon is short (5-minutes) and the temperature is constrained in a limited range. As it was shown in Section 5.2, when such conditions are met, the difference between the predictions performance of linear and nonlinear models is small. Moreover, the receding horizon formulation of the MPC strategy allows to absorb the prediction errors of the models, because the optimization is repeated at each discrete time interval. In the following, we will use the assumption that the power consumption of the freezer can be modulated instead of being on-off. From Appendix A, the prediction of the freezer temperature for the time horizon $i = 0, \cdots, N-1$ is given by Eq. (A.17) as

$$\boldsymbol{T} = \Phi v_0 + \Theta(B)\boldsymbol{P} + \Theta(E)\boldsymbol{T_r}, \tag{31}$$

where the symbols Φ, $\Theta(B)$, $\Theta(E)$ are as defined in Appendix A and $v_0 = [v_{a,0}, v_{b,0}]^T$ is the measured state vector of Model B. The bold notation indicates column vectors obtained stacking the time variant scalar values of the respective quantities, i.e. $\boldsymbol{T} = [T_1, \cdots, T_N]^T$, $\boldsymbol{P} = [P_0, \cdots, P_{N-1}]^T$, $\boldsymbol{T_r} =$

$[T_{r,0}, \cdots, T_{r,N-1}]^T$. The group of inequality constraints in (28) can be written utilizing Eq. (31), as shown in (33) and (34) where the known terms (i.e. the temperature limits , the measured current state and the temperature predictions of the room, that can be assumed constant because regulated) have been moved on the right-hand-side terms. In a similar way, the group of inequality constraints in (29) can be written as in (35) and (36). The complete formulation of the proposed optimization is given as

$$\boldsymbol{P^o} = \arg\min_{\boldsymbol{P}} \boldsymbol{p}^T \boldsymbol{P} \tag{32}$$

$$\text{s.t.} \quad \Theta(B)\boldsymbol{P} \leq \boldsymbol{T_{max}} - \Phi v_0 - \Theta(E)\boldsymbol{T_r} \tag{33}$$

$$-\Theta(B)\boldsymbol{P} \leq -\boldsymbol{T_{min}} + \Phi v_0 + \Theta(E)\boldsymbol{T_r} \tag{34}$$

$$\mathbb{I}_{N\times N}\boldsymbol{P} \leq \boldsymbol{P_{max}} \tag{35}$$

$$-\mathbb{I}_{N\times N}\boldsymbol{P} \leq -\boldsymbol{P_{min}}, \tag{36}$$

which is convex as both the cost function (32) and the inequality constraints (33)-(36) are affine functions of the decision variable $\boldsymbol{P}$. The proposed optimization can be promptly solved using off-the-shelf software, such as Matlab with the *linprog* function.

7.2. Simulation results

In this section, we compare by simulations the performance of a conventional thermostatic controller and the proposed MPC. For the MPC, deterministic simulations conditions are assumed, i.e. both the price signal forecast and the freezer temperature prediction are known without uncertainty. The ambient temperature T_r is constant and the consumer behavior,i.e. door openings and variable food content, is not included in the simulations. The price signal utilized for the MPC optimization problem is shown in Fig. 10 and is a historical time series of the 5-minutes electricity price of the Canadian power system operator IESO [23].

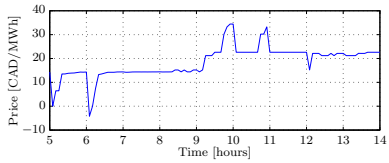

Figure 10: The 5 minutes real time electricity price of IESO utilized to test the MPC strategy.

The simulated operation of the thermostatically controlled freezer is depicted in Fig. 11, which shows the freezer temperature and power consumption in the upper and lower panel, respectively. The thermostatic control is realized as:

$$P_i = \begin{cases} P_{\text{nominal}}, & \text{if } T_i < T_{\text{set-point}} - h \\ 0, & \text{if } T_i > T_{\text{set-point}} + h \\ P_{i-1}, & \text{otherwise} \end{cases}, \tag{37}$$

where P is the power consumption, T is the temperature of the freezer and i denotes a discrete time interval. $T_{\text{set-point}}$ and h are respectively the set-point and hysteresis of the thermostat and, in the proposed simulations, are -16 and 1°C. These values were conveniently chosen in accordance with the food refrigeration regulations which indicate a maximum cold storage temperature of approximately $-17\,°\text{C}$ [24].

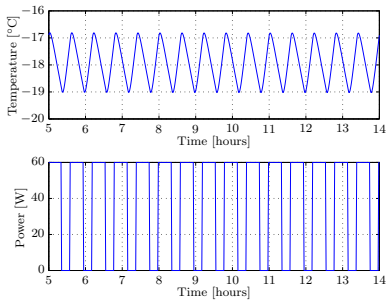

Figure 11: The freezer temperature and power consumption of the thermostatic controller.

The freezer operation with the MPC controller is illustrated in Fig. 11. Similarly to the case of the thermostat controller, the highest freezer temperature $T_{\max}$ is chosen as $-17\,°\text{C}$, while $T_{\min}$ is $-25\,°\text{C}$. From Fig. 11, it is visible that the MPC tends to consume less energy when the electricity price is expensive by storing energy using the available thermal mass. For example, in the time interval between hour 8 and 10, the freezer power consumption is initially increased to reduce the temperature and in order to reduce the consumption when the electricity price is larger.

The total cost of the electricity required for the operation of the two discussed controllers and considering the price signal of Fig. 10 are summarized in Table 10. In comparison to the conventional thermostatic controller, the MPC strategy achieves a 8.1% operation cost reduction.

8. Conclusions

In this paper, the application of a grey-box modelling methodology to the model identification of a domestic freezer was described. The objective of the

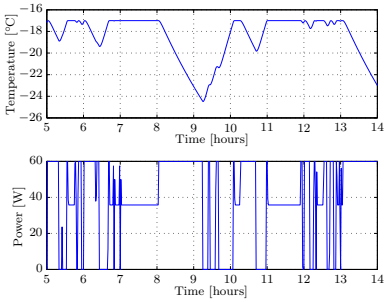

Figure 12: The freezer temperature and power consumption of the MPC controller.

Table 10: Electricity cost of the controllers during 24 hours operation.

Controller	Total electricity cost [CAD]
Thermostat	0.0913
MPC	0.0839

system identification effort was to model the physical processes associated with the operation of the freezer (heat transfer and refrigeration cycle coefficient of performance). The model identification was carried out utilizing measurement from an instrumented commercially available domestic freezer and maximum likelihood estimation. A number of linear and nonlinear dynamic models were presented in increasing order of complexity, validated through the residuals analysis and cross-validatated to detect model overfitting. It was shown that including in the models a nonlinear description of the refrigeration process based on the reversed Carnot cycle improves the performance of the modelling process, allowing to explain the most of the time dynamics observable from the measurements. As an application of the presented models, a convex model predictive control (MPC) strategy was formulated with the objective of providing demand response using a freezer according to a dynamic electricity price. The simulations results show that the MPC strategy was able to shift the consumption of freezer and decrease the operation cost of 8%. The main outcome of the paper is an experimental proof-of-concept that grey-box modelling can be effectively used to identify reliable models of a domestic refrigeration useful for temperature and electricity consumption predictions. The future work is in the direction of integrating the proposed models with pattern recognition techniques in order to identify consumer behavior.

Appendix A.

Let $A_c \in \mathbb{R}^{n\times n}$ and $B_c, C \in \mathbb{R}^n$ the matrices of the following generic linear continuous time state-space model

$$\dot{x}(t) = A_c x(t) + B_c u(t) \tag{A.1}$$
$$y(t) = Cx(t), \tag{A.2}$$

where $\boldsymbol{x}(t) \in \mathbb{R}^n$ and $y(t) \in \mathbb{R}$ are respectively the state and output of the system. The discrete state space representation of the linear model above is

$$x_{i+1} = Ax_i + Bu_i \tag{A.3}$$
$$y_i = Cx_i, \tag{A.4}$$

where the system matrices A and B can be obtained, for example, using the backward Euler method as

$$A = A_c T_s + \mathbb{I}_{n\times n} \tag{A.5}$$
$$B = B_c T_s, \tag{A.6}$$

where T_s is the discretization time. Developing (A.3) and (A.4) for $i = 1$ and $i = 2$, respectively, yields

$$x_1 = Ax_0 + Bu_0 \tag{A.7}$$
$$y_2 = C\big(Ax_1 + Bu_1\big). \tag{A.8}$$

Replacing (A.7) into (A.8) gives

$$y_2 = CA\big(Ax_0 + Bu_0\big) + CBu_1. \tag{A.9}$$

Iterating the same procedure, the output of the system at a generic time instant n is:

$$y_n = CA^n x_0 + CA^{n-1}Bu_0 + \cdots + CA^0 Bu_{n-1}. \tag{A.10}$$

Using the matrix product notation, the model output for the time instants $i = 1, \cdots, n$ can be written as:

$$\begin{bmatrix} y_1 \\ y_2 \\ \vdots \\ y_n \end{bmatrix} = \begin{bmatrix} CA \\ CA^2 \\ \vdots \\ CA^n \end{bmatrix} x_0 + \begin{bmatrix} CB & 0 & \cdots & 0 \\ CAB & CB & \cdots & 0 \\ \vdots & \vdots & \ddots & \vdots \\ CA^{n-1}B & CA^{n-1}B & \cdots & CB \end{bmatrix} \begin{bmatrix} u_0 \\ u_1 \\ \vdots \\ u_{n-1} \end{bmatrix}. \tag{A.11}$$

In a more compact form, the expression above can be written as:

$$\boldsymbol{y} = \Phi x_0 + \Theta(B)\boldsymbol{u}, \tag{A.12}$$

where the following quantities have been introduced

$$\Phi = \begin{bmatrix} CA \\ \vdots \\ CA^n \end{bmatrix} \tag{A.13}$$

$$\Theta(B) = \begin{bmatrix} CAB & 0 & \cdots & 0 \\ \vdots & \vdots & \ddots & \vdots \\ CA^{n-1}B & CA^{n-1}B & \cdots & CB, \end{bmatrix} \tag{A.14}$$

and the bold variables u and y are column vectors obtained stacking the respective time variant scalars. In the case the system (A.3) has an additional input v_i such as

$$x_{i+1} = Ax_i + Bu_i + Ev_i \tag{A.15}$$

$$y_i = Cx_i, \tag{A.16}$$

the system output (A.12) can be written as

$$\boldsymbol{y} = \Phi x_0 + \Theta(B)\boldsymbol{u} + \Theta(E)\boldsymbol{v}, \tag{A.17}$$

i.e. adding the input and the respective transition matrix $\Theta(E)$.

References

1. Annual energy outlook 2012. Tech. Rep.; US Energy Information Administration; 2012.

2. Xydis G. Wind energy to thermal and cold storage—a systems approach. *Energy and Buildings* 2013;56:41–7.

3. Douglass P, Garcia-Valle R, Sossan F, Ostergaard J, Nyeng P. Design and evaluation of autonomous hybrid frequency-voltage sensitive load controller. In: *IEEE International Conference on Innovative Smart Grid Technologies (ISGT)*. 2013:.

4. Christakou K, Tomozei DC, Le Boudec JY, Paolone M. Gecn: Primary voltage control for active distribution networks via real-time demand-response. *Smart Grid, IEEE Transactions on* 2013;PP(99).

5. Hovgaard TG, Larsen LF, Edlund K, Jørgensen JB. Model predictive control technologies for efficient and flexible power consumption in refrigeration systems. *Energy* 2012;44:105–16.

6. Hovgaard TG, Boyd S, Larsen LF, Jørgensen JB. Nonconvex model predictive control for commercial refrigeration. *International Journal of Control* 2013;86:1349–66.

7. Hermes CJ, Melo C, Knabben FT, Gonçalves JM. Prediction of the energy consumption of household refrigerators and freezers via steady-state simulation. *Applied Energy* 2009;86(7).

8. Hovgaard T, Larsen LFS, Skovrup M, Bagterp Jø rgensen J. Power consumption in refrigeration systems-modeling for optimization. In: *Advanced Control of Industrial Processes (ADCONIP), 2011 International Symposium on*. 2011:234–9.

9. Hermes CJ, Melo C. Assessment of the energy performance of household refrigerators via dynamic simulation. *Applied Thermal Engineering* 2009;29(5).

10. Costanzo GT, Sossan F, Marinelli M, Bacher P, Madsen H. Grey-box modeling for system identification of household refrigerators: A step toward smart appliances. In: *IEEE International Youth Conference on Energy (IYCE)*. 2013:.

11. Kristensen NR, Madsen H. Continuous time stochastic modelling. 2003.

12. Madsen H, Thyregod P. Introduction to General and Generalized Linear Models. Chapman & Hall/CRC Texts in Statistical Science Series; Chapman & Hall/CRC; 2011.

13. Nelder JA, Wedderburn RW. Generalized linear models. *Journal of the Royal Statistical Society Series A (General)* 1972;:370–84.

14. Thermal insulation materials made of rigid polyurethane foam. Tech. Rep.; Federation of European Rigid Polyurethane Foam; 2006.

15. Herter K, Wayland S. Residential response to critical-peak pricing of electricity: California evidence. *Energy* 2010;35:1561–7.

16. Zarnikau JW. Demand participation in the restructured electric reliability council of texas market. *Energy* 2010;35:1536–43.

17. Cappers P, Goldman C, Kathan D. Demand response in u.s. electricity markets: Empirical evidence. *Energy* 2010;35:1526–35.

18. Keane A, Tuohy A, Meibom P, Denny E, Flynn D, Mullane A, O'Malley M. Demand side resource operation on the irish power system with high wind power penetration. *Energy Policy* 2011;39(5):2925–34.

19. Hedegaard K, Ravn H, Juul N, Meibom P. Effects of electric vehicles on power systems in northern europe. *Energy* 2012;48(1):356 –68.

20. Sossan F. Indirect control of flexible demand for power system applications. Ph.D. thesis; Technical University of Denmark, Department of Electrical Engineering; 2014.

21. Hammerstrom DJ, Ambrosio R, Carlon TA, Desteese JG, Kajfasz R, Pratt RG. Pacific Northwest GridWise Testbed Demonstration Projects Part I . Olympic Peninsula Project. *Contract* 2007;:157.

22. Boyd S, Vandenberghe L. Convex Optimization. Cambridge University Press; 2004.

23. Independent Electricity System Operator . IESO power data. 2014. URL: http://www.ieso.ca/Pages/Power-Data/default.aspx.

24. University of Nebraska-Lincoln . Refrigerated and freezer storage. 2014. URL: http://food.unl.edu/safety/refrigerator-freezer.

Paper B

A Comparison of algorithms for controlling DSRs in a control by price context using hardware-in-the-loop simulation

A Comparison of Algorithms for Controlling DSRs in a Control by Price Context Using Hardware-in-the-loop Simulation

Fabrizio Sossan
IES Risø-DTU
Roskilde, Denmark
Email: faso@risoe.dtu.dk

Henrik Bindner
IES Risø-DTU
Roskilde, Denmark
Email: hwbi@risoe.dtu.dk

***Abstract*—With an high penetration of energy production from fluctuating energy sources, the reallocation of power system ancillary services - traditionally assigned to conventional power plants - is required in order to provide stable and reliable power system operations. Demand Side Resources, DSRs, are electric loads whose consumption can be controlled or scheduled and so they can be conveniently used for supplying power system services. A shift in the power usage of Demand Side Resources can be induced through a brodcasted price signal. In this paper the performances of three different algorithms suitable for controlling domestic electric space heating using a price signal are compared. A population of houses is simulated in a software platform and, in order to pretend more realism from the simulation, their behaviors are modified in real time using a temperature feedback signal which comes from a real building. The experimental results of using a model predictive controller on a real building are also shown.**

This study is part of the Flexpower project whose aim is investigating the possibility of creating an electric power system with a big participation of DSRs in the regulating power market.

I. Introduction

Demand side resources, or DERs, are electric loads that provide services that are naturally coupled to some kind of storage; this allows to control, schedule or shift their usage without having a big direct impact on the quality of the services they are providing to the users. Examples of demand side resources are space or water heating, electric vehicles or also dedicated small storage systems. Because their flexibility, DERs are suitable to be controlled in order to gives support to power system services with respect to their constraints, physical limits and local settings. DERs exploitation is based on the consideration that the contribution from the single unit is small but the aggregated response of a big number of devices might be relevant. Demand side resources can be directly controlled (for example by a power reference signal), they can react in order to response to a deviation of the grid frequency or, a time shift in their electric power usage can be achieved using a price signal for the electric energy: this economic incentive should induce the user to consume more power when the energy is cheap (and in the case to store it) and to reduce the consumption when the price for the energy is high. Price signal is a convenient form of control since the decision is computed locally while in the case of direct control the information (local conditions or user preferences for example) should be propagated from each devices up to some aggregator which should send a control signal to drive each of them. The critical part of a control-by-price approach is the price signal itself because, for producing it, the response of the distributed demand side resources should be known because it is required in the market bidding.

In this paper the performances of three algorithms with price responsiveness capability for controlling domestic electric space heating through a broadcasted price signal are compared. The proposed algorithms have different level of requirements: two of them work basing their decision on historical data of the price signal; the third one is a model predictive controller (MPC) and it uses both price and real weather forecast.

In this approach, the price signal is artificial and it is built with the aim of highlighting the pros and cons of each control algorithm. The algorithms have been compared adopting both a final user point of view, evaluating the deviation from the optimal comfort level (the indoor temperature set-point in this case) and the total cost for the energy used, and the power system one; from the power system perspective, it would be useful having a devices with a good price responsiveness capability, able to reduce or to decrease the power consumption steadily for a long time and predictable in the behavior.

The control algorithms have been tested in a Java simulation platform with a population of houses. For pretending more realism from the simulation, an *hardware-in-the-loop* approach has been used: the thermal dynamics of a real building have been introduced in the simulation and they are used for perturbing in real time the behaviors of all the houses inside the population.

Detailed descriptions about the simulation platform, the hardware in the loop feedback, the thermal models, the control algorithms and how their performances have been compared are given in Section II.

Section III is for presenting and discussing the results of the simulations: both the aggregated response of the population of buildings and the experimental result of the model predictive

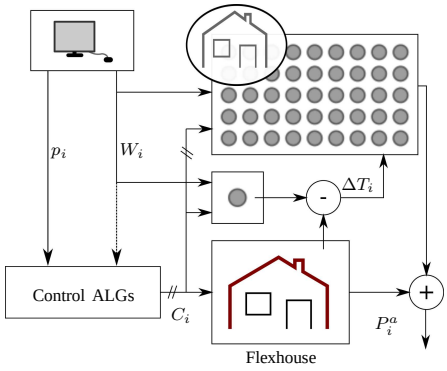

Fig. 1. The experimental setup used for the proposed simulations with the Flexhouse building as the *hardware-in-the-loop* for reproducing the real environmental conditions. Weather forecast W_i and the price p_i signal are used.

controller applied on a real house are reported. A comparison of the performances obtained with the different control algorithms is then presented.

Section IV is for conclusions.

II. Methods

The software tool used for performing the simulations is a Java dynamic simulator which allows to implement generic models and control algorithms. The functionalities of the simulation platform have been integrated with our power system facility, SYSLAB [1], in order to perform a real time hardware in the loop simulation introducing the thermal dynamics of a real building, Flexhouse [2].

The diagram of the simulation scenario is shown in Figure 1. The box with the small gray circles represents the population of houses that is implemented in the simulator. The disturb signal ΔT_i, which is obtained comparing the indoor temperature of Flexhouse with its model implemented in the simulator, perturbs the behavior of all the models in order to reproduce the effect of the real environment and operating conditions (uncertainties in the modeling and in weather forecast). Of course environmental local conditions like wind, outside temperature and solar radiation, act on Flexhouse.

The output of each implemented control algorithm is a signal that drives the electric heaters. In the case of Flexhouse, the same control signal is applied both to the real building and to the model inside the simulation platform in order to compare the real behavior with the simulated one.

The output of the simulation is the temperature profile and the power usage of each building: the sum of them gives the aggregated electric power consumption. Also the experimental data regarding Flexhouse activity are made available by the simulation platform.

In this experimental setup, the price signal p_i is simulated and it is built for trying to demonstrate which algorithm performs better within this framework. In accordance with Flexpower project, the price for the electric energy is released every five minutes.

Weather forecast W_i for the area are delivered by a FTP service and they are produced by Risø-DTU Meteorological Department; they are used both by the model predictive controller and for evolving the state of thermal models. Weather forecast are released every day and with a time resolution of one hour: smaller time steps are required for computing the models evolution so the same resolution of the price signal, five minutes, is achieved simply using linear interpolation.

Despite local conditions measurements, such as outdoor temperature or solar radiation, are available in SYSLAB, they are not used by the implemented control algorithms because it would not be realistic in an future diffusion of the control by price since it would increase the complexity of the system for the many sensors to add around.

A. Thermal models

Reference [3] present several linear thermal models for Flexhouse. They are reported in increasing order of complexity (states number) and they are built using a grey-box approach where the parameters are computed using a maximum likelihood estimator with real measurements from Flexhouse. The one selected for this implementation is the simplest one, a 1-state linear model. This model is used both for describing Flexhouse dynamics and the population of buildings; for this last purpose, the parameters of the model have been slightly perturbed following a normal distribution for taking into account small differences in size and thermal conductivity features.

The population of the buildings is composed by four identical groups of fifty houses each. Each group of buildings is driven by a different type of controller (presented later) and the temperature evolution of each model is perturbed at each step by the noisy input discussed before.

For a better description of the thermal behavior of a building, a two states model could be used for representing the transients both of the air and of the building envelope. The reason why a simpler 1-state model has been chosen is that Flexhouse only disposes of the indoor air temperature information so this is the only measure available for initializing the model (a state estimator could be considered in the case of linear models with larger order). Anyway the hardware in the loop approach gives to the simulated population of house an even more realistic footprint to the thermal transient. The problem still remains in the model predictive controller, where the 1-state model could not give a good prediction on the future indoor temperature during transient (the steady state response is the same) resulting in a worse performance of the controller.

B. Control algorithms

The control algorithms for whom the performances are compared have different levels of complexity and requirements.

The simplest one is the traditional thermostatic controller and it has been included mainly for having a comparison with the current situation.

The second algorithm is a simple evolution of the traditional thermostat where a price response capability has been added: in the temperature hysteresis cycle, the controller can choose to switch on the heating for storing thermal energy if the proposed price for the electric energy is cheaper than the prices paid in average (in the past) or otherwise to shutdown it.

The third control algorithm is proposed by [4] and [5]; again, the decision process is based upon considerations on the historical prices. At each time i, when a new price for electric energy is proposed, the temperature set-point for the thermostatic controller is deviated from the optimal one using the quantity ΔT_i defined in the Equation 1:

$$\Delta T_i = -k * \hat{p}_i \tag{1}$$

$$\hat{p}_i = \frac{p_i - \overline{p}_i}{\sigma_i} \tag{2}$$

where p_i, $\overline{p}_i$ and σ_i in Equation 2 are respectively the current price, the moving average and standard deviation of the price history for the last 24 hours. Coefficient k is a positive constant and sets the price responsiveness capability of the controller. $\hat{p}_i$ is called *relative price*. The result achieved by this controller is to produce a temperature deviation ΔT proportional to the relative price and in general it is negative when the price is greater than the average of the old ones: so the new temperature set-point will be smaller than the previous one and vice-versa.

The fourth and last controller uses a thermal model for computing the future temperature states of the house and it minimizes a cost expression in the form of Equation 3 with finding an appropriate heating power profile; the target of the algorithm is to reduce future deviations from the temperature set-point paying as few as possible for the electric energy.

$$J = k_1 q(T(t_f)) + \int_0^{t_f} k_2 q(T(t)) + r(u(t))\overline{p}(t)\ dt \tag{3}$$

The symbols T and u, both time dependent, are for indoor temperature and heating power respectively. The integration interval starts from the current instant, 0, until the length of optimization horizon t_f. The functions $q(T)$ and $r(u)$ are numerical weighting barrier functions that assume high values when the independent variable approaches not admissible values. Their shape is shown in Figure II-B. Function $\overline{p}(t)$ is the price signal that, multiplied by the electric power used by the heaters and integrated in time, gives a money value. Since the integral looks ahead in time, $\overline{p}(t)$ is a price forecast series. As said before, the price signal is artificial and, in this approach, it is assumed to know the price forecast without error. The factor k_1 determines the price responsiveness capability of the controller. The goal of the optimization process is finding the optimal control law $u^o(t)$ that is able to minimize the cost expression J of Equation 3. For finding the minimizing control $u^o(t)$, a numeric algorithm based on the gradient descent method[6] has been used and it is applied each time a new price for the electric energy is released (five minutes). The indoor temperature T should be treated as stochastic variable but in this approach the problem formulation is left deterministic since the receding horizon configuration brings a natural feedback into the system because the algorithm retrieves a new indoor temperature reading every five minutes, together with the price signal and weather forecast.

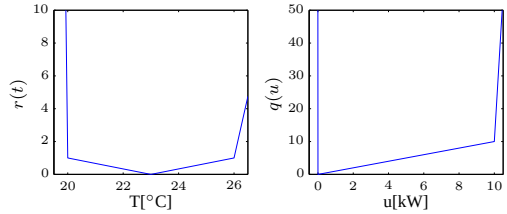

Fig. 2. The weighting functions $q(T)$ and $r(T)$ used in the cost expression of the model predictive controller.

Both a final user and power system point of views have been taken into account in the comparison of the performances of the different algorithms. These three indicators have been evaluated.

1) temperature comfort penalty function: it is computed as the integral in time of the temperature deviation from the set-point (chosen as $23°C$ for all the population of simulated buildings and Flexhouse). States of under-temperature have been weighted 1.2 times more than over-temperature conditions; a second temperature penalty function is considered and it is the integral in time of the temperature deviation when it is out of the admissible comfort interval (defined as $23 \pm 3°C$).

2) total cost for energy: it is simply the integral in time of the electric power used for heating multiplied by the price signal;

3) price responsiveness capability: it is defined as the variation of heating power produced by a control algorithm with respect to price variation (dP/dp).

The first two indicators take into account the user comfort and economic benefit, while the last one is important from power system perspective since it gives a measurement of the control capability that each algorithm adds, in this case, to domestic electric heating. The second indicator, the total cost for the energy, gives also a measurement of the capability of the algorithm to move electric power consumption in instants of time with lower energy prices.

The number of on-off cycles produced by the algorithms has not been take into account in this analysis; anyway this is a relevant aspect since the lifetime of the electromechanical devices acted to powering heaters is heavily affected by the number of switching cycles.

III. Results and Discussions

As introduced before, the simulation here presented is obtained applying the heating power setting computed by the predictive controller to both a real building (Flexhouse) and its model. The difference between the two responses is then

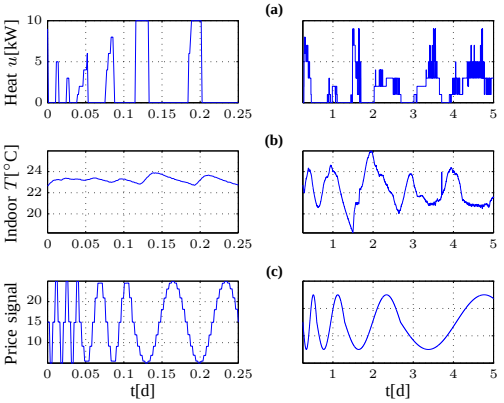

Fig. 3. The experimental data from Flexhouse with the model predictive controller. Plot *a* shows the heating power, *b* is the indoor temperature and *c* is the artificial price signal.

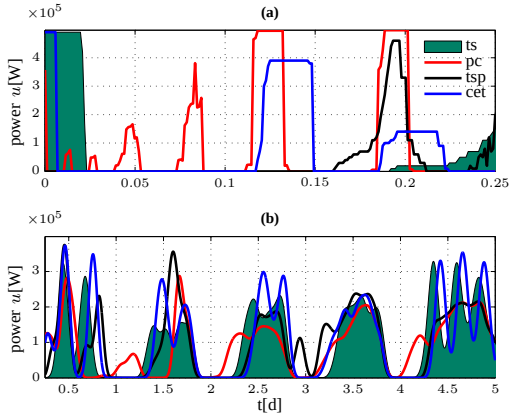

Fig. 4. A comparison of the output of the four different controllers. The two plots are consecutive and with different time scale. Data in the plot *b* have been filtered with a low pass filter for a better visualization of the main frequency components.

used for perturbing the state of all the other buildings inside a real time simulation, where the behavior of 200 houses (divided in four identical groups of 50 buildings with each group driven by one of the four algorithms discussed before) is reproduced. The temperature set-point for all the buildings is $23°C$ and the allowed offset is $\pm 3°C$. An artificial new price is broadcasted every five minutes together with real weather forecast. The price signal is a sine wave with decreasing frequency. For convenience of visualization, some of the plots here presented are split in a two parts with each of them having a different x (time) scale. The optimization horizon length of the predictive controller is five hours; as said before, it uses real weather forecast and the price signal forecast is supposed known without error.

Time $t = 0$ in the plots refers to 18:16 pm of October the 13^{rd} 2011 and the simulation last for 5.2 days.

Since the price signal is artificial and it was created for enabling the comparison between algorithms, its unit of measure on the plots is not specified and it is intended as a generic monetary value for unit of energy (i.e. $/kWh).

The firsts plots in Figure 3 shown the experimental results of the application of the model predictive controller to Flexhouse. It is visible the attempt of the controller to move the electric energy consumption when the price is low. With the decreasing of the frequency of the price signal, the controller starts to lose the capability of shifting the energy usage because the house does not have enough thermal inertia to maintain the indoor temperature in a acceptable range.

Figure 4 shows the aggregated response of the four different groups of buildings; each of them is driven by a different controller according to the plot legend: *ts* stays for thermostatic controller, *tsp* is for second algorithm discussed in Section II, *cet* is the third and *pc* is the model predictive controller. The data in the bottom graph have been elaborate with a low pass filter for a better visualization. As Figure 4 shown, the output produced by each controller with price responsiveness capability is very different from the green area that is the thermostat action; this means that they are all exploiting the flexibility offered by the price signal but, anyway, in different ways. Again, with the increasing of the period of the price signal, all the controllers tend to show a behavior more and more similar to the thermostatic controller action because the thermal inertia is not enough for both being able respond to slow price variation and maintaining the indoor temperature in an acceptable comfort level.

Figure 5 shows the average temperature profiles for the four different groups of buildings. Plot *a* shows the instant deviation from the indoor temperature set-point ($23°C$). Plot *b* shows the accumulated error computed as the integral of the deviation, where the states of under temperature have been weighted 20% more than states of over temperature. Plot *c* shows the accumulated error when the temperature is not in the admissible range $23 \pm 3°C$. Plot *b* shows that the thermostatic controller is the more precise in keeping the temperature close to the optimal set-point; plot *c* shows that the model predictive controller is the one that performs best in keeping the temperature of the buildings in the defined acceptable range. It is worth to notice the behavior of the two thermostatic based controllers (black and green profiles): in fact they always should be able to maintain the temperature in the thermostatic interval but, in the days of the simulation, the weather was cold ($7/12°C$) and sunny in the Copenhagen area and during the day hours the sun was able to warm the buildings in a significative way. This

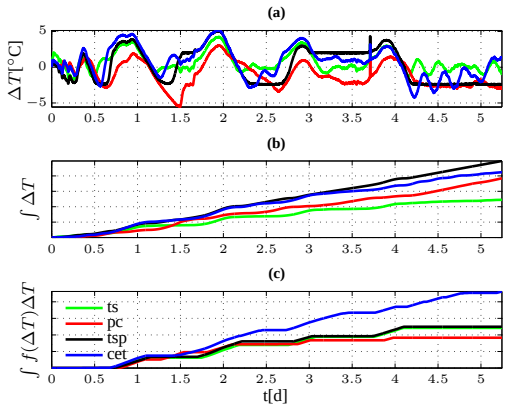

Fig. 5. Plot *a* shows the temperature deviation from the set-point (23°C) for the different algorithms. Plot *a* is the accumulated error (with states of under temperature have been weighted 1.2 times more). Plot *c* is the accumulated error for the temperature deviation from the comfort area that is 23 ± 3°C.

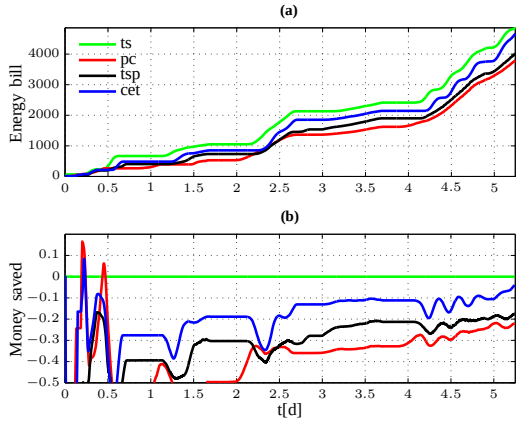

Fig. 6. Plot *a* shows the instant values of the electric bill. Plot *b* shows the money saved with respect to the traditional thermostatic controller in a price signal context.

explain why the thermostatic based controllers have this accumulated error different than zero; in this case the model predictive controller takes advantage of the weather forecast and it is able to perform even better than them. The control algorithm that corresponds to the blue line does not show a good performance in plot *c* because the way the temperature offset is computed (Equation 1) can easily lead to temperature references quite different from the real desired optimal one.

Figure 6 shows the cost of the energy for the different control algorithms. Plot *a* is the instant energy bill and plot *b* represents the average instant amount of money that the final user would save (in a variable price context of course) applying the different algorithms with respect to using traditional thermostatic controller. Plots in Figure 6 show that the model predictive controller is the algorithm that performs best together with the very simple modified thermostatic controller. It is worth to notice that, despite weather forecast are real, the price signal is supposed known and so in the case of the energy bill the performance of the model predictive controller could be worse if wrong forecast are provided. Anyway, with good price forecast the MPC controller is the algorithm supposed to still give the best result because it is the only that, using forecast, takes advantage of looking into the future for a better trading of the thermal energy stored in the buildings. So, for example, if the price forecast are indicating an increment in the future energy price, MPC algorithm is the only one that is able to start to store thermal energy at some point (with switching the heating on) in order to avoid to pay more money for the same energy amount later.

Figure 7 shows the price responsiveness for the proposed algorithms. Price responsiveness is defined as $\frac{dP}{dp}$, that is the variation of electric power usage achieved by an algorithm given a certain variation of the price of the energy. Each point on the plot is the mean of a distribution of values that are the different responses that the algorithm gives to such variation of price. The standard deviation σ for each distribution is reported on each mean value with the vertical bar on the plot: how the bars show, the aggregate response is not really predictable and may vary in a very significative way because it is function of a wide number of parameters, such as time, outside temperature, wind speed, solar radiation, thermal features of the buildings, thermal history and so on. Anyway the continue lines in the plot of Figure 7, that are the fourth grade polynomials obtained applying least square method to the mean values of the distributions, show a clear tendency we could expect about the behavior of the algorithms that is that the controllers with price responsiveness capability are able to reduce the power consumption when there is a positive variation of the price and vice-versa; as the flat green lines shows, the thermostatic controller does not offer price responsiveness at all. The algorithms that show the best price responsiveness capabilities are the model predictive controller and the one named *cet*.

With computing the average of the standard deviation of the populations along the x-axis, it is possible to get an idea of which algorithm would result in the best predictability of the price response for this simulation: the controller with the less standard deviation is *cet*, then *tsp* and finally the model predictive controller.

An interesting point of the price responsiveness of Figure 7 is to see if increasing the number of buildings of one order of magnitude could improve its shape in the sense of having smaller values for the standard deviations and, so, increasing the predictability of the behaviors of the buildings; in fact these curves could be used for estimating the prediction of power

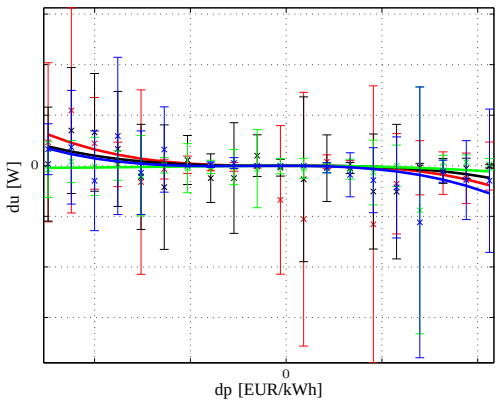

Fig. 7. The price responsiveness for the four different algorithms that is defined as the variation in the power consumption as a function of a variation in the price; vertical bars show the standard deviations for the different responses.

usage variation given a electric energy price and they could be used for bidding in the electric market for computing a price signal.

IV. Conclusion

In this paper the performances of three different algorithms suitable for controlling domestic electric space heating through price signal are compared. Simulations have been realized using a simulation platform that is able to take into account a temperature feedback signal coming from a real building in order to perturb in real time the behavior of all the buildings for pretending more realism from the simulation. Besides, the experimental results of using a model predictive controller on a real house have been presented. Real weather forecast for the area are used for the model predictive controller and they are provided by Risø-DTU Meteorological Department. The price signal used in the simulation is artificial and created for enabling the comparison between the algorithms.

Control algorithms are compared taking into account the comfort level they can achieve (measured as the deviation from the optimal indoor temperature), the total cost for the energy they require and the price responsiveness capability, defined as the change in the electric power usage when a variation in the electric energy price is proposed.

All the algorithms here presented show a positive capability of moving the energy consumption from moments where the energy is expensive to cheaper energy time frames (Figure 7) and maintaining a reasonable comfort level in the buildings. All the algorithms start to lose effectiveness when the frequency of the price signal decreases; this because the thermal inertia of the buildings is not big enough to maintain the indoor temperature in the allowed range.

Anyway the algorithm that shows the best global performance is the model predictive controller; in the case of the indoor temperature comfort level, it behaves even better than the thermostatic based controllers (Figure 5.c) because, taking advantage of weather forecast and the thermal model, can predict the effects of solar radiation (that in the days of the experimental simulation was important) and take appropriate counteractions.

Model predictive controller is also able to produce the cheapest energy bill if compared with the other two algorithms. In the case of the proposed simulation, we assume perfect foresight for the price signal and this would not be the case in a real application where errors in forecasting are expected. Anyway in presence of good forecast for the price signal, the model predictive controller should still be the best one also in terms of energy cost since it is the only one that can look into the future and, for example, start to store energy if it detects a future increase in the price; this allows a better management of the energy stored in the buildings.

From the point of view of the infrastructure, model predictive controller does not have more requirements than other controllers since they all need to receive a price signal and some kind of hardware to implement the algorithm; once the communication requirements for enabling the transmission of price signal is set up, weather and price forecast are services that can be added to the system without having impact on the complexity of the hardware architecture.

References

[1] O. Gehrke, *A Guide to LaTeX*, 3rd ed. Harlow, England: Addison-Wesley, 1999.

[2] Y. Zong et al., *Model Predictive Control Strategy for a Load Management Research Facility in the Distributed Power System with High Wind Penetration - Towards a Danish Power System with 50% Wind Penetration*, APPEEC, 2011.

[3] P. Bacher et al., *Models for Energy Performance Analysis*, IMM Technical Report, 2010.

[4] D. Hammerstrom et al., Pacific Nortwest GridWise Testbed demonstration Projects, Part I. Olympic Penninsula Project National Technical Iformation Service, U.S. Dept. Commerce, 2007.

[5] P. Nyeng and J. Østergaard, *Information and Communications Systems for Control-by-Price of Distributed Energy Resources and Flexible Demand*, IEEE Transactions on Smart Grid, Vol.2, No.2, June 2011.

[6] R.F. Stengel, *Optimal control and estimation* Dover publications, 1993.

Paper C

Scheduling of domestic water heater power demand for maximizing PV self-consumption using model predictive control

Scheduling of Domestic Water Heater Power Demand for Maximizing PV Self-Consumption Using Model Predictive Control

Fabrizio Sossan, Anna Magdalena Kosek, Sergejus Martinenas, Mattia Marinelli, Henrik Bindner
Center for Electric Power and Energy
Technical University of Denmark
4000 Roskilde, Denmark
{faso, amko, smar, matm, hwbi}@elektro.dtu.dk

***Abstract*—This paper presents a model predictive control (MPC) strategy for maximizing photo-voltaic (PV) self-consumption in a household context exploiting the flexible demand of an electric water heater. The predictive controller uses a water heater model and forecast of the hot water consumption in order to predict the future temperature of the water and it manages its state (on and off) according to the forecasted PV production, which are computed starting from forecast of the solar irradiance. Simulations for the proof of concept and for validating the proposed control strategy are proposed. Results of the control approach are compared with a traditional thermostatic controller using historical measurements of a 10 kW PV installation. Economic results based on the Italian self consumption tariffs are also reported. The model of the water heater complex is a mixed grey and white box and its parameters have been estimated using a real water heater device.**

Keywords – Smart grids, Power demand, Solar generation, Demand Side Management

I. Introduction

In the last decade, worldwide evolution of installed photo-voltaic capacity shows an exponential growth with an increase of nearly 70% in Europe between 2010 and 2011 given by an increment of 30 GW of new installations [1]. According to [1], the PV installation capacity in Europe is expected to increase in the incoming years, because of national government targets and convenient feed-in tariffs. In 2009, Germany introduced tariffs for promoting self-consumption allowing users to receive incentives for each consumed watt during PV production periods [2], [3]. The same kind of incentive has been introduced in Italy in 2013.

The photo-voltaic energy self-consumption is relevant for allowing the transition towards a more efficient power system, improving power balance, voltage stability and reduction of power losses. Several solutions for controlling a battery storage to absorb the excess of PV production and reuse it during peak hours have been proposed. Braun et. al. [4] presents a energy management strategy using a PV installation coupled with lithium batteries. [5] proposes a centralized controller that optimizes the use of lead acid batteries taking into account consumption patterns and schedule of common domestic white goods while [6] proposes a battery control strategy for absorbing fluctuations of renewable sources. Few attempts of absorbing PV production using so-called Demand Side Resources have been proposed. DSRs are electric loads which have an intrinsic natural flexibility due, for example, to thermal inertia. DSRs allow to defer electric power usage without compromising the quality of the services they are supplying to the users and they are generally proposed as a resource for supporting power system regulating power [7] or frequency regulation [8].

In this paper, a MPC strategy for scheduling the consumption of an electric water heater according the forecasted PV production is presented. The choice of the demand side unit to control has been done according to the fact that the power required by water heater is not correlated with sun irradiance. In case for example of [9], the power demand is negatively correlated with the sun irradiance, because the sun contributes to warm the building envelope, and therefore the self-consumption strategy might be not effective. On the contrary, air conditioning units would be very convenient for PV self-consumption policies since their power demand is positively correlated with sun irradiance during the warm season. The advantage of exploiting flexible demand other than batteries, it is that some flexible units are already present at household level and it is definitely worth investigating their usability before considering to place new storage devices.

The model predictive control strategy uses a grey box model of a single element electric water heater whose parameters have been estimated from a real device. An optimization algorithm is finally used for scheduling the power consumption of the heater in order to use electric energy when photo-voltaic power is available and to respect user comfort (*i.e.*, hot water should always be available when required). Simulation results of the receding horizon MPC strategy are proposed. Predictive control is compared with a traditional thermostatic controller and economic results based on real self-consumption and feed in tariffs are proposed.

The paper is organized as follows: Section II presents the water heater model, it formulates the optimization problem needed for realizing the MPC strategy and it shows how the controller is applied for controlling the water heater. Section III contains simulation results of the receding horizon MPC strategy. Section IV presents discussion and conclusions are finally reported in Section V.

II. METHODS

The target of the proposed control strategy is to maximize photo-voltaic self-consumption, shifting the power usage of a domestic electric water heater. The optimal control problem is formulated as linear optimization and the cost expression is shown in Eq. 1.

$$\min_{P_e} \quad \sum_{i}^{N} \left| \frac{max(P^s) - P_i^s}{max(P^s)} \right| P_i^e \tag{1}$$

$$\text{subject to} \quad T_{i+1} = f(T_i, T_i^{room}, q_i, T_i^{inlet}, P_i^e) \tag{2}$$

$$T_{min} \leq T_i \leq T_{max} \ \wedge \ P_{min}^e \leq P_i^e \leq P_{max}^e \tag{3}$$

Index i refers to a discrete time instant. The time series P^s is the forecast for the produced PV energy. Photo-voltaic forecast model is introduced in subsection II-B. P^e is the power consumption profile of the water heater and it is the target variable for the optimization process. Constraint 2 is evaluated using the mathematical model of the electric water heater, which is presented in paragraph II-A: T is the average temperature of the water inside the tank, T^{room} is the temperature of the room where the heater is placed and T^{inlet} is the temperature of the cold water which replaces the consumed hot water; quantity q is the amount of consumed hot tap water. For this simulation, a static pattern for the hot water consumption profile is used [10]. The same pattern has been used as forecast (*i.e.,* forecast are assumed perfect). Inequalities 3 set the upper and lower bounds for the water temperature and limit the electric power consumption of the heater. N is the length in number of discrete time steps of the optimization horizon length, the receding time horizon has been chosen to be 12 hours in order to encompass the day ahead cycle of PV production.

The pseudo-code which shows how the MPC strategy is applied is shown in listing 1. The MPC problem is solved at each iteration for the whole receding horizon length (12 hours) but only the first control is actuated at each cycle. The sampling time is 15 minutes.

while *true* **do**
  P^s = update production forecast;
  T_0 = read current water temperature;
  T = produce water temperature forecast(T_0, q);
  u^{opt} = solve optimization problem(T, P^s);
  actuate heating power(u_0^{opt});
  wait for sampling time
end

Algorithm 1: MPC receding horizon formulation

The output of the MPC is the energy that the heater should consume in the time frame. In case of a real device, the on-off state could be modulated in order to obtain the right amount of energy. This policy is still acceptable because the self-consumption is primarily about maximizing the amount of energy which is consumed and not following a precise power profile.

A. Water heater model

In this section a model for a single element electric water heater is presented. Thermal stratification of the water due to buoyancy effect is not described in this model.

Thermal loss towards the environment: Thermal loss to external environment is due to heat conduction loss through the surface of the tank and the natural convection which moves heat from the tank surface to the environment. Heat loss Q is modeled as heat conduction through the surface of the water tank:

$$Q(t) = -A \ \frac{T(t) - T^{room}(t)}{R} \tag{4}$$

where A is the surface of the tank, R the thermal resistance of the insulation material and T^{room} the ambient temperature. It is assumed that the room temperature is not affected by the heater thermal loss (bigger thermal inertia).

Thermal loss due to water consumption: Given an amount of water with mass m which is consumed in the time interval ΔT and replaced in the tank by new water at temperature T^{in}, the new average temperature of the water in the tank T_{i+1} can be expressed as combination of the temperatures of cold and hot water weighted on the mass ratio (m_t is the mass of water associated with the volume of the heater tank):

$$\begin{aligned} T_{i+1} &= \frac{m}{m_t} T^{in} + \frac{m_t - m}{m_t} T_i \\ T_{i+1} - T_i &= \frac{m}{m_t}(T^{in} - T_i) \end{aligned} \tag{5}$$

Assuming the mass flow rate $q(t)$ piecewise constant, the mass can be expressed as $m = q(t)\Delta t$ where Δt is the sampling time and Eq. 5 becomes:

$$\frac{T_{i+1} - T_i}{\Delta t} = \frac{q_i}{m_t}(T^{in} - T_i)$$

and the contribution in terms of heat flux is:

$$Q(t) = C_p q(t)(T^{in}(t) - T_i(t)) \tag{6}$$

Contribution from heating element: The heat to the water is supplied through the Joule losses in the heating conductor, so:

$$Q^{in}(t) = P_e(t) \tag{7}$$

Final model is obtained merging the contribution of Eq. 4, Eq. 6 and Eq. 7:

$$\begin{aligned} C_p m_t \dot{T}(t) = &- A\frac{T(t) - T^{room}(t)}{R} + \\ &+ C_p q(t)(T^{in}(t) - T_i(t)) + P(t) \end{aligned} \tag{8}$$

Reorganizing the terms yields to:

$$\begin{aligned} \dot{T}(t) = &- A\frac{T(t) - T^{room}(t)}{RC_p m_t} + \\ &+ \frac{T^{in}(t) - T_i(t)}{m_t} q(t) + \frac{P(t)}{C_p m_t} \end{aligned} \tag{9}$$

Defining the thermal mass $C_w = C_p m_t$ and a lumped coefficient $R_e = A/R$ for accounting the conduction losses through the water tank, Eq. 9 becomes:

$$\begin{aligned} \dot{T}(t) = &- \frac{T(t) - T^{room}(t)}{R_e C_w} + \\ &+ \frac{T^{in}(t) - T(t)}{C_w/C_p} q(t) + \frac{P(t)}{C} \end{aligned}$$

which can be rewritten as:

$$\dot{T}(t) = \left(-\frac{1}{R_e C_w} - \frac{q(t)}{C_w/C_p} \right) T(t) + \\ + \frac{1}{C_w} P_e(t) + \frac{1}{R_e C_w} T^{room} + \frac{q(t)}{C_w/C_p} T^{in}(t) \quad (10)$$

a time variant multiple input single output model. Analogue model has been described in [11] and [12]. For performing simulation, Eq. 10 is discretized with a sampling time of 900 s.

A mixed white and grey box modelling criteria has been adopted for assigning the values of thermal capacitance and resistance of the water tank model. The thermal capacitance has been assigned considering the water as the predominant thermal mass of the whole water heater complex, so:

$$C_w = \frac{V_t}{1000} \, \rho \, C_p \quad (11)$$

where V_t is the capacity in liters of the tank (30 l), ρ is the water density (1000 $kg \cdot m^{-3}$) and C_p is the specific heat at constant pressure (4183 $J \cdot kg^{-1} \cdot K^{-1}$). The thermal conductivity of the tank has been estimated using temperature measurements of the water inside the tank and with a simple numeric procedure which consists in measuring the electric power (without any hot water tap consumption) and divide its average by the difference between the average water temperature and the room temperature. So, the thermal resistance R_e of Eq. 10 is:

$$R_e = \frac{\bar{T} - T^{room}}{\bar{P}_e} \quad (12)$$

B. PV production forecast model

The production of the PV plant is predicted starting from forecast for the sun irradiance on the horizontal plan and translated into production values using a PV model. Solar irradiance forecast has one hour resolution and it is provided by DTU Wind Energy, Meteorology Section [3] through an FTP server. The input-output diagram of the PV model is shown in Fig. 1. Geographical information is needed by the model for computing the azimuth and the altitude of the sun in the sky. Given the installation characteristics of the plant, the model computes the quantity of solar radiation which is incident to the panel. Finally a thermal characterization of the PV cells, which is function of ambient air temperature, sun radiation and wind speed, is used for computing the losses and indeed the efficiency of the photo-voltaic effect.

C. Simulation set-up

The simulations here presented are used for showing the capability of the model predictive controller to move the consumption of the heater during hours with PV production. The MPC uses solar irradiance forecast relative to 4th May 2013. Water consumption profile is from [10] and it has been resized for the need of two people (considering the small size of the water boiler in analysis). Water consumption forecast are the same as the consumption profile and, indeed, they are assumed to be perfect. In order to evaluate the performances of the MPC strategy, the water heater consumption profile is compared with a traditional thermostatic controller and real

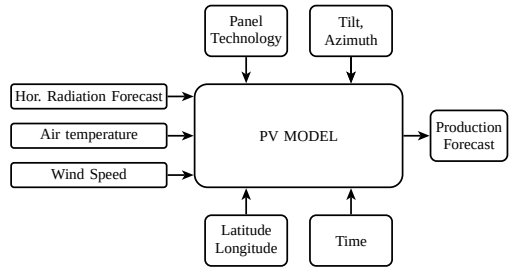

Fig. 1. The PV model allowing to obtain the forecast for the photo-voltaic production.

production data for the same day of a 10 kW SYSLAB PV plant [1] – normalized and referred to a smaller 2 kW PV installation – are used for evaluating the economic income for adopting such solution using Italian feed-in and self-consumption tariffs.
A summary with the relevant information for the simulation is reported in Table I.

TABLE I. SIMULATION SETUP

Component	Attribute	Value
PV plant	Nominal power	2 kW
Water Heater Model	Nominal power	1.26 kW
	Tank capacity	30 l
	R (model parameter)	2 $K \cdot W^{-1}$
Thermostatic controller	Temperature set point	$55 \pm 5°C$
MPC controller	Optimization length	12 hours

III. RESULTS

Fig. 2 compares the forecasted PV production with a real production profile, obtained normalizing the measurements from a 10 kW PV ground installation. Production forecast are computed starting from forecast of the sun irradiance on the horizontal plan which comes with a resolution of one hour. In this case the production forecast is not able to detect local drop of power (due to fast clouds passage) but, for the day under consideration, it is able to capture the average component especially during the central part of the day.

Fig. 3 compares the power consumption profiles of the heater obtained by the two controllers, MPC and thermostatic. The yellow surface shows the measured and normalized PV production.

Fig. 4 shows the electric energy which has been bought from the grid in order to satisfy the demand required by the two water heater controllers.

Fig. 5 presents the portion of electric energy produced by the PV which has been self consumed by the electric water heater.

Fig. 6 shows the part of PV production which has been sold to the national grid because it has not been not self consumed.

[1]SYSLAB is laboratory for intelligent distributed power systems at Technical University of Denmark, part of PowerLabDK (www.powerlab.dk).

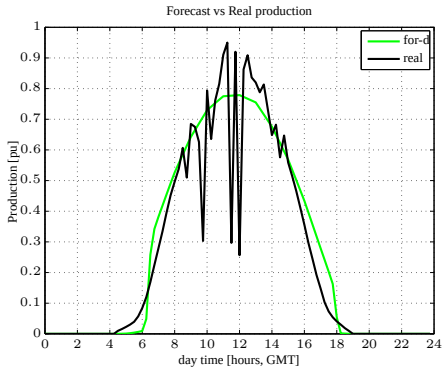

Fig. 2. Forecasted production against real production based on data for 4th, May 2013.

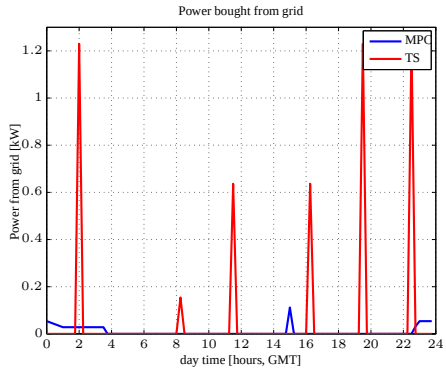

Fig. 4. Instant power which is bought from the grid in case of traditional thermostatic controller, *red line*, and predictive control strategy, *blue* line.

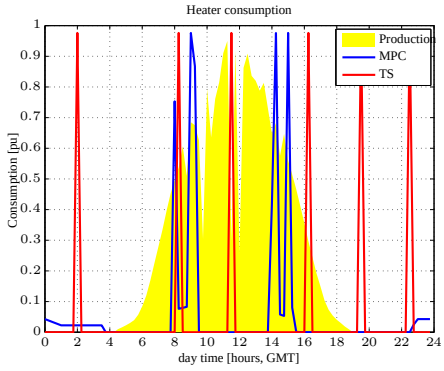

Fig. 3. Power consumption profiles for the two control strategies against the absolute value PV production. Values are in *per unit*.

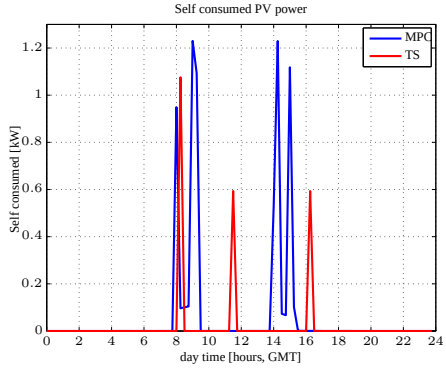

Fig. 5. Self consumed PV power for traditional thermostatic controller, *red line*, and predictive control strategy, *blue* line.

Fig. 7 shows the average temperature of the water inside the tank of the water heater for the two temperature control algorithms along with the water consumption profile on the right axis.

Table II shows the composition of the energy demand in terms of energy bought or self consumed and the amount of energy sold to the grid for each control algorithm. An estimation of the energy bill – referred to the day in analysis – produced by each controller is also given in the last column. it is evaluated using the Italian tariffs for PV feed-in and self-consumption as a reference. The assumed tariffs are [€·kWh^{-1}]: 0.23 for consumption [13], 0.20 for PV production and 0.126 for self consumed energy [14].

TABLE II. SUMMARY OF CONTROLLERS OPERATIONS ON 24 HOURS SIMULATION

Controller	Energy sold	Energy bought	Self consumed	Energy bill
Thermostat	11.86 kWh	1.28 kWh	0.57 kWh	2.31 €
MPC	10.75 kWh	0.21 kWh	1.67 kWh	2.15 €

IV. DISCUSSION

Table II shows that the proposed MPC strategy increases to 297% the amount of active power which is consumed by the water heater during the time with PV production. The PV production forecast, Fig. 3, are able to detect the average component of the PV real production. Fast changes in the PV production profile cannot be captured because the original solar irradiance forecast are given with a resolution of one hour. The amount of money which the MPC allowed to save is 0.16 € on a time span of 24 hours and considering the condition as the day in analysis. For the analyzed day, the capacity factor has been 26%: considering an annual capacity factor of 8%, it can be assumed, ideally, to dispose of 112 days with an analogue production profile; assuming also the same quality for the forecast both for PV production and water consumption, the annual ideal economic revenue would be around 18 €.

Fig. 6 shows that the flexibility in the power demand of the electric water heater in analysis (capacity 30 l) is definitely not enough for absorbing all the PV production. Increasing the size of the tank would increase the flexibility of the system because of the greater thermal inertia. Enlarging the

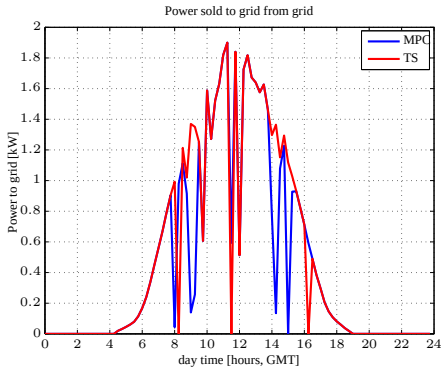

Fig. 6. PV power that has been sold to the grid in case of traditional thermostatic controller, *red line*, and predictive control strategy, *blue* line.

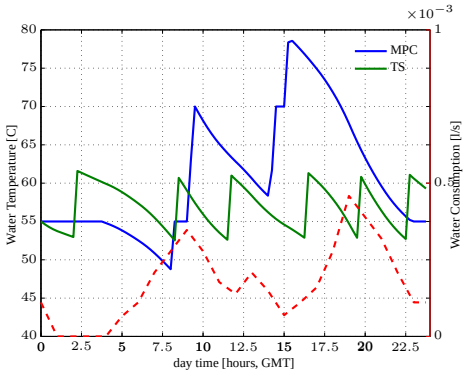

Fig. 7. Average temperature of the water inside the tank for the MPC controller and the thermostatic one. On the right axis the water consumption profile used for simulation.

range of allowed hot water temperature would also concur to increase the flexibility of the system. It is worth noting that the controller algorithm does not use the information about the real time production of the PV panel, *i.e.*, the MPC strategy is based uniquely on the irradiance forecast and it is not corrected accounting for the current production. This setup reduces the complexity of the system because it does not require communication between the PV inverter and the MPC controller. Considering the instantaneous PV prediction error, even if it increases the complexity of the system, could be beneficial for producing better results for forecasts with a large error.

Fig. 7 shows how the MPC controller exploits the thermal inertia of the water for absorbing the production from the PV installation. When no PV production is available, the MPC let the water temperature to settle at $55^\circ\ C$: whenever the PV installation is producing, the MPC demands more electric power to be consumed in order to increase the temperature of the water and have it ready for consumption for longer time. At time $t = 2.5\ h$ the temperature of the water drops to $50^\circ\ C$ because the lower temperature constraint is implemented as a soft one in the cost function and, therefore, the controller allows the water temperature to go below the lower limit when it foresees PV production in the immediate future.

V. Conclusions

This paper presents a model predictive control strategy for maximizing PV self-consumption exploiting the flexible demand of an electric water heater. The proposed control approach has been tested in simulation using sun irradiance forecast and real production data. Simulations showed that the MPC controller is able to move the consumption of the heater during the period when there is production from the PV plant. A comparison with a traditional thermostatic controller showed a energy bill reduced of 15% (according Italian feed-in and self-consumption tariffs) for a total save of around 0.15 € for the day considered for simulations. The energy self consumed by the MPC is raised to around 300% than the thermostatic controller. Such results represent a good achievement in terms of self consumed power if considered that an electric water heater is a device which is commonly present in a household context.

References

[1] "Global market outlook for photovoltaic until 2016," tech. rep., EPIA, European Photovoltaic Industry Association, May 2012.

[2] T. Drizard, "German energy policy: reconciling energy storage and feed-in tariffs through self-consumption tariffs," 2009.

[3] A. Hahmann, D. Rostkier-Edelstein, T. Warner, F. Vandenberghe, Y. Liu, R. Babarsky, and S. Swerdlin, "A reanalysis system for the generation of mesoscale climatographies," vol. 49, pp. 954–972, May 2010.

[4] M. Braun, M. Budenbender, Z. Perrin, D. Feng, and Magnor, "Photovoltaic self-consumption in Germany," in *24th European Photovoltaic Solar Energy Conference*, September 2009.

[5] E. Castillo-Cagigal, A. Caamao-Martn, D. Gutirrez, F. Masa-Bote, J. Monasterio, E. Porro, J. Matallanas, and Jimnez-Leube, "Self-consumption of pv electricity with active demand side management: The gedelos-pv system," in *25th European Photovoltaic Solar Energy Conference*, September 2010.

[6] S. Grillo, M. Marinelli, S. Massucco, and F. Silvestro, "Optimal management strategy of a battery-based storage system to improve renewable energy integration in distribution networks," *Smart Grid, IEEE Transactions on*, vol. 3, no. 2, pp. 950–958, 2012.

[7] F. Sossan and H. Bindner, "Evaluation of the performance of indirect control of many dsrs using hardware-in-the-loop simulations," in *CDC, 2012 Maui, HI, US*, December 2012.

[8] P. Douglass, R. Garcia-Valle, P. Nyeng, J. Ostergaard, and M. Togeby, "Smart demand for frequency regulation: Experimental results," *Smart Grid, IEEE Transactions on*, vol. PP, no. 99, pp. 1–8, 2013.

[9] Y. Zong, L. Mihet-Popa, D. Kullmann, A. Thavlov, O. Gehrke, and H. Bindner, "Model predictive controller for active demand side management with pv self-consumption in an intelligent building," in *3rd IEEE PES Innovative Smart Grid Technologies Europe (ISGT Europe), Berlin*, September 2012.

[10] S. Kalogirou and Y. Tripanagnostopoulos, "Hybrid pv/t solar systems for domestic hot water and electricity production," *Energy Conversion and Management*, vol. 47, no. 1819, pp. 3368 – 3382, 2006.

[11] P. Dolan, M. Nehrir, and V. Gerez, "Development of a monte carlo based aggregate model for residential electric water heater loads," *Electric Power Systems Research*, vol. 36, no. 1, pp. 29 – 35, 1996.

[12] M. Nehrir, R. Jia, D. Pierre, and D. Hammerstrom, "Power management of aggregate electric water heater loads by voltage control," in *Power Engineering Society General Meeting, 2007. IEEE*, pp. 1–6, 2007.

[13] Eurostat, "Household electricity prices including all taxes.," May 2013.

[14] Gestore Servizi Energetici, "Quinto conto energia," 2012.

Paper D

An auto tuning substation peak shaving controller for congestion management using flexible demand

An Auto Tuning Substation Peak Shaving Controller for Congestion Management Using Flexible Demand

Fabrizio Sossan and Mattia Marinelli
Center for Electric Power and Energy
Technical University of Denmark
4000 Roskilde, Denmark
{faso, matm}@elektro.dtu.dk

***Abstract*—This paper presents a substation controller for shifting the electrical consumption during peak hours and reducing congestions in the distribution network indirect controlling deferrable electric demand. The controller produces a single control signal which is broadcasted to all the substation electric loads and which is used for inducing a shift in the power consumption when a congestion is occurring. The controller auto tunes its parameters on-line in order to adapt to different substations and power consumption profiles. Simulations for validating the proposed control strategy are presented. Simulations have been using the MV CIGRE' reference network. Substations loads are composed both by conventional consumption and flexible demand. Flexible demand is composed by a population of 346 Demand Side Resources, DSRs, which are represented by buildings equipped with electrical space heating.**

Keywords – Power distribution, Power demand, Smart grids, peak shaving, indirect control, Congestion Management

I. Introduction

Exploiting the flexibility at demand side level is becoming of increasing focus in order to supply power system services to the grid. The electric loads which exhibit flexibility in the electric power consumption are the ones with an intrinsic storage capability such as space heating and cooling units and refrigeration devices. This kind of electric loads are usually referred with the term Demand Side Resources, DSRs, and their power consumption can be deferred according the needs of the power system as long as operational constraints and user comfort levels are respected. Exploitation of DSRs potentiality is based on the assumption that the power contribution from the single demand side unit is modest but the aggregate response obtained from a large population of DSRs might assume relevant size for the power system. Two mainstream approaches has been proposed for controlling DSRs: direct and indirect control. In the former case, the power consumption of each DSR is directly controlled and supervised by one (or more) aggregation layer [1]. In the latter case, a shift in the power consumption of the demand side units is induced by broadcasting a control signal [2]. Indirect control is also referred as control-by-price when the control signal is the price for the electric energy the users should pay. The indirect controlled units are let free to respond to the price signal on voluntary basis according local preferences and evaluating the associated economic advantage for shifting their power consumption [3]. Direct control is demanding in terms of ICT infrastructure and communication requirements, while indirect control results in a less complex setup because it requires only one way communication [4] needed to transmit the real time control signal. For this reason indirect control does not allow to know to the exact response from the single demand side unit and the electric power and energy contribution can be only estimated in terms of aggregate response [5], [6].
Exploiting DSRs flexibility has been proposed for providing regulating power or for restoring power system reserve in the future power system where a higher penetration of production from renewable energies is expected and conventional generation might not have enough flexibility. In this paper a demand side management strategy for solving congestions in the distribution network is proposed. Each network substation is equipped with a controller which produces a signal for indirect controlling the underneath demand side units with the aim of reducing a congestion whenever it arises. The local controller is a PI based and it has auto tuning capability meaning that it can detect the sensitivity of the associated flexible demand allowing the controller to be replicated in all the substations without requiring any manual tuning of the parameters. Simulations for showing the proof of concept have been realized using CIGRE' medium voltage reference network is used in the proposed simulations. The population of controllable DSRs are buildings heated by electric space heating which exhibit a certain flexibility in the consumption due to the thermal inertia of building envelope and air content. In the grid, seven substations are present with both conventional residential and commercial electric load. The penetration of nominal flexible demand at substation level is 43% (calculated as ratio between flexible demand and flexible demand plus conventional consumption). Power system simulations are performed in Matlab Simulink and the DSRs population is simulated using thermal models in Python.
The simulation setup together with the proposed congestion controller are discussed in Section II. Section III presents the results. Discussion of results is provided in Section IV. Finally, conclusions are provided in Section IV.

II. Methods

The simulation setup for validating the proposed congestion management strategy consists of a power network whose electric demand is composed both by conventional and flexible electric loads. The network layout is described in Section II-A) while the DSRs population, which represents the flexible demand, is described in Section II-B. In each substation of network the congestion controller is placed. Congestion controller is discussed in Section II-C.

Power system simulations have been performed in Matlab

Simulink while the DSRs have been simulated using a Python simulation platform. The two simulations environment are synchronized and they exchange information at each simulation time step, 300 s.

A. Electric network layout

The network used for the study is the CIGRE' MV European Reference. A comprehensive description of this network can be found in reference [7]. For sake of clarity, the main aspects are here reported. The European MV distribution feeders are three-phase and either of meshed or radial structure, with the latter dominating rural installations. The benchmark allows flexibility to model both meshed and radial structures. Each feeder includes numerous laterals at which MV/LV transformers could be connected. The nominal voltage is 20 kV and the system frequency is 50 Hz. The study has been performed in the feeder 1 (urban) which is shown in Figure 2 and whose main information are here listed:

- 11 MV buses and 11 LV (Low Voltage) buses;
- 4590 kVA of transformer MV/LV capacity;
- 2.82 km OHL (OverHead lines) and 12.2 km Cable lines.

Three configuration switches are present but for this study are left in open status.
At the current stage, 7 MV/LV substations out of 11 possible are used for simulations. Low voltage network in the substations is not represented in details. Substations are composed 3 controllable loads:

- lumped flexible demand load;
- lumped residential base load;
- lumped commercial base load (not present in all substations);

The power consumption of the lumped flexible load corresponds to the aggregated consumption of a demand side resources population which is described in Section II-B. The number of units in each population has been chosen according to the nominal power of the substation. The residential and commercial base loads are subject to predefined daily consumption patterns which are described in [7]; their (active) power consumption profile are shown in Figure 1 where $t = 0h$ refers to midnight. Because the flexible demand is assumed to be electric domestic space heating, the curve consumption of the conventional residential load has been scaled to 0.7 pu.

B. DSRs population

The controllable demand side population is composed by 346 buildings equipped with electric radiators for space heating. Demand side units are spread among the 7 substation of the network according the nominal power capacity of each of them. Each building has a nominal heating power capability of 10 kW and its thermal dynamics are simulated using a second order dynamic model. In order to represent a heterogeneous population, the parameters of the models have been slightly variated around nominal values following a normal distribution for accounting variation in size and insulation characteristics.

The nominal thermal model has been built using grey box modeling on a real building [8], Power Flexhouse [9]. Power

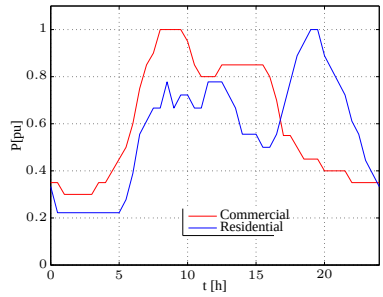

Fig. 1. Static daily patterns for the conventional residential and commercial consumption. Because flexible consumption is also domestic, residential consumption profile has been scaled in amplitude by a factor 0.7.

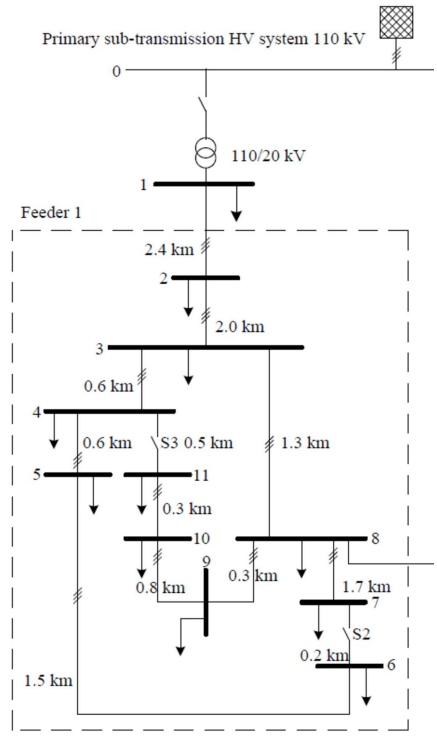

Fig. 2. Network layout of the CIGRE' feeder used for simulations .

Flexhouse is an automated free standing building connected to SYSLAB grid, a low voltage distributed power system facility at DTU Risø campus, Denmark. Power Flexhouse thermal model is described by a system of differential equations reported in Equation 1 and Equation 2. The two temperature states are for the indoor air, T^{in}, and heaters surfaces. The electric power P is the controllable input which is managed by the demand side algorithm described in Section II-B1. Quantities S and T^o are two not controllable inputs and

they are respectively solar irradiation on the horizontal plan [W·m^{-2}] and outdoor air temperature [$^{\circ}C$]. The model is simulated in discrete domain with an integration time of 300 s.

$$\dot{\underline{x}} = \begin{pmatrix} -2.73\times10^{-5} & 9.15\times10^{-6} \\ 1.48\times10^{-3} & -1.48\times10^{-3} \end{pmatrix} \underline{x} + \begin{pmatrix} 0 & 1.81\times10^{-5} & 7.38\times10^{-4} \\ 1.48\times10^{-2} & 0 & 0 \end{pmatrix} \begin{pmatrix} P \\ T^{\text{out}} \\ S \end{pmatrix} \quad (1)$$

$$T^{in} = (1 \quad 0)\,\underline{x} \quad (2)$$

1) DSRs indirect control algorithm: Each building is controlled with a simple control algorithm that, indirectly, adjusts the electric energy consumption according to the signal that is sent from the substation congestion controller: the demand side algorithm, whose formula is shown in Equation 3, produces an offset value for the indoor temperature set point (Equation 4) at each instant of time i when a new control signal, p_i, is available.
In Equation 4, $\bar{p}$ is the mean of the control signal over the last 12 hours and k is a coefficient for setting the responsiveness of the algorithm (it equals 10 in the proposed simulations).
The indoor temperature set point, Equation 4, is maintained using a simple thermostatic controller.

$$\hat{p}_i = \frac{p_i - \overline{p}_i}{\overline{p}_i} \quad (3)$$

$$T^{in}_{set\ point} = 21^{\circ}C - k\ \hat{p}_i \quad (4)$$

Roughly, Equation 3 and Equation 4 tell that if the current control signal is higher than the average of the past ones, the indoor set point is decreased and vice-versa. It is worth noting that such algorithm has a null contribution at steady state, so no deviation to the indoor reference is applied when the control signal is constant for sufficient long time (12 hours in this case). This allows to not affect the user comfort level at steady state.

C. Congestion controller

The overview of the implemented control approach is shown in Figure 3: a substation controller detects congestions (which occur when the power transit exceeds the substation transformer nominal value) and, in order to solve them, it produces a control signal in order to reduce and shift the consumption. P_{e_i} is the power transit at the substation transformer and it comprises both conventional and flexible demand. Subscripts i refer to time instants. Electric power is here expressed in pu, per unit, and it is referred to the nominal power of the substation transformer ($P[pu] = P/P_{nom}$) according to the specification of the reference network.

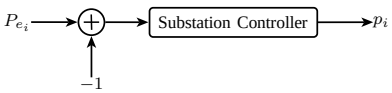

Fig. 3. General overview of the proposed control approach. The substation controller measures the power transit and it produces a control signal p_i in order to reduce the power transit and shift the consumption.

Considering Figure 3, if the sensitivity of the aggregated flexible demand (s_i and defined in Equation 5) to an unitary variation of the control signal is known at each instant of time $t = i$, then the amount of overload could be measured and multiplied by s in order to know the exact variation of the control signal needed to resize the power transit below its nominal value. The problem is that the quantity s is function of the states of the DSRs for a given substation and time variant, therefore, considered the characteristics of indirect control (one way communication), it is unknown.

$$s_i = \frac{\Delta price_i}{\Delta P_{e_i}} \quad (5)$$
$$\Delta P_{e_i} = P_{e_i} - P_{e_{i-1}}$$
$$\Delta price_i = price_i - price_{i-1}$$

The proposed controller is a closed loop PI regulator whose input is the deviation from the nominal power, 1 pu; its diagram is shown in Figure 4.

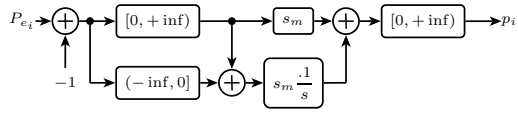

Fig. 4. The proposed substation controller for congestion management.

The gain of both proportional and integral parts is proportional to s_m. Coefficient s_m is defined in Equation 6 as the smallest variation in the observed (past) aggregated power consumption for a unit of price.

$$s_m = \min\{s_i\} \quad (6)$$

The aim of the proportional part of the regulator is to give a one shot guess (given by s_m times the amount of overload) of the deviation in the control signal amplitude to send to the units. In general, the guess will not be able to solve the congestion because, as said before, the exact value s_i would be needed. In particular here, s_m is chosen as the smallest value among a set of past s_i and it might easily overestimate indirect control capability leading to an control signal which is not high enough. The task of the integral part of the regulator is indeed to correct the proportional action and produce the magnitude of the control signal in order to try to restore the nominal power transit.

The input of the proportional part of the regulator is limited to the interval $[0, +\inf)$ because it has to act only when a congestion is occurring. However a negative input $(-\inf, 0]$ is allowed for the integral part of the controller in order to remove the offset price when no congestion is occurring.
The indirect control signal produced by the controller is in the range $[0, +\inf)$, *i.e.* the controller discouraging consumption.
The integral part of the controller has an anti wind-up loop part which is not shown in the diagram of Figure 4.
It is worth noting that the parameter s_i in Equation 5 is not influenced by the conventional load which does not react to any change of the control signal.
Congestion controllers are placed in all the 7 substations and they adjust their gains automatically on-line using Equation 6 evaluating the variations of aggregate power consumption

given changes of the indirect control signal. An initial training phase of the controller is required to detect the sensitivity of the flexible demand. No manual individual tuning is needed for the controllers.
In order to allow the value s_m to be updated with newer ones, the stored value of s_m is multiplied by a forgetting factor equal to $e^{\lambda/12}$ with λ as the *age* of the parameters in hours.
In the proposed simulations, the substation controller can send a new control signal once every 5 minutes.

III. Results

Simulations here proposed are performed using the urban feeder of the medium voltage CIGRE' reference network. Electrical demand is composed by a mix of conventional and flexible. Each substation is equipped with an auto tuning controller whose task is to send a unique control signal to all substation electrical loads in order to shift the power consumption every time a congestion occurs.

Two simulation scenarios are proposed. Scenario *a* is with no congestion control while, in Scenario *b*, all substation controllers are activated. Both scenarios present same network configuration, conditions and consumption profiles.

Simulations last for 24 hours, starting from midnight. The time series used for evolving thermal models of buildings (outdoor temperature and solar radiation are from real measurements).
Coherently with the notation used before, the power transits in the plots are expressed in pu, that is transit power divided the nominal capacity of the substation transformer.

In scenario *a*, congestion control is not present. Flexibility in the electrical demand is not exploited and electric space heating units are let free to consume according their thermal energy needs. The power transit of each substation, from substation 1 to 7, and the price signal of scenario *a* are shown in Figure 5.

In scenario *b*, the substations congestion controllers are activated. Power transits at each substation are shown in Figure 6. Substation 0 is not shown in the figures because the power transit never exceed the nominal value.

Voltages profiles at each substations transformers are shown in Figure 7. Green and blue profiles are when congestion controllers are activated and switched off respectively.

IV. Discussion

Figure 5 and 6 show the power transit at each substation respectively when the demand side units are not controlled and when the proposed substation congestion controller is shifting their consumption.

Scenario *a* in Figure Figure 5 depicts a situation where all the substation are congested during evening hours.

Figure 6 shows how in scenario *b*, the substations controllers starts to raise the price signal as soon as they detect an overload; consequently the DSRs tend to reduce their power consumption. A closer inspection to the power profiles of the different substations in Figure 6, during the time frame where the congestions occur, shows that 1) the power consumption

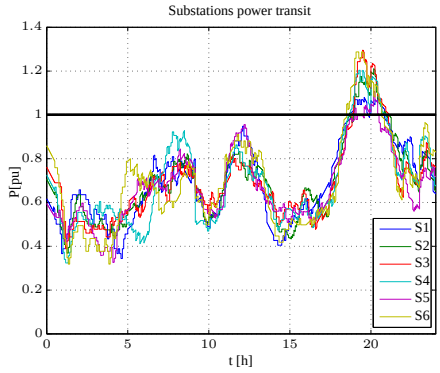

Fig. 5. Scenario *a*. Congestions are occurring in all the substations in the evening hours.

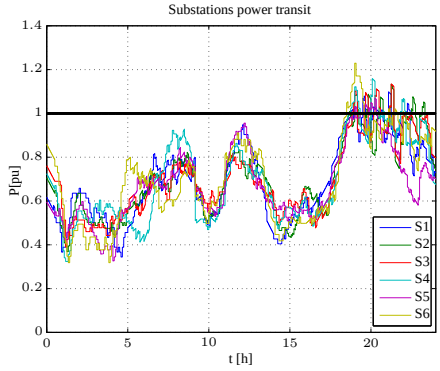

Fig. 6. Scenario *b*. Congestion controllers are activated in each substation and the consumption is trimmed thanks to acting on flexible demand.

oscillates around 1 pu or 2) it slowly decreases to one, 3) the peak values are reduced but the 'wave' of high consumption last longer than scenario *b*.
Case 1) occurs when the identified value s_m for a certain substation is underestimating indirect control capability: in this case only the proportional regulator contributing to the control signal. After the indirect control signal is sent, the power transit is reduced below its nominal value: because the proportional regulator is not feeded anymore, the power consumption returns to a value higher than 1 pu and the cycle starts again.
In case 2), the value s_m is overestimating indirect control capability and the proportional regulator 'one-shot guess' is not able to solve the congestion: in this case the integral action of the regulator start to increase the magnitude of the indirect control signal causing the aggregated power consumption of the loads to drop slowly.
Explanation for case 3) is that the controller, for solving the congestion, raises the amplitude of the control signal: once the congestion is solved, the controller - removes the price offset causing the DSR to increase a little the consumption again; this sort of regulator wake effect concurs in keeping an high

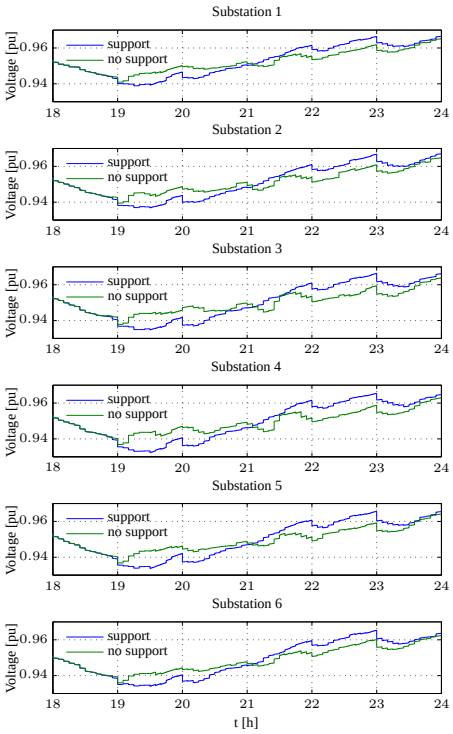

Fig. 7. Voltage profiles at the different substations.

level of consumption even after the congestion is solved.

TABLE I. SUBSTATIONS POWER TRANSIT VALUES DURING CONGESTION

Power transit	Scenario	S1	S2	S3	S4	S5	S6
peak value	*b*	1.08	1.21	1.30	1.20	1.11	1.29
	c	1.08	1.09	1.11	1.16	1.07	1.23
mean	*b*	1.05	1.09	1.15	1.11	1.02	1.16
	c	0.98	0.98	0.98	1.	1.01	1.02

Table I reports some relevant information of the power transits of each substation. Data are referred to the time frame $\sim 18.5h < t <\sim 20.7h$ where congestion is occurring. The controller is able to trim the consumption peak values in all substations and in particular the mean values of the power transits are kept very close to the nominal ones.
In this simulation the proposed controller is able to reduce the congestions in all the substations meaning also that the simple auto tuning procedure here presented is well performing.
As a result of the shift and reduction of the power demand, also the substations voltage profiles in Figure 7 appear to improve.

V. CONCLUSION

This paper proposes a controller for peak shaving and managing congestions in the distribution network using flexible electrical demand. The controller is auto tuning meaning that it adjusts the parameters by itself on-line and it does not require any manual intervention. In order to show the proof of concept, the performance of the controller have been tested using seven substations of the urban feeder of the medium voltage CIGRE' reference network. Electric loads, which are placed at distribution level, are composed by a mix of conventional and flexible demand (with a penetration of flexible demand of 43% over the total). Flexible electrical demand is represented by a population of Demand Side Resources, DSRs, spread at substation level. Electric space heating has been chosen as demand side unit. Each DSR is equipped with a simple control algorithm which indirectly adjusts the power consumption according the signal received form the substation congestion controller and respecting local user comfort conditions. The congestions controllers have been replicated identically in all the 7 substations and each of them produces a unique broadcast signal for controlling the substation flexible demand. One way communication is assumed and only the measure of the aggregate power consumption at substation level is needed. Simulations showed that the proposed controller can effectively use the flexible demand in order to reduce the power transit during peak hours and that the auto tuning procedure is able to adapt controller parameters to different substations and assure the performances. Voltage profiles of the substations have also improved. Future work is in the direction of evolve the current controller to a model predictive control strategy which might improve the overall performances because it can better manage the flexibility [3]. Besides, distributed generation in the CIGRE' reference network will be considered.

REFERENCES

[1] F. Bliek, A. van den Noort, B. Roossien, R. Kamphuis, J. de Wit, J. van der Velde, and M. Eijgelaar, "Powermatching city, a living lab smart grid demonstration," in *Innovative Smart Grid Technologies Conference Europe (ISGT Europe), 2010 IEEE PES*, pp. 1 –8, oct. 2010.

[2] D. J. Hammerstrom, P. Investigator, R. Ambrosio, T. A. Carlon, J. G. Desteese, R. Kajfasz, and R. G. Pratt, "Pacific Northwest GridWise Testbed Demonstration Projects Part I . Olympic Peninsula Project," *Contract*, p. 157, 2007.

[3] F. Sossan and H. Bindner, "A comparison of algorithms for controlling dsrs in a control by price context using hardware-in-the-loop simulation," in *Power and Energy Society General Meeting, 2012 IEEE*, pp. 1–6, 2012.

[4] P. Nyeng and J. Ostergaard, "Information and communications systems for control-by-price of distributed energy resources and flexible demand," *Smart Grid, IEEE Transactions on*, vol. 2, pp. 334 –341, june 2011.

[5] F. Sossan and H. Bindner, "Evaluation of the performance of indirect control of many dsrs using hardware-in-the-loop simulations," in *CDC, 2012 Maui, HI, US*, December 2012.

[6] O. Corradi, H. Ochsenfeld, H. Madsen, and P. Pinson, "Controlling electricity consumption by forecasting its response to varying prices," *Power Systems, IEEE Transactions on*, vol. 28, pp. 421 –429, feb. 2013.

[7] C. T. F. C6.04.02, "Benchmark systems for network integration of renewable and distributed energy resources," tech. rep., Cigre' Internationl Council on large electric systems, July 2009.

[8] H. M. P. Bacher, A. Thavlov, "Models for energy performance analysis," tech. rep., DTU - IMM, 2010.

[9] Y. Zong, D. Kullmann, A. Thavlov, O. Gehrke, and H. Bindner, "Active load management in an intelligent building using model predictive control strategy," in *PowerTech, 2011 IEEE Trondheim*, pp. 1 –6, june 2011.

Paper E

Dynamic behaviour of a population of controlled-by-price demand side resources

Dynamic Behaviour of a Population of Controlled-by-price Demand Side Resources

Fabrizio Sossan, Xue Han and Henrik Bindner
Center for Electric Power and Energy, DTU Elektro
Technical University of Denmark
Roskilde, Denmark
{faso, xueh, hwbi}@elektro.dtu.dk

***Abstract*—It is described that controlling or shedding by price the power consumption of a population of thermostatic loads introduces in the aggregate consumption dynamic effects that cannot be disregarded if electrical flexible demand is meant to supply power system services. It is shown that inducing a desynchronization in the consumption contributes to damp the oscillations. Results are supported by Monte Carlo simulations of a population of buildings equipped with electric space heating whose consumption is indirect controlled by a dynamic price of the electricity.**

I. Introduction

The increasing cost of traditional sources for electricity generation and the thrust towards a more sustainable impact of human activities on planet Earth are leading the need of integrating more renewable energy in the power system. The axiom on which the power system is based is that the electric generation has to match the consumption and this is accomplished by regulating the production to respond to system frequency variation. Increasing the share of generation from renewable sources decreases the amount of controllable production in the grid limiting the penetration that renewables can achieve.

A solution that is envisaged for restoring the lack of controllability is controlling the electric power demand. Such a solution is dated back in time [1]. However it has been revitalized in the recent years because the promising transition to smart grid constitutes an adequate enabling technology for realizing it in large scale and in an automated way. Control-by-price or indirect control is often mentioned as a way for supplying regulating power and supporting the ancillary services of the electric grid. The need of regulating power of the grid is reflected into a dynamic energy price that is used for inducing a shift (or sometimes a shedding) in the power consumption of demand side resources (DSRs). DSRs are electric loads whose consumption can be shifted without impacting the quality of the primary services they are supplying to the consumers. The paradigm of controlling flexible demand is that the contribution in terms of electric power support from the single DSR is not relevant for the power system while the aggregate and coordinate contribution from a large population of DSRs might have important size and hence the capability of impacting the operation of the electric grid. Nevertheless flexible consumption cannot be regarded as a fully controllable virtual unit as the aggregate electric power consumption primarily depends on consumers demand and DSRs operational constraints.

Load kickback effect, are investigated originally under the circumstances of restoration from a power system outage [2]. It is due to the fact that the usual diversity of different loads is lost and they have temporary synchronized behaviour. Under the smart grid frame, the kickback effect may happen as well: the ancillary services instruct the DSRs to perform same or similar actions to their flexible consumption. [3] presented the load kickback model of water heaters. The kickback curve is formulated as a function of curtailed energy using regression method. In [4], the software EnergyPlus is used to identify the payback effects of the components inside the building (e.g., space-heating and air-conditioning systems) by specifying the thermostat model. The kickback effects are observed from a large population of thermostat loads in some studies [5] and a control strategy for reducing it is proposed in [6]. However, given the increasing importance of demand response in the power system, the dynamic behavior of the aggregate demand should be investigated specifically.

In this paper, the dynamic behavior of the aggregate response of an indirect controlled population of DSRs is studied. A sensitivity analysis through Montecarlo simulations is performed considering a homogeneous (i.e. same kind of DSR but not same characteristics) population of 100×10^3 thermostatic controlled loads (building electric space heating) and it is shown how controlling them with an identical indirect control signal (e.g. price signal) introduces time dynamic effects that need to be taken into account if flexible demand is meant to supply regulating power to the grid or other power system services. It is also shown that inducing a diversification in the state of DSRs provide to desynchronize the aggregate consumption hence leading to a more desirable behavior for the power system. This conclusion can be considered for developing price responsive controller for indirect control capable of producing better behaving aggregate power consumption.

The paper is organized as follows: Section II describes the indirect control setup, building thermal models, price responsive control algorithm along with the description of the Monte Carlo simulations scenario. In Section III a detailed description of the kickback effect is provided and supported by simulation results. Monte Carlo simulations of the population are provided and discussed in Section IV. Conclusions are stated in Section V.

II. Indirect control setup

The indirect control setup that is considered for supplying power system services is the one shown in Fig. 1. An indirect

control signal, say the electricity price $p(t)$ (however no market considerations are given in the sequel), is used for inducing a shift in power consumption of a population of DSRs.

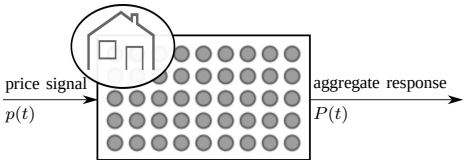

Fig. 1. Indirect control setup. A price signal indirect controls a population of 10^5 buildings equipped with electric space heating.

The population is composed by 10^5 buildings equipped with electric space heating. The aggregate power consumption $P(t)$ of the population is simulated with a bottom-up approach and combining together the individual power requirement of all buildings. Each building is described by a first order dynamic model and it is discussed in Section II-A. Each space heating unit is equipped with an price responsive control algorithm that is discussed in Section II-B. The simulations are performed using a Monte Carlo approach, i.e. buildings and control algorithms have identical form across the population but their parameters are variated according statistical distributions (Section II-C).

A. Building thermal model

The temperature T_j of each building j of the population is simulated with the first order thermal model given in Eq. 1 where input quantities ϕ_s, T^{out} are time series for solar irradiance [Wm^{-2}] and outside temperature [°C] respectively and $u_j(t)$ is the controllable input (on/off) and the parameter D_j is the nominal power consumption of the space heating. The parameters C_j, R, A_j are respectively the lumped thermal capacity of the building, the thermal resistance of the building towards the exterior environment and the window area. C_j and A_j are parameters depending on the size of the building and the criteria with which they have been assigned is explained in the sequel. $\eta_j(t)$ in Eq. 1 is a zero mean Gaussian noise term which is introduced for further differentiating the behavior of the models in the Monte Carlo simulations.

$$C_j \frac{dT_j(t)}{dt} = -\frac{1}{R}T_j(t) + D_j u_j(t) + A_j \phi_s(t) + \frac{1}{R}T^{out}(t) + \eta_j(t) \quad (1)$$

The parameters of the thermal model in Eq. 1 of Power Flexhouse are reported in Table I. Power Flexhouse is a free standing building and it is used as facility for testing demand side management strategies at DTU Elektro, Denmark [7].

TABLE I. POWER FLEXHOUSE I ORDER THERMAL MODEL PARAMETERS.

Name	Unit	Value
C_{FH}	[kW °C^{-1}]	12.3×10^3
S_{FH}	[m^2]	125
A_{FH}	[m^2]	10.7

The values of the parameters in Table I (which are obtained by grey-box modelling) are used as base values for deriving those of all the other models in the population. While the value of the thermal resistance R is kept constant across the population (it is assumed that the buildings have same insulation characteristic), the values C_j and A_j are respectively obtained using the expressions in Eq. 2 and Eq. 3 where S_j is the size [m^2] of the building j and S_{FH} is the one of Power Flexhouse.

$$C_j = \frac{S_j}{S_{FH}} C_{FH} \quad (2)$$

$$A_j = \sqrt{\frac{S_j}{S_{FH}}} A_{FH} \quad (3)$$

In other words each C_j and A_j are scaled according the size of the building they represent (an explanation of the empirical relationships in Eq. 2 and Eq. 3 is provided later). The size S_j [m^2] of each building is a Gamma distributed random variable and it is given in Eq. 4. The histogram of 100×10^3 realizations from Eq. 4 is shown in Fig. 2. The distribution in Eq. 4 and the associated parameters k, θ have been obtained performing a statistical analysis of the size of the class of buildings whose Power Flexhouse is representative using data from the Danish National Register of Buildings (BBR) [8].

$$S_j \sim \Gamma(k, \theta) \quad \text{with } k = 22.35 \vee \theta = 1/6.71 \quad (4)$$

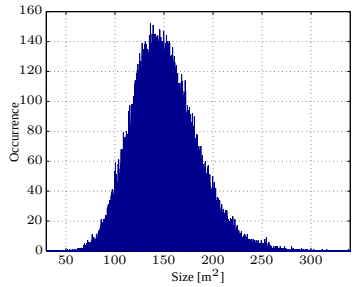

Fig. 2. Stochastic realizations from the Gamma distribution in Eq. 4.

The motivations for Eq. 2 and Eq. 3 are hereafter explained. The thermal capacity of building is due both to its air content and envelope thermal mass. Assuming constant building height, the air volume is linear with the building size S_j. Assuming rectangular shape and same sides ratio of the buildings, the lateral surface of the building is proportional to the square root of building size S_j. Assuming constant thermal resistance, the thickness of the insulation layer ($R \propto$ thermal conductor thickness on exchange area) has to grow linearly with the lateral surface hence linearly with the square root of the building size S_j. As the volume of the insulation layer and walls is given by the lateral surface times the envelope thickness (and both are linear with the square root of the building size) it can be concluded that the volume of the building envelope is also linear with S_j. In case of parameter A_j, it is assumed that the window area of each building j is proportional to the building lateral surface hence to the square root of the building size S_j and t given in Eq. 3. A is the estimated value of Power Flexhouse window area and it is given in Table I.

B. Price responsive building temperature controller

Each building j of the population is equipped with a price responsive controller that acts on the top of a thermostat (feedback controller with hysteresis) as shown in Fig. 3.

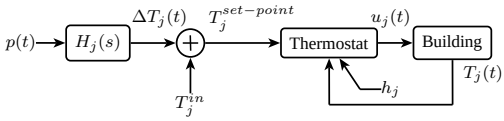

Fig. 3. Price responsive local controller + house thermostatic controller.

The price signal is elaborated by the high pass filter $H_j(s)$ whose expression is given in Eq. 5, where a_j is the temperature variation induced by an unitary stepwise change of $p(t)$ and τ_j is the filter time constant (s is the Laplace operator).

$$H_j(s) = \frac{\Delta T_j(s)}{p(s)} = \frac{a_j s}{s + \tau_j} \tag{5}$$

The steady state contribution of $H_j(s)$ is null, meaning that if the price signal does not change for sufficient long time, the original set-point is restored. This is because it is assumed that the consumers are not willing to affect their temperature comfort at steady state (nondisruptive load control).
The set-point of the thermostat $T_j^{set-point}(t)$ is given in Eq. 6 where T_j^{in} is the user indoor comfort temperature.

$$T_j^{set-point}(t) = T_j^{in} + \Delta T_j(t) \tag{6}$$

The quantity h_j in the thermostat block of Fig. 3 is the hysteresis of the controller and $u_j(t)$ represents the state of the space heating.

C. Parameters variations in the Monte Carlo simulations

Monte Carlo simulations, i.e. accounting for stochastic variations of the parameters, are performed for considering differences of both building and price responsive controller characteristics across the population. Table II shows the PDF according to which the parameters are picked and the correlation coefficients between them. Correlation among S_j (hence thermal capacity C_j) and both D_j and τ_j is introduced because the space heating nominal power and the time constant of the filter are assumed to related to the size of the building.

TABLE II. PARAMETERS DISTRIBUTIONS AND CORRELATION COEFFICIENTS ASSUMED FOR MATRIX FOR MONTE CARLO SIMULATIONS

-	PDF	C_j	A	ϕ_h	T_j	h_j	a_j	τ_j
C_j	$\Gamma(22,663)$	1	.99	.99	0	0	0	.85
A	$\Gamma(88,.13)$	.99	1	.99	0	0	0	.84
D_j	$80 \cdot S_j + \mathcal{N}(.25^2,1)$	.99	.99	1	0	0	0	.84
T_j^{in}	$\mathcal{N}(21,.15^2)$	0	0	0	1	0	0	0
h_j	$\mathcal{N}(1,.10^2)$	0	0	0	0	1	0	0
a_j	$\mathcal{N}(-1.5,.1^2)$	0	0	0	0	0	1	0
τ_j	$\frac{(S_j-150)}{.1} + \mathcal{N}(7e3,1)$	.85	.84	.84	0	0	0	1

III. DESCRIPTION OF THE KICKBACK EFFECT

The simulation in support of this discussion is obtained with the setup in Section II-C with the exception that the threshold of the thermostats and the parameters of the controllers are constant across the population. This is for facilitating the visualization and the description of the dynamics phenomena associated to the aggregate consumption. Solar radiation and ambient temperature (needed by thermal models) have been arbitrarily set to 0 and $10\,^{\circ}\mathrm{C}$ respectively and they are assumed constant both in time and across the population.

The aggregate power consumption response of the buildings (Fig. 4-I) to a step variation of the price signal (Fig. 4-II) is analyzed in this section. Four points of interest have been identified along the consumption profile of Fig. 4-I and they are indicated by the colored marks. In the sequel, the instants of time that corresponds to the marks are analyzed. Fig. 4-III shows the temperature deviation that the indirect control algorithm (Section II-B) applies to each building.

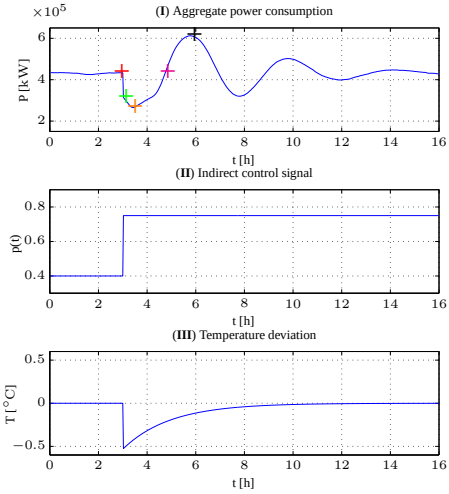

Fig. 4. Population power consumption **(I)** when controlled by price signal in (**II**). The temperature deviation produced by the algorithms is shown in (**III**).

Red mark (steady state): the aggregate power consumption does not exhibit any variation. This is a steady state situation and, statistically, for each thermostat turning on, there is one turning off and vice-versa. The histogram in Fig. 5 shows that the distribution of the distance between the temperature of each building and the respective set-point (i.e. $T_j(t) - T^{set-point}$) is uniform across the population. The buildings moving rightward are those whose space heating is *on* and those which eventually pass the right threshold are the ones switching off. The units moving leftward are cooling down (space heating off) and those which pass the left threshold are the ones switching on, hence contributing positively to the aggregate power consumption. The red bars in the histogram of Eq. 7 shows the distribution of the units state.

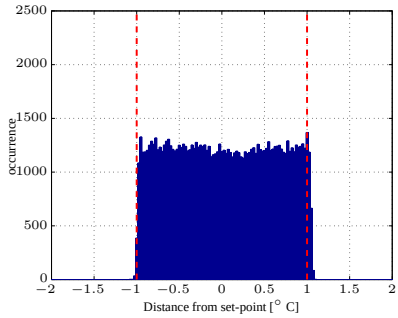

Fig. 5. Histogram of the distance of the temperature of each building from the respective set-point $(T_j(t) - T_j^{set-point})$ at the red mark of Fig. 4-I.

Green mark: the price signal variation is perceived by the indirect control algorithms which therefore decrease the temperature set-point of the respective building. All the units that are in *on* state and whose temperature is higher that the new thermostat set-point are switched off. This provokes a drop in the power consumption. By comparing Fig. 5 and Fig. 6, it is possible to notice that the histogram is shifted on the right of the thermostatic interval (whose thresholds are denoted by the two red dotted lines). A consequence of this is that – for a certain period of time – no units will be able to trigger the consumption on because they need to cool down in order to reach the new left thermostatic bound. This unbalance causes the aggregate power consumption to decrease further as shown by the power profile behavior between the green and orange marks in Fig. 4-I. The blue bars in the histogram in Fig. 7 show the distribution of the state of the space heating units for the instant of time under consideration and, as expected, the group of units in the *off* state for the instant in analysis is larger than in the steady state.

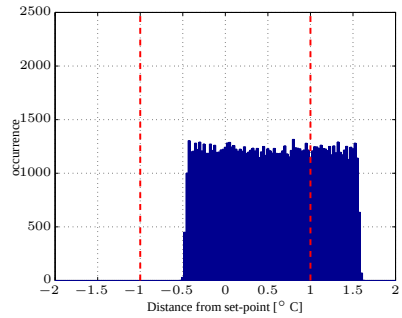

Fig. 6. Temperatures distances distribution at the green mark in Fig. 4-I..

Orange mark: the power consumption profile reaches the minimum value. The histogram in Fig. 8 shows a large number of units being in the proximity of the left thermostatic threshold and hence close to trigger the consumption on (if off). It is worth to note that while time passes, the indirect control algorithm gradually removes the temperature offset (Fig. 4-III) hence 'accelerating' the movement of the population in the histogram towards the center.

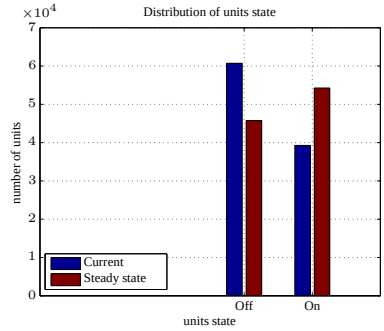

Fig. 7. Distribution of the units state across the population at steady state in the proximity of instant of time indicated with the green mark in Fig. 4-I .

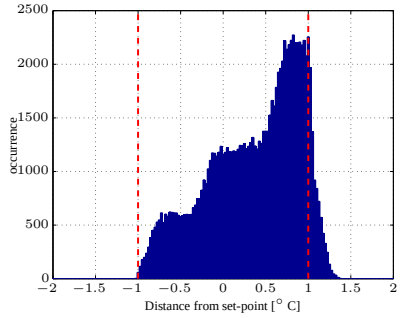

Fig. 8. Temperatures distances distribution at the orange mark in Fig. 4-I.

Magenta mark: here the aggregate power consumption assumes the same value as at steady state (red mark). However this situation does not result in a equilibrium point because the flow of units trespassing the right thermostatic threshold does not equal the flow in the opposite side. By comparing the histograms in Fig. 8 and Fig. 9 it is possible to notice that there is a 'wave' moving leftwards, hence composed by units that are cooling down. This unbalance will cause the aggregate power consumption to increase because a large number of units is expected to trigger the consumption on in the near future. This will cause more units to consume power concurrently and hence provoking a *kickback* effect on the aggregate power consumption (black mark).

Black mark: it corresponds to the peak of the kickback effect of the aggregate response. After the black mark, the aggregate power consumption in Fig. 4-I undergoes to a period with dumped oscillations before reaching a new steady state at time $t \approx 15$ h. The steady state power consumption does not differ than the initial one because the indirect control algorithm does not introduce any steady state contribution for not altering the user comfort.

IV. Monte Carlo simulations

Simulations are performed with the setup discussed in Section II-C, therefore accounting for variations across the population of buildings characteristics, parameters of price responsive controller and parameters of the thermostat. Fig. 10 shows the aggregate power consumption behavior to a step

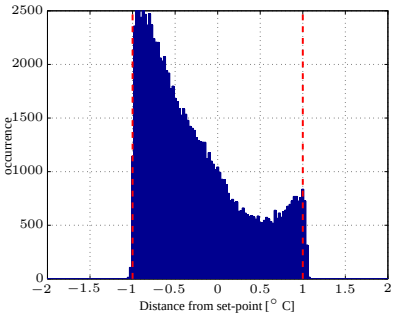

Fig. 9. Temperatures distances distribution at the magenta mark in Fig. 4-I.

variation of the price signal for three different values of the standard deviation of η [1] (the noise term in Eq. 1) and it resembles the response of a second order system at different damping ratios. Initially, the variation of the price signal provokes a synchronization of the state of those units that switch off. A small variance noise term does not promote a diversification of the consumption for those units have been switched off that hence tend to trigger the consumption together for long time causing undamped oscillations. A large variance reduces the deep of the initial power contribution but it contributes to restore a diversification in the consumption hence the peak of the kickback effect is reduced in amplitude and spread in time. Such a characteristic is surely more desirable for the power system point of view. However the noise term is not a controllable parameters and according indirect control paradigm, a desynchronization cannot be induced by price as the signal for indirect control is the same for all DSRs.

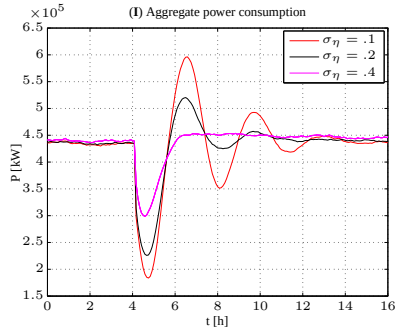

Fig. 10. Population power consumption for three values of the variance of the Gaussian noise term η in Eq. 1.

One might wonder if dynamic effects are reduced by shedding the consumption instead of shifting it. Fig. 11-I shows the aggregate power consumption of the same population discussed above with the difference that the temperature offset is not high pass filtered (Fig. 11-III). Oscillations are still present because the initial drop of power provoked by the variation of the price signal does not match the power variation at steady state.

[1] Standard deviations in Fig. 10 refer to the discretized thermal model (sampling time 300 s). For example, $\sigma_\eta = .1$ means than in five minutes the evolution of the model could be perturbed up to $\pm 0.2\,^{\circ}\mathrm{C}$ at 95% of probability.

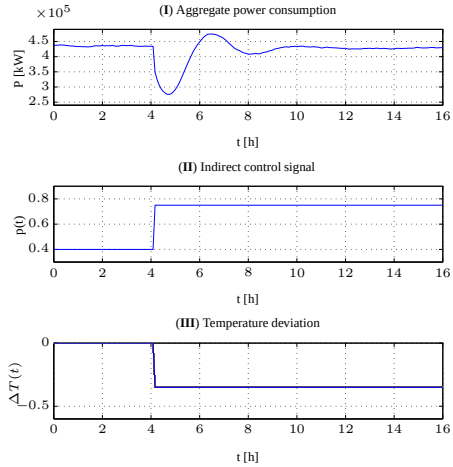

Fig. 11. Consumption shedding instead of shifting.

V. Conclusions

The topic of indirect controlling a large population of DSRs is addressed. It is shown that a variation of the price signal provokes a synchronization in the consumption of the DSRs that can lead to unwanted oscillations of the aggregate power response. The same phenomena is observed to happen also when the consumption is curtailed rather than shifted. It is shown that diversificating the state of DSRs composing the population reduce the peak of the kickback effect. This suggests that a random component could be taken into account in the local price responsive controller in order to dump the oscillations and avoid a deep a kickback.

References

[1] C. Gellings, "The concept of demand-side management for electric utilities," *Proceedings of the IEEE*, vol. 73, no. 10, pp. 1468–1470, 1985.

[2] D. Miller and T. Sleva, "Cold load pickup issues," tech. rep., Power System Relay Committee of The IEEE Power Engineering Society, May 2008.

[3] S. Lee and C. Wilkins, "A practical approach to appliance load control analysis: a water heater case study," *power apparatus and systems, ieee transactions on*, no. 4, pp. 1007–1013, 1983.

[4] N. Ruiz, I. Cobelo, and J. Oyarzabal, "A direct load control model for virtual power plant management," *Power Systems, IEEE Transactions on*, vol. 24, no. 2, pp. 959–966, 2009.

[5] C. Perfumo, E. Kofman, J. H. Braslavsky, and J. K. Ward, "Load management: Model-based control of aggregate power for populations of thermostatically controlled loads," *Energy Conversion and Management*, vol. 55, pp. 36–48, 2012.

[6] N. A. Sinitsyn, S. Kundu, and S. Backhaus, "Safe protocols for generating power pulses with heterogeneous populations of thermostatically controlled loads," *Energy Conversion and Management*, vol. 67, pp. 297–308, 2013.

[7] DTU, "Powerflexhouse," 2013.

[8] "Bygnings-og boligregistret." www.bbr.dk.

Paper F

A MPC replacement strategy for electric space heating including cogeneration of a fuel cell-electrolyzer system

A model predictive control strategy for the space heating of a smart building including cogeneration of a fuel cell-electrolyzer system

Fabrizio Sossan[a,*], Henrik Bindner[a], Henrik Madsen[b], Dimitri Torregrossa[c], Lorenzo Reyes Chamorro[c], Mario Paolone[c]

[a] *DTU Elektro, Frederisborgvej 399, 4000, Roskilde, Denmark*
[b] *DTU Compute, Richard Petersens Plads, 2800, Lyngby, Denmark*
[c] *EPFL DESL, 1015, Lausanne, Switzerland*

Abstract

The objective of this paper is to analyze the value of energy replacement in the context of demand response. Energy replacement is defined as the possibility of the consumer to choose the most convenient source for providing space heating to a smart building according to a dynamic electricity price. In the proposed setup, heat is provided by conventional electric radiators and a combined heat and power generation system, composed by a fuel cell and an electrolyzer. The energy replacement strategy is formulated using model predictive control and mathematical models of the components involved. Simulations show that the predictive energy replacement strategy reduces the operating costs of the system and is able to provide a larger amount of regulating power to the grid. In the paper, we also develop a novel dynamic model of a PEM fuel cell suitable for micro-grid applications. The model is realized applying a grey-box methodology to the experimental proton exchange membrane fuel cell of the EPFL-DESL micro-grid.

Keywords: Demand Response, Control-by-price, Energy replacement, Combined heat and power generation, Proton exchange membrane fuel cell, Model predictive control, Grey-box modelling.

1. Introduction

In the recent years, flexible demand became of renewed interest as a promising resource to restore the lack of control capacity of the power system caused by the increase of the proportion of energy production from renewable generation. Flexible demand is that part of the consumption that can be shifted in time without compromising the quality of the primary services it is supplying

*Corresponding author
Email address: fabrizio.sossan@elektro.dtu.dk (Fabrizio Sossan)

to the consumers. The electric loads capable of flexible operation are said demand side resources (DSRs) and are, for example, the electric thermal loads such as space heating devices and refrigeration units; in this case, the flexibility is given by the associated thermal mass that allows a temporary deferral of the power consumption without causing significant variations of the temperature. The utilization of flexible demand has been proposed to support the primary control of frequency and voltage, and provide regulating power to the grid [1–8].

In this paper, we introduce the concept of *energy replacement* applied to the provision of space heating to a smart building. Energy replacement consists in coupling a traditional source of space heating, i.e. electric radiators, together with combined heat and power (CHP) generation units. The CHP source is a storage system composed by a proton exchange membrane fuel cell (PEMFC), an electrolyzer and tanks for storing the reactants. The control of the energy replacement setup is realized by means of model predictive control (MPC), which achieves to schedule the operation of the energy resources according to a dynamic electricity price and while respecting the temperature comfort of the consumer. From the power grid operation point of view, such a setup is expected to provide larger flexibility because energy can be stored not only in the building thermal mass, but also by producing and storing the reactants of the PEMFC-electrolyzer system. The electricity price reflects the need of regulating power of the grid, and, in general, is meant to act as an economic incentive for the flexible demand to shift the consumption. This approach is known as control-by-price, and is extensively advocated in existing literature as a simple framework to enable demand response, since it relies on a few ICT requirements. We show by simulation that, in comparison with conventional space heating setups [9–11], the proposed predictive control strategy achieves a reduction in the operation cost and is able to manage effectively the extended amount of flexibility provided by the CHP system. The topic of the integration of CHP devices at demand side level with the objective of enhancing the performance of demand response was previously considered in [12]. We extend such a development by including dynamic models of the fuel cell and building, showing, as mentioned above, how energy can be stored by means of both producing reactants and exploiting the thermal mass of the building envelope. In the process of developing the energy replacement strategy, we propose a novel dynamic model of a PEMFC suitable for micro-grid applications. The model is realized applying a grey-box modelling methodology and is identified using measurements from the experimental 15 kW PEMFC of the DESL facility at EPFL.

The paper is organized as follows: Section 2 describes the setup of the replacement strategy, the models of the components and the MPC algorithm. In Section 3, the simulation results are presented and discussed. Finally, conclusions are stated in Section 4.

2. Methods

2.1. The energy replacement concept

The objective of the energy replacement strategy is to provide heat to a smart building combining the operations of several energy resources while minimizing the total cost of the operation and according to the requirements of the grid, which reflects its need of regulating power into a dynamic price of the electricity. The configuration of the energy replacement setup is sketched in Fig. 1: space heating is supplied by the electric radiators and recovering the waste heat associated to the electrochemical conversions operated by the FC and electrolyzer. From Fig. 1, the reactants required by the FC are produced by the electrolyzer, and are mechanically compressed by electric compressors and stored in tanks. It is worth to note that high pressure electrolysis could avoid the use of the compressors since the reactants are already produced at high pressure [13]. Although, in this setup, the configuration with mechanical compression is chosen because is more general in terms of components.

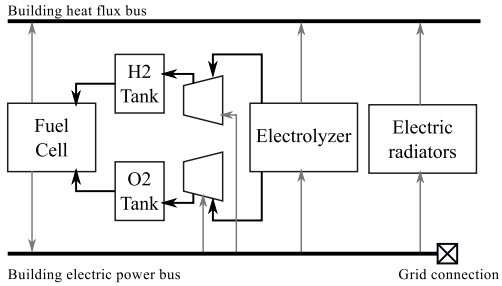

Figure 1: The setup of the energy replacement strategy. Building space heating is provided by conventional electric radiators, the FC and electrolyzer. The reactants are mechanically compressed and stored in the tanks.

The control of the energy replacement strategy is realized using the MPC. It consists in an optimization problem that minimizes the associated penalty function, while obeying the constraints of the system. The formulation of the MPC strategy requires the mathematical models of the components in Fig. 1. The model of the FC is identified using a grey-box approach and using measurements from a 15 kW PEMFC: the modelling methodology, the experimental setup and the model are described in Section 2.2. The models of the compressors and tanks of the reactants are realized using a first principles approach and are described in Section 2.4 and Section 2.5, respectively. The mathematical models of the electrolyzer and building are from literature and are presented in Section 2.3 and Section 2.6, respectively. The formulation of the MPC problem is described in Section 2.7.

2.2. Fuel cell grey-box model

2.2.1. Stochastic grey-box modelling

The PEMFC model is identified using the grey-box methodology, which is a framework that allows to identify a model incorporating its physical knowledge together with measurements from a real device. The adopted grey-box modelling process consists in formulating a candidate model as a function of unknown parameters that are estimated from measurements using maximum likelihood estimation (MLE). The objective of MLE is determining the parameters of the model that maximize the likelihood of the model, i.e. maximize the probability that the model can explain the set of available measurements. The mean and variance of the 1-step ahead prediction of the candidate model with parameters $\boldsymbol{\theta}$ at the time step k are defined as

$$\hat{\boldsymbol{y}}_{k|k-1} = E[\boldsymbol{y}_{k|k-1}(\boldsymbol{\theta})] \tag{1}$$

$$R_{k|k-1} = \mathrm{Var}[\boldsymbol{y}_{k|k-1}(\boldsymbol{\theta})], \tag{2}$$

respectively, where $\boldsymbol{y}_{k|k-1}$ indicates the prediction of the model provided the information up to $k-1$. The 1-step ahead prediction error of the model is defined as

$$\boldsymbol{\epsilon}_k = \boldsymbol{y}_k - \hat{\boldsymbol{y}}_{k|k-1}, \tag{3}$$

where $\boldsymbol{y}_k$ is the measurement at the time interval k. Assuming that the predictions of the stochastic model are Gaussian distributed, the likelihood function is defined as

$$L\big(\boldsymbol{\theta}, \boldsymbol{y}(k)\big) = \Bigg(\prod_{j=1}^{k} \frac{\exp\big(-\frac{1}{2}\boldsymbol{\epsilon}_j^T R_{j|j-1}^{-1} \boldsymbol{\epsilon}_j \big)}{\sqrt{\det(R_{j|j-1})}\sqrt{2\pi}^{k}} \Bigg) p(\boldsymbol{y}_0|\boldsymbol{\theta}), \tag{4}$$

which is the joint probability of the prediction errors obtained as the product of the single conditional probability density. The parameters of the model are found by minimizing the logarithm of the function in Eq. (4). The MLE routine that is utilized to estimate the FC model is implemented in the software package CTSM [14], which is available as a library for the programming language for statistical computing R. In order to capture all the dynamics inherent the system to identify, the device to model should be excited in a wide range of frequency during its operation. This is usually accomplished by controlling the device using a pseudo binary random signal (PRBS), that is a binary signal with a fixed period and duty cycle randomly picked from an uniform distribution. In the case of the FC, the PRBS was replaced by a stepwise signal (shown in Fig. 2) characterized by random durations and amplitude variations. Once the parameters are estimated, the candidate model is validated by means of performing the residual analysis, which allows to determine if the model is able to capture all the dynamics observable in the set of measurements. The FC dynamic model is formulated using stochastic differential equations (SDEs), which allow to obtain, as an outcome of the estimation process, the uncertainties

related to both the system disturbances and measurements noise. In general, this is a useful feature since a characterization of the disturbances allows to determine the statistics of the predictions of the model and implement Kalman filtering for state reconstruction and prediction. In the following sections, the experimental setup and the FC model are described.

2.2.2. Experimental setup

DESL laboratory at EPFL in Lausanne implements an experimental micro-grid for studying the interaction between distributed power generation and the electric power system. The micro-grid is composed by a number of distributed energy resources, among which a 15 kW PEMFC. The FC system, originally developed for automotive application, is composed by the supply system of the reactants, the FC and the associated cooling system. All the components of the FC system are controlled and supervised by an internal controller, which is accessible through a CAN bus and returns information regarding the state of the system, temperature and voltage of the stack, and maximum current that the FC can deliver. The FC is supplied by a 240 and 480 m^3 tanks at 200 bar for hydrogen and oxygen, respectively, for an equivalent of 1 MWh of stored energy. A further pipeline provides nitrogen to the FC, that is used to purge the reactants circuit and the membrane after each use. The electric output of the FC is connected to a programmable direct current (DC) load. All the measurements are sampled at 10 Hz and are logged by a software in LabView, which is also used to set the current consumption reference of the DC load. The experiment requirements are to measure the FC stack terminal voltage, FC stack temperature and to control the current supplied by the FC by means of the electronic load, in a similar way as done in [15]. The FC measurements that are used to identify the model of the FC are shown in Fig. 2.

2.2.3. Model formulation

In a FC, the not unitary efficiency of the electrochemical conversion causes a drop of the voltage available at the terminals of the stack. The voltage of a PEMFC can be described by the equivalent electric circuit shown in Fig. 3, where E is the modified Nerst potential and v_{act}, v_{conc}, R_{ohm} are the activation loss, concentration loss and ohmic loss, respectively [16]. All the three types of voltage losses depend on the FC temperature and reactants partial pressures. Activation and concentration losses are evident at low and high values of the FC current, respectively, while ohmic loss is linear with the current.

As far as the dynamic properties of PEMFCs systems are concerned, the dominant time constants are those associated to the temperature evolution of the FC stack ($O(2)$) and operation of the supply system of the reactants ($O(0)$), while the electric dynamics are very fast ($<<O(-3)$) [17]. In the existing literature, dynamic models of PEMFCs systems were developed mainly in connection to automotive applications, and they describe how the FC voltage is affected by the dynamics of the supply system [18–24]; in such models, the temperature dynamics are disregarded as it considered that the FC is operating in continuous mode, hence with the temperature regulated at the nominal value by an active

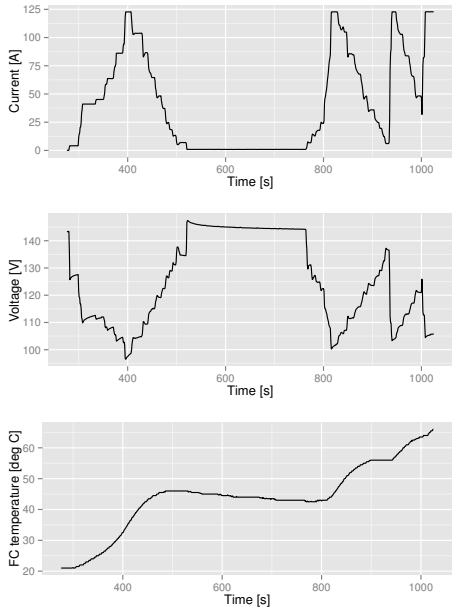

Figure 2: The measurements used to estimate the FC model. The three plots show the FC current (that is controlled by the electronic load), the DC voltage and the temperature of the stack, respectively.

cooling system. In the case of CHP applications, the dominant time constants of the system are those associated to the temperature dynamics of the building, i.e. $O(10^4$ s). In this context, the dynamics of the supply system of the reactants can be neglected since they are much faster than the dominant time constants. On the contrary, the thermal transient is of longer duration and should be taken into account, especially if the FC is meant to operate in a discontinuous mode, as it is the case of the proposed energy replacement strategy. These requirements motivate the need of developing a new dynamic grey-box model for PEMFC systems specific for micro-grid applications. The developed model of the FC is composed by two parts: a static model that describes the voltage of the FC as a function of the FC current and temperature, and a dynamic model that describes the temperature evolution of the FC stack.

Model of the FC stack terminal voltage. The model proposed to describe the voltage of the PEMFC is shown in Fig. 4. The ideal voltage source OCV denotes the open circuit voltage, while the controllable voltage source v_{act} and resistor R_{ohm} denotes the activation and ohmic losses, which are a nonlinear

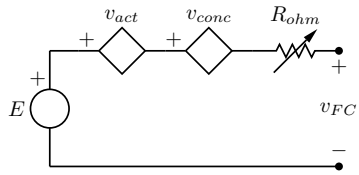

Figure 3: The conventional description of the FC stack voltage [16].

and linear functions of the FC current i_{FC}, respectively. At this stage, the concentration loss is not modelled because it was not observable in the set of available measurements (indeed the maximum FC DC current was below 120 A).

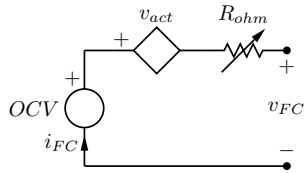

Figure 4: The proposed model of the FC stack voltage.

The mathematical formulation of the model corresponds to the KVL applied to the circuit in Fig. 4, that is:

$$v_{FC} = OCV - v_{act} - R_{ohm}. \tag{5}$$

In the model, the value of OCV is chosen as a constant because no clear correlation with the temperature was observed in the measurements. Theoretically, the OCV of a single cell is defined by the modified Nernst potential [25], which is given as

$$\begin{aligned} E'(T_{FC}, p_{H_2}, p_{O_2}) = 1.229 - 0.85 \times 10^{-3}\,(T_{FC} - 298.15) + \\ + 4.3085 \times 10^{-5} T_{FC} \left[ln(p_{H_2}) + \frac{1}{2} ln(p_{0_2}) \right], \end{aligned} \tag{6}$$

where T_{FC} is the temperature [K] of the stack, p_{H_2} and p_{O_2} are the partial pressures [atm] of hydrogen and oxygen, respectively. The derivative of Eq. (6) with respect to the temperature, calculated at the operational value of the reactants pressure and zero current (2.50 atm and 2.55 atm for oxygen and hydrogen, respectively), gives a value of approximately $0.8 \times 10^{-4}\,\mathrm{V\,K^{-1}}$: the linear dependency of the modified Nerst potential with the temperature is very small, thus assuming a constant value for OCV in Eq. (6) is reasonable. Even

if the number of the FC cells composing the stack might be known, it can be inferred by the following expression:

$$n_{FC} = \frac{OCV}{E'}, \tag{7}$$

where E' is as in Eq. (6).

A candidate function for describing the activation loss v_{act} of Eq. (5) is the Tafel's equation:

$$v_{act} = a \cdot ln(i_{FC}) - b, \tag{8}$$

where a and b are two coefficients to be determined empirically [18, 26]. In the proposed model, we assume that the coefficient b does not depend on the temperature, so it can be considered as part of the FC OCV; moreover, we replace the Tafel's equation with the following one

$$v_{act} = a' \cdot \sqrt{i_{FC}}, \tag{9}$$

which is a function of similar shape as Eq. (8), but is defined over the whole set of possible values of the FC current, i.e. $i_{FC} \geq 0$; this is done with the objective of avoiding numerical instability of the algorithm that estimates the parameters of the model. In order to account for the temperature dependency of the activation loss, the parameter a' of Eq. (9) is replaced by a linear function of the FC temperature. Hence, the final expression that describes the activation loss is given as

$$v_{act}(T_{FC}, i_{FC}) = (\alpha \cdot T_{FC} + \beta)\sqrt{i_{FC}}, \tag{10}$$

where α and β are parameters to be estimated.

The ohmic loss associated to the FC operation is described by a resistance; in a similar way as done for the activation loss, we describe the resistance as a linear function of the temperature. The ohmic loss is given as

$$R_{ohm}(T_{FC}) = \gamma \cdot T_{FC} + \delta, \tag{11}$$

where γ and δ are parameters to be estimated.

Model of the FC temperature. The equivalent electric circuit that describes the evolution in time of the FC temperature T_{FC} is shown in Fig. 5, where Q_{FC} is the heat generated by the electrochemical conversion, C is the lumped thermal capacity of the FC, R is the lumped thermal resistance of the FC envelope, while Q_{ext} is the heat loss due to conduction and natural convection that occurs between the FC and the environment, which is at temperature T. The controlled current generator Q_c of Fig. 5 denotes the heat extracted by the FC cooling system, which is thermostatically controlled and is activated once the temperature of the FC reaches the nominal operating value of ≈ 80°C; in order to reduce the number of variable to identify, the quantity Q_c is excluded from the estimation

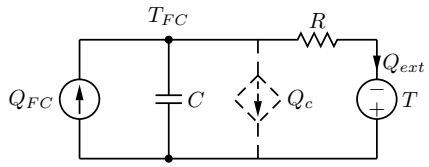

Figure 5: The model proposed to describe the temperature dynamics of the FC. The current generator Q_c is sketched with the dashed line because it is not considered in the identification process.

process by means of using a set of measurements where the cooling system is *off*, i.e. with $T_{FC} < 80°\text{C}$.

The first order differential equation that describes the circuit of Fig. 4 constitutes the deterministic skeleton of the FC thermal model. The complete formulation of the thermal model of the FC is given as

$$dT_{FC}(t) = \left(\frac{Q_{FC}}{C} - \frac{T_{FC}(t) - T(t)}{RC} \right) dt + \sigma dB(t), \tag{12}$$

where $B(t) \in \mathcal{N}(0,1)$ is a Wiener process, i.e. a stochastic process with independent normal distributed increments, and σ is a scale coefficient to estimate. By combining the equations (10) and (11), the amount of heat Q_{FC} generated by the FC corresponds to the Joule losses associated to the voltage generator v_{act} and resistance R_{ohm} of Fig. 4, and is given as

$$Q_{FC}(T_{FC}, i_{FC}) = \big((\alpha \cdot T_{FC} + \beta)\sqrt{i_{FC}} + (\gamma \cdot T_{FC} + \delta) i_{FC}\big) i_{FC}. \tag{13}$$

Identification results. The parameters of the electric model and thermal model are estimated using the procedure described in Section 2.2.1. In order to provide a warm start to the optimization underlaying the MLE problem, the parameters of the electric model are previously estimated using measurements of the voltage, current and temperature of the FC and applying conventional least squares. The estimated values of the mean and standard error of the parameters of the FC model are summarized in Table 1.

As a support to the validation process of the model, we perform the residuals analysis, which consists in evaluating any autocorrelation in the 1-step ahead prediction error of the model, or residual, that was defined in Eq. (3). In the ideal case, the prediction error should be white noise, meaning that the model was able to capture all the dynamics observable in the measurements. Fig. 6 shows the autocorrelation function (ACF) of the predictions of the model (black profile) and the 90% confidence interval of the ACF of white noise (blue line). Since the autocorrelation of the residuals is similar to the one of white noise, the model is considered statistically significant.

Fig. 7 compares the measurements of the temperature of the FC with the 2

Table 1: The estimated parameters of the FC model.

Name	Mean	Standard error
OCV	144.2	0.89
α	-1.15×10^{-1}	4.95×10^{-4}
β	1.01×10^{1}	1.91×10^{-4}
δ	-4.89×10^{-1}	2.82×10^{-3}
γ	9.11×10^{-3}	3.40×10^{-5}
Rs	1.09×10^{-1}	4.89×10^{-2}
Cs	2.27×10^{4}	9.55×10^{2}
σ	-9.07×10^{-2}	5.10×10^{-3}

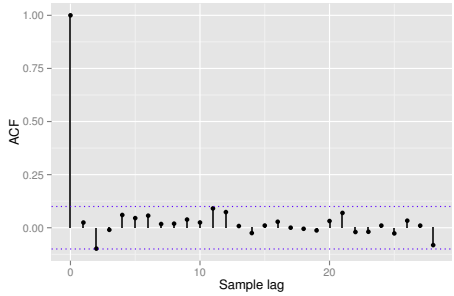

Figure 6: Autocorrelation function (ACF) of the 1-step ahead predictions of the FC model and the 90% confidence interval of the ACF of white noise with the black and blue colors, respectively.

minutes ahead prediction of the identified thermal model, and it qualitatively shows that the prediction is able to track the measurements.

Fig. 8 compares the experimentally obtained polarization curve, i.e. FC voltage as a function of the FC current, with the one estimated using the identified electric model.

2.3. Electrolyzer Model

The electrolyzer is a device that realizes the inverse process of a FC, that is the production of pure hydrogen and oxygen through the electrochemical conversion of water. Nowadays, three mainstream electrolysis technologies are available: alkaline, PEM and SOFC. For this study, a PEM electrolyzer is chosen because it works at low temperature (20-80 °C) and allows a small size of the stack [27], thus is potentially suitable for small scale applications. In [28], a nearly linear function of the stack temperature is used to describe the efficiency of the conversion cycle. Since accurate measurements for estimating the thermal model of the electrolyzer are not available at this stage, the efficiency is assumed as a function of the current only. The adopted model is based on

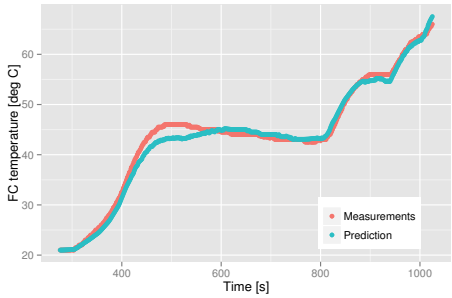

Figure 7: The temperature of the FC stack according to the measurements and as predicted by the estimated thermal model (2 minutes ahead prediction).

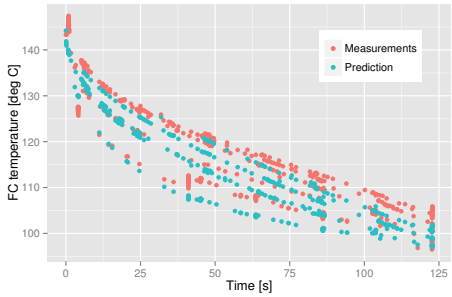

Figure 8: The polarization curve of the FC according to the measurements and as predicted from the model of the FC voltage.

the measurements proposed in [29], which shows a positive correlation between the stack temperature and the conversion efficiency (similarly to the fuel cell) that, with a current of 100 A, goes from 78% to 84% respectively at ambient and nominal temperature. We describe the voltage of the electrolyzer v_{EL} as

$$v_{EL} = 33.1 - 43.0 \times 10^{-3}\, \mathrm{i}_{EL}, \tag{14}$$

where i_{EL} is the current absorbed by the electrolyzer. In a similar way as done for the FC, the heat associated to the operation of the electrolyzer Q_{EL} is calculated as the Joule loss associated with the model of the voltage, that is

$$Q_{EL} = i_{EL}^2 \cdot 43.0 \times 10^{-3}. \tag{15}$$

2.4. Tank Model

As known, the mass m [kg] of a generic gas inside a tank is given as

$$m = \int \dot{m}_{\text{in}} - \dot{m}_{\text{out}} dt, \tag{16}$$

where $\dot{m}_{\text{out}}$ and $\dot{m}_{\text{in}}$ denote the outlet and inlet flow of the gas in $[\text{kg}\,\text{s}^{-1}]$, respectively. Assuming the gas as ideal, the pressure p of the gas can be expressed with the law of the perfect gas as

$$p = \frac{m\bar{R}T}{V}, \tag{17}$$

where R is the specific gas constant $[\text{J}\,\text{kg}^{-1}\,\text{K}^{-1}]$, V is the volume of the tank $[\text{m}^3]$, and T is the gas temperature [K]. Replacing Eq. (16) into Eq. (17) gives

$$p = \frac{\bar{R}T}{V} \int \dot{m}_{\text{in}} - \dot{m}_{\text{out}} dt. \tag{18}$$

Based on the fact that the only possible path for the electrons is the FC membrane, the inlet and outlet flows of the hydrogen can be computed as a function of the electrolyzer and FC currents i_{EL} and i_{FC}:

$$\dot{m}_{\text{in}} = n_{EL} \frac{i_{EL}}{F} \tag{19}$$

$$\dot{m}_{\text{out}} = n_{FC} \frac{i_{FC}}{F}, \tag{20}$$

where n_{EL} and n_{FC} are the number of cells of the stack of the electrolyzer and FC, respectively. The complete model of the hydrogen tank is shown in Eq. (21) ($\bar{R} = 4.124\,\text{J}\,\text{g}^{-1}\,\text{K}$).

$$p_{H_2} = 1 \times 10^{-3} \frac{\bar{R}T}{FV} \int n_{EL} i_{EL} - n_{FC} i_{FC} dt \tag{21}$$

The model of the tank of the oxygen can be obtained in a similar way as done for the hydrogen. Although, the models of the tank and compressor of the oxygen are not implemented because the consumption and production rates of the oxygen are determined by the stoichiometric coefficients of the water reaction formula ($2H_2 + 0_2 \rightarrow 2H_2O$), and, as far as the formulation of the MPC is concerned, they can be implemented using algebraic relationships rather than dynamic ones.

2.5. Compressor model

The derivative of the isoentropic compression work required to compress the mass flow rate $\dot{m}$ at temperature T_{env} [K] from pressure p_1 to p_2 [Pa] is given as

$$\dot{W}_{isoen} = \dot{m}\bar{R}T_{env} \frac{k}{k-1} \left(\frac{p_2}{p_1}^{\frac{k-1}{k}} - 1 \right), \tag{22}$$

where k is the adiabatic index (≈ 1.4), and $\bar{R}$ [J kg^{-1} K^{-1}] is the specific constant of the gas that undergoes the compression. The mechanical power required for the compression is defined as

$$\dot{W}_{mech} = \frac{\dot{W}_{isoen}}{\eta_{isoen}}, \tag{23}$$

where η_{isoen} is the isoentropic efficiency of the compressor. Using the same approach as in [30, 31], η_{isoen} is assumed constant at 0.8. Finally, the electric power needed to drive the compressor is

$$P_{co} = \dot{W}_{mech} \frac{1}{\eta_m}, \tag{24}$$

where $\eta_m = 0.9$ is the lumped efficiency of the electric motor that drives the compressor. In a similar way as done for the tank, the mass flow rate $\dot{m}$ in Eq. (22) can be calculated as function of the electrolyzer current. The final expression of the compressor model is thus given as

$$P_{co} = n_{EL} \frac{i_{EL}}{F} \bar{R} T_{env} \frac{k}{k-1} \left(\frac{p_2}{p_1}^{\frac{k-1}{k}} - 1 \right) \frac{1}{\eta_m}, \tag{25}$$

with $\bar{R} = 4.124\,\mathrm{J\,g^{-1}\,K}$.

2.6. Building thermal model

The building indoor temperature, say $T(t)$ [°C], is described by the following first order differential equation [32]:

$$C \frac{dT(t)}{dt} = -\frac{1}{R} T(t) + \frac{1}{R} T_{out}(t) + A\phi_s(t) + \phi_h(t), \tag{26}$$

where T_{out} is the outdoor temperature [°C] , ϕ_s is the solar radiance on the horizontal plane [W m^{-2}], ϕ_h is the heat supplied to the building [W], and the parameters C, R, A are the lumped thermal capacity of the building, the thermal resistance of the building envelope and the windows surface, respectively. The values and units of the parameters are shown in Table 2. According to the energy replacement strategy, the heat supplied to warm the building is composed by the following terms

$$\phi_h(t) = P(t) + Q_c(t) + Q_{EL}(t) + Q_{ext}(t), \tag{27}$$

where $P(t)$ is the electric power consumption of the heaters, $Q_c(t)$ is the heat extracted by the active cooling system of the FC, Q_{EL} is the waste heat associated with the operation of the electrolyzer and Q_{ext} is the natural thermal loss of the FC. It is worth noting that a more accurate description of the dynamics of the building temperature could be achieved using a second order model because it allows to account for the different transients due to thermal masses of the building envelope and air [33]. However,the main focus of this study is on describing the lumped thermal capacity of the building rather than a detailed description of the temperature transients, hence the first order model is used.

Table 2: The parameters of the building thermal model [32].

Name	Unit	Value
C	$\mathrm{J\,°C^{-1}}$	1.23×10^7
R	$\mathrm{°C\,W^{-1}}$	4.87×10^{-3}
A	$\mathrm{m^2}$	10.7

2.7. Energy replacement model predictive control

The objective of the MPC strategy is to schedule the operation of the resources of the energy replacement setup minimizing the total cost of operation, while obeying the constraints of the components and respecting the temperature comfort of the consumer. The symbols used in this section are defined in Table 3 and Table 4. The former table defines the variables of the optimization problem (state variables and decision variables), while the latter summarizes the parameters.

Table 3: Variables of the MPC optimization problem.

Symbol	Description	Type	unit
T	Building indoor temperature	state variable	°C
T_{FC}	FC stack temperature	state variable	°C
Q_c	heat extracted by the FC cooling system	decision variable	W
i_{FC}	FC current	decision variable	A
v_{FC}	FC stack voltage	variable	V
i_{EL}	Electrolyzer current	decision variable	A
v_{EL}	Electrolyzer voltage	variable	V
p_{H_2}	hydrogen pressure in the tank	state variable	bar
P_{co}	Compressor electric power	state variable	W
S	Fuel cell start-up	state variable	–
n	Fuel cell start-up counter	integer variable	–

The cost expression of the optimization underlaying the MPC problem is

Table 4: Parameters of the MPC optimization problem.

Symbol	Description	Value	Unit
$T_{FC,MAX}$	FC nominal stack temperature	75	°C
$i_{FC,MAX}$	FC maximum current	150	A
$i_{EL,MAX}$	Electrolyzer maximum current	120	A
$p_{H_2,MAX}$	Max hydrogen pressure in the tank	6	bar
$p_{H_2,MIN}$	Min hydrogen pressure in the tank	2.1	bar
V	Tank volume	2.5	m^3
N	Optimization horizon length	50	h
n_{max}	Maximum fuel cell off-on cycles	3	times/day
p	Dynamic electricity price		

given as

$$J = \sum_{k=0}^{N} \big[- P_{FC,k} + P_{EL,k} + 2P_{co,k} + P_k \big] p_k + \sum_{k=0}^{N} \big(s_k S_k + \lambda_k \big[n_k - n_{max} \big] \big), \tag{28}$$

where s_k and λ_k are weights. In Eq. (28), the first summation is the total electricity cost and is calculated as the net power consumption times the electricity price: in this case, the electric power required to compress the oxygen is approximated with the one required for the hydrogen. In the second summation of Eq. (28), the first term accounts for the FC startup cost ($S_k \in \{0, 1\}$ is 1 when the FC state goes from off to on, 0 vice-versa) and the second term is a soft constraint that penalizes those schedules that require the FC to go through more than n_{max} off-on cycles. The startup variable S_k is calculated as following

$$S_k = \mathrm{sgn}\big(i_{FC,k} \cdot (i_{FC,k} - i_{FC,k-1}) \big). \tag{29}$$

The FC power $P_{FC}(k)$ in Eq. (28) is expressed as

$$P_{FC,k} = v_{FC,k} i_{FC,k}, \tag{30}$$

where v_{FC} is determined using the FC voltage model (given in Eq. (5)) and i_{FC} is a decision variable of the optimization. In a similar way, the electrolyzer power $P_{EL,k}$ is

$$P_{EL,k} = i_{EL,k} v_{EL,k}, \tag{31}$$

where $v_{EL,k}$ is determined using the model in Eq. (14) and $i_{EL,k}$ is a decision variable of the optimization. Finally, the compressor power P_{co} in Eq. (28) is expressed using the compressor model in Eq. (25).

The operational constraints implemented in the MPC are the following self-explanatory inequalities:

$$0 \leq i_{FC}(k) \leq i_{FC,MAX} \tag{32}$$
$$0 \leq i_{EL}(k) \leq i_{EL,MAX} \tag{33}$$
$$p_{H_2,MIN} \leq p_{H_2}(k) \leq p_{H_2,MAX} \tag{34}$$
$$T_{FC}(k) \leq T_{FC,MAX} \tag{35}$$
$$i_{FC}(k+1) - i_{FC}(k) \leq \Delta i_{FC,MAX} \tag{36}$$
$$P_{MIN} \leq P(k) \leq P_{MAX} \tag{37}$$
$$T_{MIN} \leq T(k) \leq T_{MAX}, \tag{38}$$

which apply for $k = 0, \ldots, N$. The inequality (35) limits the temperature of the FC: this task is accomplished through Q_c, which is a decision variable of the optimization problem. The comfort of the user is preserved by the pair of inequalities in (38).

In addition to the operational constraints, the optimization problem is subject to the mathematical models previously introduced, in particular:

- the FC operation is described by the models of the stack voltage, the heat loss and the stack temperature, which are given in Eq. (5), Eq. (13) and Eq. (12), respectively.
- the electrolyzer operation is described by the models of the voltage and heat loss, given in Eq. (14) and Eq. (15), respectively;
- the tank is described by the dynamic model in Eq. (21);
- the electric power consumption of the compressor for the hydrogen is described by the model in Eq. (25);
- the temperature of the building is described by the dynamic model in Eq. (26).

The dynamic models are discretized using rectangular integration and with a sample time of 200 s. The MPC problem is given by minimizing the cost expression J in Eq. (28) using i_{FC}, i_{EL}, P and Q_c as decision variables. The optimization problem if of non linear mixed integer type, is formulated in GAMS and solved using CONOPT algorithm.

3. Results

In this section, the simulations results of the energy replacement MPC are presented. In order to show the achieved cost savings and the capability of the proposed strategy to manage the larger amount of flexibility, a traditional

MPC setup is used as a benchmark. The traditional MPC setup is a building equipped with electric space heating that is controlled by the same MPC as the energy replacement, but without any CHP unit. In the following, the traditional MPC setup and the energy replacement MPC will be referred to as *Setup A* and *Setup B*, respectively. In the simulations, measured values of the outdoor temperature and insulation are utilized (sunny early spring period, ambient temperature between 2 and 6 °C and maximum peak insulation on the horizontal plane 500 [$\mathrm{W\,m^{-2}}$]). Simulations are performed assuming a deterministic context, i.e. all the forecast required by the MPC are known and the models are error free. Simulations are performed using, initially, an artificial price signal and, subsequently, using the regulating power price of the Nord Pool day-ahead market.

3.1. Artificial electricity price

Following the same approach proposed in [34], the flexibility of the two setups is probed using a sine wave as an artificial price signal. Three price signal scenarios are analyzed, and each of them is characterized by a different frequency of the sine wave. The price signal scenarios are shown from Fig. 9 to Fig. 11 and they correspond to a period of the price signal of 5, 14 and 50 hours, respectively.

Figures from 12 to 17 show the simulation results for each price signal scenario and setup. Each figure is composed by two stacked plots; the plot in the upper panel shows the building temperature (blue profile) and the temperature comfort range (red profile), which is chosen as 20 ± 1°C and 20 ± 1.5°C during the day and night hours, respectively; the plot in the bottom panel shows the net power consumption of the building: negative values indicate that the building exports power to the grid and vice-versa. In Scenario I, the price signal (Fig. 9) exhibits fast variations, and, in both setup, the respective MPC strategies are to able to shift the consumption during the periods when the cost the electricity is low while keeping the average temperature of the building in the middle of the comfort zone.

In the case of Scenario II, the variations of the price signal are slower than the previous case. The MPC controller of Setup A let the temperature of the building to lay at the lowest allowed limit during the periods with higher electricity cost, while, when the price is lower, it stores energy in the thermal mass by increasing the temperature of the building (Fig. 14). In the case of Setup B, the extended flexibility provided by the CHP system allows the controller to keep the average temperature of the building in the central part of the comfort area, as shown in Fig. 15.

Finally, scenario III is characterized by a slow varying price signal. The MPC controllers of both setup are able to modulate the power consumption according to the amplitude of the price signal. In comparison to the previous scenario, the temperature dynamics of figures 16 and 17 are similar because, since the electricity price varies slowly, the limited thermal mass of the building do not allow to maintain the temperature in the middle of the comfort zone. In

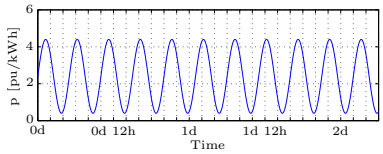

Figure 9: The price signal of Scenario I.

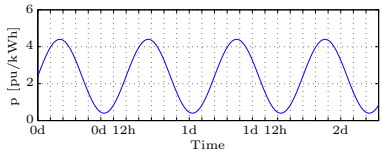

Figure 10: The price signal of Scenario II.

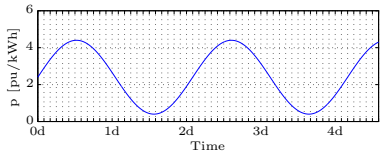

Figure 11: The price signal of Scenario III.

both Setup A and B, the controllers saturate the storing capacity of the building and let the temperature to lay at the limits of the comfort zone.

In order to evaluate in a numerical form the flexibility of the two setups, we evaluate the correlation index between the price signal and the power consumption. The correlation index is defined as

$$r = \frac{\mathrm{Cov}[p, P]}{\sqrt{\mathrm{Var}[p] \cdot \mathrm{Var}[P]}}, \tag{39}$$

where P is the total net power consumption of the building and p is the price signal. The correlation index is used as an indicator for measuring how much the power consumption is affected by the variation of the electricity cost. For an ideal fully deferrable load, the correlation coefficient should be -1, because the power consumption is always in anti-phase with the price signal. In the case of a conventional electric load, the flexibility is a function of the consumer comfort, and the value of the correlation coefficient is expected to assume larger values than -1. The correlations coefficients calculated the three price signal scenarios are given in Table 5. As expected, the power consumption of Setup B

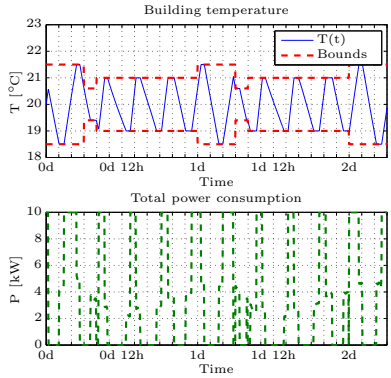

Figure 12: Scenario I, Setup A.

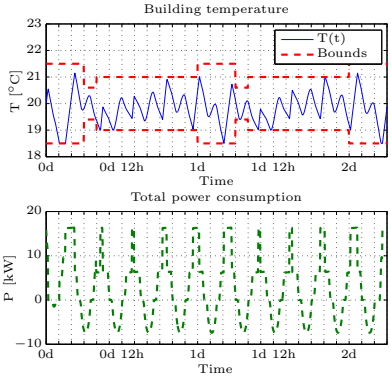

Figure 13: Scenario I, Setup B.

has considerable larger negative correlation of the price signal than Setup A, meaning that the proposed energy replacement strategy is able to schedule the operation of the different energy resources and exploit the larger amount of flexibility.

In order to illustrate more into details the operation of the energy replacement setup, the power consumption profiles and the contributions of heat of the energy resources of Setup B is shown in Fig. 18 and Fig. 19, respectively. In the former figure, it can be seen that when the electricity price is low, the electric radiators and the electrolyzer sustain the space heating of the building, and the compressors are activated in order to store the reactants. On the contrary,

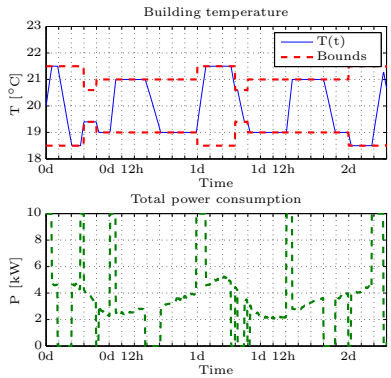

Figure 14: Scenario II, Setup A.

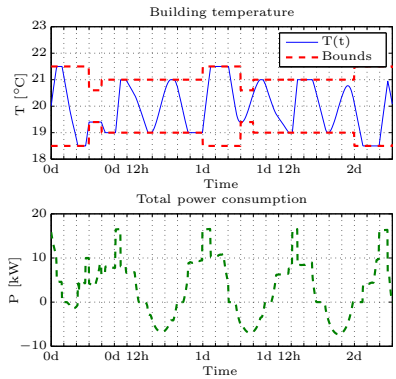

Figure 15: Scenario II, Setup B.

Table 5: The correlation indexes between the power consumption and the price signal calculate with Eq. (39)

Setup	SI	SII	SIII
Setup B	-0.91	-0.81	-0.67
Setup A	-0.82	-0.48	-0.22

when the electricity price is large, the FC is activated in order to export electric power to the grid and provide space heating to the building.

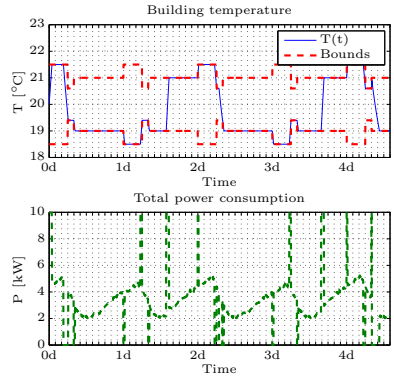

Figure 16: Scenario III, Setup A.

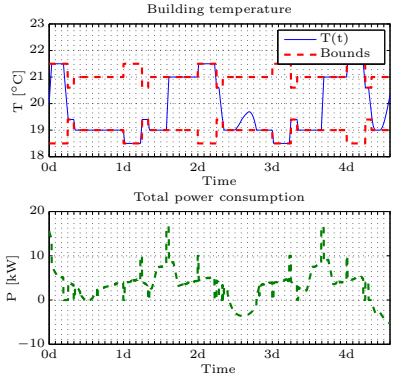

Figure 17: Scenario III, Setup B.

3.2. NordPool market electricity price

The simulations of this section are performed using the hourly electricity price of the NordPool day-ahead market [35]. The electricity price is shown in Fig. 20.

Fig. 21 shows the temperature profile and the net power consumption of the building controlled with the energy replacement MPC, while Fig. 22 shows the temperature dynamics for Setup A.

Table 6 summarizes the total electricity cost for Setup A, Setup B and Setup A', which is the same as Setup A except that the radiators are con-

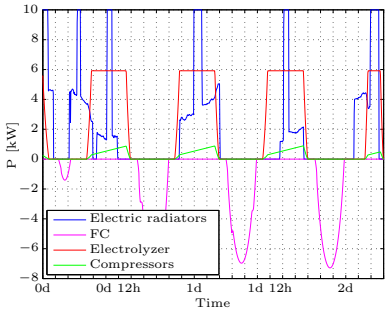

Figure 18: The operation of the energy replacement setup (Setup B) during Scenario II: the power profiles.

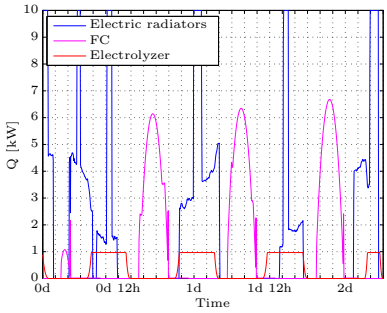

Figure 19: The operation of the energy replacement setup (Setup B) during Scenario II: the heat profiles.

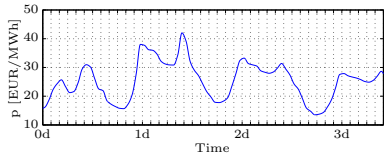

Figure 20: The hourly electricity price of the NordPool day-ahead market. The initial instant of time refers to the 4^{th} of August.

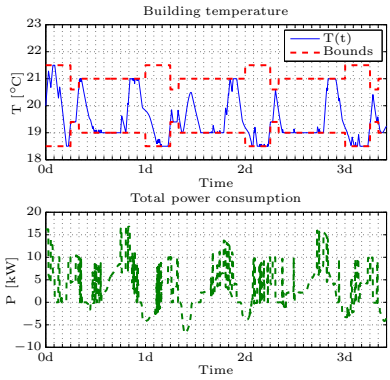

Figure 21: Energy replacement strategy (Setup B) with the NordPool electricity price.

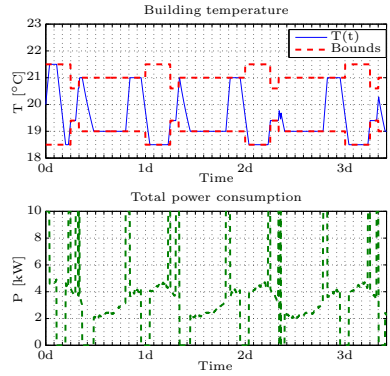

Figure 22: Setup A with the NordPool electricity price.

trolled by a thermostatic controller rather than the MPC. From Table 6, it can be seen that the proposed energy replacement setup allows to save the 20% and 25% if compared to Setup A and Setup A', respectively.

Table 6: The total electricity cost calculated using the Nord Pool regulating power price of Fig. 20.

Setup	Electricity cost [EUR]
Setup B (energy replacement MPC)	7.27
Setup A (MPC with only electric radiators)	9.10
Setup A' (thermostatic controlled radiators)	9.70

4. Conclusions

A model predictive control strategy with the objective of exploiting the potential of combined heat and power generation of a fuel cell and an electrolyzer system was presented. This application was referred to as *energy replacement* to indicate the possibility of the consumer to switch among the most convenient source to provide space heating to a smart building according to a dynamic electricity price, which reflects the need of regulating power of the electric grid. We showed that the proposed model predictive control strategy is able to schedule effectively the operation of the different energy resources and outperforms other space heating setups in terms of amount of regulating power that can provide to grid and operation cost, which is reduced of up to 25%. In the process of generating these results, this paper presents a novel PEMFC model suitable for smart-grid and micro-grid applications. The model has been realizing applying grey-box methodology using measurements from the 15 kW PEMFC of the EPFL-DESL facility. As a summary, the key contributions of the paper are:

- the concept of *energy replacement*, which offers a larger flexibility than conventional space heating setup and enhances the support that flexible demand can provide to the future power system;
- a model predictive control strategy for combining the operation of conventional heating system and combined heat and power generation devices;
- a novel grey-box model of a PEMFC suitable for smart and micro-grid applications.

References

1. Ela E, Tuohy A, Milligan M, Kirby B, Brooks D. Alternative approaches for incentivizing the frequency responsive reserve ancillary service. *The Electricity Journal* 2012;25(4):88–102. URL: `http://www.sciencedirect.com/science/article/pii/S1040619012000929`. doi:http://dx.doi.org/10.1016/j.tej.2012.04.015.

2. Xu Z, Ostergaard J, Togeby M. Demand as frequency controlled reserve. *IEEE Transactions on Power Systems* 2011;26(3).

3. Affonso CM, da Silva LC. Potential benefits of implementing load management to improve power system security. *International Journal of Electrical Power & Energy Systems* 2010;32(6):704–10. URL: `http://www.sciencedirect.com/science/article/pii/S014206151000013X`. doi:http://dx.doi.org/10.1016/j.ijepes.2010.01.004.

4. Douglass P, Garcia-Valle R, Sossan F, Ostergaard J, Nyeng P. Design and evaluation of autonomous hybrid frequency-voltage sensitive load controller. In: *IEEE International Conference on Innovative Smart Grid Technologies (ISGT)*. 2013:.

5. Papaioannou IT, Purvins A, Tzimas E. Demand shifting analysis at high penetration of distributed generation in low voltage grids. *International Journal of Electrical Power & Energy Systems* 2013;44(1):540–6. URL: `http://www.sciencedirect.com/science/article/pii/S0142061512004140`. doi:http://dx.doi.org/10.1016/j.ijepes.2012.07.054.

6. De Rijcke S, De Vos K, Driesen J. Balancing wind power with demand-side response. In: *5th IEEE Joint IAS, PELS & PES Benelux Chapter Young Researchers Symp., Leuven, Belgium*. 2010:.

7. Corradi O, Ochsenfeld H, Madsen H, Pinson P. Controlling electricity consumption by forecasting its response to varying prices. *Power Systems, IEEE Transactions on* 2013;28(1):421 –9. doi:10.1109/TPWRS.2012.2197027.

8. Christakou K, Tomozei DC, Le Boudec JY, Paolone M. Gecn: Primary voltage control for active distribution networks via real-time demand-response. *Smart Grid, IEEE Transactions on* 2013;PP(99). doi:10.1109/TSG.2013.2275004.

9. Halvgaard R, Poulsen N, Madsen H, Jørgensen J. Economic model predictive control for building climate control in a smart grid. In: *IEEE International Conference on Innovative Smart Grid Technologies (ISGT)*. 2012:.

10. Sossan F, Bindner H. A comparison of algorithms for controlling DSRs in a control by price context using hardware-in-the-loop simulation. In: *IEEE Power and Energy Society General Meeting*. 2012:.

11. Zong Y, Kullmann D, Thavlov A, Gehrke O, Bindner H. Application of model predictive control for active load management in a distributed power system with high wind penetration. *IEEE Transactions on Smart Grid* 2012;3.

12. Houwing M, Negenborn R, De Schutter B. Demand response with micro-chp systems. *Proceedings of the IEEE* 2011;99(1):200–13. doi:10.1109/JPROC.2010.2053831.

13. Schug C. Operational characteristics of high-pressure, high-efficiency water-hydrogen-electrolysis. *International journal of hydrogen energy* 1998;23(12).

14. Kristensen NR, Madsen H. Continuous time stochastic modelling. 2003.

15. Torregrossa D, Blumier D, Miraoui A. Regressive method for the determination of fuel cell pem parameters in order to develop a fuel cell pem emulator. In: *Industry Applications Society Annual Meeting, 2009. IAS 2009. IEEE*. 2009:doi:10.1109/IAS.2009.5324869.

16. Pukrushpan J. Modeling and control of fuel cell systems and fuel processors. Ph.D. thesis; The University of Michigan; 2012.

17. Rodatz S, Paganelli G, Guzzella L. Optimizing air supply control of a pem fuel cell system. In: *American Control Conference, 2003. Proceedings of the 2003*; vol. 3. 2003:2043–2048 vol.3. doi:10.1109/ACC.2003.1243375.

18. Pukrushpan J, Stefanopoulou A, Peng H. Modeling and control for pem fuel cell stack system. In: *Proceedings of the American Control Conference*; vol. 4. 2002:3117–22.

19. Sedghisigarchi K, Feliachi A. Dynamic and transient analysis of power distribution systems with fuel cells-part i: fuel-cell dynamic model. *Energy Conversion, IEEE Transactions on* 2004;19(2):423–8. doi:10.1109/TEC.2004.827039.

20. Rekioua D, Bensmail S, Bettar N. Development of hybrid photovoltaic-fuel cell system for stand-alone application. *International Journal of Hydrogen Energy* 2014;39(3):1604 –11. URL: `http://www.sciencedirect.com/science/article/pii/S0360319913006496`. doi:http://dx.doi.org/10.1016/j.ijhydene.2013.03.040.

21. El-Sharkh M, Rahman A, Alam M, Byrne P, Sakla A, Thomas T. A dynamic model for a stand-alone {PEM} fuel cell power plant for residential applications. *Journal of Power Sources* 2004;138(12):199–204. URL: `http://www.sciencedirect.com/science/article/pii/S0378775304006925`. doi:http://dx.doi.org/10.1016/j.jpowsour.2004.06.037.

22. Deng L, Deng XR, Ma N, Wei P. Dynamic modeling of a pem fuel cell stack thermal system. In: *Advanced Computer Control (ICACC), 2010 2nd International Conference on*; vol. 2. 2010:473–7.

23. Fang L, Di L, Ru Y. A dynamic model of pem fuel cell stack system for real time simulation. In: *Power and Energy Engineering Conference (APPEEC)*. 2009:.

24. Bjazic T, Ban Z, M.P. F. Linear model of PEM fuel cell power system for controller design purposes. In: *30th Jubilee International Convention : Computers in Technical Systems*. 2007:.

25. Amphlett JC, Baumert R, Mann RF, Peppley BA, Roberge PR, Harris TJ. Performance modeling of the ballard mark iv solid polymer electrolyte fuel cell i. mechanistic model development. *Journal of the Electrochemical Society* 1995;142(1).

26. Larminie J, Dicks A. Fuel Cell Systems Explained. J. Wiley; 2003. ISBN 9780768012590. URL: `http://books.google.dk/books?id=5rp22BEdibcC`.

27. Carmo M, Fritz DL, Mergel J, Stolten D. A comprehensive review on pem water electrolysis. *International Journal of Hydrogen Energy* 2013;38(12):4901–34. URL: http://www.sciencedirect.com/science/article/pii/S0360319913002607. doi:http://dx.doi.org/10.1016/j.ijhydene.2013.01.151.

28. Grgn H. Dynamic modelling of a proton exchange membrane (pem) electrolyzer. *International Journal of Hydrogen Energy* 2006;31(1):29–38. URL: http://www.sciencedirect.com/science/article/pii/S0360319905000868. doi:http://dx.doi.org/10.1016/j.ijhydene.2005.04.001.

29. Dale N, Mann M, Salehfar H. Semiempirical model based on thermodynamic principles for determining proton exchange membrane electrolyzer stack characteristics. *Journal of Power Sources* 2008;185(2):1348–53. URL: http://www.sciencedirect.com/science/article/pii/S0378775308016686. doi:http://dx.doi.org/10.1016/j.jpowsour.2008.08.054.

30. Hovgaard T, Larsen LFS, Skovrup M, Bagterp Jø rgensen J. Power consumption in refrigeration systems-modeling for optimization. In: *Advanced Control of Industrial Processes (ADCONIP), 2011 International Symposium on*. 2011:234–9.

31. Lee JM, Cho B. A dynamic model of a pem fuel cell system. In: *IEEE Conference on Applied Power Electronics*. 2009:720–4.

32. P. Bacher A. Thavlov HM. Models for energy performance analysis. Tech. Rep.; DTU-IMM; 2010.

33. Madsen H, Holst J. Estimation of continuous-time models for the heat dynamics of a building. *Energy and Buildings* 1995;22:67–79. URL: http://www.sciencedirect.com/science/article/pii/037877889400904X. doi:http://dx.doi.org/10.1016/0378-7788(94)00904-X.

34. Sossan F, Bindner H. Evaluation of the performance of indirect control of many DSRs using hardware-in-the-loop simulations. In: *IEEE Conference on Decision and Control (CDC)*. 2012:.

35. Nord Pool Spot . Nord pool spot. 2013. URL: http://www.nordpoolspot.com/.